Applications of reticular diversity in metal-organic frameworks : an ever-evolving state of the art

Applications of reticular diversity in metal–organic frameworks: an ever-evolving state of the art

Aleksander Ejsmont,[1] Jacopo Andreo,[2,3] Arianna Lanza,[4] Aleksandra Galarda,[1] Lauren Macreadie,[5] Stefan Wuttke,[2,3,*] Stefano Canossa,[6] Evelyn Ploetz,[7,*] and Joanna Goscianska[1,*]

[1]*Faculty of Chemistry, Adam Mickiewicz University in Poznań, Uniwersytetu Poznańskiego 8, 61-614 Poznań, Poland*

[2]*BCMaterials, Basque Center for Materials, UPV/EHU Science Park, 48940 Leioa, Spain*

[3]*Ikerbasque, Basque Foundation for Science, 48013, Bilbao, Spain*

[4]*Center for Nanotechnology Innovation @NEST, Istituto Italiano di Tecnologia, Piazza S. Silvestro, 12, Pisa, 56127, Italy*

[5]*School of Chemistry, University of Sydney, Sydney, 2006, NSW, Australia*

[6]*EMAT, University of Antwerp, Groenenborgerlaan 171, 2020 Antwerp, Belgium*

[7]*Department of Chemistry and Center for NanoScience (CeNS), Ludwig-Maximilians-Universität München (LMU), Butenandtstraße 11, 81377 Munich, Germany*

*Email: stefan.wuttke@bcmaterials.net, evelyn.ploetz@cup.uni-muenchen.de, and joanna.goscianska@amu.edu.pl

Abstract

Metal–organic frameworks (MOFs) are exciting materials due to their extensive applicability in a multitude of modern technological fields. Their most prominent characteristic and primary origin of their widespread success is the exceptional variety of their structures, which we termed ‘reticular diversity’. Naturally, the ever-emerging applications of MOFs made it increasingly common that researchers from various areas delve into reticular chemistry to overcome their scientific challenges. This confers a crucial role to comprehensive overviews capable of providing newcomers with the knowledge of the state of the art, as well as with the key physics and chemistry considerations needed to design MOFs for a specific application. In this review, we commit to this purpose by outlining the fundamental understanding needed to

carefully navigate MOFs' reticular diversity in their main fields of application, namely host–guest chemistry, chemical sensing, electronics, photophysics, and catalysis. Such knowledge and a meticulous, open-minded approach to the design of MOFs paves the way for their most innovative and successful applications, and for the global advancement of the research areas they are employed in.

Keywords: Metal–organic framework; Pore chemistry; Host–guest interaction; Conductivity; Chemical sensing; Photovoltaics; Catalysis

Abbreviations

AAS	Atomic absorption spectrometry
AI	Artificial intelligence
AIE	Aggregation-induced emission
ALD	Atomic layer deposition
AMP	Aminomethyl propanol
An	Anthracene
an2py	*trans*,*trans*-9,10,-bis(4-pyridyl-ethenyl)anthracene
ASA	Arsinilic acid
azdc	Azobenzene-4,4′-dicarboxylate
bdc	1,4-dicarboxy-benzene
bdc-NH_2	2-amino-1,4-benzenedicarboxylate
BET	Brunauer–Emmett–Teller
BHJ	Bulk heterojunction
bht	Benzenehexathiol
Bodipy	Boron-dipyrromethene
bpa	4,4′-ethylenedipyridine
bpdc	Biphenyl-4,4′-dicarboxylate
bpe	1,2-bis(4-pyridyl)ethylene
bpptztz	2,5-bis(4-(pyridine-4-yl)phenyl)thiazolo[5,4-d]thiazole
bpy	bipyridine
btc	1,3,5-tricarboxylate
btdd	bis(1*H*-1,2,3-triazolo[4,5-b],[4′,5′-i])dibenzo[1,4]dioxin)
bte	4,4′,4″-(benzene-1,3,5-triyl-tris-(ethyne-2,1-diyl))-tribenzoate
bte-NO_2	3,3′,3″-nitro-4,4′,4″-(benzene-1,3,5-triyl-tris-(ethyne-2,1-diyl-))tribenzoate
CAP	Chloramphenicol
CB	Conduction band
CD	Cyclodextrin
COF	Covalent organic framework
CP5	Carboxylatopillar[5]arene
CSMCRI	Central Salt & Marine Chemicals Research Institute
CT	Charge transfer
CUS	Coordinatively unsaturated site
DABCO	1,4-diazabicyclo[2.2.2]octane
dae	Diarylethene
dcphOH-ndi	Carboxylate appended naphthalene diimide
DEF	Diethylformamide
DFT	Density functional theory
DMA	*N*,*N*-dimethylacetamide
DMEDA	*N,N'*-dimethylethylenediamine
DMF	Dimethylformamide
DMSO	Dimethyl sulfoxide
dobdc	1,4-dioxido-1,3-benzenedicarboxylate
dobpdc	4,4′-dioxidobiphenyl-3,3-dicarboxylate

DOX	Doxorubicin
DPA	Dipicolinic acid
dpa	9,10-diphenylanthracene
dppztz	2,5-bis-(4-(4-pyridinyl)-phenyl)-thiazolo-[5,4-*d*]-thiazole
dpta	4-amino-3,5-diphenyl-1,2,4-triazole
DSSC	Dye-sensitized solar cell
EMF	Electro-motive force
emi	1-ethyl-3-methylimidazolium
EPR	Electron paramagnetic resonance
ESA	Excited-state absorption
ET	Energy transfer
etim	Ethylimidazole
ETU	Energy transfer upconversion
Fc	Ferrocene
FRET	Förster resonance energy transfer
FTIR	Fourier-transform infrared
FTO	Fluorine-doped tin oxide
Fu	Fluorouracil
G	Guest
GO	Graphene oxide
H	Host
HAADF-STEM	High-angle annular dark-field scanning transmission electron microscopy
HAB	Hexaaminobenzene
HENU	Henan University
HER	Hydrogen evolution reaction
hhtp	Hexahydrotriphenylene
hitp	2,3,6,7,10,11-hexaiminotriphenylene
hmba	Hydroxymethylbenzoate
HP	Hairpin probe
hpdc	1*H*-pyrazole-3,5-dicarboxylate
HPLC	High-performance liquid chromatography
HPU	Henan Polytechnic University
IBU	Inorganic building unit
Ibu	Ibuprofen
IC	Internal conversion
ICP-OES	Inductively coupled plasma atomic emission spectroscopy
IL	Ionic liquid
IRMOF	Isoreticular metal-organic framework
ISC	Intersystem crossing
isq	*o*-diiminobenzosemiquinonate
IVCT	Inter-valence charge transfer
JBNN	Jumping beyond nearest neighbor
LED	Light-emitting diode
Lip	Liposome

LiPS	Lithium polysulfide
LLCT	Ligand-to-ligand charge transfer
LMCT	Ligand-to-metal charge transfer
LSMO	$La_{0.67}Sr_{0.33}MnO_3$
LUCO	Lowest unoccupied crystal orbital
Ma	Maleimide
MC	Missing cluster
MCP	Methyl-cyclopentane
MD	Molecular dynamics
m-dobdc	4,6-dioxido-1,3-benzenedicarboxylate
me-im	2-methylimidazole
men	*N,N′*-dimethylethylenediamine
MFM	Manchester Framework Material
MIL	Materials Institute Lavoisier
ML	Missing linker
MLCT	Metal-to-ligand charge transfer
MMCT	Metal-to-metal charge transfer
MMM	Mixed-matrix membrane
MO	Metal oxide
MOF	Metal-organic framework
MTV	Multivariate
mtb	4,4',4",4"'-methanetetrayltetrabenzoate
MUV	Materials of University of Valencia
NCP	"N-confused" porphyrin
NDI-py	N,N′-bis(4-pyridyl)-1,4,5,8-naphthalene diimide
NF	Ni-foam
NIR	Near-infrared
NMR	Nuclear magnetic resonance
NNH	Nearest-neighbor hopping
NP	Nanoparticle
NTDI	Naphthalene-tetracarboxydiimide
NU	Northwestern University
NZF	Nitrofurazone
OA	Oleic acid
OBU	Organic building unit
OER	Oxygen evolution reaction
OMS	Open metal site
ORR	Oxygen reduction reaction
OSV	Organic spin valve
PA	Photon avalanche upconversion
PAF	Porous aromatic framework
PCBM	[6,6]-phenyl-C_{61}-butyric acid methyl ester
PCET	Proton-coupled electron transfer
PCN	Porous coordination network

PET	Photoinduced electron transfer
PETN	Pentaerythritol tetranitrate
PIZOF	Porous interpenetrated zirconium–organic frameworks
POM	Polyoxometalate
POMOF	POM-based metal-Organic Framework
PSI	Post-synthetic insertion
PSII	Photosystem II
PSM	Post-synthetic modification
PVP	Polyvinylpyrrolidone
PXRD	Powder X-ray diffraction
pz	Pyrazine
pzc	Pyrazine-2-carboxylate
QCR	Quartz crystal resonator
QD	Quantum dot
Rh	Rhodamine
RhB	Rhodamine B
$Ru(bpy)_3$	Ru^{II} polypyridine
Rubpy	$Ru(2,2'\text{-bpy})_3$
SALE	Solvent-assisted linker exchange
SALI	Solvent-assisted linker incorporation
SBHA	Suberoylbis-hydroxamic acid
sbpdc	4,4′-dibenzoate-2,2′-sulfone
SBU	Secondary building unit
SCO	Spin crossover
SC-SC	Single-crystal-to-single-crystal
sdc	*trans*,-*trans*-4,40-stilbenedicarboxylate
SDZ	Sulfadiazine
SEC	Size-exclusion chromatography
SG	SYBR Green I
SIFSIX	SiF_6^{2-}
SLI	Sequential linker installation
SSLiB	Solid state lithium battery
tatab	4,4′,4′′-*s*-triazine-1,3,5,-triyltri-*m*-aminobenzoate
tba	t-butyl alcohol
tbapy	1,3,6,8-tetrakis(*p*-benzoate)pyrene
TBU	Ternary building unit
TCNQ	Tetracyanoquinodimethane
tcpp	Tetrakis(4-carboxyphenyl)porphyrin
tdc	2,5-thiophene dicarboxylate
TFA	Trifluoroacetic acid
TGA	Thermogravimetry
TL	Truncated linker
TMS	Transition metal sulfide

TMU	Tarbiat Modares University
TOF	Turnover frequency
TON	Turnover number
tppZn	Tetraphenylporphyrinato Zn(II)
ttf	Tetrathiafulvalene
ttftb	Tetrathiafulvalene-3,4,5,6-tetrakis(4-benzoate)
tztz	thiazolo[5,4-*d*]thiazoles
UC	Upconversion
UCL	Upconversion luminescence
UCNP	Upconversion nanoparticle
UiO	Universitet i Oslo
USTC	University of Science and Technology of China
UV	Ultraviolet
VB	Valence band
Vis	Visible
VOC	Volatile organic compound
VR	Vibrational relaxation
XRD	X-ray diffraction
XTA	X-ray transient absorption
ZIF	Zeolitic imidazolate framework
ZJU	Zhejiang University

1. Introduction

Since its entrance in countless synthetic laboratories around the globe, the rational engineering of metal–organic frameworks (MOFs) approached more and more the process of building and furnishing a laboratory of its own [1]. As we decide the architecture of our workplace based on practicality and the positioning of the necessary equipment and furniture that allow a laboratory at the meter-scale to operate efficiently, when designing a new MOF structure we plan thoughtfully the division of confined spaces, their accessibility, and the installation of functional entities in what we estimate as optimal sites [2,3]. There is, however, a rather obvious difference between setting up a laboratory at the meter and at the Ångström scale: the precision and reliability of the process of construction itself.

MOFs are assembled from an alternation of organic building units (OBUs) and metal-containing inorganic building units (IBUs) [3,4] and the endless chemical variety of their constituents generates miscellaneous MOFs' structures [5–7]. However, the very process of controlling such assembly remains perhaps the greatest and most long-standing challenge in researching these cutting-edge miniaturized laboratories [2]. Indeed, being MOFs synthesized by self-assembly instead of direct manipulation of their components, our approach to their construction remained substantially unchanged over the last decades and consists in driving the aggregation of building blocks by finely tuning synthesis variables such as temperature, solvent mixture, reactants, additives, *etc.* [8].

The practice of constantly perfecting and making more precise and reliable assembly of MOFs can be considered at the heart of their engineering and the primary source of their structural—hence functional—sophistication [9]. Major leaps in this respect included the attention shift from the systematic change of building blocks' chemical structure to tuning linkers' and framework's metrics altogether (isoreticular MOFs [10]), to even regulating the framework's mobility by employing conformationally-flexible linkers and/or geometrically versatile IBUs [11,12]. Another more recent and increasingly popular area of MOFs chemistry is the engineering of partly aperiodic frameworks. It aims not only to achieve control on the crystalline structure of MOFs but also to purposefully introduce building-block vacancies [13] and heterogeneities [14,15] with specific spatial distributions in the main crystal lattice.

Given this premise, herein we focus on the concept of 'reticular diversity' (Fig. 1), which we coined to describe the variability of structure and composition of framework assemblies. Reticular diversity is a key concept in MOFs chemistry as it does not only reflect the countless possibilities of synthesizing frameworks with different geometries, composition, complexity,

metric and degree of order, but also includes the perspective of combining all these aspects in the design of a single extremely sophisticated material. Such an inclusive and open-minded approach to MOFs research is becoming a solid foundation of the most advanced realities in the field, and an exciting new source of innovation that lies largely unexplored.

With this in mind, we present an overview of recent applications (especially in the last 5 years) of MOFs' reticular diversity in a comprehensive series of research areas.

Aiming to introduce the most relevant properties of MOFs, we start by describing the chemistry of their most crucial component: their pores. Subsequently, the major applications of MOFs as host–guest systems, sensors, electronic- and photonic materials, catalysts are extensively reviewed after providing, for each field, the basic theoretical background needed for a useful critical understanding. Each section also delivers the general context for its specific research field, the major challenges, and the state of the art, and finally presents a perspective look at the future possibilities of MOF materials.

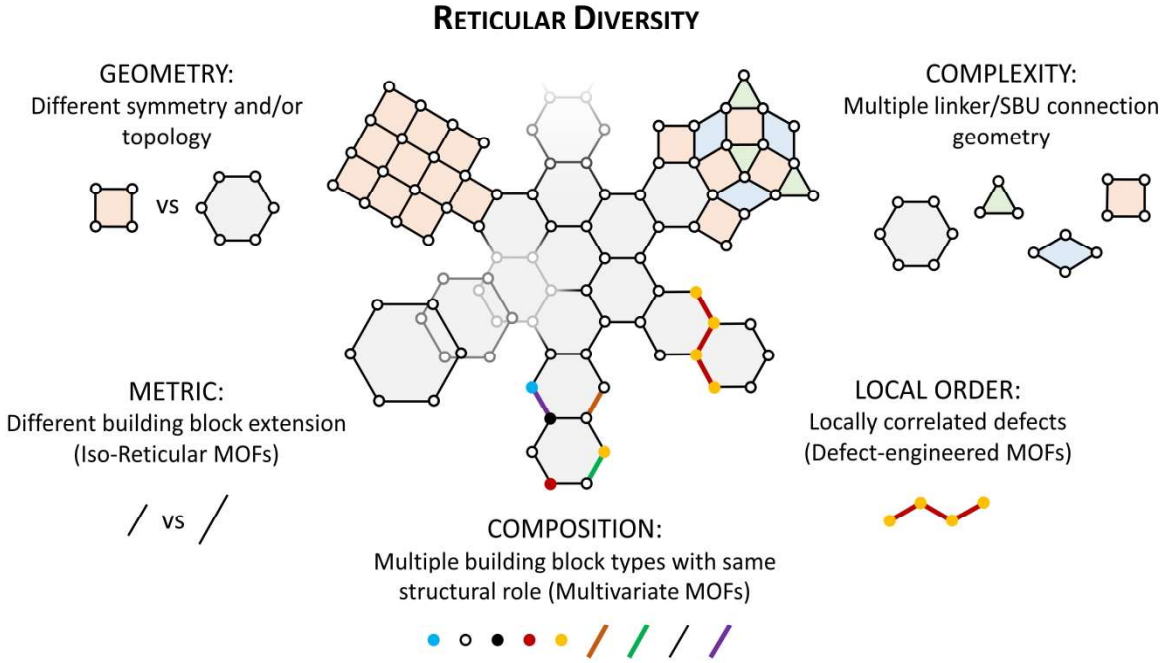

Figure 1. General scheme of the main current possibilities of reticular diversity of MOFs.

2. Pore chemistry

The uniqueness of framework materials is their combination of functionality and regular porosity [2]. These two aspects are inextricably interdependent and affect one another. The application of the final material is governed by the physicochemical properties of the

framework which, in turn, arise from their designed structural and chemical details. The origin of the macroscopic function can be traced back to the characteristics of the pore at the atomic scale. Hence, we can consider pore chemistry as the core of functionality in framework materials and therefore the starting point for material design (Fig. 2).

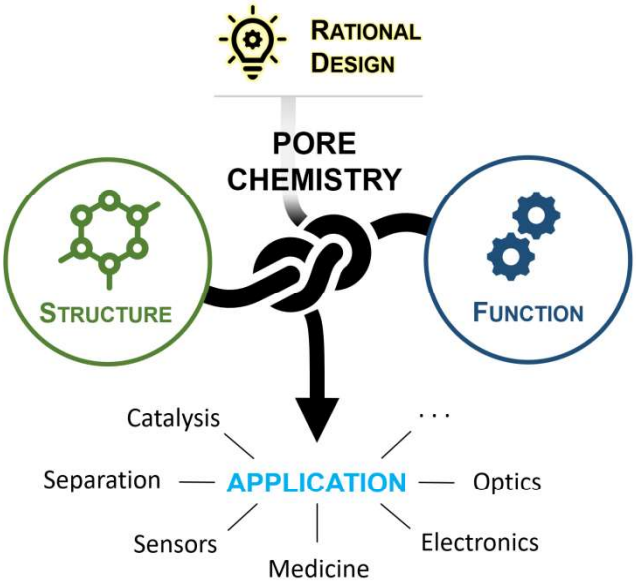

Figure 2. The rational design of MOFs focused on their pore chemistry, where the intrinsic connection between structure and function makes them valuable for a wide variety of applications.

In this chapter, we wish to explore a recently proposed mindset for reticular pore chemistry starting from the atomic scale [2]. We will be stepping into the pore space itself and thus distinguishing the origin of the influencing features that drive function. The geometrical and physical characteristics of the void are the first aspect to be considered. We ask ourselves, what are the pore walls comprised of? Are there additional guests present or missing parts? Functional groups can be identified in the pore, which are atoms or groups of atoms that can either be part of the framework backbone or belong to guests hosted in the cavities. Defects, *i.e.* local irregularities of the periodic framework, can act as functional sites as well. Hence, all the above-mentioned aspects will be considered in section 2.1. as target sites for MOF functionalization.

In combining suitable building blocks, chemists usually adopt two possible approaches for the synthesis of crystalline reticular materials with pre-conceived functions (section 2.2.). Firstly, functionality can be introduced along with the structural building blocks in a pre-synthetic approach. This is identified as a self-assembly process which results in the formation of a

crystalline material with embedded sites of functionality. The second approach is based on the generation or modification of functional sites by means of physical or chemical transformations carried out on a pre-formed framework, over one or more post-synthetic steps.

Section 2.3. presents different conceptual methods to specifically position the functional sites with respect to the MOF scaffold and the void space, by exploiting covalent bonds, supramolecular interactions, or other ways to mechanically confine atoms and molecules. Finally, the controlled distribution of functional sites inside the pore and over the framework is explored in section 2.4. as a strategy to tune the functions and achieve complex synergies.

The design of framework materials relies on the rationalization of all these entangled aspects and therefore requires organic, inorganic, and physical chemistry to be blended in a discipline named reticular chemistry. Our intention to describe those four principles (*i.e.* targets, approaches, methods, and strategies for functionalization) is to emphasize the importance of considerate pore design, which ultimately underpins the desired functionality of the material.

2.1. Functionalization targets

The complex ′anatomy′ of reticular frameworks offers several options for the location of functional sites. In this section, we will identify what features at the atomic scale can be the sources of functionality. This makes the primary target of the design process (Fig. 3). Porosity, framework backbone, included guests and defects will be discussed to highlight how each component can be exploited as a modification point to incorporate functionality.

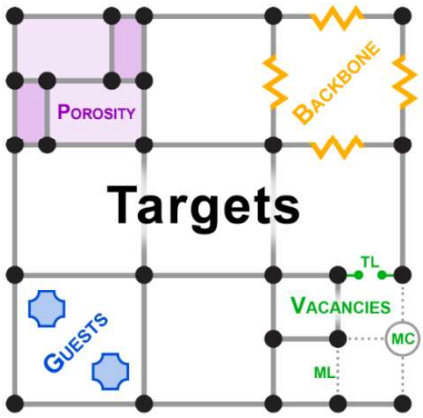

Figure 3. MOF's functionality targets: porosity, backbone, guests, and framework vacancies. Different types of vacancies can be distinguished (ML= missing linker; MC= missing cluster; TL= 'truncated linker').

2.1.1. Porosity

Porosity, implying the presence of permeable voids or cavities in a solid, is a key concept in material sciences [16]. Significant and well-defined structural voids are a distinctive feature of framework materials and are crucial for their functionalization and most of their applications. Strictly speaking, the term 'pore' indicates an opening that allows and regulates the transfer of matter through an interface or barrier. However, the meaning of 'pore' is often extended in MOF literature to serve as a synonym for void, cavity or channel, and in this text, we will adopt similar lexical flexibility [17].

Porosity is typically described in terms of volume, surface area, size- and shape distribution of the cavities and all these characteristics strongly influence the sorptive properties of MOFs [18]. In addition to pore size, other inherent structural factors such as shape, the orientation of each pore relative to the neighboring ones, and topological arrangement of the void space have relevant effects on the mechanical, physical, and chemical properties of the material. Moreover, the pore environment can also be described in terms of overall framework charges [19], presence of extended π-systems or aromaticity [20], hydrophilicity/hydrophobicity [21–23], contoured surfaces [24], and chirality [25–27].

Most applications of MOFs are based on their ability to adsorb and/or react with chemical species in the cavities (see chapter 3), however, the interest for porosity extends beyond this well-established scope, to fields such as optics, electronics, heat insulation *etc.* [28–33]. From low density at the atomic scale, a variety of technologically relevant features descends, such as low specific weight, high thermal insulation or low electric susceptibility. Porous frameworks take these properties to ranges rarely encountered for crystalline materials, while, at the same time, preserving the anisotropy and direct structure-property correlativity, typical of crystals.

2.1.2. Functional sites on the backbone

Within the framework, a functional group can: (*i*) have a structural role by participating in the metal-ligand coordinative bonds; (*ii*) act as guest-interactive sites or (*iii*) co-participate in both roles (Fig. 4). The pore dimensions and framework conformation determine the accessibility of the installed functional groups and sites.

OBUs are polytopic organic molecules that typically act as linkers, or struts, joining the IBUs into a regular 3D structure. At the same time, OBUs can enrich the framework backbone with potentially any type of organic functional group. IBUs can consist of single metal ions or, in

most cases, of polynuclear aggregates containing several metal ions, which are often referred to as secondary building units (SBUs).

Because the linkages between OBUs and IBUs are based on coordinative bonds, coordinating functional groups such as carboxylate, sulfonate, phosphonate, disulfido, and nitrogenated heterocycles can adopt a structural role by bridging metal nodes [34,35].

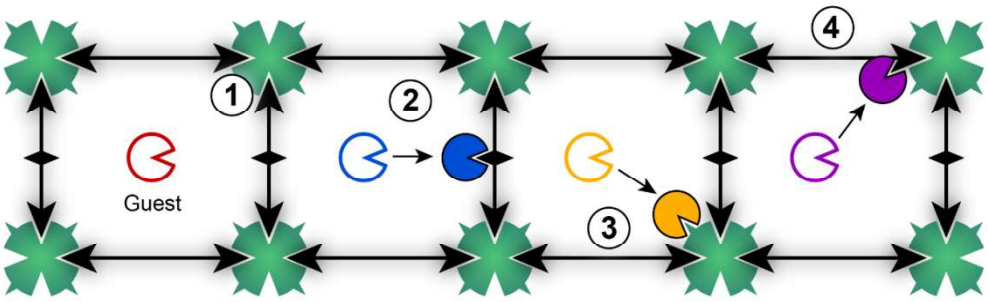

Figure 4. Examples of functional groups in a MOF with respect to the backbone building blocks: 1) functional group with a structural role (linkage); 2) guest-interactive group on the linker; 3) guest-interactive site in the IBU; 4) functional group acting both as linkage and guest-interactive group.

There is virtually no limit to the type of functional groups that can be present on the MOF backbone and influence the overall pore chemistry by acting as guest-interactive sites. In section 2.2.2. we will show that certain functional groups can be exploited for subsequent reactions and transformations of the framework. Moreover, the presence of metals in MOFs enriches such materials with physicochemical properties typical of inorganic or organometallic compounds. For chemical processes such as catalysis, open metal sites (OMS, also termed coordinatively unsaturated sites, CUS) are especially important [36]. These are metal ions belonging to IBUs or appended to binding sites on the linkers, which are coordinatively unsaturated and ideally accessible from the channels. On such sites, the metal-mediated functionality can be initiated after chemisorption of guests or substrate molecules.

2.1.3. Guests

Extra-framework component, *i.e.* ions, molecules, or supramolecular assemblies that do not participate in the network topology can be considered as guests. It is common for reticular frameworks to contain guest molecules, which are most often solvent molecules or unreacted linkers. The nature of the guests that can be absorbed in (and released from) the channels, is affected by the physicochemical properties of the pore, *e.g.* size, shape, acidity, and hydrophilicity/hydrophobicity. Furthermore, reticular structures often show a certain extent of

mechanical flexibility [12], which can allow for dynamic adjustments and unusual cooperative sorption-desorption processes [37–39]. Very large guests (*i.e.* larger than the pore aperture) can be incorporated *in situ* if they are present during self-assembly, and from solutions in exceptional cases [40–43]. Guests can also have an indirect structural role by contributing to structural formation [44,45] and stabilization [46], especially for CUS and structural defects [47].

The presence and chemical nature of guests can dramatically modify the framework conformation [48] or influence its dynamics in complex ways [49,50]. For example, the diameter of guest-filled channels for some MOFs can be unexpectedly smaller than the guest-free counterpart [51,52]. Importantly, guests can alter the chemical behavior of reticular materials, by carrying additional chemical functionality and by interacting with the framework through suitable binding sites. The detailed qualitative and quantitative determination of the guest content is important to characterize, and typically requires a combination of complementary analytical methods.

2.1.4. Framework defects and vacancies

Defects are imperfections (or irregularities) of the framework lattice, such as vacancies, compositional alterations, disorder, and dislocations. Both compositional and occupational variations are highly investigated aspects of reticular materials. A general tendency observed in MOF literature is to use the term ‘defect’ to especially indicate structural vacancies. Partial substitution of building blocks is also a frequent occurrence and this type of compositional ‘defectivity’ is typically referred to as heterogeneity or variability, which will be discussed in section 2.4.1.

Vacancies are sites that locally break the regular periodic arrangement of atoms or ions of the static crystalline parent framework because of missing or dislocated atoms or building units [53]. In MOFs, interruptions of the framework are often due to missing linkers, while missing nodes are less frequently reported [54,55]. ’Truncated linkers’ are a peculiar type of defects due to whereby molecules mimicking linker fragments, but having lower bridging multiplicity, coordinate to the metal clusters, thus locally interrupting the framework connectivity [56].

Most physical properties of crystalline solids arise from the average structure and some of them are negatively affected by the presence of impurities or lattice vacancies. However, many other properties and functions can be only explained by lattice defects. This general observation is valid also for reticular framework materials, in which vacancies and other lattice disruptions can trigger novel functions or allow enhanced performances compared to the ideal structure.

The first evident effect of vacancies is an increased porosity and surface area relative to the perfect, defect-free material [57,58]. Moreover, the mechanical properties, availability of OMS, hydrophilicity, or acidity can also be affected. Improved ion conductivity [59], and catalytic activity [60] have been also reported as a consequence of framework vacancies. Therefore, these types of defects are important functional targets and efforts to introduce, quantify, and characterize vacancies have been pursued [61], making 'defect engineering' a part of the design of framework materials [53].

A certain amount of lattice defects is always inherently formed as a result of growth faults or dislocations which occur during any crystal formation process. Parameters that influence the nucleation and growth rate will also affect the periodicity, which is directly linked to the concentration of lattice defects. For example, rapid crystallization of bicarboxylate-based MOFs was reported to cause missing linker defects, with a concomitant decoration of the IBUs by OH groups [62]. Conversely, increasing the temperature and initial linker/metal ratio can decrease the concentration of linker vacancies [63].

2.2. Functionalization approaches

The framework can be functionalized for one or more of the above-discussed targets. For this purpose, a functionalized framework can be imagined as a variation of a blank, non-functionalized scaffold, constructed by different building blocks following the principles of reticular chemistry. In this section, we will introduce the two mainly explored approaches for their functionalization (Fig. 5). One route is *de novo* functionalization, in which the structural building blocks are modified with the desired functional group in a pre-synthetic approach and/or the synthesis protocol is adjusted to allow for the generation of the desired functional sites. A second option is to adopt a post-synthetic approach, *i.e.* to functionalize a previously synthesized precursor framework by physical or chemical transformations of the building units.

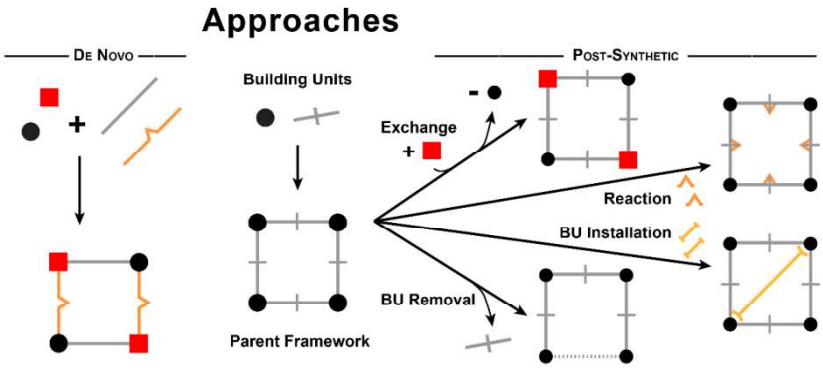

Figure 5. Two main approaches for the functionalization of MOFs: a *de novo* approach and post-synthetic modification (PSM). BU stands for building unit.

2.2.1. *De novo* functionalization

Conceptually, the most straightforward method to prepare a framework material with desired functionalities is *via* self-assembly of the building blocks which are already functionalized. A wide variety of homogeneous and heterogeneous synthetic procedures can be applied, which are extensively described in previous literature [8,64,65], and, noteworthy, solvent-free synthesis can also be pursued [66,67]. The *de novo* approach consists of introducing functionalities from the start, for example as substituents on the linkers or as additional reactants in a one-step MOF synthesis. When the function of the material is purely based on its physical properties (*e.g.* magnetism, dielectric constant, luminescence), it is an intrinsic characteristic that arises from the nature of the building blocks and the framework structure [68]. However, there are cases in which chemical functional sites originate from the self-assembly. For example, a metal ion in an IBU can be coordinatively unsaturated and therefore ready for an application (*e.g.* in catalysis) that relies upon coordinative chemisorption. In the situation where the desired functional sites are carried by the organic linkers, they must not hamper the desired self-assembly process. In the design of a functionalized MOF, we can typically introduce functional groups that are stable and coordinatively innocent [69], or that are expected to be less reactive than the groups designated for coordination to the metal cluster based on criteria such as hard/soft acid-base theory [70,71]. These "unreacted" functional groups are sometimes referred to as functional tags [69] and can be used for further post-synthetic modification (PSM, see section 2.2.2.) if desired.

The *de novo* approach enshrines a much higher complexity in the case of the synthesis of multivariate frameworks [72,73]. These are heterogeneous products, based on the combination of interchangeable building blocks (multiple nodes or linkers), having the same structural role but different chemical features. In general, from a direct, "one-pot" reaction, one would expect high homogeneity and perfect mixing of the interchangeable constituents available, as they are equally dispersed in the reaction mixture. However, a homogeneous distribution of components in the final products can only be expected if: (*i*) the alternative constituents have the same reactivity and (*ii*) the reaction conditions remain constant during the framework assembly. In the ideal case, multivariate frameworks are obtained [74,75], whereas the most common pitfall is the separation of the building blocks and preferential crystallization into distinct phases due to different metal-ligand affinity or solubility. The stoichiometric ratio or the reaction conditions could be varied to optimize the mixing of variated constituents and compensate for their different reactivity. Such parameters influence the nucleation and growth rate and,

therefore, affect the tendency to form segregated domains *versus* high mixing of the interchangeable building units.

Besides metal ions and linkers, additional small molecules can be added as modulators during the synthesis of MOFs. Their role is to control the rate of crystal growth, thus allowing to control crystal size, size distribution, and morphology of the products [76]. Modulators competitively and, importantly, reversibly bind to the metal centers, slowing the crystallization process and allowing for a controlled nucleation and crystal growth. HF, HCl, and several low molecular weight monocarboxylic acids are the commonly employed modulators, as their conjugate bases can act as competitive monotopic ligands and the modulating effect depends mainly on their concentration and pK_a. If a modulator is added in too high concentration, the crystallization can be entirely inhibited and MOF formation will not occur [77]. On the other hand, modulators can remain in the final product acting as truncated linkers and therefore can be used to introduce framework defects [53,61,78–80].

To allow the applicability of any material, sustainability is an essential aspect. In the production of a synthetic compound, minimizing the number of steps allows us to minimize energy consumption, solvent usage, and to maximize yield and 'atom economy' in general [81]. In this view, direct one-step synthesis of a functionalized framework is highly desirable and reticular chemistry makes it conceptually easy to design isoreticular frameworks decorated by different functionalities. In practice, the compatibility of pre-synthetically functionalized building blocks with the reaction conditions must be evaluated and identifying the appropriate conditions for the formation of the desired product can be a tedious task requiring a great deal of time and resources. It is often not possible to introduce functionalities *de novo*, due to interference of the desired functional groups with the self-assembly process. For example, alcohols, aldehydes, carboxylic acids, nitriles, azides, alkylamines, thiols, phosphines, *etc.* can be advantageous, as they open the possibility for many further reactions. However, their reactivity is also a hindrance due to their ability to interact with metals or encouraging side-reactions with other groups on the linker.

2.2.2. Post-synthetic functionalization

PSM approach can allow the formation of a functional framework that is otherwise difficult or impossible to obtain through a direct synthetic approach [82–85]. Porosity is essential to make PSM possible. Without void space it would be not possible to install additional functional groups without drastically altering the framework topology. Moreover, porosity allows the reactants to diffuse inside the bulk and to react throughout virtually the whole volume of the

material. PSM of framework materials can involve: (*i*) exchanging non-active components with suitable active analogs [86]; (*ii*) reactions of some precursor of functional groups which are present in the framework [69]; (*iii*) installing additional building blocks or introducing guests [86]; (*iv*) removing building blocks thus introducing vacancies [63] (Fig. 5, right).

These actions can be directed to the linkers and metal clusters, as well as to the guests, by applying the tools of organic synthetic chemistry, coordination chemistry, supramolecular chemistry, electrochemistry, *etc.* under the broader concept of framework chemistry [18,34,87–89]. PSM can aim to add, remove or exchange guest species and in fact the most common way of altering the functionality of a MOF by PSM is its 'activation' [90,91]. This involves the removal of guest species and labile terminal ligands, upon heating and/or vacuum treatment. For this aim, an intermediate soaking or washing step can be performed to exchange the original guests with more volatile species. Drying with supercritical CO_2 has also emerged as a green method for activating MOFs [92]. Activation changes the pore chemistry by revealing functional sites (such as OMS or H-bond donor or acceptors on the pore surface) that were otherwise saturated by guests. The exchange of guest molecules or counter-ions from framework materials, can also serve to alter their properties (such as flexibility, fluorescence or magnetism) [93–95] or to introduce reactive precursors on which further chemical PSM can be initiated.

Because of the lability of M–L coordinative bonds [96], non-substituted or non-active linkers can be exchanged by homologous molecules, without altering the overall topology. This process is referred to as SALE (solvent-assisted linker exchange) [86,97–99]. Exchange of neutral N-donor linkers is generally easier to perform and control, *e.g.* in layered-pillared MOFs [86,100,101]. However, anionic linkers, such as carboxylates [97], are amenable to be exchanged too [102]. SALE has successfully been applied also to imidazolate frameworks [103–105]. Interestingly, this exchange is not limited to the linkers of the same size. Isoreticular framework expansion could be obtained by replacing the original linear ditopic linkers by longer ones [102].

The organic backbone of framework materials can be post-synthetically modified by performing virtually any reaction allowed by both organic chemistry and the chemical stability of the framework. Typically, this requires a reactive tag or ′handle′ to be present and accessible on the scaffold. Primary amines are very versatile precursors, and probably the most exploited [106,107]. NH_2 groups can sometimes be introduced pre-synthetically on the linkers to produce amino-functionalized isoreticular MOFs in relatively simple reactions. Subsequently, they can

be covalently modified by reactions involving nucleophilic addition with a wide range of substrates. This allows the introduction of functionalities such as carboxylic acids, amines, carbamates, cyanates, urea, and azides onto the organic backbone of the MOF through the formation of amide or imine linkages. Similar strategies can be performed on aldehyde-tagged backbones. Protected terminal alkyne tags can be also introduced pre-synthetically and, after deprotection, can be exploited for cycloaddition reactions with azides under mild conditions, in so-called 'click reactions'. Similar reactions are seen by reacting alkyne substrates with azide-bearing linkers, whereby the azide group can be derived from an amino group by preliminary PSM [18,108,109]. Another route is to protect a functional group on an organic linker before forming the framework, and then perform a post-synthetic deprotection reaction to reveal the desired functionality [109]. Several reaction steps can be performed and highly specialized functions can be achieved with framework materials exhibiting 'enzyme-like complexity' [110].

If unreacted or newly formed coordinative sites are present, their post-synthetic metalation can be a facile and straightforward method to obtain heterometallic materials [71,111,112].

Frameworks without chemical tags are a particularly challenging target for organic PSM. However, photochemical reactions, such as cycloadditions can occur on unsaturated linkers in suitable arrangement [113,114]. An exceptional example of direct, covalent PSM of a MOF that contains no chemical tag was reported for MIL-101(Cr) in which initial nitration of the aromatic linker with nitric acid was possible without damaging the framework [115].

The installation of additional linkers in a parent MOF also referred to as post-synthetic insertion (PSI) [84], solvent-assisted linker incorporation (SALI) [116], and sequential linker installation (SLI) [117], is a unique category of PSM that can occur in mild conditions. This modification allows the framework connectivity to change, thus increasing its topological complexity and, typically, enhancing the mechanical robustness [118]. While the installation of additional struts will decrease the available void volume, it also reveals the possibility to tailor the channel size and shape for enhanced selectivity and to create compartments within the framework [119,120] which can allow trapping and/or controlled release of guests [121,122]. PSI can be used to transform 1D and 2D coordination polymers into 3D MOFs. In fact, to date, PSI of linkers in 3D MOFs was reported almost exclusively concerning the insertion of various functionalized ditopic carboxylates into preformed Zr-MOFs [86]. This is likely due to the stable and highly connected, large IBUs that Zr-based MOFs typically offer [123,124], where the installation can occur by substitution of the terminal –OH/–OH_2 ligands [118].

PSM directed on IBUs is emerging as a powerful strategy to add and control functions that are influenced by the metal. Analogous to the four general types of actions outlined above, four types of modifications can also be distinguished for IBUs: (*i*) post-synthetic substitution of cations, known as transmetalation; (*ii*) variation of the cation oxidation state; (*iii*) incorporation of new species at the IBU, and (*iv*) generation of vacancies [125].

The exchange of the metal nodes is typically performed by immersing the MOF in a metal ion solution, for several days at room or elevated temperatures to result in a partial or complete transmetalation [14,126–128]. Besides the soaking time and reaction conditions, the solvent and the cation identity play a major role in the exchange rate and the degree of substitution [129–131]. Transmetalation is not limited to cations with the same valence as the original cations, because additional positive charges can be compensated by additional monotopic counter anions that decorate the IBU without affecting the framework topology. A very promising application of transmetalation is to introduce redox-active species, *e.g.* transition metals in the reduced state that are incompatible with the typical synthetic conditions [132]. Although cation exchange occurs more readily for MOFs with labile M–L bonds, it has also been applied to some stable MOFs families such as UiO-66, MIL [133], and ZIFs [134]. Moreover, starting from labile frameworks, stable final products can be obtained by post-synthetic metathesis and oxidation [135].

Overall, post-synthetic functionalization is a powerful approach to obtain highly functionalized frameworks in one or several PSM steps. Its main advantage is the possibility to incorporate a wide range of functional groups that could otherwise not be achieved during a pre-synthetic approach [136]. PSM necessarily involves heterogeneous reactions, which has the advantage to allow easy separation of the product from the reaction mixture. However, in heterogeneous conditions, parameters such as crystallite size and diffusion of reactants must also be taken into consideration and it can be challenging to achieve consistent functionalization throughout the entire framework bulk. Nevertheless, this aspect can be exploited to obtain advanced features, such as functionalization domains or gradients, or core-shell structures. Therefore, unless the modification is selective and, importantly, quantitative, PSM leads to multivariate framework materials with an unknown distribution of the functionality throughout the framework. Indeed, after conversion, the final framework will likely contain some unreacted precursors. The final goal of reticular framework chemistry [2,87,88] is to combine the knowledge and methods of all fields of synthetic chemistry to manipulate and influence extended solids with molecular precision. However, the control over both—the type of substituent and the degree of modification—is the main, open challenge of post-synthetic functionalization. Finally, the

ability to generate topologically identical, but functionally diverse, frameworks in a systematic way can help to elucidate the structure–function relationship.

2.3. Functionalization methods

After having examined the features defining pore chemistry at the atomic scale, and the practical approaches for functionalization, we take a step back to rationalize what relationships can exist between the functional sites and the framework scaffold, allowing for different methods for immobilization of the active species (Fig. 6). A distinction can be made based on the forces binding the functional components to the MOF backbone, and it can be useful for general considerations about the stability of such active groups in the material. This aspect of structural design is important for the final application. There are cases where the functional sites must be firmly anchored to the framework and withstand several performance cycles, while in other cases easy cleavage, dynamicity, or reversibility of the interactions is required.

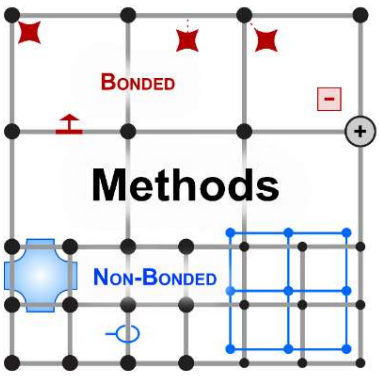

Figure 6. The functional sites can be immobilized in the MOF with different methods, based on their possible interactions with the backbone.

2.3.1. Bonded functional groups and active species

Functional groups can be covalently bonded to the framework, at the OBU or the IBU. The species tethered in this fashion will be difficult to cleave or wash away during repeated activity cycles. On the other hand, the post-synthetic installation of such groups will be in general more demanding due to their direct influence on the linker structure and chemistry.

When the functionality is provided by a guest, the active species is attached to the host framework *via* a non-covalent interaction, most likely H-bonds [137] or other interactions [45,138] and/or can be acting as a counter-ion to an ionic framework [139]. In some cases, the same guest can interact in more than one way with a framework. For example, a Lewis base

can accept H-bonds from donors from the framework or coordinate an OMS, and the selection of one or the other binding sites can depend on minimal external stimuli [140,141]. Moreover, the interplay between Brønsted and Lewis acidity/basicity implies that the host-guest systems based on these interactions will be influenced by pH. Host-guest interactions are fundamental for the applications of MOFs as adsorbents or nanocarriers and will be discussed in more detail in chapter 3.

2.3.2. 'Non-bonded' functional species

Covalent bonds and supramolecular interactions are not the only way to install functionality in a framework. Active guests can be ′mechanically′ trapped in a pore, virtually without the need for any interaction, simply because their hydrodynamic radius exceeds the channel opening. In analogy to a ship in a bottle, bulky guests, such as polymers [142,143] or inorganic nanoparticles [144], can be assembled inside the framework after it has been impregnated with small reactive precursors [145].

Flexibility or plasticity of either the host framework or the guest can allow confining active species in the cavities after adsorption. It has been possible to adsorb even small proteins inside framework materials, which is facilitated by the inherent flexibility of such biomacromolecules [43,146,147]. Similarly, conformational changes of flexible spacers, as well as the reorientation of rigid linkers or, more in general, a phase transition of the framework, can cause the shrinking or closure of previously accessible channels and pockets. Amorphization, which can be induced by thermal treatment, compression, or ball-milling is one of such transformations and it has been applied to encapsulate guests of various sizes such as iodine or drugs [148–150]. The opposite effect, *i.e.* the opening of diffusion pathways among seemingly non-connected cavities or throughout seemingly non-porous structures, can also occur in response to suitable physicochemical stimuli. This phenomenon is often referred to as the 'gate-opening' process [151] and has important implications for the sorption-desorption behavior of framework materials. The addition of bonded guests or SLI can also be used to block the channels and prevent the escape of non-interacting guests.

Finally, another way of immobilizing active species is to create a topological entanglement between them and the host framework during self-assembly or *via* PSM [152–155], or to create interpenetrated networks. This allows complex architectures to be conceived, where two or more components are not chemically bonded to each other, and yet are ′interlocked′ (*i.e.* mechanically bonded) and impossible to separate unless covalent bonds are broken.

2.4. Strategies for functionalization

Our examination of pore chemistry in the previous sections has highlighted that the adaptability of pore spaces is almost unlimited: not only can we choose among a multitude of organic and inorganic functional groups, but also among different methods to anchor functionalities to the framework scaffold. Taking the stance from a wider, global scale, we realize that the reticular structure offers us a three-dimensional pinboard and, in this section, we will explore the strategies we can undertake to pin the functional sites to it. Firstly, we can combine different functionalities in one single framework, with different criteria, to create complex (Fig. 7 A) or heterogeneous (Fig. 7 B) networks. Secondly, we can control the degree of functionalization and, to some extent, the arrangement of the functionalities in space.

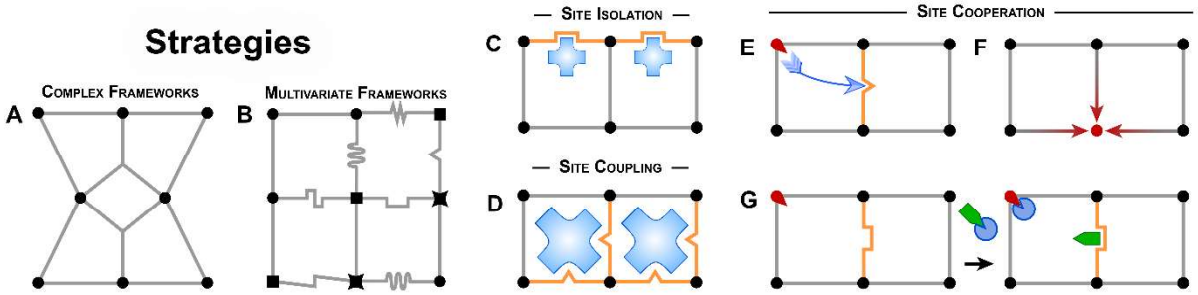

Figure 7. The arrangement of multiple functional sites within the framework volume. Functional building blocks of different types combined to give complex (A) or heterogeneous (B) frameworks. Functional sites of the same kind isolated (C) in the framework or coupled (D) to achieve a common function. Various types of functional synergies achieved by cooperation among different types of functional sites (E-G).

2.4.1. Complex, heterogeneous, and multivariate frameworks

The structural and chemical complexity of framework materials can be increased to achieve more sophisticated functions. First of all, we distinguish between complexity and heterogeneity, to highlight whether building blocks differ in terms of structure (topologically and metrically) or terms of chemistry [18]. This distinction is not a simple formalism, as it relates to the likelihood of multiple building blocks adopting a long-range ordered arrangement in a framework, which leads to implications on the structural characterization and rationalization of the final properties. Combining multiple structurally different organic linkers and/or metal nodes results in framework complexity, which is evident from the observed structure and topology. In an ideally non-defective structure, building blocks with different

geometries and structural roles must indeed occupy distinct (crystallographic) sites in the framework in an ordered fashion.

This core principle of reticular chemistry can be applied to construct complex MOFs, based on multiple OBUs, multiple IBUs, or both. The differences between building blocks can be chemical (*i.e.* different donor groups or different metals) or topological (*i.e.* two or more types of linkers with the same donor groups and different multiplicity, or homometallic IBUs with different geometries). MOFs constructed with chemically different linker molecules are often referred to as multifunctional MOFs [15]. There are many examples of the reaction of metal ions with polycarboxylic acids and nitrogenated linkers in one or more reaction steps, to obtain pillared layers [156,157] or other topologies [158]. MOFs based on linkers with the same functional groups but different geometry are instead referred to as multicomponent MOFs and many examples have been reported such materials containing up to four different di- and tricarboxylate moieties [159–163]. Importantly, the number of components and the topological complexity can be increased by SLI in one or more PSM steps [120,164–167]. Complex heterometallic MOFs can be assembled following a multi-SBU approach [88,168,169], multiple reaction steps [170] or by using metal–organic polyhedra [171,172] as "ternary building units" (TBUs) [173,174]. However, multimodal networks can also be observed in homometallic MOFs where nodes with different geometries coexist [175–178].

Heterogeneous (*i.e.* multivariate) MOFs are obtained from the combination of multiple building blocks that are chemically different but interchangeable from a structural perspective. Analogous linkers with different substituents can occupy the same site positions in the framework, as can isomorphous IBUs based on different metals. High degrees of heterogeneity can be achieved by mixing several variations of the same linker and/or compatible metal ions, giving rise to so-called multivariate MOFs [1,72–74,179].

2.4.2. Arrangement of functional sites

The reticular design allows for the combination of building blocks based on their geometrical and physicochemical features into complex architectures. Moreover, upon the combination of different functional features, properties extending beyond the simple sum of the individual constituents typically arise and often a synergistic effect can be observed. Indeed, the final properties depend also on the distribution of the different functional sites over the entire framework architecture [2].

The active sites have limited positional and orientational freedom as they are immobilized into the underlying framework. The solid-state nature of the framework also ensures that the

functionalities are relatively ′concentrated′ in a confined space (Fig. 7 C, D). Simultaneously, porosity ensures that the active sites are accessible throughout the bulk of the material. The combination of these two aspects makes framework materials excellent candidates for many physicochemical processes, as an alternative for both solid-state and in solution applications. As an example, a framework-based catalyst can offer a higher local concentration of active sites with respect to a homogeneous catalyst and, at the same time, offer a higher surface area than a conventional heterogeneous or supported catalyst.

In the case of multivariate frameworks, functional variations are superimposed onto a metrically and compositionally well-defined structural canvas [1] and the percentage ratio of each functionality can be varied. Although the elucidation of the exact spatial arrangement of chemically different building blocks is not trivial, the most common scenarios are either an ideally perfect mixing of the components which result to be randomly distributed or, conversely, a tendency to segregate in domains within the crystal lattice (including the formation of core-shell structures). The distribution can be a result of the reaction conditions, for example, due to temperature or concentration gradients during the self-assembly, linker solubilities, or variable reaction kinetics and/or diffusion rates in multivariate syntheses and PSM treatments [14,18].

Another scenario can also be anticipated, albeit quite rare, in which also structurally interchangeable components self-assemble into an ordered structure. Finally, due to the high complexity described above, aperiodic structures showing partial ordering (correlated disorder), paracrystallinity, *etc.* are very often encountered in multivariate reticular materials. As a consequence, a thorough characterization of the complex framework should extend beyond the determination of the average crystal structure, and combine several techniques to reveal further details explaining the structure–behavior relationships that emerge (*e.g.* superstructures, disorder, defect structures) [180].

2.4.3. Cooperation of functional sites

A deep understanding of the spatial arrangement of functional sites underpins the ability to control specificity and stereo- or regioselectivity of the desired function, in addition to pursuing the design of synergies through the cooperation of neighboring groups (Fig. 7 E) [2,181–183] in analogy to active sites in enzymes [184]. Cooperation can involve two or more functionalities simultaneously or in sequence [185]. However, cooperation can also occur in the ’backstage‘ in cases where some ancillary functional groups tune the activity of other, primary, functional groups, *e.g.* with induction effects (Fig. 7 F) [186,187]. Another type of

cooperation can be anticipated, where some secondary groups provide function by preventing undesired processes (*e.g.* trap unwanted reactants or by-products) (Fig. 7 G) or protecting the architectural stability of the framework (*e.g.* by acting as buffers or inducing self-repairing of the structure [180]).

As our understanding of the structure–property relationship progresses, we move steadily towards the design of increasingly advanced systems, making it possible for reticular framework-based materials to potentially outperform conventional materials in a broad range of applications.

3. Host–guest interactions

For many years, humanity has been curious to explain and understand various processes occurring in nature, driving research towards imitating and adapting these to their needs. Originating from scientific observation, through to the development of very complicated molecular theories, including the foundations of nanotechnology, knowledge in this area has expanded significantly. Specifically, growing global attention has seen devotion to research into processes occurring beyond the molecular level and to a higher level of molecular organization—the supramolecular level. The field based on the intermolecular interactions, in which structural blocks experience strong interactions through non-covalent bonds, is defined as host–guest chemistry (Fig. 8) [188,189]. The concept of complementary host and guest molecules was introduced by three chemists—Donald Cram at the University of California, Charles Pedersen at Dupont Chemicals, and Jean-Marie Lehn at the University of Strasbourg—who received the Nobel Prize in 1987 for their outstanding achievements [190]. Host–guest chemistry was developed first in aqueous or organic solutions [191]. Understanding the structure, stoichiometry, or class of intermolecular interactions, in addition to quantitative descriptions of thermodynamics and kinetics, is most often reduced to comprehensive host–guest studies.

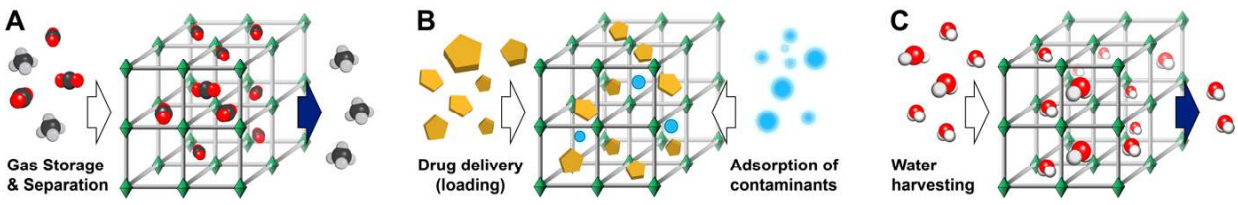

Figure 8. Host–guest interactions scheme. (A) Gas storage and separation. (B) Targeted incorporation of guest molecules for drug delivery and adsorption of contaminants. (C) Water harvesting.

The principles of host–guest chemistry are promoted by cross-disciplinary research in MOF materials. In contrast to traditional studies, the inherent poor solubility of MOFs limits research to the crystalline form. A very important aspect of host–guest chemistry employing MOF materials is the mutual connection between the guest species and the MOF pores. This concept is known as molecular recognition, which is the heart of chemical sensing (see chapter 4) [192,193]. The creation of the host–guest complex requires mutual complementarity of the molecules that comprise it. More specifically, this involves achieving appropriate binding energy, which is determined by the electronic and geometric features of the species involved, and their arrangement. Molecular recognition is treated as conformational and stereochemical selectivity which, in relation to supramolecular complexes, means that the guest and the host must be complementary [188,189,194]. In the situation where the guest structure changes in response to external stimuli, the host conformation is simultaneously transformed, according to various guest shapes [195]. Only by understanding the supramolecular interactions of a host–guest system at a molecular level (Fig. 9), we can use this knowledge for practical applications.

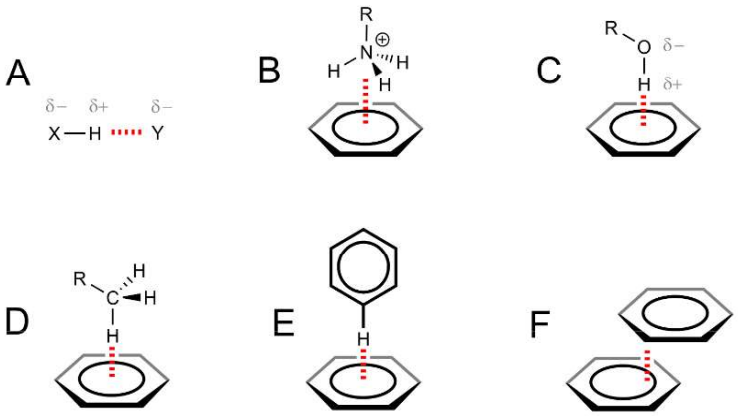

Figure 9. Schematic illustrations of selected non-covalent interactions, which are important in biological and synthetic, supramolecular systems. (A) hydrogen bonding; (B) cation-π interaction; (C) polar–π interaction; (D) CH–π interaction; (E) aromatic CH–π, or T-shaped stacking interaction; and (F) π–π stacking interaction (licensed under CC-BY [196]).

Hydrogen bonded interactions (60–170 kJ/mol) are one of the most important non-covalent interactions in host–guest chemistry. The selectivity, strength, and directionality linked intrinsically with hydrogen bonding processes have allowed the creation of complicated and efficient molecular hosts, capable of selective binding to a wide range of complementary guests. Effectiveness and selectivity of hydrogen bonding interactions can be reversibly modulated by an external stimulus [197]. Hydrogen bonds also strengthen other intermolecular interactions, including π–π and van der Waals interactions [198,199]. π–π interactions are weak, electrostatic interactions (below 50 kJ/mol) that occur between aromatic rings, often in

a situation where one compound is electronically rich and the other electronically poor. There are two types of π–π systems known: face-to-face and edge-to-face (Fig. 10). The face-to-face arrangement is energetically unfavorable because of the repulsion of negatively charged π-electron clouds leading to relatively weak interactions. The edge-to-face interaction can be considered as a weak hydrogen bonding interaction, occurring between the electron deficit hydrogen of one aromatic ring and the electron-rich π-cloud of an adjacent ring. These types of interactions often govern the crystal packing of numerous, small aromatic hydrocarbons. In addition to face-to-face and edge-to-face systems, a whole group of indirect geometrical connections is known [199,200].

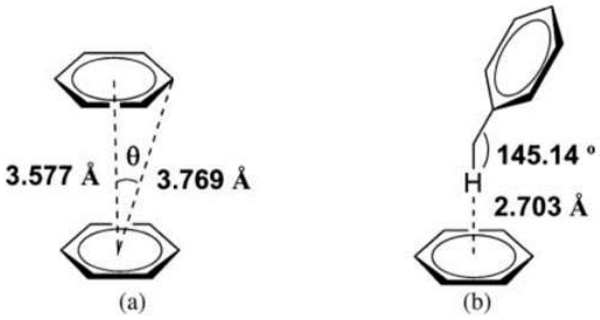

Figure 10. (a) Face-to-face π–π stacking; (b) edge-to-face π–π stacking (Reprinted with the permission [201]. Copyright 2011, Taylor & Francis).

In recent years, cation–π interactions (5–80 kJ/mol) have become an important type of non-covalent interactions, which are used in the design of novel host–guest systems. It is a stabilizing force between a positive charge and the face of an aromatic ring, leading to enhanced separation efficiency and highlights a new MOF application. The halogen bond has opened also new avenues in the field of separation of many industrially important compounds. According to IUPAC, the halogen bond is formed between an electrophilic region associated with a halogen atom in a molecular entity and a nucleophilic region in another, or the same, molecular entity [202].

The success of MOFs to act as host species relies on the availability of their internal space (so-called 'cavity') to occupy by other molecules (guests) and on the ability to tune their pore confinement [199,203]. The cavity plays a decisive role in the outcome of host–guest complexes. The guest molecules might be immobilized within the confined space of the host framework if their shape and size allow their presence in the available space. They can have an impact on MOF structure formation and stabilization [199]. Specific and unique molecular recognition between the host MOF pores and guest molecules allows the design of MOFs with functional pores directed towards desired applications. Furthermore, these pores can be

precisely tuned by adjusting their dimensions to encourage size-exclusive effects for the separation of small molecules and can be further optimized to their full potential for the storage of gas molecules (Fig. 8 A) [2,193].

To describe the host–guest interaction, classical methods of physical organic chemistry (*e.g.* Van't Hoff thermodynamic analysis) are primarily used. This approach can determine thermodynamic parameters such as $\Delta G°$, $\Delta H°$, $\Delta S°$ through monitoring the extent of guest inclusion or through competition experiments with a guest of known binding affinity. Moreover, it should be mentioned that both thermodynamic and kinetic parameters are related to the number of interactions, the kinetics, and the strength of individual interactions [204]. Host–guest systems show marked entropy–enthalpy compensation. This combination leads to more negative enthalpy, which is often accompanied by a loss in entropy [19]. Overall, this results in an enhancement of affinity due to the enthalpy change. In host–guest chemistry, the relative stability of reactants and products for a series of reactions is often associated with the rate of the reaction. This perspective assumes that the associated reactions are 'similar' and related to the structural transition state and the pathway of the reaction. This ultimately defines the reaction rate and therefore, the mechanism of the reaction must be equivalent to the reactions being compared [205,206].

When the host (A) and guest (B) molecules combine to form a single complex (AB), the equilibrium is represented as:

$$\mathrm{A} + \mathrm{B} \leftrightharpoons \mathrm{AB} \qquad \text{(Eq. 1)}$$

Assuming we are dealing with an ideal dilute solution, the association constant K_a and the dissociation constant K_d (which is the reciprocal of K_a) can be defined as:

$$K_a = \frac{[HG]}{[H][G]} \qquad \text{(Eq. 2)}$$

$$K_d = \frac{[H][G]}{[HG]} \qquad \text{(Eq. 3)}$$

The larger the K_a value, the stronger the binding of the guest to the host, while for the K_d value the relationship is inverse.

As outlined above, the important thermodynamic parameters are enthalpy and entropy. Therefore, significant chemical insight can be gained by determining the standard enthalpy change ($\Delta H°$) and the standard entropy change ($\Delta S°$) associated with a coupling event. The

connection between free energy, enthalpy, and entropy of a reaction is based on the Gibbs-Helmholtz equation [207]:

$$\Delta G^\circ = \Delta H^\circ - T\Delta S^\circ \quad \text{(Eq. 4)}$$

The interaction between host and guest molecules results in a decrease of the Gibbs free energy (ΔG°), leading to a thermodynamic driving force for host–guest interactions. A change in heat between reactants and products in their standard (1 M) state at constant pressure, if no work is done, is a change in standard enthalpy of a chemical process. To check for a change in enthalpy, the easiest solution is to associate it with changes in bond strength. However, small changes in bond angle, strain, and torsion angle, arising through steric interactions between host and guest, results in subtle changes for the bond strengths formed within the complex. Due to the difficulty in enumerating these different effects, we can simply classify a host–guest complexation as being endothermic (ΔH° is positive) or exothermic (ΔH° is negative). From a thermodynamic perspective, the entropy of a system is a measure of its disorder. The overall free energy of the system decreases as disorder increases. For a small molecule, at 1 M concentration, entropic contributions can be organized in order of importance: $S^\circ_{translational} \cong S^\circ_{rotational} > S^\circ_{vibrational} > S^\circ_{symmetry} \approx S^\circ_{mixing}$. For a host–guest complexation, changes in translational and rotational entropy dominate, although sometimes a loss of the other forms of entropy for the complexed host and guest can be also important. As in a solution, the guests are more diluted, the entropy of the system increases. In the solution, the entropic change will increase when the host, guest, and host–guest distributions of species shift toward free host and guest, rather than the host–guest complex. If the solutions are further diluted, the decomplexation of a host–guest complex is observed [208,209].

Kinetic analysis of the host–guest interaction is necessary to determine a mechanism of complex formation. It enables detection and studies of individual transformation steps and provides valuable insight into the phenomena of molecular recognition and self-assembly [210]. When the pores of MOF materials are chemically and geometrically tailored to selectively bind a target guest molecule, it is possible to direct its uptake and release (Fig. 11) [211].

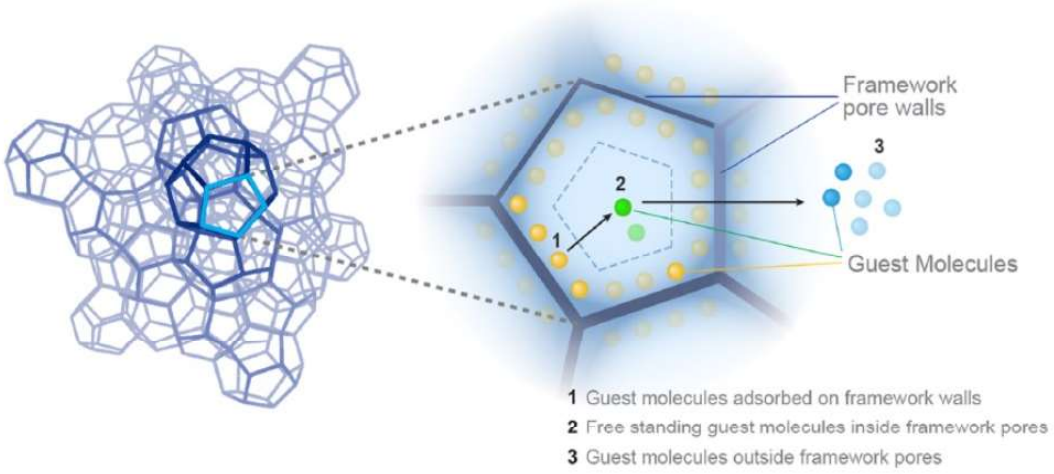

Figure 11. The release process of guest molecules from porous frameworks through three energy states (Reprinted with the permission [211]. Copyright 2017, American Chemical Society).

In order to predict and precisely program the release of guest molecules from a MOF porous system, a kinetic model in the form of the cumulative distribution (Weibull distribution) based on the host–guest interactions can be used:

$$y = 1 - e^{-(kt)^n} \quad \text{(Eq. 5)}$$

where y is the fraction of released guest molecules at time t, k is the release rate constant, which reflects host–guest interactions, and n is the guest–guest interaction parameter.

The interaction between the MOF framework and guest molecules can be described using the Arrhenius equation to correlate the release rate constant (k), with the energy activation (E_a):

$$k = Ae^{-E_a/RT} \quad \text{(Eq. 6)}$$

The negative natural logarithm of this parameter is directly connected with the interaction energy:

$$-\ln k = \frac{E_a}{RT} - \ln A = \frac{E - E^*}{RT} \quad \text{(Eq. 7)}$$

E presents the energy of the interaction between guest molecules and MOF structure, while E* is a reference state with $k=1d^{-1}$.

As mentioned above, one of the most important MOF characteristics is their potential to bind molecules in a specific way based on special pre-designed host–guest interactions [2]. It is necessary to compile literature data that will allow for a deep analysis of what kind of strategy is useful to design MOF materials with functional sites tailored for unique recognition of guest

molecules of varying size and geometry. Therefore, in the following sections we focus on the description of preparation and functionalization methods of MOF materials to optimize their utility properties for application in gas storage and separation, adsorption of different contaminants, water harvesting, and drug delivery.

3.1. Gas storage and separation

Gases are commonly used as energy resources for industry and daily life. Until now, fossil fuel burning covered approximately 85% of the global energy demand [212]. The main challenges associated with employing gases for energy purposes involve their transportation, storage, and conversion. The conversion processes are usually performed under harsh conditions and consume vast amounts of energy because of their extremely low boiling point and density coupled with their high critical pressure and diffusivity. Therefore, recent years have seen a surge in efforts towards designing porous materials, including MOFs and COFs, that will be highly useful for gas separation and storage purposes [213]. From an industrial perspective, MOFs can be employed for effective gas capturing, especially concerning CO_2 and H_2 [214–216]. Precise control and tuning of small pore/window sizes within porous MOFs are important. This strategy allows for the highly efficient separation of specific gases *via* the size-exclusion effect, in which small gas molecules (*e.g.* H_2, C_2H_2, CO_2, CH_4) can pass through the pore channels while large ones are deterred [212]. Most interactions between MOFs and gas molecules are van der Waals interactions, which can be enhanced by a confined pore environment. In addition, it is crucial to immobilize open metal sites and functional groups on the pore surface to direct strong interactions with gas molecules, especially for gas storage and separation at moderate temperatures. The ability of MOF materials to capture CO_2 can be optimized by the creation of active sites on their surface *via* the functionalization with nitrogen bases or polarizing organic functional groups. The basic functional groups and the exposed metal sites strongly interact with CO_2, resulting in increased adsorption capacities [217–219]. The highest CO_2 uptake (79.7 wt%), at 293 K and 20 bar, was reported by Li and co-workers [220] who developed the MOF UiO(bpdc) (bpdc = biphenyl-4,4'-dicarboxylate), synthesized by a solvothermal reaction of bpdc linkers with $ZrCl_4$. This value is comparable to those observed for MOF-177 and MIL-101(Cr) under similar conditions and is also larger than the experimental or theoretical CO_2 adsorption capacities of UiO-67 and UiO-68.

In 2019, Ullah *et al.* [221] exploited PSM to tether aminomethyl propanol (AMP) to a sample of IRMOF-3, using three different AMP concentrations (25, 50 and 75 wt%), to obtain AMP@IRMOF-3. The potential impact of CO_2-philic surface functional groups on the

selective adsorption of CO_2 was investigated at different temperatures (298, 323, 348 K). Despite a decrease in the MOF surface areas as a result of the bulky AMP tethered substituents, the adsorption capacity towards CO_2 was improved from 1.39 mmol/g (IRMOF-3) to 3.90 mmol/g (AMP@IRMOF-3). It is worth noticing that functionalization with amines has a significant impact on the CO_2 uptake capacity at lower pressures. In this region, CO_2 uptake is more dependent on the CO_2 interaction with nitrogen-rich amine functional groups rather than on the overall adsorbent surface area. Moreover, it was shown that the presence of a nitrogen-containing functional group on the surface of AMP@IRMOF-3 did not significantly enhance the adsorption capacity towards other gases, such as methane. This is due to weak interactions between the CH_4 molecules and both the IRMOF-3 and AMP@IRMOF-3 frameworks. Hence, AMP@IRMOF-3 can be viewed as a promising candidate for selective CO_2 capture from natural gas sources [221].

The strategy of appending amine functionalities to the pore walls in MOFs is further evident in the research by McDonald and co-workers [222]. Here, Mg_2(dobpdc) (dobpdc^{4-}=4,4′-dioxidobiphenyl-3,3-dicarboxylate) was functionalized with *N*,*N*′-dimethylethylenediamine (mmen). This functionalization resulted in a high adsorption capacity towards CO_2 under flue gas conditions and remarkable, unexplained, step-shaped adsorption isotherms that shift markedly with temperature [222]. Initially, it was assumed that CO_2 was trapped by uncoordinated amine groups. However, a careful investigation of the MOF-CO_2 interactions revealed that the increase of adsorption is owed to CO_2 insertion into metal-amine bonds, causing a reorganization of the amines into well-ordered chains of ammonium carbamate (Fig. 12).

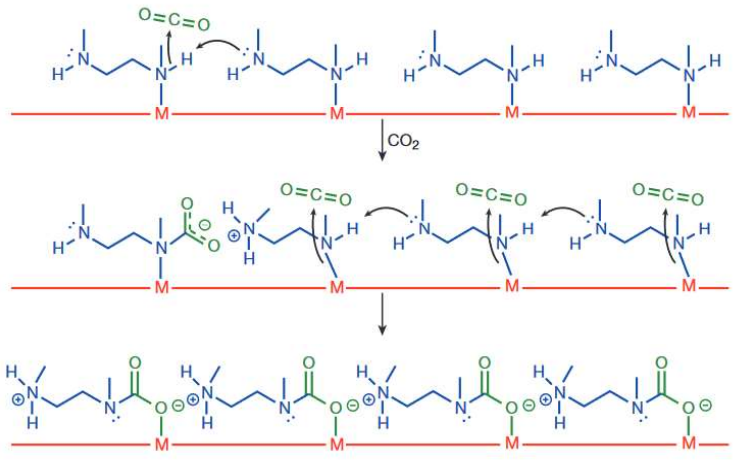

Figure 12. A cooperative insertion mechanism for CO_2 adsorption (Reprinted with the permission [222]. Copyright 2015, Nature Research).

Consequently, large CO_2 separation capacities can be achieved with small temperature swings, and reasonable regeneration energies (about 2.2-2.3 MJ per kg of CO_2 captured). This is lower than what is currently achieved with the widely adopted aqueous amine solutions [222].

In 2017, Flaig *et al.* [223] covalently tethered two primary alkylamines -(CH_2NH_2) to linker 3,3″-dioxido-[1,1′:4′,1″-terphenyl]-4,4″-dicarboxylate to functionalize IRMOF-74-III under dry and humid conditions. In the low-pressure range (<0.133 bar) the IRMOF-74-III-$(CH_2NH_2)_2$ captures 2.33 times more CO_2 than its monoamine counterpart IRMOF-74-III-CH_2NH_2 through a chemisorption mechanism. Here, solid-state NMR shows that the major chemisorption product is carbamic acid, in contrast to other primary amine-functionalized solid adsorbents that capture CO_2 mainly as ammonium carbamates. However, the equilibrium of reaction products shifts to ammonium carbamate in the presence of water vapor. It was a new finding that presented the possibility to control the chemistry of CO_2 capture in MOF materials and highlighted the importance of geometric constraints and the mediating role of water trapped within the pores of MOFs [223].

Toxic gases including carbon monoxide (CO), sulfur dioxide (SO_2), hydrogen sulfide (H_2S), chlorine (Cl_2), nitric oxide (NO), nitric dioxide (NO_2), and ammonia (NH_3) are anthropogenic pollutants released into the atmosphere. Global emissions of CO, SO_2, and NO_2 are predominant due to the burning of fossil fuels. MOFs have shown to be efficient adsorbents of NO_2 and SO_2, because of the presence of CUSs. In 2017, Cui *et al.* [224] reported the selective recognition and tight packing of SO_2 clusters *via* synergistic host–guest and guest–guest interactions induced with pore chemistry control in inorganic anion pillared MOFs (SiF_6^{2-}, SIFSIX). It was shown that the binding sites of the anions and aromatic rings in SIFSIX materials capture every atom of SO_2 through $S^{\delta+}\cdots F^{\delta-}$ electrostatic interactions and $O^{\delta-}\cdots H^{\delta+}$ dipole–dipole interactions. In addition, the guest–guest interactions between SO_2 molecules further promote gas trapping within the pore space. Due to these interactions, it is possible to remove SO_2 from other gases even at very low concentrations. Exceptional SO_2 capacity (11.01 mmol/g) at atmospheric pressure was observed for SIFSIX-1-Cu, while the highest SO_2 uptake at low-pressure was achieved with the use of SIFSIX-2-Cu-i (4.16 mmol/g SO_2 at 0.01 bar and 2.31 mmol/g at 0.002 bar) [224].

Molecular hydrogen (H_2) is a promising compound to use as a transportation fuel. Its combustion does not result in the production of offensive pollutants or carbon dioxide [225]. One of the issues with H_2 uptake is that MOF pores cannot be fully utilized for H_2 storage at moderate temperatures, due to the weak van der Waals interactions between pore surfaces and H_2. To increase their H_2 uptake, it is essential to optimize the pore surfaces [193]. Enhancing

the pore volume and surface area of MOFs significantly increases the gravimetric hydrogen uptake at high pressure, where functionality has little impact [226]. Nevertheless, the perfect pore size of an adsorbent for optimal hydrogen adsorption should be similar to the diameter of a hydrogen molecule (van der Waals radius of 1.2 Å, kinetic diameter of 2.89 Å) [227]. At room temperature, chemisorption is dominant and unsaturated metal sites play a key role in H_2 adsorption [228]. Among MOF materials, the most promising for H_2 storage is Ni_2(*m*-dobdc) (*m*-dobdc^{4-} = 4,6-dioxido-1,3-benzenedicarboxylate), developed in 2018 by Kapelewski and co-workers [229]. This material has open metal cation sites that strongly interact with H_2 and are isomeric with M_2(dobdc) (M = Co, Ni; dobdc^{4-} = 1,4-dioxido-1,3-benzenedicarboxylate). These materials were tested for H_2 storage and it was found that Ni_2(*m*-dobdc) was an exceptional physisorptive storage material yielding the volumetric capacity of 11.0 g/L at 100 bar and 298 K and 23.0 g/L with a temperature swing between -75 and 25 °C. Its high capacity is related to the presence of highly polarizing Ni^{2+} adsorption sites, which generate large binding enthalpies and dense packing of H_2 within the material.

Collectively, these efforts to garner MOFs as specific gas sorption materials contribute toward their involvement in gas separation techniques, which include cryogenic distillation, membrane- and adsorption-based technologies. For many years, adsorption processes have become key gas separation tools in the industry. They play an important role in future energy and environmental technologies. In these processes, gas separation is achieved based on the differences in the affinity of various components to the surface of an adsorbent. MOFs are very efficient adsorbents used in gas separation and purification [230]. Regarding their application in this area, it is useful to divide them into rigid and flexible/dynamic materials. Rigid MOFs have relatively stable and solid framework structures, with permanent porosity. Flexible MOFs are characterized by dynamic, ‘soft’ frameworks that conformationally react to external stimuli, such as temperature, pressure, and guest molecules. In rigid MOFs, the adsorption selectivity may be related to the molecular sieving effect and/or preferential adsorption based on the different strengths of the adsorbent–adsorbate and adsorbate–adsorbate interactions (Fig. 13). Furthermore, the nature of the guest–surface interactions is crucially important in these cases [230].

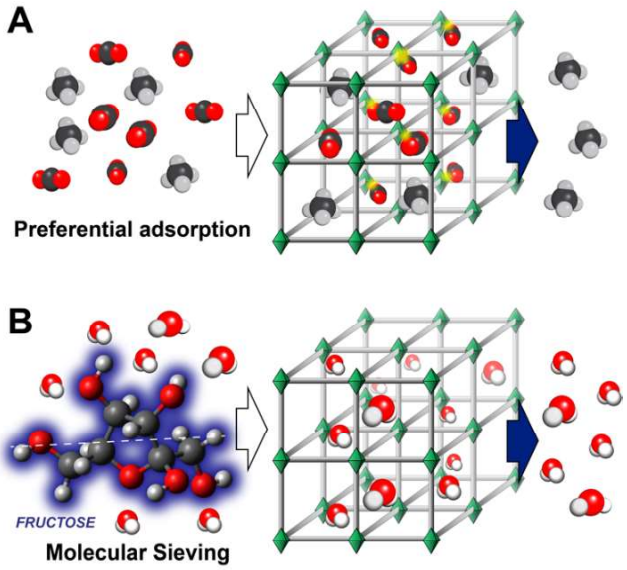

Figure 13. Schematic illustration of selective gas adsorption in rigid MOFs. (A) Preferential adsorption. (B) Molecular sieving effect.

In some rigid MOFs, adsorption selectivity can be assigned to the thermodynamic equilibrium effect or the kinetic effect in each equilibrium time. This is known as preferential adsorption. In these cases, the selectivity is connected with adsorbate properties such as quadruple moment, polarity, and accessible hydrogen bonding, in addition to the surface properties of the pores. The selective gas adsorption in some MOFs can be associated with both the pore size and the interactions between adsorbate molecules and the pore walls [230].

The selective gas adsorption in flexible MOFs (Fig. 14) is more complicated than for rigid MOFs. Framework rearrangements during the adsorption-desorption process result in hysteretic behaviors of sorption isotherms. Beyond adsorbate–surface interaction and size/shape exclusion, structural rearrangement should be considered as well.

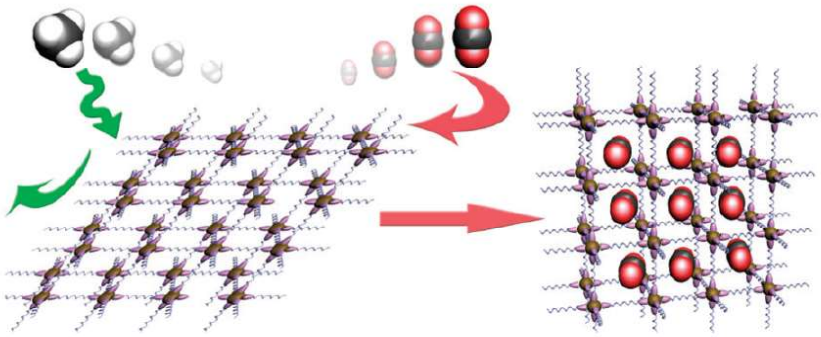

Figure 14. Schematic illustration of selective gas adsorption in a flexible MOF (Reprinted with the permission [230]. Copyright 2009, Royal Society of Chemistry).

Selective gas adsorption in flexible MOFs can be divided into the following three categories:

(i) selective adsorption based on size/shape exclusion accompanied by pore size/shape change—molecules of adsorbates enter the pores and interpenetrated frameworks can alter the pore size through modulating inter-framework distances;

(ii) selective adsorption based on adsorbate–surface interactions accompanied by pore size/shape change—the surface properties of pores determine the adsorption selectivity of various gases;

(iii) selective adsorption based on gate-opening or structural rearrangement induced by adsorbate–surface interactions—crucial for flexible MOFs with small pores to allow guest entrance; the pores can expand when exposed to certain gas adsorbates.

Hydrophobicity/hydrophilicity of the channel surface also impacts the adsorption selectivity. Influence on the framework flexibility can have molecules with dipole and quadrupole moments or H-bonds formation. The most challenging aspect of flexible MOFs is the direct synthesis of materials with pre-defined gate behavior and functionality. Identification and characterization of the relevant host–guest, host–host and guest–guest interactions play a key role in the different forms of flexible and dynamic processes [230,231].

Separation of CO_2 is fundamental to improve the fuel combustion properties of natural gas. In 2020 Ullah and co-workers [232] modified MOF-200 with graphene oxide (GO) to investigate the influence of post-synthetic functionalization on selective CO_2/CH_4 adsorption. It was found that modification of MOF-200 with GO leads to an increase in CO_2 uptake despite the reduction of the surface area and pore size of the material. A decrease in pore size results in an enhancement in the interactions of pore walls with the CO_2 molecules, which may be the cause of high sorption capacity relative to CO_2. With an increase in the temperature of the system, the adsorption capacity decreased suggesting an exothermic process. In addition, the PSM with GO does not improve the CH_4 uptake. It is caused by the bigger size of CH_4 molecules and weaker interactions between the gas molecules and the adsorbent framework. The selectivity towards CO_2 over CH_4 was enhanced by approximately 31.8% for MOF-200/GO (18.4) compared to MOF-200 (13.9) [232].

In recent years, MOFs have been used as fillers in mixed-matrix membranes (MMMs), where typically molecular sieving and solution-diffusion mechanisms favor gas separation. In 2017, Maserati *et al.* [233] introduced a phase-change MOF, mmen-Mg_2(dobpdc) (dobpdc^{4-}=4,4′-dioxidobiphenyl-3,3′-dicarboxylate), into a MMM which can be used to increase the solubility of a specific gas in the membrane, and thereby its permeability and selectivity. Diamines were grafted within these Mg_2(dobpdc) nanocrystals to exploit their CO_2 adsorptive properties in an

MMM for CO_2/N_2 separations. It was assumed, that new diamine-functionalized Mg_2(dobpdc) nanocrystals integrated into MMMs increase the CO_2 permeability while maintaining high CO_2/N_2 selectivity, relative to the neat polymer matrix. The dynamic uptake and release of CO_2 along diamine molecules is a key to the operation of the membrane attached to open metal sites lining the MOF channels [233].

In 2018 Liu *et al.* [234] prepared a composite adsorbent based on MIL-101 loaded with *N,N'*-dimethylethylenediamine (DMEDA) by a PSM method. The DMEDA-MIL-101 material displayed high capacity and selectivity in post-combustion CO_2 capture despite a 52% decrease in BET specific surface area and pore volume in comparison to MIL-101. Using the standard composition of the flue gas from power plants (around 15% CO_2 and 75% N_2 at a total pressure of 1 bar) selectivity of 31.7 (298 K) for DMEDA-MIL-101 was noted. Moreover, at 273 K and 298 K under 1 bar total pressure, the CO_2 capacity increased of about 8.7% and 18.7%, respectively. This improvement in capacity and selectivity towards CO_2 is caused by higher isosteric heat of CO_2 adsorption as a consequence of the interaction between amines and CO_2. Pristine and functionalized with amine groups materials are stable and maintain crystal frameworks until 650 K. It was proved that chemical features of the pore surface influence low-pressure CO_2 adsorption and CO_2/N_2 separation at ambient temperature [234].

The separation of ethylene/ethane mixtures is a very important industrial process, however, considered challenging to conduct because of the similar molecular sizes and volatilities of these two components. MOFs are good materials for hydrocarbon separation, including the above-mentioned gases. As was shown by Zhang and co-workers [235], the introduction of both OMSs and π-complexation into MOF leads to high ethylene-ethane adsorption selectivity at 318 K. It was especially observed for sample MIL-101-Cr-SO_3Ag exhibiting higher ethylene-ethane adsorption selectivity than benchmark zeolites and PAFs. It was related to the π-complexation between Ag(I) ions and the double bond of ethylene molecules, which is reflected in the high isosteric heats of adsorption of C_2H_4 [235].

3.2. Adsorption of contaminants from liquid phase

Textile industries use over 700,000 tons of dyes, which represent one of the top three pollutants being not biodegradable due to their complex structure and chemical stability. Given their often toxic, carcinogenic, and mutagenic nature, organic dyes are a serious threat to living organisms and the environment [236–238]. Therefore, the best-case scenario is that they should be completely removed from the ecosystem [239]. The research performed, on the laboratory and technical scale, indicate that adsorption methods are of special importance for the treatment of

dyes in wastewater due to their high efficiency, simplicity, mild conditions, availability of adsorbents, and the ability to work at a relatively wide range of concentrations [240–243]. The challenge of this area is to find a suitable adsorbent, which has a high adsorption capacity and selectivity, as well as potential reusability. MOFs have been extensively studied for the adsorptive removal of organic dyes from aqueous solutions because of their large surface area and the existence of multiple different interactions between dye molecules and the MOFs' external surface, *e.g.* hydrogen bonding, π–π stacking, and electrostatic interactions [244–246]. In comparison to other frequently used adsorbents such as activated carbons, mesoporous silica, and zeolites, MOFs are more versatile because their structure and physicochemical properties can be tuned by altering different components [247]. They have mostly microporous structure and therefore dye molecules are too large to enter inside the pore. Hence, dyes are adsorbed on the external surface of MOFs and their surface properties have a great impact on the efficiency of adsorption processes [248,249].

In 2019, Zha *et al.* [250] developed a super-hydrophobic MOF *via* the reaction of UiO-66-NH_2 with a functionalized carboxylic acid-containing numerous branched hydrocarbon chains. Here, the aim was to improve its adsorption capacity towards the cationic dye Rhodamine 6G (Rh 6G). Isosteric acid was covalently bonded to the UiO-66-NH_2 surface by an amidination reaction to give UiO-66-NHCOR. Experimental results showed that UiO-66-NHCOR was more effective in the removal of Rh 6G from aqueous solutions than pristine UiO-66-NH_2. It was observed that more than 99% of Rh 6G at the initial concentration of 500 mg/L can be adsorbed on the surface of UiO-66-NHCOR (adsorption capacity: 478 mg/g) within 10 minutes while only 52% for UiO-66-NH_2 material (adsorption capacity: 243 mg/g). A possible adsorption mechanism was proposed by employing FTIR spectroscopy. After adsorption, hydrogen bonding, π–π stacking, and hydrophobic interaction were noted between Rh 6G and UiO-66-NHCOR (Fig. 15). The UiO-66-NH_2 frameworks are characterized by a high density of hydrophilic active sites (zirconium oxo-clusters and free-NH_2) therefore water molecules can be adsorbed on the surface and access the MOF voids. Hence, hydrophobic modification of UiO-66-NH_2 can reduce the competitive uptake of water during dye adsorption in aqueous solution [250].

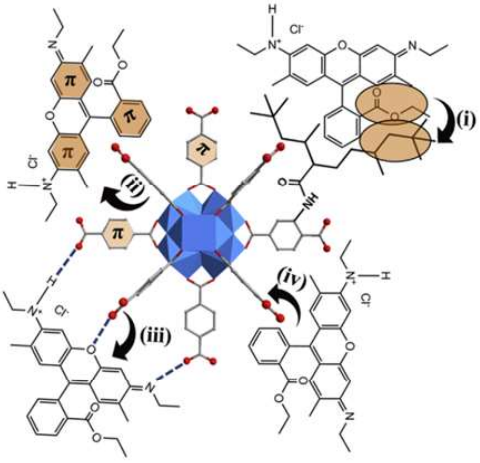

Figure 15. Possible mechanism of Rh 6G adsorption on UiO-66-NHCOR: (*i*) π–π stacking, (*ii*) hydrogen bonding, (*iii*) hydrophobic interaction, and (*iv*) pore filling (Reprinted with the permission [250]. Copyright 2019, Elsevier).

Nowadays, organoarsenic compounds are considered novel organic pollutants, which should be removed from the environment prior to their degradation to toxic inorganic arsenite (As(III)) and arsenate (As(V)) [251,252]. In 2018, Lv *et al.* [251] found that an amino-functionalized indium-based MOF (NH_2-MIL-68(In)) can be used as an efficient adsorbent in the removal of *p*-arsanilic acid (*p*-ASA) from wastewater. The *p*-ASA-adsorption mechanism onto NH_2-MIL-68(In) is based on synergetic interactions involving π–π stacking and hydrogen bonding. NH_2 groups present on the surface of MIL-68(In), formed hydrogen bonds with the NH_2 species from *p*-ASA molecules, and the hydroxyl groups bonded to the As, resulting in an enhanced level of N···H–O(N) interactions. NH_2-MIL-68(In) exhibited excellent reusability and after regeneration with an acidic ethanol solution, it still demonstrated high adsorption capacity (401.6 mg/g) towards *p*-ASA [251].

Metal ions with a density over 5 g/cm^3 such as arsenic, cadmium, chromium, copper, lead, mercury, nickel, and zinc ions are pollutants that contaminate both surface and groundwater. They are toxic, persistent, and can have a negative influence on the wellbeing of flora and fauna [253]. In 2016, Saleem *et al.* [254] applied UiO-66-NH_2 material, modified with methyl isothiocyanate in the process of removal of Pb^{2+}, Cr^{3+}, Cd^{2+}, and Hg^{2+} from aqueous solutions [254]. Their adsorption performance was then compared to that of unmodified UiO-66 and UiO-66-NH_2 samples. The material functionalized with sulfur-containing groups showed the largest adsorption capacity towards Pb^{2+}, Cr^{3+}, Cd^{2+}, and Hg^{2+} due to the high affinity of sulfur, to metal ions.

In 2017, Wang *et al.* [255] followed this trend and functionalized Zr-MOFs with amine groups and investigated their ability to remove cadmium and lead ions. The material obtained achieved

high adsorption capacity (177 mg/g) towards Cd^{2+} at an initial concentration of 40 mg/L (pH 6 and temperature 30 °C) in 2 hours and 167 mg/g at the same conditions towards Pb(II). The amino groups which possess free electron pairs, act as the Lewis bases which coordinate the metal ions representing Lewis acids [256].

3.3. Water harvesting

In the atmosphere there exist about 13 sextillion (10^{21}) liters of water [257]. Water is crucial to every field of life and as such, increasing the standard of life and demographic growth requires huge water resources, especially in arid regions. Amongst of all water on earth, 2.5% is freshwater, but most of it is held in glaciers (68.7%), accumulated in groundwater (30.1%), and only a tiny fraction being directly available in lakes and rivers (0.4%). This is a recyclable resource, which can be harvested. The difficulty with finding a practical application of this process is associated with finding a material capable of simple water capture and release (capture cycle). Of equal importance is also ensuring sufficient cooling energy for a material, such that the temperature of the collecting equipment is lower than the water evaporation temperature in order to enable liquid water formation (collecting cycle). Classical desiccants, such as $CaCl_2$, zeolites and silica gel, adsorb water with high efficiency, however, their strong affinity to water makes their regeneration energy-intensive and economically impractical [258–261]. Hence, developing new materials for water harvesting from the air is crucial. Next-generation adsorbents should be characterized by: (*i*) high chemical stability, (*ii*) tailorable hydrophilicity, and (*iii*) an adjustable pore diameter to modulate the sorption kinetics. MOFs and COFs are ideally suited to behave as new adsorbents [262] and address water harvesting applications [263]. This is due to their unique porosity, mechanochemical variability, the combination of both hydrophilic and hydrophobic moieties in the same structure and available topologies [264]. The exceptional surface area of MOFs (up to 10,000 m^2/g) can, technically, host a significant amount of water within their pores. While the affinity of MOFs to water could be enhanced by creating open metal sites during activation, unfortunately, this is a strategy advised against due to the high binding constant of water to the uncoordinated metal sites. This consequently leads to difficulties in desorbing water even at a lower relative pressure [265]. However, the attachment of hydrophilic functional groups to the organic linker could be a rational solution for better water adsorption. High adsorption capacity can be achieved also by expanding the MOF pore size and increasing the length of organic linkers (Fig. 16). However, the increase in the pore size can change the water adsorption mechanism from pore filling, which is desirable for water harvesting applications, to capillary condensation [266].

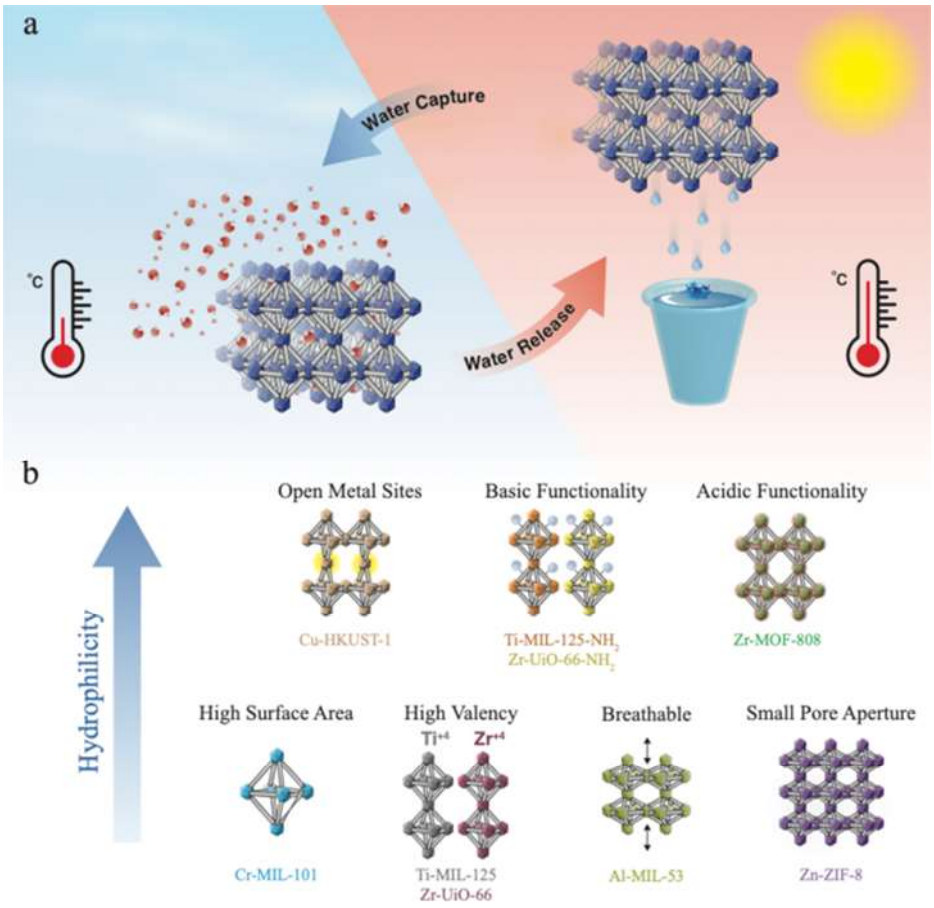

Figure 16. Schematic illustration of the MOF water harvesting system (a) and a general overview of MOFs employed in the present study (b), highlighting different functionalities and representative MOFs (licensed under CC-BY [267]).

In 2019, Shi *et al.* [268] synthesized a series of MIL-101(Cr)-X/$CaCl_2$ composites as potential water adsorbents, functionalized with different hydrophobic (−CH_3, −F) and hydrophilic (−SO_3H, −NH_2) groups. $CaCl_2$ was chosen as an added composite because of its high heat energy storage density, fast hydration rate, and low cost. Investigations showed that the hydrophilic functionalized derivatives displayed a higher sorption capacity towards water than the hydrophobic and non-functionalized MIL-101(Cr). MIL-101(Cr)-SO_3H/$CaCl_2$ can adsorb up to 0.6 g of water at 30 °C and relative humidity of 32%. This was a substantial improvement compared to the non-functionalized MIL-101(Cr)/$CaCl_2$ (adsorbing up to 0.47 g/g). This was explained due to the formation of hydrogen bonds between water molecules and hydrophilic functional groups (−SO_3H and −NH_2), leading to higher heat of adsorption. Moreover, it should be mentioned that the introduction of hydrophilic groups also improves the cycle stability of these particular composites [268].

In 2017, Dinca and co-workers [269] applied the mesoporous MOF [Co_2Cl_2btdd] (btdd = bis(1*H*-1,2,3-triazolo[4,5-b],[4′,5′-i])dibenzo[1,4]dioxin)) as an adsorbent to capture water

vapor at low relative humidity. The material synthesized adsorbed 82% water by weight below 30% relative humidity and when simulated under desert conditions it would deliver 0.82 g_{H2O}/g_{MOF}, significantly more than in the case of previously reported adsorbent MOF-841 [270]. Moreover, it demonstrated a cooling capacity of 400 KWh/m^3 per cycle, which is amongst those recorded as the best for materials capable of generating a 20 °C difference between ambient and output temperature. Co_2Cl_2btdd contains open metal sites that coordinate water prior to pore filling. This effectively decreases the pore diameter and renders it to be essentially equal to the critical diameter of water. The water uptake occurs *via* reversible continuous pore filling. Studies were repeated six times under typical desert climate conditions of 35% relative humidity at 25 °C (night) and 5% relative humidity at 45 °C (day). These results showed that after six cycles the initial water capacity of the material was decreased only by 5.1 wt%. Co_2Cl_2btdd is predicted to be easily regenerate under mild conditions [260,269].

In 2018, Fathieh *et al.* [258] synthesized MOF-303 [Al(OH)(hpdc)] (hpdc = 1*H*-pyrazole-3,5-dicarboxylate), which exhibits hydrophilic one-dimensional pores with a diameter of 6 Å and a pore volume of 0.54 cm^3/g. These parameters facilitate a large maximum water capture capacity of 0.48 g/g. In addition, the material shows high hydrolytic stability, which was proven by 150 adsorption-desorption cycles without detectable degradation. Furthermore, blending MOF-303 [Al(OH)(hpdc)] with 33 wt% of nonporous graphite improved its thermophysical and adsorptive properties (increase of 114% in water production) [258].

The applicability of COFs for water harvesting have been also explored. Among them, the most interesting is two-dimensional imine-linked COF-432, with a voided square grid topology [264]. COF-432 has remarkable long-term stability upon water uptake and release cycling. Moreover, it exhibits non-hysteretic water sorption isotherms with an abrupt uptake step at low relative humidity and low heat of adsorption. These properties render COF-432 as a material with a high water-capacity and a low regeneration energy barrier. It shows maximum water uptake of 0.3 g/g at 34% relative humidity and a working capacity of 0.23 g/g in the relative humidity range between 20 and 40%. COF-432 does not exhibit hysteretic water sorption behavior like other COFs and as such reduces the energy needed for regeneration. The stability of water cycling was confirmed by conducting 300 uptake and release cycles, after which working capacity remained unchanged. The pore surface of COF-432 is largely non-polar, but imine bonds could play the role of adsorption sites for water molecules [264]. Highly favorable hydrogen bonds are formed between the imine functional groups and the water guest molecules, which cooperate and create infinite chains of water molecules in the framework channels, leading to a denser structure [271].

3.4. Programming of drug delivery

MOF nanoparticles are good candidates for biomedical applications due to their porous nature, modular structure, and readily chemical functionalizability. They can be commonly used as active compound carriers, bio-imaging and therapeutic agents [272–276]. The porosity and topology of MOFs can be modulated through post-synthetic modification, variations of the metal node, and pre-designed ligand geometries. Organic linkers (*e.g.* carboxylates, imidazolates, or phosphonates) in the hybrid structure of MOFs provide biocompatibility and high sorption capacity towards different drugs, while inorganic groups can be optimized for controlled release profiles. The synthesis of mesoporous MOFs is crucial, as the small micropore size limits the drug uptake and loading capacity. Drug molecules and peptides/proteins with a small molecular weight (< 7000 g/mol) can be easily loaded into MOF particles. Naturally, proteins with a large molecular weight (> 10,000 g/mol) need large pores/channels in order to be incorporated into the MOF. In the case of large molecules, such as peptides and enzymes, ideally, MOFs would operate on a dual-action of directed cargo transportation and protection from premature decomposition [277]. 'Smart' MOFs, reacting to external stimuli such as pH, light, temperature, or pressure have been employed to regulate guest release (Fig. 17) [278–281]. Considering the location of cargos and cargo–carrier interactions, its loading methods could be divided into three strategies: encapsulation, direct assembly, and post-synthesis. The incorporation of cargos into "void" volumes of MOFs *via* non-covalent or covalent interactions, is called encapsulation. This strategy enables the loading of many chemotherapy drugs, nucleic acids, and enzymes. Matching between the size of selected cargos and pore structures of MOFs carriers is the key parameter for successful encapsulation [282–287]. In addition to direct encapsulation strategies, certain drug molecules can be directly used as ligands through participating in the formation of the framework [288,289]. The application of this strategy has allowed loading chemotherapeutic drugs, such as zoledronate, pamidronate, methotrexate into MOFs. In the post-synthetic strategy, MOF nanoparticles with the desired size, morphology, and physicochemical properties are prepared and isolated first [290], followed by carefully characterization [291,292] and the introduction of cargos into the porous framework *via* forming coordination bonds with metal nodes or covalent bonds with the functional sites of linkers [80,249,293]. The cargos can be located on the internal and/or external surface of the MOF nanoparticles [284].

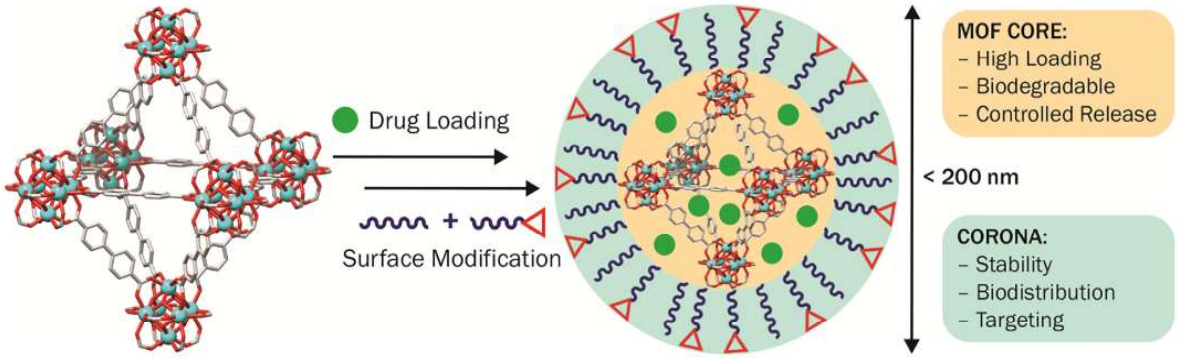

Figure 17. Scheme showing the ideal properties of a MOF-based drug delivery system, using the structure of UiO-67, $[Zr_6O_4(OH)_4(bpdc)_6]_n$ (bpdc = 4,4'-biphenyldicarboxylate), as an example (Reprinted with the permission [294]. Copyright 2019, Elsevier).

In recent years MOFs have been tested for application in the fields of controllable drug release and efficacious treatment of cancer [295]. Bones are by far the most common, metastatic places, primarily in the case of lung, breast, and prostate cancers as well as kidney and thyroid cancers [296]. The pH in bone tumor tissues is more acidic than in blood and normal tissues (pH 7.4), hence when bone tumor cells breakdown bone and release minerals, the concentration of Ca^{2+} in the blood is extremely high. Tumors also produce parathyroid hormone, vitamin D sterols, prostaglandin E what results in bone resorption. Unique mechanical and biocompatible properties, stable structure, and extremely low toxicity of zirconium compounds accelerate the burgeoning biomedical applications of Zr-based MOFs [294,297]. In 2016, Tan *et al.* [298] designed mechanized Zr-MOFs with multi-stimuli responsive supramolecular gatekeepers that combine thermotherapy with chemical and biochemical triggers. These MOFs were loaded with the 5-fluorouracil (5-Fu) high performing anticancer drug at room temperature. After loading 5-Fu into the Zr-MOF, carboxylatopillar[5]arene (CP5) rings were introduced to encircle the A stalks *via* host–guest complexation to generate [2]pseudorotaxanes as the movable elements of the mechanized Zr-MOFs, thereby realizing the drug encapsulation (Fig. 18). It was found that adding an excess of CP5 results in an encapsulation capacity that is more than 2 times greater (247 mmol/g) than previously reported for the Zn^{2+}-triggered version. This confirmed the important role of supramolecular switches CP5 system, which showed a stimuli-responsive host–guest performance for controlled drug release. The research hypothesis was that drugs will be released in a controlled way from smart containers near the targeted lesions to kill the cancer cells and help to regenerate bone, reduce undesirable side effects and tune the pH and Ca^{2+} concentration in the body. MOF nanoparticles can comprise 5-Fu drug molecules at neutral pH but release them under acidic pH. The release rate of 5-Fu is pH-dependent. In a

neutral pH, 5-Fu molecules were strongly held within nanopores, which is rarely observed in the case of MOF-based drug delivery systems. At pH 5 the supramolecular gates opened and 5-Fu could start to release. In this pH, 18% of the drug was released during 1 h, while at pH 4, 54% of 5-Fu was released in the same period. Therefore, the responsive drug delivery system can reduce undesired drug release during its transportation in blood circulation and improve the effective release of drug in tumor tissues. Moreover, CP5-capped MOF nanoparticles have the ability to respond to Ca^{2+} due to the stronger binding between CP5 and Ca^{2+} [298].

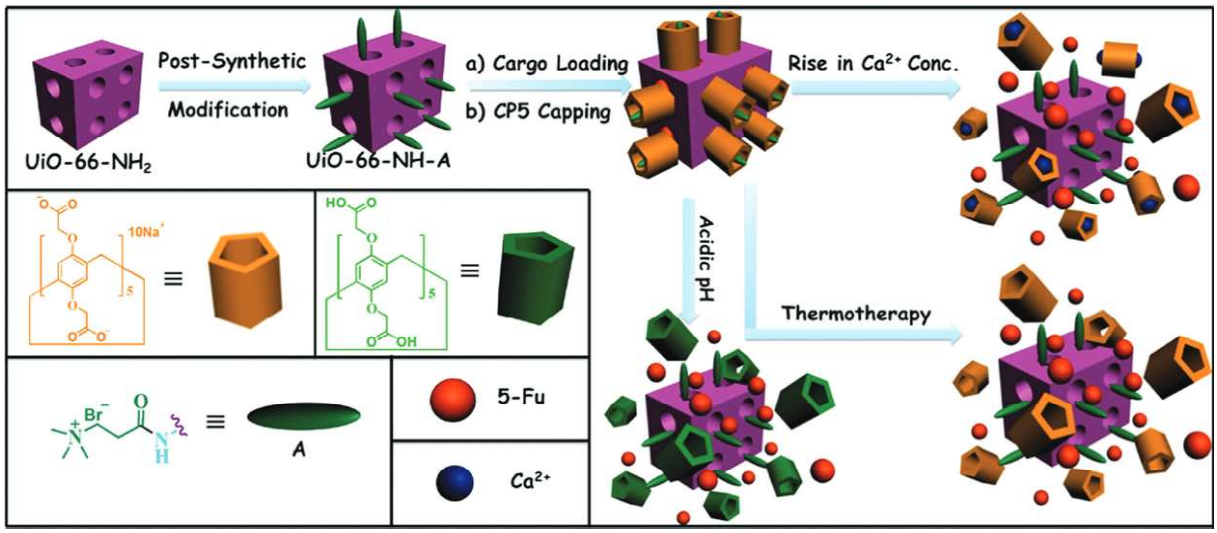

Figure 18. Schematic representation of stimuli-responsive mechanized Zr-MOFs (UiO-66-NH_2) with positively charged A stalks encircled by carboxylatopillar[5]arene (CP5) rings on the surfaces. The mechanized UiO-66-NH_2 can be operated by pH changes, Ca^{2+} concentrations, and thermotherapy to regulate the release of 5-Fu (Reprinted with the permission [298]. Copyright 2016, Royal Society of Chemistry).

The ability to bind molecules in a specific way on the basis of the host–guest interactions is a very important property of porous materials [211]. Type and number of functional groups in the porous structure can influence the interactions with guest molecules, therefore their release can somewhat be anticipated and programmed. In 2017, Dong and co-workers [211] applied the well-known MOF, MIL-101(Fe), composed of Fe_3O IBUs and benzene dicarboxylate (bdc) linkers, to construct multivariate MOFs (MTV-MOFs) with functional groups –H, $–NH_2$, and $–C_4H_4$ appended to the bdc. They were loaded with three molecular guests - ibuprofen (Ibu), rhodamine B (RhB) and doxorubicin (DOX). It was found that by the modifying the linker ratios in one MTV-MOF the release rate of the guest molecules can be precisely tuned between 0.30 and 1.14 per day for Ibu, 0.005 and 0.16 d^{-1} for RhB, 0.008 and 0.022 d^{-1} for DOX. The

co-release of guest molecules can also be achieved, in which the suppression or reinforcement is in good accordance with the release of the single guest molecule. Here, maximum guest release can be programmed between 17 and 29 days (DOX). Functional groups in MTV-MOFs are crucial in interacting with probe molecules, thereby controlling their release behavior. With the increasing percentage of $–NH_2$ groups, the Ibu is released slowly whereas in the case of RhB and DOX, the release is rapid. It can be explained by diversity in host–guest interactions. An interaction between the $–NH_2$ groups and Ibu molecules is stronger than between $–NH_2$ groups and RhB or DOX. However, $–C_4H_4$ exhibits stronger interactions with RhB or DOX than with Ibu, due to its large π system. Stronger interactions between the functional groups on the pore wall and the probe molecules cause a slow release, while weaker interaction will accelerate the process. Combining two functional groups interacting strongly and weakly with probe molecules in MTV-MOF allows opportunities to tune the release rate over a wide range up to 32-fold [211]. It was established that using the right type and proportion of functional groups makes it possible to achieve zero-order release ideal for active pharmaceutical ingredient release systems [179,211].

In 2017, Preiß *et al.* [299] applied two representative MOF nanoparticles, MIL-100(Fe) and MIL-101(Cr) in the uptake and release processes of fluorescein. MIL-100(Fe) exhibits a maximum payload capacity of 649.4 μg/mg, while for MIL-101(Cr) this was 413.5 μg/mg. It was revealed that loading and release rates of fluorescein are highly dependent on pH. Fast loading kinetics with high affinity was observed in distilled water (at low pH), while slower loading kinetics (lower affinity) was noted at high pH (7.4-8.4). Opposite trends were established for the release process, with high affinity and slow release at low pH (and in water). It should be mentioned that for MIL-101(Cr) less than 3% of fluorescein was released to the receptor fluid within 90 minutes at any pH tested, while in the case of MIL-100(Fe) the amount of fluorescein released increased with rising pH from 3% at pH 5.1 to 40% at pH 7.4. Possibly, under these conditions, binding of fluorescein to MIL-101(Cr) is irreversible or exhibits extremely long off-times. It may also be caused by electrostatic interactions that can confine the guest molecules inside the MOF pores [299].

During therapy, cancer cells become immune to drugs. A potential solution to address this problem can be the treatment with multiple drugs at once to destroy resistant cancer strains and prevent the formation of new resistant strains [300,301]. Although combination therapy is more effective, it is also challenging, due to the different physicochemical properties of each drug. The hybrid nature of MOFs makes the materials suitable to simultaneously incorporate several drugs.

In 2017, Illes *et al.* [302] loaded iron-based MOF nanoparticles (MIL-88A) with multiple drugs (Suberoylbis-hydroxamic acid (SBHA) alone, or irinotecan and floxuridine together) in different ratios. In the next step, drug carriers were coated with a lipid shell allowing control of interactions with intracellular fluids. It was found that the liposome-coated MIL-88A nanoparticles (Lip-MIL-88A) can successfully adsorb a significant amount of biologically active compounds (20 wt%) and then release their cargo. The liposome coating prevents leakage of the cargo. In cell experiments, Lip-MIL-88A nanoparticles were absorbed by cells and enabled a significant intracellular release after three to four days of incubation. The mixture of irinotecan and floxuridine in the 3:1 ratio shows the best results reducing the cell viability to 28.6%. The liposome-coated MOF nanoparticles are promising drug delivery systems because of uncomplicated loading and effective intracellular release, which can in the future improve cancer chemotherapy [302].

4. MOFs in chemical sensing

There is no area of industry where sensor enhancements are redundant and, as such, superior and more efficient chemical sensors are constantly pursued and desired [303–307]. The increasing importance of sensors is apparent from our evolutionary need for constant sensory awareness. Nowadays, technology is continuously developing and becoming an inseparable part of human life. As a growing technological generation, the desire for rapid communication of our personal, dynamic states is in demand, particularly when pre-mediated changes can be predicted. Sensors can be considered as an interface between nature and us as they monitor environmental changes, having a pivotal impact on augmenting reality [308,309]. Apart from augmented reality and using sensors to strengthen cognition [310], the growing interest of artificial intelligence (AI) and obtaining sensors imitating human senses has become a new widely explored field in the last decade [311]. To meet such an ongoing demand, further development of subtle sensing systems must be cooperatively considered multidisciplinary by researchers in areas including chemistry, physics, and engineering. Mentioned fields have significant involvement in the sensor design and when coupled with the numerous considerations required to identify the correct chemical make-up, they dictate the number and variety of chemosensors.

4.1. Chemical and physical aspects of sensing

According to the IUPAC, a chemical sensor is a device that converts chemical information (component concentration and matrix composition), originated from an analyte's reaction or

system's physical property, into an analytically useful signal [312]. The chemical sensor contains a chemically selective recognition phase, often separated from the sample through a membrane (to prevent from interferents), and a transducer to convert chemical information to a useful signal (Fig. 19). The recognition phase (receptor) is a component of the chemical sensor, which is directly in contact with analyte. The receptor can interact with chemicals in two different ways. The first way is surface interaction, where analyte molecules are adsorbed onto the receptor; the second method is interphase–bulk interaction, in which analyte molecules are absorbed in the active layer phase of the receptor [313]. The most important quality of the sensor is selectivity, which is the capability to respond selectively to one species in the presence of others. Usually, it involves shape recognition (stereospecificity) of the intended analyte to be detected. Besides the geometrical fitting to the binding sites in the recognition phase of the chemical sensor, molecules need to match the type of interaction with them *e.g.* hydrophilic-hydrophilic [314].

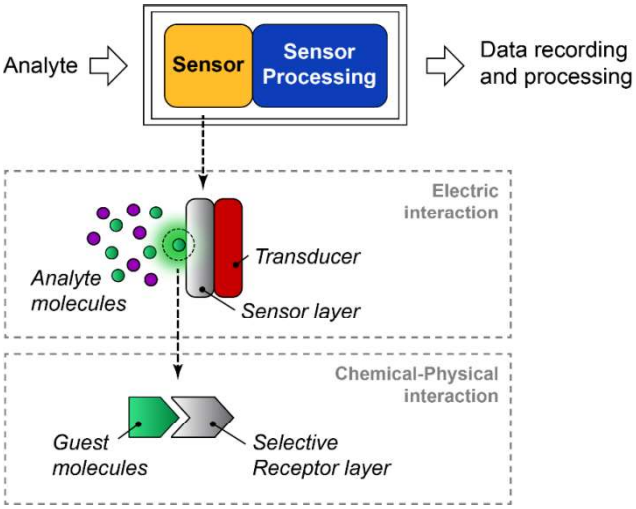

Figure 19. Scheme of a typical chemical sensor.

Classification of chemical sensors is based on either the receptor's stimulus *i.e.* gas, ion, bio- or humidity, or on the type of transducer's signal *i.e.* electrochemical, photometric, acoustical/mechanical, magnetic, or calorimetric. To receive information about the detected component in the analyte, the chemical signal needs to be transduced and amplified. MOFs can be applied in chemosensing as a transducing element due to their various framework functionalities (Fig. 20). Firstly, host–guest interaction may result in the framework changes, with subsequent material properties alteration such as photoluminescence, which is considered as direct detection with signal transduction and propagation. Additionally, receptor information

intake if correlated with MOF material can induce the framework, particularly MOF's electrons in linkers (conductivity) or magnetic properties of metal nodes. Usually, a material that amplifies the signal further is a semiconductor, which transfers fractional charge or donates/accepts an electron. For that energy states and Fermi level must be considered, which are derived from the Fermi-Dirac statistics. Quantum mechanics are necessary especially in the description of indistinguishable electrons and holes [315]. Electrochemical transducing is based on converting a chemical reaction into an electrical signal and it strictly depends on redox reaction kinetics between all electroactive components present in the reaction. This includes detected molecules, transducer material, and environmental parameters [316]. The optical photometric transducer, instead of the chemical reaction, converts radiant power generated from the Lambertian source as fluorescence, chemiluminescence, or bioluminescence into measurable signal [317]. Such a signal is absorbed by an atom/molecule and, based on the Lambert-Beer law, the length of the light path, the intensity of transmitted light and the concentration of the measured sample are taken into account [318]. Whereas optical sensor utilizes electromagnetic radiation, the mechanical sensor uses acoustic waves. Usually, the quartz crystal resonator (QCR) is applied in such systems to propagate the signal (wave to electronic) due to their piezoelectric effect, *i.e.* electric charge generation induced by mechanical stress [319]. Magnetic sensing includes many technologies such as Hall-effect, flux-gate, search-coil, magnetoresistive magnetometers and more [320]. Based on most of these, there is Faraday's law of induction which states that "a change in magnetic flux is associated with an electro-motive force (EMF)" [321]. Magnetic components in the transducing part of the chemical sensor generate an electrical current through alterations of magnetic field properties or by a motion of the electrical conductor. The last transduction mechanism relies on temperature variations in the form of heat consumption, generation or transfer usually as an exo-/endothermic reaction between the sensor and chemical species [322]. The sensor is heated by the resistor and its temperature is measured by the heat flow from the analyzed substrate to the environment. Changes in the heat during the kinetically controlled catalytic chemical reaction between the sensor layer and molecules are the operative principle of most calorimetric gas sensors, which are also called pellistors.

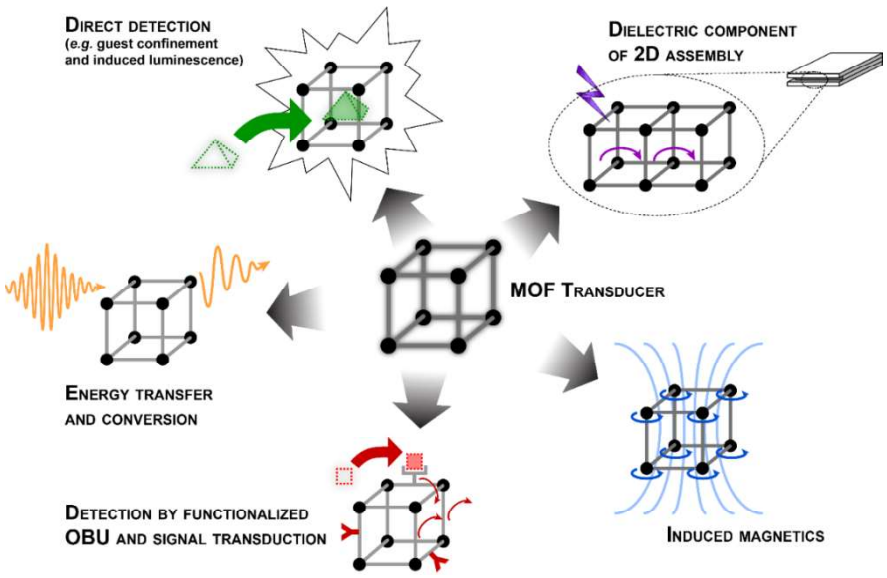

Figure 20. Visual presentation of MOF transducers. MOF as a direct detector and transducer in *e.g.* host–guest sensing and induced luminescence; a dielectric transducing element in 2D assembly; magnetically responsive material; transducing platform for functionalities as detectors; converter and propagator of electromagnetic waves.

Other commonly used terms for sensors include detector and dosimeter, where neither is interchangeable. A detector is a type of sensor that indicates the presence or absence of a chemical substance, occurring when analyte concentration exceeds a set threshold value. A dosimeter measures the dose of a chemical accumulated over time and is predominantly a single-use device as the effect is usually irreversible. Any sensor coupled with another non-sensing apparatus, such as an alarm, creates a performing system which is called an actuator.

The combination of chemistry and physics in chemical sensing is based on the recognition–amplification connection. Recognition, as an information intake of a specific change (*e.g.* compound concentration, system content) in real-time, is influenced by the receptor selectivity and can be chemically modulated. The developed recognition phase can be predesigned purposely to react for requisite environmental changes and ignore unnecessary or undesirable alterations. For instance, in 2019 Esrafili and co-workers [323] reported their "design-for-purpose" approach for a highly selective MOF sensor for Hg^{2+} in the presence of other metal cations such as Cd^{2+}, Cu^{2+}, and Cr^{3+}. The group obtained luminescent Cu-based frameworks dually functionalized with malonamide group (–NH–CO–CH_2–CO–NH–) and acylamide group (–NH–CO–) with 0.1 ppm detection limit and 714 mg/g maximum capacity of mercury ions. Chemosensing of a specific compound can also be correlated with specific bacterial detection, which causes a distinct disease. In 2016 Zhang and co-workers [324] fabricated a

bimetallic, lanthanoid MOF Tb/Eu(btc) (btc = 1,3,5-tricarboxylate) for dipicolinic acid (DPA) biomarking in anthrax inducing bacteria (*Bacillus Anthracis*) or human serum. The energy transfer between Tb^{3+} and Eu^{3+} varied accordingly to DPA concentration (50-700 nM) and resulted in different fluorescence intensity being observed. This lanthanoid MOF exhibited self-calibration and due to naked-eye recognition, no transducing element was necessary. In more complex sensing systems, the amplification of recognized change is also dependable on the concentration of the analyte. However, it must be adjusted by employing physics principles to introduce appropriate transducing mechanisms to the chemical sensor. For instance, in 2018 Yang and co-workers [325] proposed an application of Cu-tcpp (tcpp = tetrakis(4-carboxyphenyl)porphyrin) nanosheets in aptasensor (DNA sensing) for detecting antibiotic chloramphenicol (CAP). The Cu-based MOF was compared to graphene oxide in the FRET (Förster resonance energy transfer) mechanism revealing greater quenching ability of the HP/SG (hairpin probe/SYBR Green I) complex by π–π stacking and/or electrostatic interactions. Consequently, it contributed to 7.5-fold higher signal amplification and overall improved sensor sensitivity.

After receiving the signal, the information is then transduced into an electrical signal. To achieve a meaningful output, the measured signal must be subtracted from the reference signal and subsequently converted to a digital signal, followed by processing using statistical methods. Collectively, these steps require numerous specific properties from the sensor to be sufficiently performed and provide the researcher with a useful result. Essential terms and phenomena need to be considered when designing sensors, especially when it comes to comparing their effectiveness and efficiency. The static features include measurable sensor transient properties for instance:

(i) sensitivity—a slope of the sensor response curve, expressed as a signal value per concentration unit;

(ii) selectivity—the ability of the sensor to measure the particular component concentration in the presence of others;

(iii) detection limit—concentration at which the average value of the measured signal is equal to the value of two standard deviations;

(iv) repeatability—receiving the replicable information if measurements are carried in the same environment;

(v) reproducibility—the ability to repeat reliable results when conditions are changed.

The dynamic features can be measured in a steady state after the stabilization of transient effects. These features give information on how a sensing system handles the correlation

between the input signal and response to the stimuli and the output signal and impact on the external measurable quantity [326].

Changes in free enthalpy between the recognition phase and chemical species are equal contributors to the driving force and the foundation of the basis of chemical sensors. This is best described, during changes in sample activity, as the interaction of the analyzed particles with the sensor, which will only occur when standard free enthalpy is negative [314]. This activity describes molecular reactivity rather than molecular recognition and it is mainly used in activity-based sensing [327]. The sensor response and the binding equilibrium constant (??) is based on the interaction between molecules (??) and sensor (??)—more specific with the receptor, and also rates of the forward reaction ($??_{??}$) and reverse reaction ($??_{??}$) (Eq. 8). $??_X$ can be described in terms of activities of molecules in the system ($??_{??}$), activities of binding sensor site ($??_{??}$), and activities of bound molecules ($??_{??X}$) (Eq. 9). Each activity is dependent on activity coefficient (??) and concentration of the molecules (??) (Eq. 10):

$$X + S \underset{k_r}{\overset{k_f}{\rightleftharpoons}} XS \quad \text{(Eq. 8)}$$

$$K_X = \frac{a_{SX}}{a_S a_X} = \frac{k_f}{k_r} \quad \text{(Eq. 9)}$$

$$a = fC \quad \text{(Eq. 10)}$$

If the binding equilibrium constant is too high, the reversibility of the reaction is strongly hampered, and the sensor behaves more as a dosimeter. Therefore, the key element of the sensor is reversibility. Realistically, it is highly impossible to achieve a reversible sensor that provides reliable results for an extended period. This highlights the necessity for clear communication of sensor lifetime to avoid misinterpretation of the signal reading [328]. A trade-off must be reached between achieving a high value of the binding constant of the analyzed molecules and the irreversible nature of their interaction. Each receptor possesses a lower limit of molecular activity below which the sensor will not respond. This strictly depends on the transducing mechanism within the device. Here, the minimum value of a specific sensor type is fixed, and the sensor's response range is related to the overall activity of the binding centers in the receptor layer. An additional important consideration is the type of chemical interactions that direct the binding mechanism. This is influenced by the interactions either on the surface or in the bulk and the nature of the bonds' strength. This encompasses covalent bonding, hydrogen bonding, ion–ion, London forces, ion-induced dipole, dipole–dipole, and hydrophobic bonding [313].

Multiple efforts from researchers are underway to identify the 'sweet spot' of reversibility coupled with a high binding constant and sensor selectivity in analyte detection. Steady steps towards innovations, albeit often small, constitute the basis for important and breakthrough discoveries. Current goals in the sensing field are based upon envisions for future devices. These are necessary and somewhat complex, such as miniaturization, portability, low-energy supply, low cost, and integration with all parameters maintained at the highest level [329]. The aforementioned desire for detector reversibility and stability requires a material that can easily release analyzed molecules and be recycled thereafter. Thus, the interaction between the analyte–detector pair must be expandable, ideally in a linear way. The signal also must be evident to the transducer, but only persistent enough to enable modulating the information. Whereas simple detectors often do not require a complex microelectronic system, precise chemical sensors do. The circuit design is comprised of not only a sensing element but also resistors, transistors, diodes, and amplifiers. Together, these form a suitable functional material, responsive to chemical and physical stimuli. Surface modifications of electrodes in electrochemical sensors enable enhancement of their performance in sensitivity and selectivity. Additionally, this can also lead to portable sensors that can be used in the field (outdoor), making them unique to achieve what is rarely possible in other precise analytical techniques (*e.g.* HPLC or AAS) [330]. In line with these considerations, porous materials, such as MOFs, are more often considered as candidates which can address the desired requirements for chemical sensors [331,332]. In the sensing area, MOFs can act as a selectively confining element in the receptor phase [333], fluorescent-based detectors by having fluorophores as linkers [334], or 2D MOFs with flat surfaces with improved electrons transport [335]. Such dynamic MOFs can undergo reversible changes when exposed to different stimuli are often referred to as soft-porous crystals or ′third-generation MOFs′ [336]. When governing the selectivity towards the desired guest by receptor phase, alteration is the core, or at least a starting point, when one may consider MOF utility in chemosensors. Tuning MOF porosity through composition can be the first stage to a proper size exclusion [337], which can also change the overall framework properties, for instance, using short linkers can amplify magnetic interactions of metal nodes [338]. On the other hand, MOF pore functionalization focuses on matching the interaction character and its affinity, as a recognition phase, with the chemical species. Additionally, pinning other stimuli-responsive moieties in the framework broadens the "design-for-purpose" approach. This is seen in attaching chromogenic groups to increase

photo-responsiveness [339], or amine moieties to prompt chemiresistive properties of UiO-66 for acidic gases (*i.e.* SO_2, NO_2, CO_2) (Fig. 21) [340].

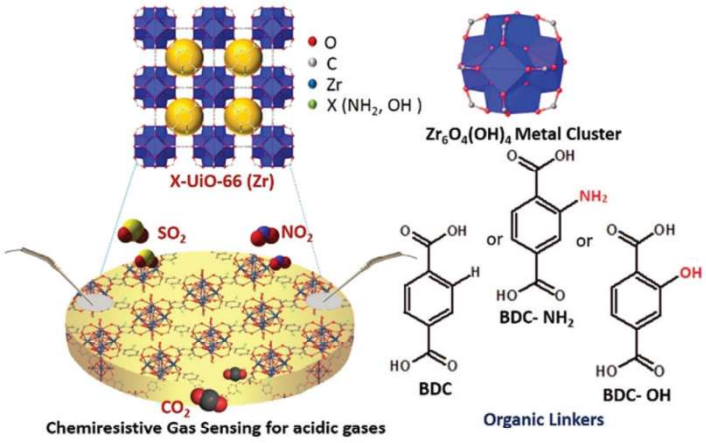

Figure 21. Illustration of chemiresistive sensing of acidic gases by the modulation of organic linker in UiO-66 (Reprinted with the permission [340]. Copyright 2019, Royal Society of Chemistry).

Considering MOFs in electrochemical sensors, the charge transport in the framework occurs *via* bond conduction through either continuous chains, the space between closely arranged linkers, or guest molecules if they are strongly bound to the scaffolding. According to band theory, MOFs are usually good insulators (conductivity is below 10^{-10} S), due to the low atomic density and strong localization of the electron wave function. Their energy gap (E_g) between valence band (VB) and conduction band (CB) in most MOF materials is higher than 4 eV ($0 < E_g < 3$ eV for semiconductors; $E_g < 0$ for metals) [341]. However, new findings revealed it is feasible to achieve framework materials having mobile charge and that are conductive by anion/cation vacancy formation [16] or impurity doping (with *e.g.* I_2 [342], tetracyanoquinodimethane (TCNQ) [343], ferrocene [344], metallacarboranes [345], metal nanoclusters [346] or conductive polymers [347]). Modifications can lower band dispersion and subsequently increase conductivity in MOFs, defined as Hubbard insulators, in which the CB is parted by the Hubbard energy into sub-bands due to electron–electron repulsion [348]. In semiconductive MOFs with little band dispersion, the conductivity can be thermally activated. This transport mechanism does not involve true band transport, but the hopping mechanism occurs, which is the migration of electrons over the lattice points through molecular bridges [349]. Such transport is commonly found in disordered MOF structures where reduced dielectric screening and strong electron-phonon coupling lead to carrier localization. Interestingly, increasing the temperature of metals or crystalline semiconductors lowers

conductivity, where for MOFs we see the opposite effect. Low hopping energy activation, partial electron delocalization, and improved charge propagation are temperature-induced in MOFs [350]. Non-conductive MOFs can also be applied in electronic-devices due to their dielectric polarization and change of dielectric constant (κ) when placed in the electric field. This is especially relevant if it has the potential to achieve operation frequencies suitable for integrated electronic circuits (~10^9 Hz) [348]. In such estimations, the composition and the material density (N) must be considered before determining its applicability as semiconductor. Usually, more bulky materials have higher dielectric properties, through modulating MOF porosity and thus its density, along with atom and bond polarizability, making it possible to increase or decrease κ. The Debye equation connects the displacements of electron clouds, nuclei, and ions with the dielectric polarization. Based on the three terms, the electronic polarization ($\propto_e$), the distortion polarization ($\propto_d$) and the permanent dipoles (μ), the dielectric constant can be written as [348,351,352]:

$$\frac{\kappa - 1}{\kappa + 2} = \frac{N}{3\,\epsilon_0}\left(\propto_e + \propto_d + \frac{\mu^2}{3kT}\right) \quad \text{(Eq. 11)}$$

Besides the electric field, other physical stimuli, such as light, pressure, temperature, or magnetic field, can affect the MOFs' properties, which can be used for electrochemical sensing. The conversion of transition metal ions ($3d^4$–$3d^7$) from the low-spin state to the high-spin state (or inverse), called spin crossover (SCO), is a useful magnetic feature of MOFs in detecting devices [353]. It can trigger the adsorption or release of the guest molecules, usually in detecting volatile gases *e.g.* pyridine, SO_2, or CS_2 [333,354].

Apart from treating sensors as only directly detecting tools, they also can be a component of more complex, assembled devices. Combining the electric and magnetic properties of MOFs with tunable E_g alignment, through tailoring the framework composition and functionalization, creates opportunities to enter the photovoltaic space as light sensors in solar panels. MOFs with visible light to near-infrared light harvesting abilities capable of absorbing solar radiation and transform those into photo-excitons. To achieve the reducing wide E_g in MOFs, adopting techniques such as employing IBU and OBU (conjugated systems) rich in electrons, functionalizing linkers with additional electron-donating groups or doping with π-donor/acceptor guest molecules to create electron-delocalized states are strategical [355]. Regarding MOFs for photovoltaic applications, they can be viewed as complementary toward a bulk heterojunction (BHJ) and dye-sensitized solar cell (DSSC) architectures [348]. In the

first case, MOF organic linkers absorb light and conduct holes by exciton splitting and electron transport. In the second case (DSSC), MOFs only act as a matrix for dyes or electrolytes regenerating dyes without the need to balance the donor-acceptor role with semiconductivity [356]. MOFs seem to be a more attractive alternative for standard dyes due to the multiple light-absorbing components, to increase the width in light absorption of the full spectral range. However, their porous structure is more beneficial, since it prevents absorbers aggregation that unfavorably might change their band gaps. To absorb light and further use it in emission application the MOF band gap again needs to be narrow enough to create excitons and be conductive, thus previously mentioned modifications come in handy [357].

4.2. Designing of MOF for application in chemical sensors

The wide variety of composition and modification techniques available for MOFs are one of the main reasons they are applicable in many fields, and within these fields they can be further tuned for very particular purposes. In terms of sensing, the general goal is to achieve the ultimately specific sensor towards one type of chemical, which ideally could be done by creating a receptor phase that selectively confines, reacts, and releases by means of predesigned composition. This is made possible with adequate pores and binding sites, also with functionalized groups prone preferential interactions with desired chemical species [358,359]. Currently, it is feasible to achieve the selectivity of sensors towards similar molecules or, as some investigations report, achieving enzyme-like MOFs. Although, in this case, the need for a strong bio-affinity sensor regeneration, without subsequent damage, became the key drawback in reversibility [360,361]. Nevertheless, there are examples of MOF sensors that stand out with their performance. For example, changing the metals in the cluster of MFM-300(X) (X = Al, Fe, In, Sc) allowed an immense change in the reversibility and interactions with the transducer in I_2 detection [362]. Different metals changed the MFM-300(X) surface area (1250–1370 m^2/g) and particle morphology (either rice-shaped, octagonal rods, plates) which had an impact on I_2 diffusion in crystallites, leading to precise tunability in critical environments. I_2 detection is the first responder activity in a nuclear waste clean-up, thus iodine sensitive recognition is compulsory in fields in which radioactive materials are applied. This proved that continuous MOF synthetic optimization is necessary, and improvements of each specific feature and different parameters are required. Very often the compromise necessary to perfectly balance the MOF properties for sensing such as selectivity, reversibility, and long-term utility can be difficult to achieve. However, sometimes a unique material is identified which changes this view, such as the terbium(III) based MOF, Tb(tatab) (tatab = 4,4′,4″-*s*-

triazine-1,3,5,-triyltri-*m*-aminobenzoate) [363]. This MOF not only revealed stability in many organic solvents (*e.g.* methanol, ethanol, hexane, DMF, DMSO, or acetone) but also in aqueous solutions at a pH range of 1–13. Furthermore, it indicated responsivity towards hexane, Fe^{3+}, $Cr_2O_7^{2-}$, and explosives such as nitrophenol derivatives. All sensing processes were correlated with pH dependable fluorescent intensity, as the receptor mechanism. However, thermolysis was already observed at 95 °C, displaying relatively low thermal stability. Other MOFs have revealed a much higher thermal stability [364], for instance, Kim and co-workers [365] introduced a Mg-MOF for various gases sensing (*e.g.* H_2, NO_2, or H_2S) and operable at wide temperature range (25 to 200 °C). The detection was based on the sensor resistance change and p-type sensing behavior. This was observed with increasing resistance when exposed to the reducing gases and decreasing in the presence of oxidizing NO_2. Additionally, for NO_2 the higher the temperatures were found to enhance the response of the sensor. There are further reports of MOFs that are stable even up to 530 °C and 610 °C, which are very promising for MOF-sensor development for application in demanding thermodynamic conditions [366,367]. The thermal stability of MOFs does not always correlate with their stability in aqueous solutions. It is problematic when a MOF seems to be ideal for hydrophilic molecular detection (*e.g.* metals ions), where in fact its structure is water sensitive. An interesting example of improved metal ions sensing in an aqueous solution was introduced by Pan and co-workers in 2019 [368]. Here, a luminescence-based detection by an Eu-MOF for Cd^{2+} exhibited even higher affinity towards cadmium than famed lanthanum-based MOFs. In solutions of many different cations (*i.e.* Li^+, K^+, Na^+, Ca^{2+}, Mg^{2+}, Ba^{2+}, Sr^{2+}, Mn^{2+}, Ni^{2+}, Co^{2+}, Cu^{2+}, Zn^{2+}, Cd^{2+}, Hg^{2+}, Pb^{2+}, Al^{3+}, Cr^{3+}, Fe^{3+}) Eu-MOF indicated particularly high fluorescence emission for Cd^{2+} (up to 23 times higher compared to pure MOF solution). It also showed exceptional water stability, illustrated by PXRD (powder X-ray diffraction) analysis where crystallinity was maintained after being submerged for 24 hours in the water, and even after boiling.

The evolution of an increasingly diverse plethora of new compounds in pharmacy and other industries requires rapid detection techniques to be realized. In fields related to medicine or forensic science, the sensitivity in biomolecule detection is particularly fundamental, where tracing any sign of barbiturates or explosives are crucial [369,370]. For these purposes, sensors which provide quick information in the form of a color or fluorescent change are always in favor because of the simple and attractive naked-eye recognition, which can be processed directly by the operator, without expensive instruments. Wang and co-workers [371] introduced a Zr-based MOF (UiO-68-An/Ma) for sensitive biothiol sensing. This MOF is a bifunctional system with anthracene (An) and maleimide (Ma) groups, applied in a solid-state

fluorescent ‘turn-on’ sensor. MOF fluorescence was investigated in different amino acid solutions, where excited samples revealed exceptional thio-triggered behavior for cysteine, homocysteine, and glutathione, giving a noticeable blue emission. The obtained material was also stable in water and highly sensitive to mentioned compounds, with a visible response at only 50 μM. Even higher sensitivity for antibiotics sulfadiazine (SDZ) and nitrofurazone (NZF) was presented by Neogi and co-workers [372]. The luminescence of the two linkers incorporated in the MOF, CSMCRI-2 $[Zn_2(azdc)_2(dpta)\cdot(DMF)_4]$ (CSMCRI = Central Salt & Marine Chemicals Research Institute; azdc = azobenzene-4,4′-dicarboxylate; dpta = 4-amino-3,5-diphenyl-1,2,4-triazole), indicated good reversibility with ultra-sensitivity. For the active pharmaceutical ingredients, this MOF managed to achieve a detection limit of up to 0.7 μM for NZF and 65 nM for SDZ.

The ability to tune the pore size of a MOF drew interest in creating sensors for large molecules, such as nitroaliphatic explosives [373] or sulphonamide antibiotics [374], which remains a challenge today. Along with the sensing issue, in ‘turn-off’ luminescent detection the differentiation of large quenching of guest molecules at varying concentrations is problematic. The evolved method called ‘discriminatory array’ based on how the mammalian nose operates was introduced by Peveler *et al.* in 2019 [373], in an attempt to improve selectivity, focused on big molecule explosives. The Peveler’s group obtained an isoreticular MOF (MJ3’) to the Eddaoudi’s group MOF [375] with solvent (DMF or water) that takes up 70% of its volume space. MJ3’ $[Zn_4L(H_2O)_4\cdot(solvent)]_n$ (H_8L = 5,5′,5″,5‴-[1,2,4,5-benzenetetrayltetrakis(methyleneoxy)]tetra-1,3-benzenedicarboxylic acid) proved to be useful for quantitative analysis towards explosives, where selectivity can be interpreted by emission quenching. Particularly high quenching was observed with pentaerythritol tetranitrate (PETN), that is often difficult to detect.

Regarding sensing recognition, the ultimate goal is to achieve specificity towards a single type analyte in a similar way to biosensors, such as antibodies or enzymes. Through three-MOF arrays, the creation of a nose-like sensor became possible and enabled us to overcome the concentration limitation [376]. This is elegantly shown through designing a MOF sensor with selectivity for chiral analytes, by pinning achiral molecules on the framework. For instance, Zhang *et al.* [377] explored a homochiral luminescent cadmium based MOF $\{[Cd(L)(4,4'\text{-bipy})]\cdot DMA\cdot 5H_2O\}_n$ (bpy = bipyridine; H_2L = 4,4′-((naphthalene-1,4-dicarbonyl)bis(azanediyl))dibenzoic acid) indicated enanantioselectivity towards D/L-penicillamine. However, because of the partial similarity of the different molecules due to the

structural repetitiveness of the MOF, designing an entirely specific sensor is rarely possible [359,378].

In addition to considering the molecules' shape and determining the perfect fit of the analyte to the receptors' active sites, the overall energy of the system must be considered. In practice, the system temperature has a significant impact on the value of its equilibrium constant. When the analyte and receptor are separated, the stability of the system is enhanced due to its high entropy. The change of free energy is the leading drive in the interaction between the analyte and the sensor. Therefore, when designing a sensor, it is necessary to create conditions in which the change of negative enthalpy, as the result of the interaction between analyte and receptor, is large enough to compensate for the change of the system's entropy and temperature. Thus, a larger change of entropy results in a higher negative change of free energy, which leads to the permanent analyte–receptor state. This was presented by Yang and co-workers [379] for the Cd-based MOF sensor $[NH_2(CH_3)_2]\cdot[Cd_{2.5}(L)_2(H_2O)$ (H_3L = tricarboxytriphenylamine). This hydrophilic material revealed structural changes caused by highly polar organic solvents. By using microcalorimetry and XRD, the examined material revealed single-crystal-to-single-crystal (SC-SC) transformations, indicating dynamic changes that enhance host–guest interactions. It was possible to selectively exchange water in the MOF and thereby change its enthalpy (−4.83 kJ/mol) with DMA (*N*,*N*-dimethylacetamide) (−71.34 kJ/mol) and methanol (−87.13 kJ/mol). Surprisingly, MOF crystals also revealed reasonable selectivity towards Cu^{2+} with naked-eye detection from yellow to dark green. The enthalpy-driven and concentration-dependent response times highly differed from 9 seconds to 72 hours, with sensitivity from 10^{-4} M to 10^{-7} M. Highly sensitive MOF sensors are not solely restricted to heavy metal ions. A responsive copper ions sensor has excellent potential, for example in applications where Cu^{2+} contamination along with ocean warming and acidification negatively affect oceanic microscopic life [380]. In particular, when monitoring environmental changes, it is substantial to control nuclear waste clean-up (*e.g.* UO_2^{2+} [381]), or water/air pollution (*e.g.* ammonia [382]). However, sensitivity for gas sensing has become an ongoing challenge [362,383]. MOFs appear to be a promising tool for sensing because of their high sensitivity to vapors, due to their sieve properties, and the capability to selectively detect, trap and condense gases inside pores. This increases the concentration of the analyte within the MOF relative to gas concentrations outside the material in the exterior atmosphere [361]. Strong interactions between the MOF and gas analytes lower detection limits and enhance the detection directness, leading to overall the simplification of the sensing process. The indium based capacitive chemical sensor MFM-300 (nodes = *cis* $InO_4(OH)_2$; linkers = (biphenyl-3,3′,5,5′-

tetracarboxylic acid) by Salama's group is a prime example of MOF development towards directed sensing applications [384]. The structure of helically arranged metal nodes with specific pore morphology and an array of –OH and –CH groups created 'pocket-like' adsorption sites, befitting specifically for SO_2. As a result, MFM-300 revealed high selectivity for toxic SO_2 in the presence of other gases such as CH_4, CO_2, NO_2, and H_2 at room temperature. Of significant interest for this MOF-sensor is the outstanding stability and detection limit down to ~5 ppb.

With an increased understanding of the methods to control pore structure in MOFs, it is possible to tailor the pore to a specific size and type of guest molecule with exceptional accuracy [385–387]. An interesting size exclusion effect was presented by Fan and co-workers [388] for aldehyde sensing amongst other VOCs (volatile organic compounds) and gases (*e.g.* ammonia, formaldehyde, methanol, ethanol, acetone) at 300 °C. Here, ZnO rods were compared to a ZIF-8@ZnO rod-like core-shell structure. MOF@MO (MO = metal oxide) exhibited better selectivity than pure MO, with additional elimination of interferences signals. The ZIF-8 pore aperture size also allowed the formaldehyde molecules to selectively enter the MOF@MO composite [389]. Oxygen species such as O_2, O_2^-, O^- and O^{2-} present in the core-shell structure further enabled proceeding the detection mechanism. The simplistic mechanism of detection occurs due to electrons floating from aldehyde on the ZnO core along the axial direction (red arrow in Fig. 22), leading to the change of electrical resistance, finally providing a useful signal.

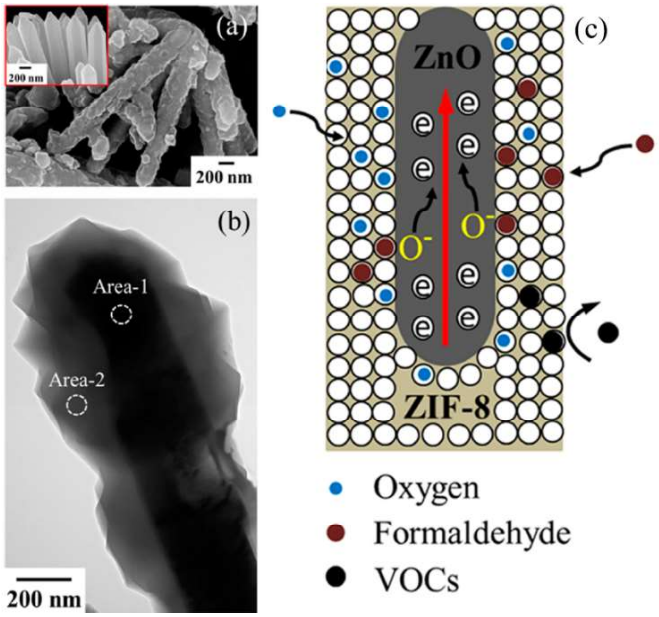

Figure 22. (a) SEM image of the ZIF-8@ZnO nanorods (Inset: SEM image of ZnO nanorods). (b) TEM image of a single ZIF-8@ZnO nanorod with core-shell heterostructure. (c) Schematic

illustration of the ZIF-8@ZnO nanorod sensor with selectivity for different volatile organic compounds (VOCs) molecules (Reprinted with the permission [388]. Copyright 2016, American Chemical Society).

Additional MOF functionalization even broadens the possible range of guest analytes and therefore careful consideration and design are first required before synthetic execution. Biswas *et al*. [390] functionalized a Zr-based UiO-66 with a new moiety, the linker 2-((pyridine-4-ylmethyl)amino)terephthalic acid. This modified UiO-66 revealed selectivity towards $O_2^{\bullet-}$ in 'turn-on' fluorescence sensing, amongst other competitive reactive oxygen radical species. Here, it was noticed that upon MOF reacting with $O_2^{\bullet-}$ the highly fluorescent linker was released to the aqueous solution. The much higher linker fluorescence intensity (~1.3×10^5 cps) than the MOF (~2.2×10^4 cps) enhanced the photoluminescence of the system, thus exploiting the most common type of sensing in MOFs [391].

In addition to porous core-shell structures and functionalization, Pang and co-workers [78,331] described the strategy of creating defects in MOF structures, which can optimize sensor selective recognition. In Lu and co-workers' research [392], the influence of UiO-66 crystals size in the range of 380 nm to 1060 nm, and defects numbers of 0.15 to 0.49, were explored for organic vapor optical sensing using ethanol as the prime candidate. The sensitivity of UiO-66 was increased with decreasing the crystal size, while more missing-linker defects enhanced recovery performance.

Simulation of the human sense of smell and taste through the fabrication of electronic nose [393] and tongue [394] dictates that high selectivity is a key aspect. Sensors that can electronically replicate organs are usually 2D material-based devices, which is convenient for the aligning purposes of many layers for complex system integration [395]. This is particularly applicable when the transducer and further signal processing requires flat surfaces for better conductivity [396,397]. It is difficult to achieve crystalline, porous, and conductive materials at the same time, however, 2D nanosheets and 3D films have already proved their potential in optical and electrochemical sensors [398–400]. Typically, MOFs are known as insulating materials or at least possess very low conductivity. However, recent research into guest doping or composite fabrication has shown that tunable electrical conductivity in a MOF is possible [401,402]. Song *et al.* [403] proposed thin films in a layer-by-layer assembly of the c-MOF $Cu_3(HHTP)_2$ (hhtp = hexahydrotriphenylene), on an LSMO ($La_{0.67}Sr_{0.33}MnO_3$) electrode to create organic spin valves (OSVs) (Fig. 23). The planar coordination geometry of the c-MOF and its ability to create layers with strong electron delocalization and 2D π-conjugation between metal ions, analogous to graphene, resulted in 2500 S/cm conductivity. Presumably, by

properly adjusting the thickness of the layers the spin-tunneling transport process can be achieved. Such a concept is another proposition of Cu-based MOFs for electrically conductive and chemiresistive sensors, previously presented by Dincă *et al*. [404].

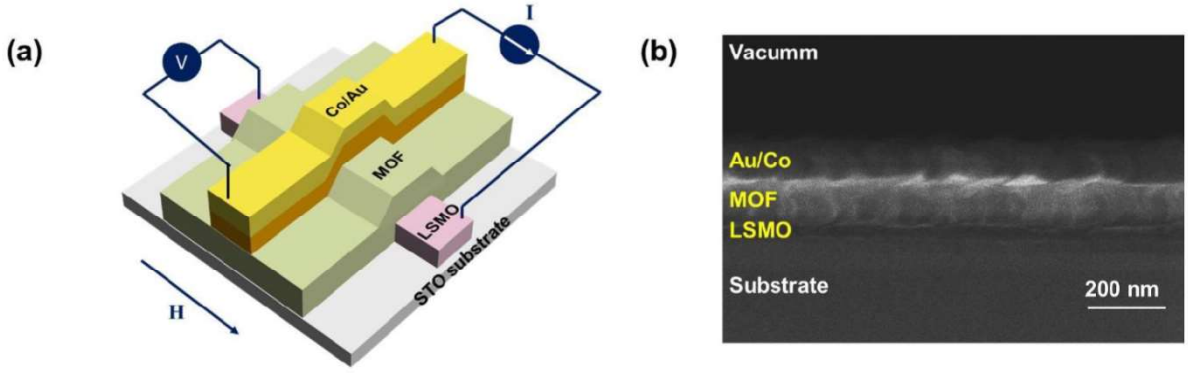

Figure 23. (a) Schematic diagram of the 2D c-MOF-based vertical OSVs (organic spin valves); (b) SEM images of the cross-section of the vertical OSV consisting of LSMO (50 nm), $Cu_3(HHTP)_2$ spacer (100 nm), Co electrode (50 nm) and Au (50 nm) (Reprinted with the permission [403]. Copyright 2020, John Wiley & Sons).

4.3. Summary

Briefly presented here, the activity of MOFs in the sensing area could never fully cover the topic of their remarkable applicability either as simpler detectors or advanced components in chemical sensors. Each of their features can be refined for specific purposes. Broad pore tuning in terms of size, volume and functionalization allows pairing with many molecules, linker modification provides different optical and conductivity characteristics, whereas metal or metal clusters cannot only have an impact on crystallite morphology but also on magnetic properties. All variations must consider sensors/analyte enthalpies to maintain sensor reversibility and long-run use. Up to now, MOFs are more often considered to be a good receptor phase due to their selective confinement but also, thanks to dielectric abilities, they could take part in signal-transducing systems. Although their commercial success is at the horizon, many efforts must be concentrated on the development of easier and less expensive fabrication processes. Nevertheless, one must remember that outstanding performance and preciseness rarely couple with low-budget manufacturing, and often sensing in medicine or military requires large expenditures of time and resources.

5. MOFs as electronic and ionic conductors

Conductivity is a key feature for electronic devices and research into new conductive materials is fundamental for the development of modern technology. In the last 20 years the focus of technological advancement shifted towards micro and nano applications, revealing new challenges [405–407]. Recently, MOFs showed conductive properties that can be tuned and improved by applying rational design strategies and PSMs [408–410]. The scope of this chapter is to provide a broad survey of conductive MOF development, focusing on the most important design principles to obtain them and their important applications (Fig. 24).

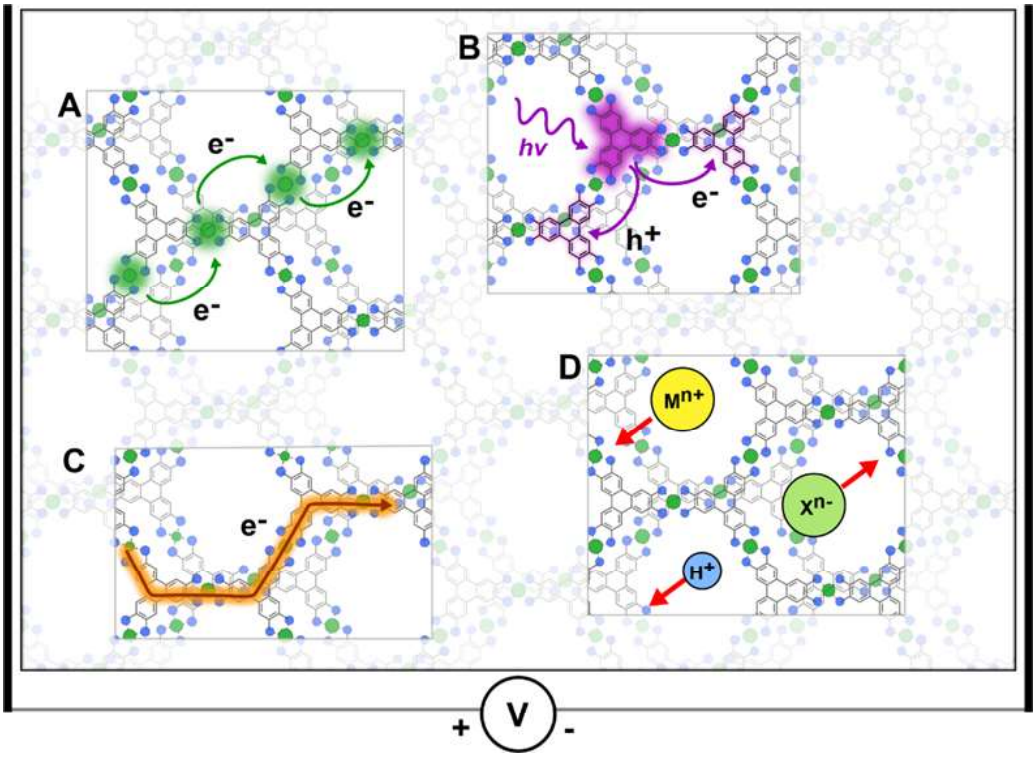

Figure 24. Schematic representation of the four types of conduction examined in this chapter: (A) semiconducting, (B) excitonic, (C) metallic, and (D) ionic.

From a physical point of view, conductivity is the capacity of a material to transport electrically charged particles (either electrons, holes, or ions) when an electric potential is applied to the material. The conductivity of a material (σ) is inversely proportional to its resistivity (ρ), and it is influenced by the length of the sample (l), its cross-section (A), and the intrinsic electrical resistance of the material (R). These properties are described in equation 11 [411].

$$\rho = R\frac{A}{l} \qquad \text{(Eq. 12)}$$

This equation represents the ideal case of a uniform material with isotropic conduction, meaning that its conductivity does not vary changing its orientation. This behavior is rarely observed in MOFs, as their crystalline structures often provide preferential directions for the

charged particles to move through. In these cases, it is necessary to consider this anisotropic behavior and apply the three-dimensional approach provided by the tensor resistivity set of equations.

As the electric current is achieved through the transport of electrical charges, the density of these charge carriers and their mobility is crucial: the higher the number of charges and their mobility, the better the material will conduct [411]. Regarding electron conduction the two main ways in which the electrons and holes can move through the material are charge hopping or band transport. In case of charge hopping, or hopping transport, the charge carriers transfer between discrete sites on which they are localized (Fig. 25). These sites have no connection between one another. In the opposite case of band transport, the sites interact with one another, forming continuous energy bands in which the charge carriers are delocalized. With this charge transport pathway, there is the formation of a valence band, that is composed by all the electronic levels that are occupied, and a conduction band, composed of all the electronic levels unoccupied in the material, and thus viable to transport the electric current.

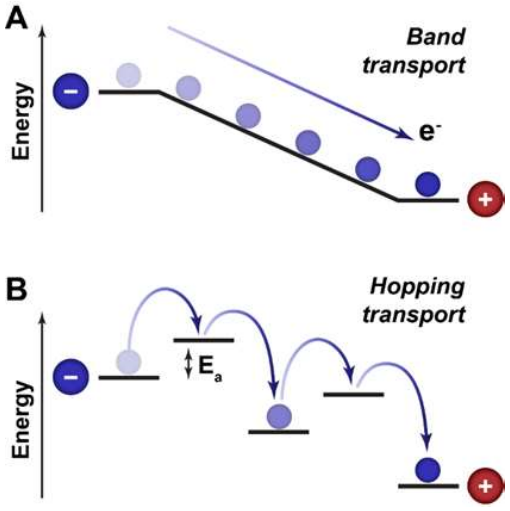

Figure 25. Schematic representations of charge transport: band transport (A) and hopping transport (B).

The energy difference, or band-gap, between the valence band and the conduction band determine the conductivity extent of the material, as a greater difference implies that more energy must be spent to promote an electron from the valence band to the conduction band. A metallic behavior is achieved when there is no band gap between the valence and the conduction band, thus freeing the electrons to pass between one and the other (Fig. 26) [412].

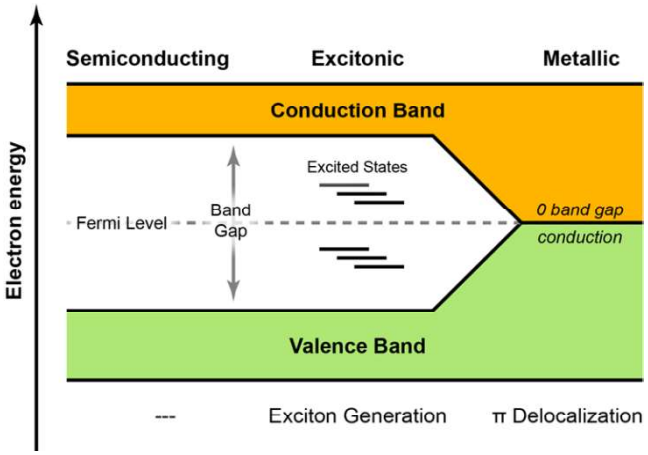

Figure 26. Band-gap structure of different types of conducting MOF materials.

The electric current in ionic conduction relies on the migration of the cations toward the anode and the anions toward the cathode, and the conductivity of the material will depend on the concentration of the ions and their relative mobility.

To facilitate the reading, we decided to divide this chapter into four subsections, based on the type of conduction MOFs exhibit.

5.1. Semiconducting MOFs

A semiconductor is a material characterized by a bandgap of between 0.1 and 3.0 eV and a comparably high electrical conductivity (0.1–100 S/cm). Semiconductors play an important role in the electronic materials field [411,413–417]. Although physical mechanisms for semiconduction in MOFs are yet to be fully explored, the most common conduction mechanism is electron hopping between metal centers [418,419]. In this case, MOFs containing metal centers with mixed oxidation states, *e.g.* Fe^{2+}/Fe^{3+}, typically result in higher conductivity compared with similar MOFs with metal centers that do not show easily duplicity of oxidation number [420]. This can be explained as the facile loss of electrons in metal ions with a large radius and low effective core charge, such as Fe^{2+} being oxidized to Fe^{3+}, with the resulting electron being responsible for conductivity [341,420–422]. Importantly, the choice of the ligand can have a substantial influence on the conductivity of the resulting MOF. 'Non-innocent' linkers (redox-active), can show high conductivities, as the hopping can be metal–metal, linker–metal or linker–linker [423–425]. In the presence of band conduction these concepts remain valid, as it is not critical if the electron levels involved in conduction are discrete or form bands. As long as the energy between the levels is low, the material will have

good conducting properties. This is supported in MOFs containing metal centers with a large number of *d* electrons, such as Fe, Co, and Ni, which present band gap shrinking [31].

Within this framework of knowledge, we can identify three key points in the rational design of semiconducting MOFs. Of most importance is the choice of an appropriate metal center, which is the fundamental factor in determining the band-gap of the overall material. The metal center should be selected to have multiple oxidation states and available *d* electrons, which will be responsible for conductivity, consisting of low redox potentials to favor ion oxidation. Equally important, the metal/linker combination should yield an appropriate topology with a comparably short distance between metal centers. Lastly, the electronic properties of the ligand (*e.g.* π=conjugation, active redox centers, or the presence of radicals), can strongly affect the overall system conductivity. This can provide a smoother flow of the electrons between metal centers or additional charge carriers, in which density is correlated with the conductivity of the material.

A striking example which puts these materials in context is $[Ni_3(HITP)_2]$ (hitp = 2,3,6,7,10,11-hexaiminotriphenylene) [426]. This 2D MOF was first synthesized and characterized by Dincă and co-workers [427], designing the material to exploit the full π-conjugated, singlet biradical character of $Ni(isq)_2$ (isq = *o*-diiminobenzosemiquinonate) to achieve a porous metal–organic graphene analog. $[Ni_3(HITP)_2]$ is easily synthesized by mixing a nickel salt and the ligand in an ammoniacal solution, but unfortunately this synthetic route affords a nanocrystalline material. This results in a practical loss of conductivity. The thin films present good electrical conductivity of 40 S/cm, while the technologically relevant pellet, obtained by pressing powder of the material at high pressure, shows a conductivity of 2 S/cm, with a loss of one order of magnitude. The $[Ni_3(HITP)_2]$ MOF has been studied for technological applications in two different fields. Firstly Miner *et al.* [428] employed $[Ni_3(HITP)_2]$ as an electrocatalyst for oxygen reduction. This important redox reaction has various applications, from hydrogen peroxide production to hydrogen fuel cells. In this work, the authors demonstrate how $[Ni_3(HITP)_2]$ is effectively a good electrocatalyst for oxygen reduction in an alkaline solution, with an efficiency competitive with the most active non-platinum group metal electrocatalysts and good stability to the working conditions over extended periods. Later Park and co-workers [429] utilized $[Ni_3(HITP)_2]$, in tandem with silicon nanoparticles, to design a composite anode material for high-performance lithium batteries. The electrode was formed by thoroughly mixing the silicon and the MOF nanoparticles in a ball mill with various ratios and then pressing the nanoparticle mixture into a pellet. The best electrode, and the main aim of the work, was obtained by a 9:1 ratio of silicon and MOF. This composite electrode showed an

excellent, reversible capacity of 2657 mA h/g, with good cycle stability, as it loses only 1% of its capacity after 100 cycles. The performance increase over pure silicon electrodes is imputable to the channels made available in the pellet by the intrinsic [$Ni_3(HITP)_2$] porosity. The porosity allows the lithium ions to migrate to the bulk of the electrode, and the possibility for the ions to electrochemically interact with the MOF itself at the metal centers. These excellent results create a platform for the design of hybrid silicon-MOF electrodes for classic high-performance lithium-ion batteries, as new and competing anode materials.

Semiconducting MOFs are showing many possible applications in a vast range of technological devices. Wei and co-workers [430] demonstrated that semiconducting MOFs may be used as an electrode material for supercapacitors (Fig. 27). Supercapacitors are a class of devices, defined to be between capacitors and batteries, capable of storing a smaller amount of energy than a battery but with a rapid charge time and higher cycle stability [431]. They are widely used in green applications, such as regenerative braking and as a power backup for random access memories [432]. A good material for this application should exhibit high conductivity and a high density of redox centers that allow a variation of the net electrical charge of the electrode to achieve high capacitance. Also, the possibility to incorporate ions into the material, and balance the change in electrical charge and high structural stability, will improve cycling lifetime.

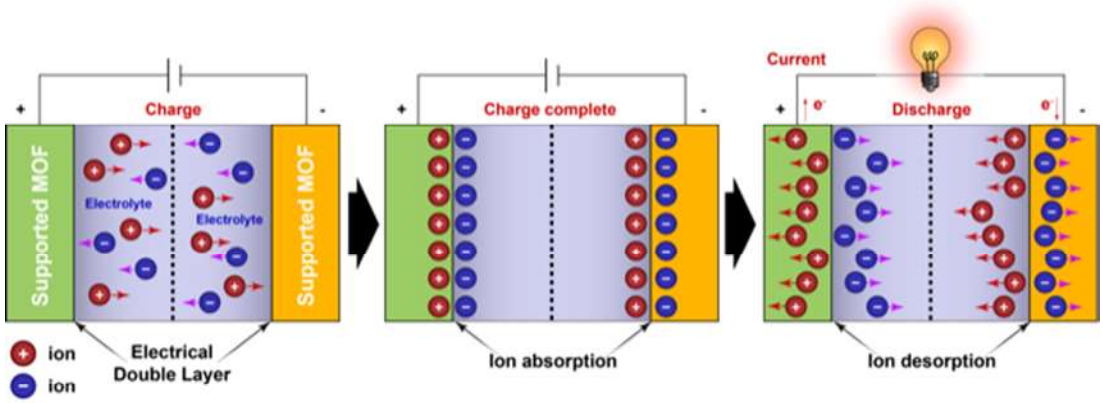

Figure 27. Schematic illustration of a charge/discharge cycle of a supercapacitor.

Possibly a semiconducting MOF has all these characteristics. As an example, Bao and co-workers [433] synthesized a new 2D cobalt MOF, Co-HAB, with the redox-active ligand hexaaminobenzene (HAB), *via* a facile route in which the resultant material is modulated by the synthetic ammonia concentration. This MOF proved to have high intrinsic conductivity, high density of redox-active sites, porosity, and good chemical and thermal stability, rendering it an ideal candidate for this type of application. Remarkably, electrodes constructed with Co-

HAB can store up to three electrons and a sodium ion per ligand, at full charge, with high cycle stability. Therefore, Co-HAB can be considered as a good electrode for supercapacitors, while its capacity to rapidly release stored energy may render it useful in other applications, such as batteries. Presently a good number of MOFs with a variety of metal centers, mostly in the upper part of the *d*-block, exhibit good properties to be employed as electrodes and have been evaluated for this application [434–437].

The first assessment of semiconducting MOFs as electrocatalysts was done by Morris *et al.* [418], successfully reducing carbon tetrachloride with a cobalt metalloporphyrin MOF. For this specific application, it is fundamental to employ a metal center, which is capable to change its oxidation state. This is because a redox reaction is conducted either using the material as a cathode, in which case the substrate will be oxidized and the metal center reduced and re-oxidized by the electric current generated by the reaction, or as an anode, on which the reaction will be the reverse, with the reduction of the substrate. After this proof of concept, more interesting redox reactions were carried out with semiconducting MOFs. For example, the aforementioned use of $[Ni_3(HITP)_2]$ for oxygen reduction, or the work of Clough *et al.* [438], in which a cobalt 2,3,6,7,10,11-hexaiminotriphenylene 2D MOF was assessed as a suitable electrocatalyst for hydrogen production from water. Recently, Hod and co-workers [439] focused on how to improve the catalytic efficiency of these materials.

Concerning the use of semiconducting MOFs in batteries, there are numerous studies on their application as electrodes and host materials [417,440]. The use of MOFs in the engineering of lithium-sulfur (Li-S) batteries is generating a field of great interest, as this typology of batteries is considered one of the strongest candidate to replace the lithium batteries currently in use [441]. Li-S batteries have up to five times higher theoretical capacity (how much power they can release in a set time) and energy density (how much energy they can store) if compared with common lithium-ion batteries (Fig. 28). Moreover, the elements that constitute them are less toxic and comparatively cheaper. Despite their theoretical capacity, Li-S batteries have two main problems that prevent their mass production and commercialization. The first is that the anode expands and contracts by 80% of its volume during each cycle, as the elemental sulfur accepts lithium ions and becomes lithium sulfide. This compromises the contact with the conductive frame of the battery and can lead to a complete failure of the device. The second issue regards the dissolution in the electrolyte and subsequent diffusion and deposition of lithium polysulfides (LiPSs), which disrupt the device functioning and drastically lowers their efficiency and cycling life by poisoning the lithium anode and disrupting the efficiency of the electrolyte.

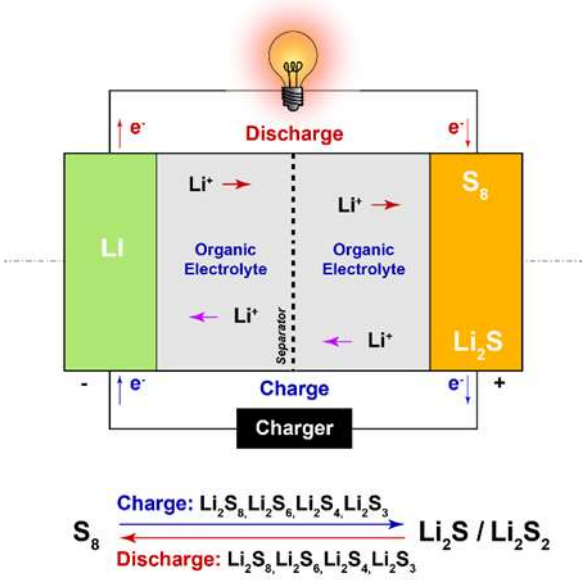

Figure 28. Schematic illustration of the charge/discharge cycle and redox reaction of a lithium-sulfur battery.

In order to address the first problem, Xie and co-workers [442] synthesized a semiconducting cadmium MOF able to provide a scaffold for the sulfur cathode. The porous framework can contain up to 72% in the weight of sulfur, and the linker extended aromatic functional groups allow electric conduction between the sulfur and the MOF. In addition, the MOF proved to efficiently prevent polysulfide species from leaking in solution, thus obtaining a high discharge capacity with good cycle stability. Following this line, Baumann *et al.* [443] utilized a Cu-MOF to encapsulate sulfur and polysulfides chains in a composite electrode material. In this study, they investigated the role of the metal center in the uptake and retention of polysulfide and found that a critical role, due to their Lewis acidity, is played by the partially exposed copper centers on the surface of the nanoparticles that constituted the host material. This suggests that MOFs with a high defectivity, coordination vacancies, or linkers functionalized with Lewis acidic groups could better perform in this role. Moreover, the use of highly conducting MOFs should improve the electron exchange rate with the sulfur hosted in their pores, thus improving the capacity of these devices. In order to address the second problem of Li-S batteries, Zhao and co-workers [444] used DFT calculations to investigate the role of a copper-benzenehexathiol (Cu-bht) MOF as an electrode coating. The DFT study showed how Cu-bht can guide the deposition of Li_2S on the cathode, interacting with the LiPSs in solution, thus improving both the efficiency and the cycling life of the batteries.

Regarding the possibility of applying conducting MOFs in sensor design, Campbell *et al.* [404] demonstrated that this class of materials can be employed in chemiresistive sensor devices. The device setup is quite simple and involves a pellet of the sensing material being placed in contact with two electrodes, while a steady potential is applied. A baseline is then achieved fluxing a carrier gas without the analyte. The device is now ready to detect the analyte, a redox-active molecule which, depending on the material, lowers or enhances its conductivity. In this work, they demonstrated that a copper *o*-phenylenediamine based MOF could be used as a chemiresistive sensor in the detection of ammonia up to 0.5 ppm in the air with a non-negligible relative humidity content (up to 60% for concentrations greater than 5 ppm).

5.2. Excitonic MOFs

An exciton is an electrically neutral quasiparticle, existing in insulators and semiconductors, and corresponds to the bond between an electron and a hole, which are attracted through electrostatics. This implies that the quantum states of the electron and hole are correlated and must lie within the band-gap of the material, although the electronic level through which the charge carriers move can be either discrete or delocalized. The difference between the band gap and the binding energy of the exciton is the minimum energy that a photon needs to generate the electron–hole pair. If a potential greater than the attraction between electron and hole is applied to the material, the exciton is split in its component and a current is established [445–449].

For optoelectronic applications, such as excitonic lasers, molecular crystals, or low-dimensional structures are employed as exciton-generating materials [450]. Here, MOFs play a unique role as a tailored framework generate more excitons than a molecular crystal, and the excitons can be transported more efficiently [451–453]. Recently, collective research has shown that the most efficient MOFs in this area are those containing chromophores as linkers, with an inter-linker separation of 1–2 nm. Chromophores act as antennae to absorb photons and transfer this energy to the metal center or to nearby linkers, where the couple electron hole is created. At the same time, the extended conjugated π-system characteristic of most chromophores permits the stabilization, and the consequent migration, of the excitons for tens or hundreds of nanometers.

Belov and co-workers [454] employed a 2D MOF to propose a new method for simultaneous all-optical data processing and storage. The 2D MOF was $[\{Zn_2(tbapy)(H_2O)_2\}\cdot 3.5DEF]_n$ (tbapy = 1,3,6,8-tetrakis(*p*-benzoate)pyrene; DEF = diethylformamide) and composed of stacked tbapy and zinc planes, supported through van der Waals interactions. This supported

the formation of intra- and interlayer excitons, with different energies of 2.95 and 3.2 eV, respectively, both of which may be independently manipulated with light input at room temperature and have a high formation efficiency. Of particular interest is the possibility of reversibly creating disorder in the crystal lattice with UV photons, achieving non-linear changes of the MOFs optical properties, effectively preventing the formation of the intralayer excitons. As these reversible changes lasted for days or occurred at an ultrafast pace, this work may act as a platform to new MOF applications in advanced photonics.

The need for light in several MOFs to achieve electrical semiconduction may also impart unusual properties to the material, as demonstrated by Castaldelli *et al.* [455]. Characterizing a cobalt naphthalene diimide based MOF (MOF-CoNDI-py-2; NDI-py = N,N′-bis(4-pyridyl)-1,4,5,8-naphthalene diimide), they observed an anisotropy in its electrical semiconduction. This meant that different wavelengths produce either an increase or a decrease in the electronic conduction of the material. Although this phenomenon was known before, this material shows one of the highest responsivities ever reported, and this peculiar characteristic may lead to the implementation of MOFs in new classes of sensors and electronic components.

More recently, Hod and co-workers [456] designed a MOF based electrode utilizing a thin film of the zirconium-porphyrin based MOF-525 supported on an electrically conductive glass (Fig. 29).

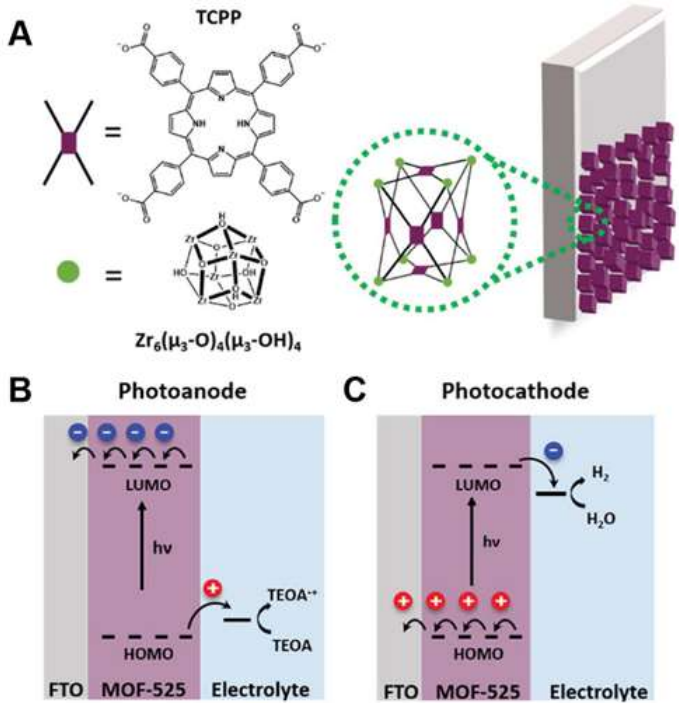

Figure 29. Structure of MOF-525 and the photoelectrode (A). Schematic representation of the photoelectrode working as an anode (B) and as a cathode (C) (Reprinted with the permission [456]. Copyright 2019, Royal Society of Chemistry).

They demonstrated that this electrode could perform both as a photoanode and a photocathode in a photo-electrochemical cell, simply by changing the electrolyte redox nature. This is due to the charge hopping mechanism of the photo-induced current. As there is no charge delocalization within the MOF, the charge-transfer rate of the MOF–electrolyte interface determines the direction in which the current is flowing. Furthermore, this work presents H_2 photocathodic evolution as a proof of concept.

To improve the performance of this new class of electrodes it will be crucial to enhance the charge transport capacity of the MOF. On this subject, Hupp and co-workers [457] demonstrated that shorter distances between chromophoric layers are essential. As isotropic conduction is not required in a thin-film electrode, as long its preferential direction remains perpendicular to the conductive support, transport distances and conduction efficiency will be improved by shortening of the pillars between the chromophores that support the charge hopping. By using different pillars in the synthesis of zinc-porphyrin thin-films, bipyridine for a layer thickness of 14.7 Å and DABCO (1,4-diazabicyclo[2.2.2]octane) for 9.9 Å, the transport distances of excitons located on the porphyrin layers roughly tripled for the DABCO thin-film.

5.3. Metallic MOFs

Metallic conductors differ from semiconductors in a key aspect: the band-gap in a metallic conductor is zero. Metallic behavior in MOFs is predominantly due to a strong overlap of the metal center orbitals with those of the linkers [31,419,458–460]. This overlap, combined with a suitable topology, ensures an orbital delocalization over the entire plane of the structure, thus making metallic MOFs metal–organic graphene analogs. This conjugation leads to a continuous distribution of electronic levels. In this way, the material assumes metallic behavior as a null-gap semiconductor. Interestingly, at present only 2D MOFs are known that show metal-like conductivity. The possibility of an anisotropic behavior has been observed in which the MOF crystal behaves as a metal-like conductor in a direction parallel to the electron delocalization, and as a semiconductor in the perpendicular direction. In an attempt to investigate this, Li *et al.* [461] used a combination of machine learning and *ab initio* simulations to predict MOF structures with metal-like conductivity. Although these materials report the highest conductivity among MOFs, to the best of our knowledge there is only one MOF that presents a conductivity higher than 1000 S/cm, Cu_3(bht) as a thin film [462]. Usually, bulk materials, especially if pressed in pellets for the conductivity measurement, present worse conductivity than thin films. This has three main reasons: the concentration of defects in the material rises in bulk materials, the grain borders between each particle do not allow for

electronic delocalization, and the particles are randomly oriented with respect to one another. As these systems are intrinsically anisotropic, most of the particles will be in a non-optimal orientation. The first example of a MOF with metallic behavior was observed in nickel bis(dithiolene) nanosheets by Nishihara and co-workers [463]. A good example of the important intersection between semiconducting and metallic MOFs is $[Ni_3(HITP)_2]$, as a study by Kawai and co-workers [464] on the thermoelectric properties of this material confirmed its intrinsic bulk metallic conduction at low temperatures, previously suggested in a DFT study [465]. The discrepancy between its observed and theoretical behavior depends on the poor crystallinity and high defect density of the material, as ordered staking between the 2D layers is fundamental for the metallic conduction of this material [466]. Unfortunately, the synthesis of new materials is often disregarded as secondary to their characterization and application. Obtaining a homogenous crystalline material is a fundamental step in the development of MOFs as functional materials, as not only is it crucial to understand their true characteristics, but also is vital to the industrialization process that leads to new devices. The defectivity of the material, although sometimes beneficial to the desired properties, is a variable that complicates the understanding of how the material achieves its characteristic properties and it should be considered during the research development. Furthermore, the computational study of Zhao and co-workers [444], focused on the improvement of Li-S batteries, demonstrated that the Cu(bht) shows metallic conduction. Also the electrocatalytic MOF used by Marinescu *et al.* [438] was later characterized at low temperature and also showed metallic conduction. These examples strongly suggest that the two fields are not only related but will both benefit from a more robust general understanding of the chemical and physical aspects that lead to these desired properties.

5.4. Ionic conduction

Ionic conductivity is the ion transport in matter following the application of electrical potential [467]. This property is fundamental in a wide range of applications, such as solid-state batteries, fuel cells, and analytic applications employing it both as sensors and for ion-exchange. Regarding this area, MOFs have been increasingly marked to show excellent potential, mainly due to their large surface area and tunability [468–470]. Here, MOFs allow the formation of membranes capable of fast ion-exchange and, through rational design, we can tailor the diameters of the pores to increase size-based selectivity. In this regard, it has been shown that the presence of smaller passages between pore cavities can significantly improve selectivity, as passing from one cavity to the next requires the ion to undergo dehydration and

subsequently, a full dehydration-hydration cycle takes places in the passage. Furthermore, a charge-based selectivity is possible in MOFs with a non-neutral framework through employing charged functional groups on the linkers which will transfer favorable ions with an opposite electrical charge.

Among ionic conducting MOFs, proton-conducting MOFs stand apart for the nature of the ion transported. This permits different strategies for transport to be employed and shows promising features for their application for fuel cells. We can classify these MOFs into four classes (Fig. 30) [471]:

- *Group 1*, includes the simplest MOF structures. Proton conductivity is sustained by carriers, such as ammonium, that are present in pores as counter-ions.
- *Group 2*, the linkers are functionalized with acidic groups that dissociate and increase proton concentration and mobility within the pores.
- *Group 3*, where globally electrically neutral carriers are present within the pores. These carriers are introduced in the pores after synthesis.
- *Group 4*, significant post-synthetic modifications are performed, *e.g.* metal center or linker substitutions, phase transitions, or the introduction of ordered structural defects.

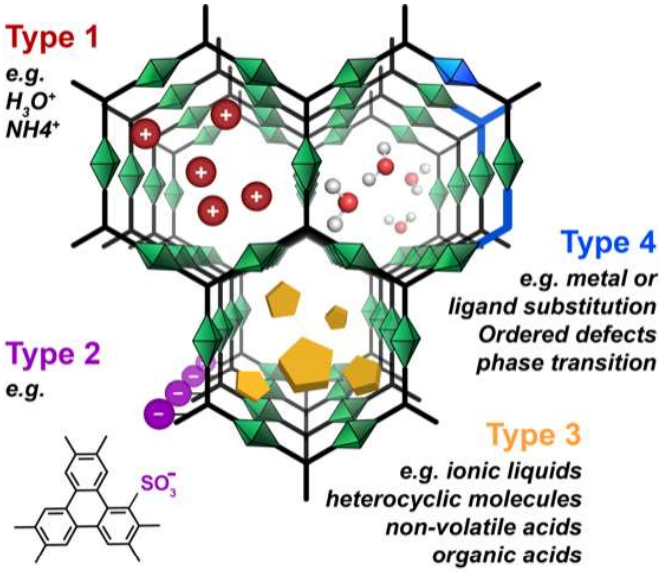

Figure 30. Schematic representation of the four main classes of proton-conducting MOFs.

Regarding applications, the main difference between these materials lies in the presence or absence of water in their pores and their contribution to proton conductivity. Proton conducting MOFs that work in humid conditions rely on a certain quantity of water in the pores to establish hydrogen bond chains which strongly facilitates proton conduction [471]. These materials must be unaffected by the presence of moisture even at high temperature, and display a typical

working temperature from 20 to 100 °C. A remarkable exception to these constraints is demonstrated by Fedin and co-workers [472] where two MIL-101 based systems were synthesized by simply saturating the pores of the MOF with either sulfuric and orthophosphoric acid. These systems showed excellent proton conductivity at high temperatures ($1 \cdot 10^{-2}$ S/cm at 150 °C with a relative humidity of 0.13 %), comparable to commercial Nafion, a sulfonated tetrafluoroethylene based fluoropolymer-copolymer widely used as proton conductor and often referred to as a benchmark.

To approach higher or lower temperatures, we need to resort to anhydrous proton conducting MOFs. These materials have a wider range of temperature in which their conduction property is maintained, ranging from −40 to 200 °C, due to the presence of non-volatile acids and/or organic molecules in their pores. The shortcoming of these MOFs is their proton conductivity, as is generally lower than that observed for water-containing MOFs.

To rationally design an ionic conductor, primary considerations are required pertaining to the kind of ion, the MOF should be tailored for and in what conditions it should operate. For non-protonic conductors one of the most important features is the pore diameter, as ions with a larger solvation sphere need larger pores to pass through the material. It is also crucial to obtain a material that will not be damaged by moisture. Regarding proton conducting materials, the first step is to decide if the MOF will be exposed to humid environments or if the working conditions will require its absence, in addition to the working temperature of the device. Another important factor to consider is the presence of protonic carriers in the pores of the material not bound to the framework, as if they leak out of the material, its proton conduction will diminish [469].

Ionic conduction is a crucial property of electrolytes in batteries. Solid-State Lithium Batteries (SSLiBs) have proven to be safer than regular lithium batteries with liquid electrolyte and are thus good candidates for their replacement. The main problem of these devices is the poor Li^+ transport at the contact interface between the solid-state electrolyte and the electrodes, resulting in a poor active loading and cycle rate capability. Wang *et al.* [473] addressed this issue with an interesting strategy by filling the pores of a UiO-67 MOF with an ionic liquid (IL) that contains Li^+ ions. This material was used as a linker between the electrodes and a metal oxidic solid-state electrolyte. As the MOF is an excellent Li^+ carrier, it reduced the interfacial resistance between the two components, providing a good ionic transport between the cathode and the solid electrolyte. To tether the MOF to the solid electrolyte it was sufficient to press the porous material on the surface of a metal oxidic pellet, commonly utilized in battery prototypes. The hybrid solid-state electrolyte composed of the MOF and metal oxide showed

high ionic conductivity ($1.0 \cdot 10^{-4}$ S/cm), a chemical window of 5.2 V and achieved good compatibility with the lithium anode due to the nano-wetted MOF. The working battery created displayed reasonable recyclability and an improved rate capability. The same concept has been developed by Kitagawa and co-workers [474] that demonstrated how the pore size of the MOF and the loading of the ionic liquid influences the proton conductivity of the material. Using PCN-777, with a cavity diameter of 3.5 nm, the surface area was measured with different loading percentage of the IL (emi)[$N(CN)_2$] (1-ethyl-3-methylimidazolium dicyanamide, proton conduction of $2.8 \cdot 10^{-2}$ S/cm). At low loading (between 12.5 and 37.5 % of pore volume) they observed the formation of the first layer of ionic liquid strongly interacting with the MOF scaffold and thus lower conductivity that the pure IL. Increasing the loading (from 50 to 75%) follows the formation of the second layer of IL, that loosely interacts with the first. Reaching a loading of 87.5% a bulk is established in the pores. This hybrid material, remarkably, reaches its full conducting potential at 63.5 % of loading, as the void space in the pores allows a high and fast ion diffusion. Moreover, higher temperatures increase the proton conductivity, reaching its maximum at around 10^{-2} S/cm at 126 °C.

Ion conducting MOFs have been employed in Li-S batteries. As we discussed in a precedent subsection, one of the main problems of these devices is the migration in the electrolyte and the subsequent precipitation of lithium polysulfides. To mitigate this problem Zhou and co-workers [475] designed a MOF membrane to intercalate between the electrodes of the battery. By choosing a MOF with pores of a suitable diameter, the membrane allows the migration of the smaller lithium ions while blocking the PLiSs. The work of Li and co-workers [476] expanded on this principle by comparing different MOFs and determining that other crucial aspects besides the pore diameter must be considered for the optimal operation of the device. In particular, the packing density of the material should be sufficient to prevent leakage of PLiSs between the MOF particles, while remaining as thin as possible in order to maximize the Li^+ migration. Also, there should not be side-reactions between the membrane and the electrolyte during the charge and discharge processes, and the membrane should be tailored to a specific voltage window in order to achieve a stable device that best performs at the desired conditions.

Electrochromic devices employ an electrical potential to modify their optical properties. This class of devices finds its applications as darkening mirrors or windows, smart glass, and displays. It is for this last application that Li *et al.* [477] designed a Na^+ conducting MOF as an ion-transport electrode. Here, the authors synthesized two nickel MOFs with linkers containing 1,4,5,8-naphthalene diimide functional groups acting as redox centers. As the voltage is applied

to the material, the organic ligands change their oxidation state and the sodium ions enter the pores to balance the electric charge. These two materials demonstrated rapid multicolor switching and high cycle stability, with high optical contrast.

5.5. Summary

Although much thorough research has been performed in the last few years to characterize, and rationalize the conduction properties of MOF materials, reticular chemistry still has a lot to offer to these systems. Even if electronic and ionic conducting MOFs are now *a priori* rationally designed to enhance their properties and augment their stability to harsh working environments, we still need to have better control over the material shape, size, and uniformity. These features are fundamental to achieve industrially applicable materials with less waste, better efficiency, and scalable, reliable manufacturing process. Regarding the fundamental aspects of these hybrid materials, much has been investigated and rationalized in the last five years, but numerous challenges still need to be addressed. In particular, there is little known about electron conductive MOFs with mixed metal centers and/or mixed linkers. This field could be promising, as correct doping of MOFs, done either directly in the synthesis or by post-synthetic metal or ligand exchange, could lead to an increase in conductivity as demonstrated by proton conduction. Furthermore, an increase in the number of MOFs with isotropic conduction pathways is desirable. As the orientation of the MOFs would not impact their properties, these materials should be easier to pack and manipulate, thus facilitating their application in electronic devices. From an applicative point of view, this class of materials is one of the most promising in the further development of lithium-sulfur batteries, a field in which they can perform as electrode materials, separators, electrolytes, and electrocatalysts.

6. Artificial Photosynthesis

Tremendous climate changes have occurred over the last years due to the constant release of carbon dioxide into our atmosphere as a consequence of the consumption of fossil fuels as the main source of energy. To stop this trend, new approaches to generate “clean and renewable” light and energy sources [478], including energy conversion and storage are key topics of current research. Several options for a CO_2-neutral production of fuels have been discussed [479]. Artificial photosynthesis is one concept within integrated devices that combine energy conversion after harvesting of sunlight and (consecutively) fuel production by energy during chemical bond-formation. In nature, light harvesting and energy-transduction occur in chloroplasts (Fig. 31 A) within highly structured lamellar membranes, called thylakoids [480].

These exhibit two different morphologies: cylindrical stacked grana and interconnecting, unstacked stroma lamellae [481] that accommodate all the molecular machinery required to perform photosynthesis. Here, asymmetry in structure and protein distribution between both thylakoid morphologies ensures the directionality of charge generation and transport [482].
Photosynthesis comprises three major steps and starts with the collection of photons in the spectral range of 400–700 nm by outer antenna chromophores within the thylakoid membrane, *i.e.* chlorophylls and carotenoids (Fig. 31 B). Next, the absorbed energy is relayed by directed energy resonance transfer reactions between chromophores within the antenna complex and delivered to the centered photosystem II (PSII). In the third step, charge separation occurs in the reaction center of PSII *via* electron transfer. The overall process from photon collection to the reaction center occurs with more than 95% efficiency [483].
Challenged by nature, great efforts are taken to mimic light harvesting and energy conversion in artificial materials with efficient and directed energy transfer. Different multi-chromophore systems [484–492] have been presented including DNA [493], polymers [489–491], polysaccharides [488], but also vesicles [492], dendrimers [494], and protein assemblies [495–498]. Absorbing chromophores are chosen from porphyrins [487] and carotenoids [499]. Enhanced artificial systems make use of an aggregation-induced emission (AIE) [500] in chromophores, such as cationic diclophane [501], tetraphenyl ethylene [502], or amphiphilic pillar[*n*]arenes [490,503] and calix[*n*]arenes [504,505]. Here, AIE fluorophores act as donor systems for directed Förster-based energy transfer to *e.g.* organic dyes [506,507]. Structured, porous systems as new materials for artificial light harvesting activities are promising since they facilitate an ordered arrangement of chromophores. This approach has been realized in mesoporous silica [508–510], zeolites [511], COFs [512–514], hybrid nanoparticles [515], but also hybrid cationic perovskite solar cells involving photonic crystals [516] or MOF-derived zinc oxide [517].

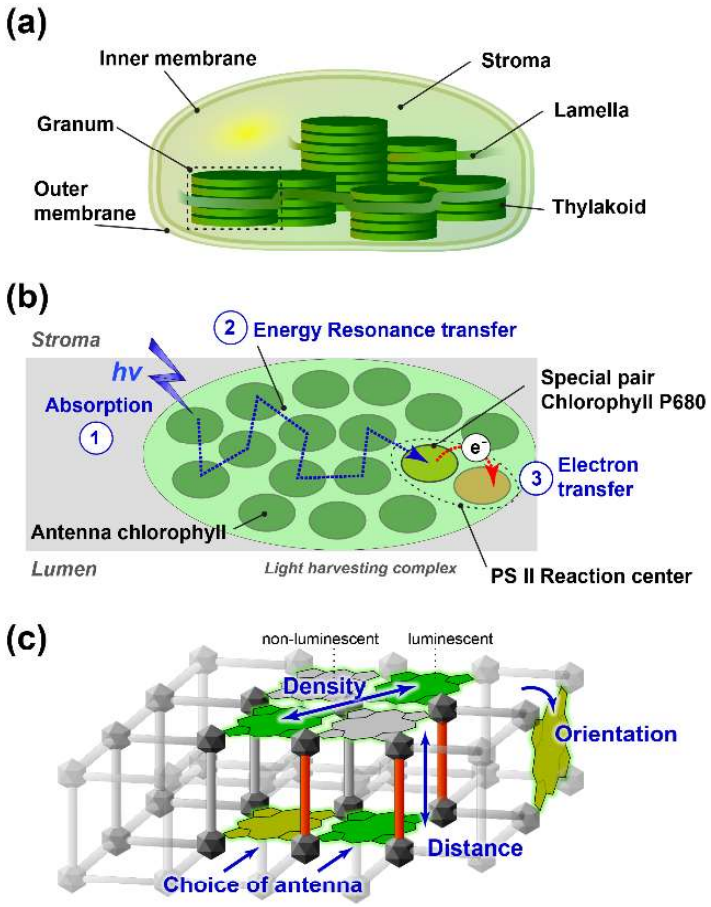

Figure 31. Photosynthesis in nature and artificial MOFs. (A) Representation of a chloroplast. (B) Three steps of light–energy–charge conversion in the light harvesting complex embedded in the thylakoid membrane (grey): absorption, energy resonance transfer, and electron transfer. (C) MOFs hold great promises for artificial photosynthesis systems due to their modular and tunable framework.

The long-range order, high crystallinity, synthetic versatility, and nearly unlimited host–guest chemistry of MOFs position them as a unique platform to design materials for light harvesting, charge transport and next-generation energy storage technologies. The orientation of antenna molecules within the framework and the distance between chromophores can easily be tuned, *e.g.* by using linkers with different lengths in an isoreticular approach (Fig. 31 C; red OBUs). The density of 'light-absorbing' units, *i.e.* the chromophoric linker or guest molecules but also luminescent metals like lanthanoids, can be varied in heterogeneous MOFs by the addition of non-luminescent species—as depicted for non-emitting antenna molecules (Fig. 31 C; grey antennas). Similarly, we have the free choice to add different types of antenna molecules (Fig. 31 C; light green antennas) or to mix luminescent metals. The high flexibility in structure and chemistry allows the incorporation of virtually any chromophore, sensitizer, or mix of both into the framework adding orthogonal absorption and emission properties originating from each of

the units to the designed framework. MOFs have therefore the substantial potential to foster all three consecutive steps in photosynthesis, especially considering their application for light harvesting and solar-cells is still at the early stage.

In the following sections, we will hence discuss the physics behind each phenomenon and review how chemistry realizes them in artificial MOFs. Similar to light harvesting complexes in nature, various chromophore classes like porphyrin-derivatives [518–520] and sensitizers have been employed as a light-absorbing antenna in MOFs. We will start the chapter with a short overview. More comprehensive reviews on incorporated light-absorbing units can be found elsewhere [521–524]. Directed energy transfer from an emitting donor to a receiving acceptor molecule benefits from the possibility of hierarchical synthesis as well as the precise control over position and orientation. Due to the high structural variability of MOFs, several energy processes between ligand–ligand, ligand–metal, metal–metal but also between guest molecules and the framework itself can pass on the absorbed energy from the antenna molecule. We will discuss the underlying mechanisms of the energy uptake and energy transport processes and reveal how MOFs are designed for directed energy transport processes. The last section is dedicated to charge-transport processes in MOFs and potential steps towards their application in photo-voltaic cells.

6.1. Light harvesting

The first step in photosynthesis is light harvesting, *i.e.* the energy uptake within the material, by absorption or inelastic scattering of the incident (solar) radiation. In recent years, various photosensitive compounds have been introduced to the MOF field with three different purposes. They contain moieties that act as: (*i*) chromophores responsible for luminescence and (non-linear) photonics, (*ii*) sensitizers, which further distribute energy to neighboring units and (*iii*) photo-switches, which are the source of photo-responsiveness leading for example to changes in conductivity [525]. As photo-switchable compounds have been reviewed recently [524], we mainly focus on photosensitive compounds with a static optical response in the following section. These include luminescent metal clusters and organic molecules. The latter can be incorporated either actively as the linker or passively as guest molecules within the framework.

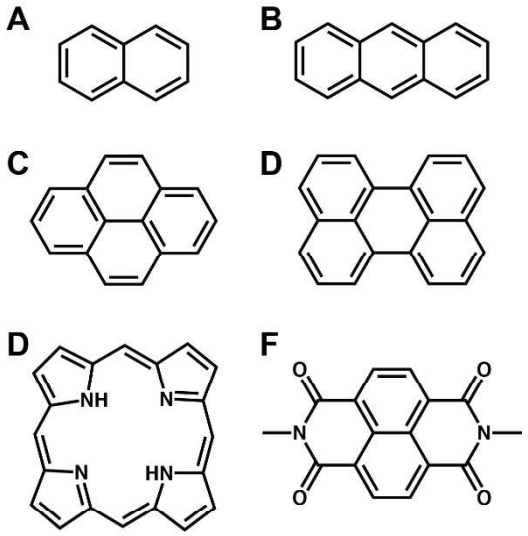

Figure 32. Chromophoric linkers applied in MOFs. (A) Naphthalene, (B) anthracene, (C) pyrene, (D) perylene, (E) porphyrin, and (F) naphthalenediimide (Reprinted with the permission [524]. Copyright 2019, John Wiley & Sons).

To act as chromophore or sensitizer, photosensitive compounds usually respond to light in the spectral range between 200-1000 nm, leading to a transient excitation into an electronically excited state of the compound within femtoseconds. In luminescent metals (*i.e.* lanthanoids) 4f-4f electron transitions are involved during absorption and de-excitation [526]. Absorption in organic fluorophores, usually within a large π-conjugated system (Fig. 32) involves transitions between the electronic singlet ground and excited state. De-excitation from the excited state occurs radiatively or non-radiatively: the molecule de-excites energetically either back directly to the electronic ground state on the pico- to the nanosecond time scale, or it decays *via* other excited electronic states within the same molecule. Alternative pathways comprise the energy transfer to neighboring units within the MOF when returning to the electronic ground state (see section 6.2.). In luminescent MOFs, organic chromophores show emissive relaxation from the excited singlet or triplet state to the ground state, which results in either fluorescence or phosphorescence depending on the nature of the excited state. The nature of de-excitation, however, strongly depends on the chemical surrounding of the photoactive compound within the MOF. Internal coupling to neighboring acceptor units can strongly affect their photoluminescence. To design MOFs for optical sensing, energy storage or other optoelectronic applications, it is crucial to understand the underlying photophysical and chemical processes of the absorbing moieties within the framework. Using MOFs as a platform for systematic studies of photosensitive units, different aspects and mechanisms of

chromophoric MOFs have been elucidated. Their findings and applications have been evaluated previously in excellent reviews on luminescence [391,527–530], sensing [348,391,527,529,531], artificial photosynthesis [521–524], photocatalysis [523], optoelectronics [348,350], photonics [529,532–534], and lasing [529,535]. Among luminescent materials, organic dyes are the most common fluorophores. These comprise resonant and charge-transfer compounds [528]. In the first case, emission originates from the excited state of a π-conjugated system, which is the basis of the most common dye families including boron-dipyrromethenes (Bodipy), fluorescein/rhodamines, porphyrins and cyanines [536]. Porphyrin linkers have been used as primary building blocks in MOFs for light harvesting purposes [518,537–539]. Charge-transfer dyes, on the other hand, rely on an intermolecular charge-transfer transition as it is the case for dansyl and coumarin derivatives. Its application was shown in optoelectronic and photoactive MOFs [540,541]. Organic dyes offer high brightness, quantum yield, and large molar absorptivity in the ultraviolet (UV) and visible (Vis) spectral range, however, they often suffer from low photostability [542]. Moreover, most organic chromophores do not absorb in the near-infrared (NIR) and hence miss major parts of the solar emission spectrum as a light harvesting agent. In contrast, transition metals exhibit primarily a stable emission (although at low absorptivity), long lifetimes, and high quantum yields. They are found in d^6, d^8, and d^{10} complexes and frequently used as photosensitizers *e.g.* in Ru^{II} polypyridine $[Ru(bpy)_3]^{2+}$ complexes (with bpy being, for example, 2,2′-bipyridine) to dope MOFs in the visible range [543,544]. The observed phosphorescence is due to the metal-to-ligand charge transfer (MLCT), which leads to oxidation of Ru^{II} to Ru^{III} and reduction of the polypyridine ligand [545]. Due to their high redox-activity, Ru^{II} often shows additional photo-induced electron transfer in MOFs, as between $[Ru(bpy)_3]^{2+}$ (Rubpy) and co-carboxylate clusters [546]. Bpy-based complexes in combination with Os^{II} or Re^{I} are equally attractive due to the long-lived and intense luminescence and redox activity. Current research focuses primarily on Ru, Os, or Re chromophores MOFs with Zn or Zr-based nodes [547]. The solar light reaching the earth's surface comprises radiation between the ultraviolet, visible and infrared range. Its total energy is spectrally distributed with about 3-5% in the UV (below 400 nm), 42-43% in the visible light (400-700 nm) and 52-55% infrared (above 700 nm) [548,549]. Most catalysts, semiconductors, and porous materials, like MOFs, primarily absorb light in the UV/Vis range. Over the last years, different approaches have been introduced beyond organic dyes and transition metals to extend the absorbing properties in MOFs by semiconducting quantum dots (QDs), core-shell nanoparticles, and lanthanoids [550–552]. Semiconducting quantum dots are employed as

sensitizers in MOFs. These particles with sizes ranging from 2 to 10 nm employ atoms of the group II and VI, *e.g.* CdSe, CdTe or group II and V, like InAs and InGaP. When being excited by light, the emission wavelength of the quantum dot is size-dependent. This effect allows for tuning the color by size control and for addressing the full spectral range from the UV/Vis to the NIR. Aside from excellent tunability, they exhibit a broad absorption and stability during illumination. For excellent light absorption, the emission band of the QD needs to be chosen such that it has the largest overlap with the energy absorption of the MOF material, which can simply be adjusted by the size of the particle. Due to the facile surface functionalization, they are often added to MOF surfaces by PSM. Recently, CdS nanoparticles were employed to decorate Eu-MOFs for enhanced photo-electrochemical properties by CdS using a broader spectral range for light harvesting [553]. In a similar approach, CdTe QD decorated Eu-MOF composites served as photo-anode in a photovoltaic device [554]. The incorporation of QDs into MOFs, however, is still challenging and a target of current research.

The last group of photoactive species exhibiting extended absorption in the NIR are lanthanoids. Most lanthanoid ions are luminescent and their emission wavelength ranges from UV (Gd^{III}) through visible (blue Tm^{III}, green Tb^{III}, orange Sm^{III}, and red Eu^{III}) to NIR (Pr^{III}, Nd^{III}, Er^{III}, and Yb^{III}), while Dy^{III} shows luminescence both in the visible and NIR region. Lanthanoids have the electronic configuration of [Xe] f^n ($n = 0–14$) and their emission primarily originates from f–f transitions. Following Laporte's rule [555], their spin-forbidden emission is usually faint, but with sharp emission lines and long-lifetimes. Due to their low sensitivity to environmental influences, lanthanoids are incorporated into MOFs with increasing occurrence over the last years [556–560]. Since direct excitation of lanthanoid ions hardly leads to photoluminescence, indirect excitation *via* a second sensitizer, also called the antenna effect, is employed (Fig. 33). The excitation is mainly described by a ligand-to-metal energy transfer or Förster-type energy transfer. Light is absorbed by the MOF organic linker, followed by energy transfer between the linker and metal ion and by consecutive emission.

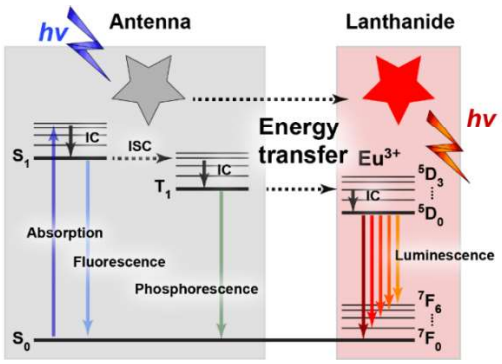

Figure 33. Enhanced luminescence in lanthanoids due to antenna sensitizer. After photoexcitation of the ligand, internal conversion, and intersystem crossing, energy transfer between the linker and the lanthanoid ion lead to photoluminescence.

6.1.1. Upconversion and multi-photon processes for extended absorption in the NIR

Upconversion (UC) relies on non-linear photophysical processes, in which the sequential absorption of multiple photons of low energetic radiation leads to the population of real, intermediate excited electronic states followed by the emission of radiation shorter in wavelength. In combination with MOF/composites structures, it has been strongly promoted and introduced to the field together with so-called upconversion nanoparticles (UCNPs). These inorganic, crystalline nanomaterials convert NIR laser excitation or sunlight into shorter emission in the UV/Vis range for various applications including biology [561–563], sensing [564], theranostics [565], and (super-resolution) imaging [566].

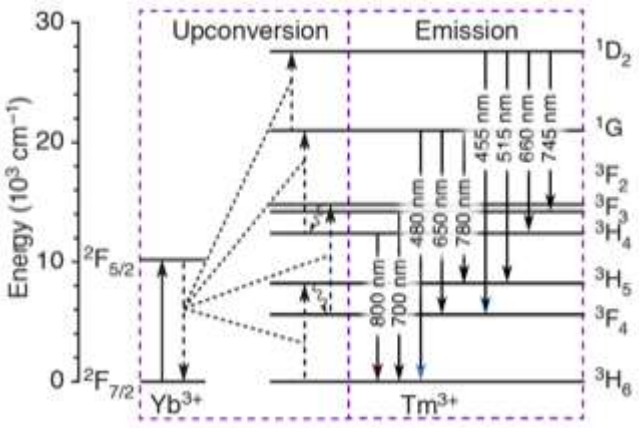

Figure 34. Upconversion in Yb^{3+}/Tm^{3+} doped sensitizer/activator ion system. Excitation light (980 nm) is absorbed by Yb^{3+} and its energy is transferred to Tm^{3+} followed by ESA and PA leading to emission in the UV/Vis range.

The multi-photon-based UC process has been reported in inorganic crystalline hosts like $NaYF_4$ that are doped with transition metal ions, *i.e.* lanthanoids, or actinoids. These feature multiple excited states within their $4f^n$ electron shells, which allow for energy coupling and transport phenomena. Trivalent lanthanoid ions, including Pr^{3+}, Nd^{3+}, Er^{3+}, and Tm^{3+} are well suited [567]. On the one hand, their ground-states possess metastable levels that can easily be excited in the NIR range. On the other hand, they offer long-lived high excited states [568] accessible to successive excitations that decay under emission in the blue/green and UV range. Co-doping with ytterbium ions is usually applied due to the strong absorption of Yb^{3+} in the IR (~ 980 nm) and highly efficient energy transfer from Yb^{3+} to other lanthanoid ions (Fig. 34). The underlying mechanism of UC depends mainly on excited-state absorption (ESA), energy transfer upconversion (ETU), and occasionally photon avalanche upconversion (PA) [567,569]. Excited-state absorption (Fig. 35 A) refers to successive multi-photon absorption from higher singlet states [570]. For mixed doping systems based on ytterbium and other trivalent ions, energy transfer upconversion plays an important role. Here, energy transfer between the sensitizer and activator is followed by higher-order excitation. The most efficient processes exciting the activator ion comprise (among others) ESA, higher-order energy transfer reactions (see section 6.2), crossed relaxation upconversion (Fig. 35 B-D) and triplet–triplet annihilation [567,571].

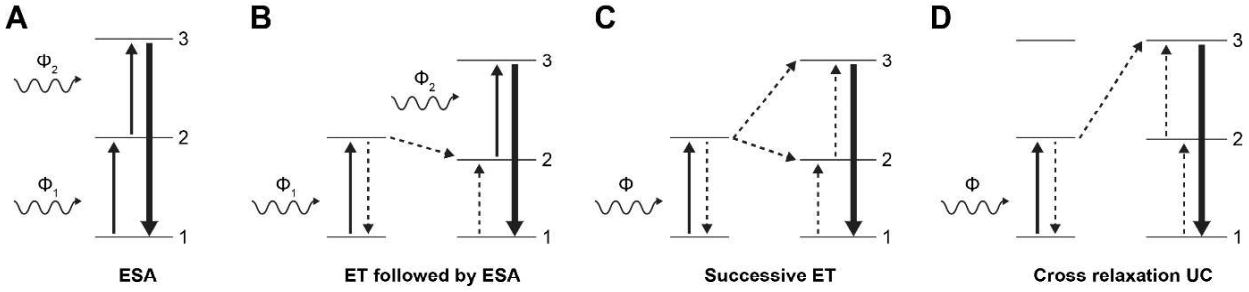

Figure 35. UC within the Yb^{3+}/Tm^{3+} doped sensitizer/activator ion system. (A) Excited State absorption. (B-D) Energy transfer upconversion processes: excitation light (980 nm) is absorbed by Yb^{3+} and its energy is transferred to a secondary ion like Tm^{3+} followed by ESA and ETU leading to emission in the UV/Vis range (Reprinted with the permission [567]. Copyright 1999, IOP Science).

Consequently, Yb^{3+} and Nd^{3+} are used as sensitizers and Er^{3+}, Tm^{3+} and Ho^{3+} as efficient activators in co-doped materials [572]. UC is not only used in inorganic materials like $NaYF_4$-based derivatives or mesoporous silica [573]. It has further been realized in various materials including COFs [574,575], MOFs [539,576,577], and MOF composites [578,579].

In a recent example [576], a series of lanthanoid-based MOFs with tunable UC luminescence emission was prepared. Using Y-MOF (([Y(bptc)$(bdc)_{0.25}(H_2O)(CH_3OH)]\cdot(H_2O)_{0.5})_n$; with bptc: biphenyl-2,5,2′,5′-tetracarboxylate and bdc as starting materials, co-doping with ytterbium and erbium was employed. After NIR excitation at 980 nm, three different emission bands at 520, 545, and 658 nm were observed, which could be assigned to the luminescent transition in Er^{3+} from $^2H_{11/2}$, $^4S_{3/2}$, and $^4F_{9/2}$ to $I_{15/2}$. The UC efficiency due to excited state absorption could strongly benefit from the presence of Yb^{3+} acting as a sensitizer.

The performance of UC-MOFs that show blue-shifted emission due to UC is frequently extended using multi-photon absorption processes occurring within linker or guest molecules. The first demonstration of multi-photon absorbing linker molecules was realized *via* two-photon absorption. A zwitterionic pyridinium linker, 2,5-bis(3,5-dicarboxyphenyl)-1-methyl-pyridinium hydroxide [580] could be successfully incorporated into ZJU-56 MOFs [581], following the multivariate strategy [582]. At the same time, Quah *et al.* [577] reported on multi-photon absorption-excited luminescence from MOFs. They successfully synthesized the chromophoric linker an2py (*trans*,*trans*-9,10,-bis(4-pyridyl-ethenyl)anthracene) and incorporated it into the 3D-MOF $[Zn_2(sdc)_2(an2py)]$ with sdc representing *trans*,-*trans*-4,40-stilbenedicarboxylate. The non-linear two-, three-, four-photon absorption properties were experimentally confirmed and characterized *via* power-dependent measurements of the strong emission around 550 nm after excitation at 800, 1200, and 1500 nm. In the same research dissemination, the second strategy was shown for NIR-absorbing guest molecules infiltrating the framework. The performance of the above-mentioned an2py-derived MOFs [577] could be further enhanced and extended by introducing guest molecules into the voids. Here, an2py served as a sensitizer in combination with the guest molecules, anthracene and perylene, that interacted *via* π–π stacking with the framework.

An inverted strategy based on host–guest interaction was presented by Gharaati *et al.* [583] who used triplet–triplet annihilation based UC between the linker, a palladium porphyrin sensitizer Pd(tcpp) and the guest, *i.e.* the annihilator 9,10-diphenylanthracene (DPA) (Fig. 36 A). After excitation of the Pd(tcpp) the excited molecule relaxed to the electronic ground state by transferring its energy to a DPA molecule *via* a triplet–triplet energy transfer. Consecutively, the excited DPA molecule interacted with a second DPA molecule. This led to the deactivation of the first molecule and electronic excitation of the second one. Deactivation occurred by radiative decay to the ground state.

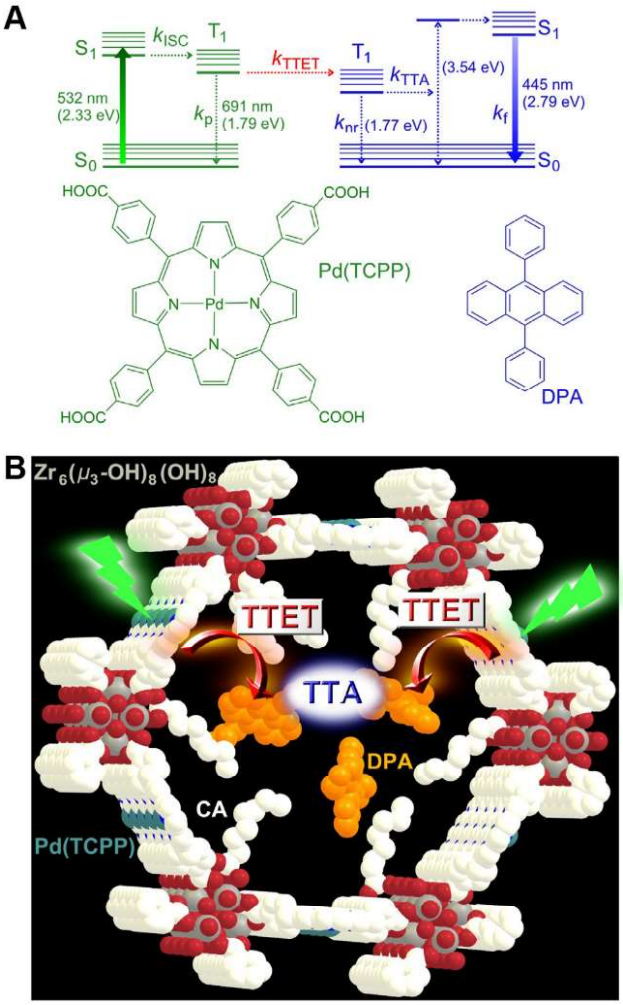

Figure 36. UC based on TTA occurring in CA/DPA@PCN-222(Pd). (A) Jablonski diagram of triplet–triplet annihilation between Pd(tcpp) and DPA. (B) Structure and function of constituents within the framework. Pd(tcpp) as linker and sensitizer; DPA as annihilator. CA acts as coordinated ′solvent′ (licensed under CC-BY [583]).

More frequently, upconversion-based MOF composite materials are reported. These are constructed from different types of nanomaterials in an organized structure and often exhibit complementary properties, but also completely new features. Taking advantage of the tunable structure and defined pore sizes, MOFs can act as protagonist and antagonist by serving on the one hand as a passively linking framework and an active medium on the other hand. Upconversion-based MOF-composite materials are excellent examples for synergistic materials with applications ranging from catalysis [549,584,585], imaging [578,579], and sensing [579], to drug delivery [539,578,585,586], and theranostics [539,578,585,586]. UCNP-MOF composites can be formed *via* self-assembly while mixing UCNP and MOF building blocks during MOF synthesis. Yuan *et al.* [578] realized UCNP-MOF composites using an *in*

situ self-assembly route driven by electrostatic interactions. This research showed that their formation occurs in three major steps (Fig. 37): (*i*) MOF nucleation, (*ii*) UCNP attachment, and (*iii*) nanocomposite formation. All composite nanoparticles exhibited characteristic Er^{3+} emission at 520, 545 and 658 nm identical to the pure $NaYF_4$:Yb/Er UCNPs. The proposed synthetic strategy offers great possibilities for the design of nanocomposites with rationally tuned structure, shape, and multifunctionality, *e.g.* broad-band absorption based on core-shell-shell and hetero MOF layers or UCNPs.

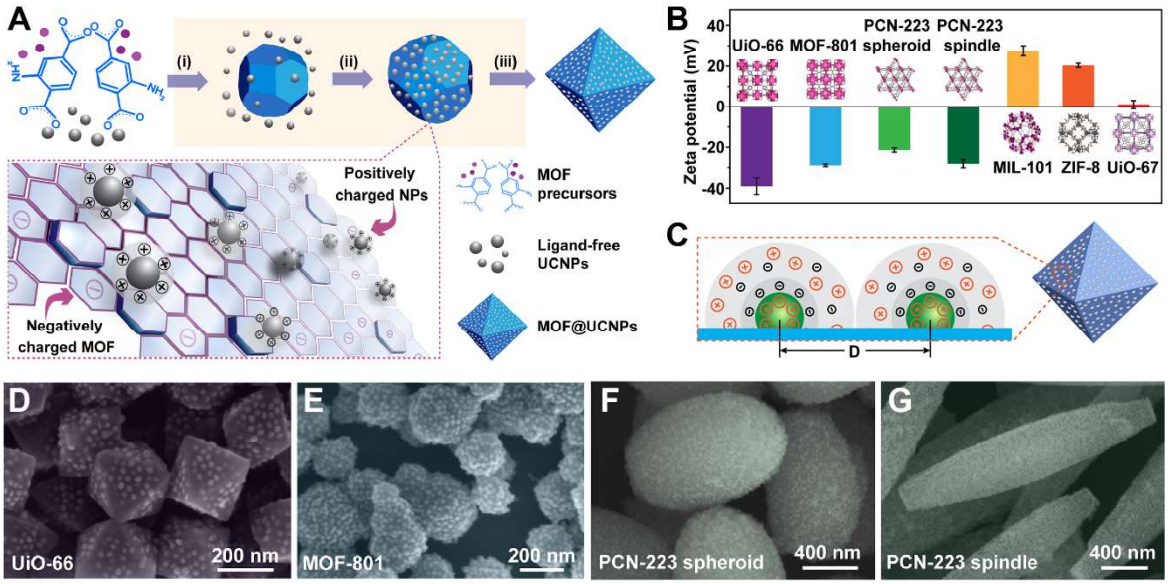

Figure 37. Self-assembly based fabrication of MOF@UCNP nanocomposites. (A) Precursors of MOF and ligand-free UCNPs are mixed during the MOF synthesis. (B) Zeta potential of different MOF species. (C) Minimal interparticle distance amounts twice the electrical double layer of the UCNP. (D-G) SEM images of MOF@ NaYF4:Yb/Er composites made of (D) UiO-66, (E) MOF-801, (F-G) PCN-223 (Reprinted with the permission [583]. Copyright 2019, American Chemical Society).

Another strategy refers to the synthesis of core-shell UCNP-MOF composites where UCNPs serve as a seed during MOF crystallization. Following this strategy, chiral core-shell hybrid nanostructures [579] could be prepared from $NaYF_4$:Yb^{3+}/Er^{3+} nanoparticles formed in oleic acid (OA) (Fig. 38 A). After purification and addition of polyvinylpyrrolidone (PVP), a ZIF-8 [$Zn(me\text{-}im)_2$] (me-im: 2-methylimidazole) layer was coated onto the UCNP nanodiscs to form hydrophilic UCNP@ ZIF core-shell nanostructures. In the last step, $NiCl_2$ as a Ni^{2+} source and chiral L-/D-penicillamine ligands as a sulfide source were employed to form NiSx-L/D NPs that were grown into the ZIF shell, consecutively. These UCNP@ZIF-NiSx-L/D NPs composites feature a strong absorption at 415 and 535 nm upon 980 nm excitation due to the

chirality of NiSx-L/D nanoparticles [587] while luminescence at 540 nm based on transitions in Er^{3+} is strongly quenched by the NiSx-L NPs. In the presence of H_2O_2, the nickel-based nanoparticles within the ZIF shell become degraded as seen by circular dichroism experiments (Fig. 38 B**)**. Concomitantly, the quenched luminescence due to UC at 980 nm is restored with an increasing amount of H_2O_2 (Fig. 38 C).

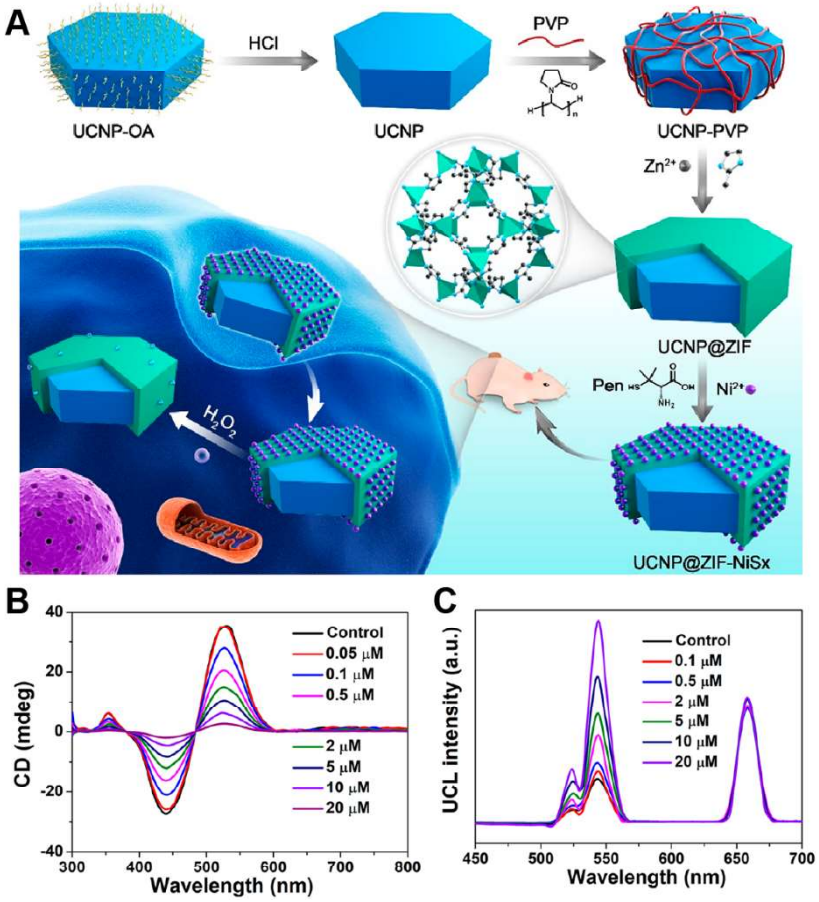

Figure 38. Core-shell synthesis of UCNP@ZIF-NiSx nanocomposites for ROS sensing. (A) Precursors of MOF and ligand-free UCNPs are mixed during MOF synthesis. (B) Circular dichroism and (C) upconversion luminescence spectra of UCNP@ZIF-NiSx in the presence of different concentrations of H_2O_2 *in vitro* (Reprinted with the permission [579]. Copyright 2019, American Chemical Society).

The identical approach [584] was used to grow MOFs on UC nanocrystals UCNPs for NIR-enhanced photocatalysis. UCNP were prepared from NaYF4:Yb^{3+}/Tm^{3+} nanoparticles that emit in the UV/Vis at 350, 360, 450 and 475 nm after 980 nm excitation, due to transitions from 1I6 and 1D2 to 3F4, and 1D2 and 1G4 to 3H6 in Tm^{3+} ions. In the next step, MIL-53(Fe) built from $FeO_4(OH)_2$ octahedra and bis-bidentate bdc-terephthalate linkers were grown on

PVP-coated UCNP. The main absorption of MIL-53(Fe) is in the range of 200-470 nm due to the transitions in the Fe(III)-O clusters with a sharp peak at 450 nm. The designed UCNP@MIL-53(Fe) composites show a complementary absorption behavior in the UV, Vis and NIR at 980 nm, however the UV and blue emission are significantly quenched. Instead of light emission from the UCNP, the excited state energy is transferred from the UCNP to the MIL-53(Fe) shell *via* a Förster-type energy transfer.

Aside from core-shell structures between MOF and UCNP, two further strategies have been presented: polymer assisted core-satellite structures [586] and Janus particles formed from MOF and UNCPs [539,585]. He *et al.* [586] introduced DNA-assembled core-satellite structures for photodynamic therapy. The core of these structures consisted of spherical, porphyrinic PCN-224 MOF particles, made of tcpp ligands and zirconium. $NaFY_4$:Yb/Er UCNP were used to efficiently collect NIR radiation, transfer their energy to the centered MOF particle, and boost the efficiency of PCN-224. Core-satellite structures could be realized with DNA-coated UC nanoparticles that were clustered around the central MOF with the aim of two complementary DNA strands attached to the UCNP and MOF particles, respectively. The resulting structure facilitated 50 % increase in singlet oxygen generation under 980 nm laser radiation.

Structures with NIR-harvesting capabilities and directional energy transport afterward were realized in heterodimeric Janus particles based on porphyrinic MOF nanoparticles and UNCPs [585]. In the first step, multi-core-shell UCNP particles were synthesized from $NaGdF_4$:Yb,Er@$NaYF_4$@$NaYF_4$:Yb,Tm@$NaYbF_4$:Nd@$NaYF_4$ (Fig. 39). In this composite structure, the $NaGdF_4$:Yb,Er core absorbs at 980 nm (Fig. 39 A, green center). Separated by a $NaYF_4$ layer (grey), a two-layer $NaYF_4$:Yb-system (blue/orange) co-doped with Tm^{3+} and Nd^{3+} was added for orthogonal upconversion luminescence (UCL). Doping with Nd^{3+} allowed for additional absorption at 808 nm. Ytterbium mediated directed energy transfer and UCL in Tm^{3+} ions (Fig. 39 B). The last $NaYF_4$ layer prevented environmental quenching and hence ensured high UC efficiency. The four-shelled UCNPs were coated with PVP for subsequent MOF growth on their surface (Fig. 39 C-D) and exhibit orthogonal UCL under NIR light excitation at 808 and 980 nm, respectively.

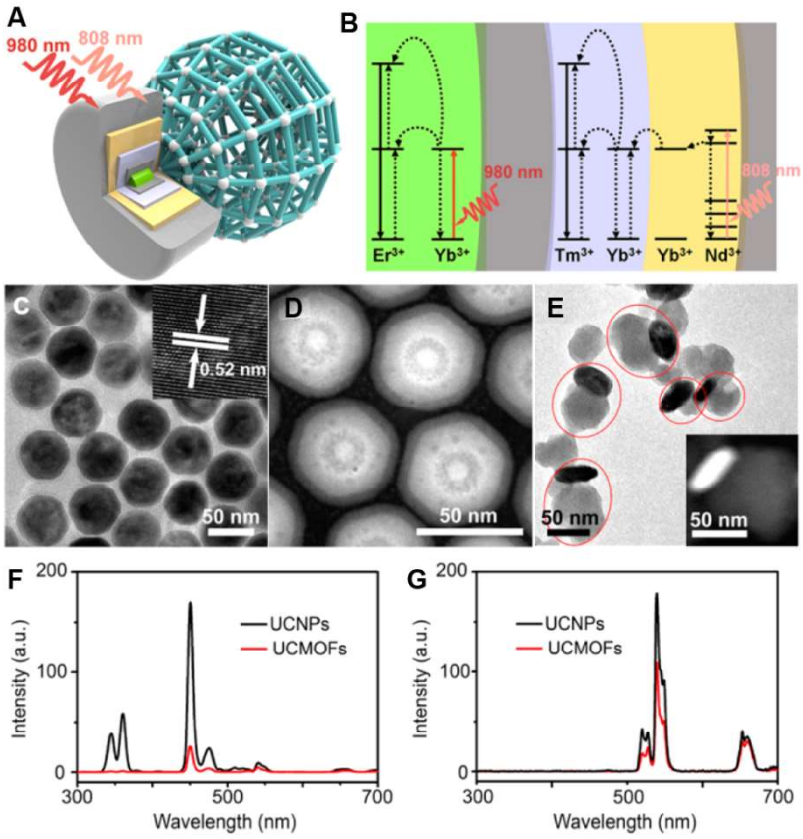

Figure 39. Multi-shell UCNP/PCN-224 MOF Janus particle for NIR-enhanced light harvesting. (A) Scheme of synthesized Janus particles formed of MOF and multishell UCNP. (B) Energy transfer mechanism for orthogonal multicolor UCL. (C-D) TEM (inset: HRTEM) and (D) HAADF-STEM of the four-shelled UCNPs. (E) TEM (inset: HAADF-STEM) image of UCMOFs. (F-G) UCL spectra PVP-coated UCNPs and UC-MOFs upon excitation with (F) 808 nm and (G) 980 nm NIR laser (Reprinted with the permission [585]. Copyright 2017, American Chemical Society).

Upon 808 nm excitation, characteristic Tm^{3+} transitions in the ultraviolet and visible blue dominated (Fig. 39 C-F). Upon 980 nm excitation, only Er^{3+} transitions in the visible green and red were observed (Fig. 39 C-G). The UCL profile of the Janus particles, however, showed that the Tm^{3+} related emission is strongly quenched. A highly efficient resonance-based energy transfer occurred between the UCL and the porphyrin-based MOF. It benefits from short distances between the outer layer of the UCNP and the MOF of 3–7 nm. The efficient energy transfer with the Janus particle facilitated their use for photodynamic therapy based on singlet-oxygen generation in combination with encapsulated doxorubicin in the MOF.

In a recent work by the Jiang lab [549], rationally designed MOF composites made of various materials for efficient light harvesting over the full solar spectrum and photo-catalysis of water were presented (Fig. 40 A, B). The designed UCNPs-Pt@MOF/Au composites employed four

different components: (*i*) core-shell structured UCNPs based on mixed doping of $NaYF_4$ with nanoparticles containing Yb^{3+}, Tm^{3+} and Er^{3+} to absorb NIR radiation (Fig. 40 C); (*ii*) platinum as an electron acceptor that improves charge separation and facilitates photo-catalysis; (*iii*) UiO-66-NH_2 ($Zr_6O_4(OH)_4(bdc\text{-}NH_2)_6$, bdc-$NH_2$ = 2-amino-1,4-benzenedicarboxylate), as a scaffold absorbing at 300-450 nm and (*iv*) plasmonic AuNPs as electron donors that absorb at 500-600 nm. The spatial separation between the platinum and gold NPs by the MOF scaffold ensured enhanced e–h separation within the composite. Concomitantly, UCNPs-Pt@MOF/Au showed a high H_2 production rate of up to 280 µmol/g over the full spectral range (Fig. 40 D). Hot electrons from Au nanoparticles and photoexcited electrons in UiO-66-NH_2 rapidly migrated to the Pt site for H_2 catalysis. Excitation of both systems is further supported by unconverted emission by the UCNPs.

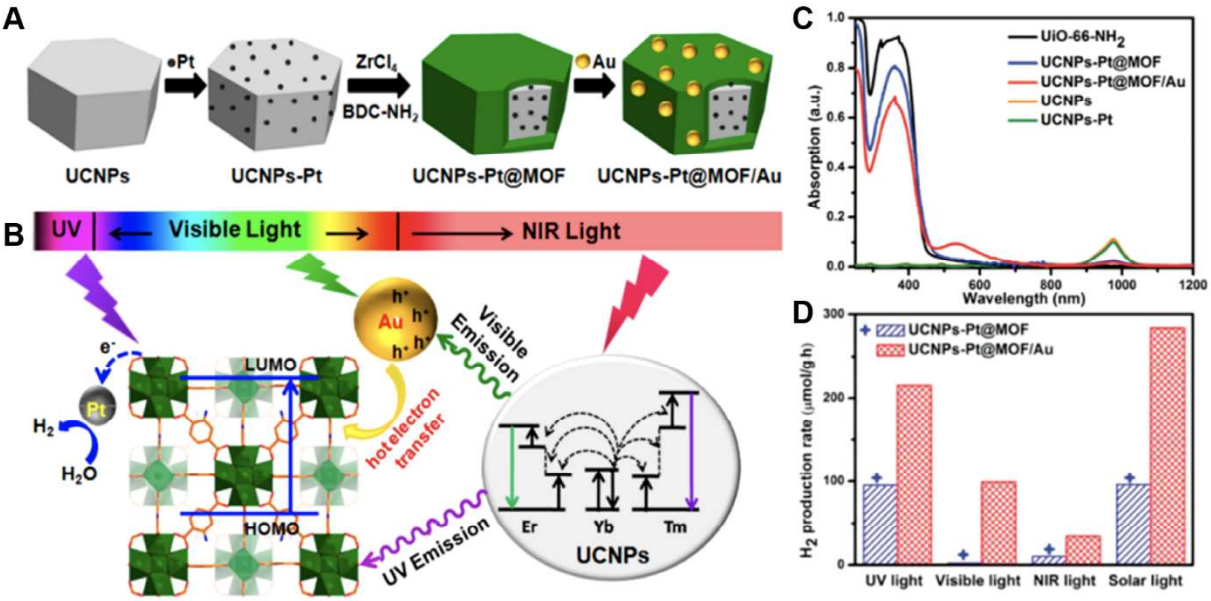

Figure 40. Plasmon and UC enhanced light harvesting in MOF composites. Schematics of (A) the fabrication process for the UCNPs-Pt@MOF/Au composites and (B) the light absorption and involved mechanism of photocatalytic H_2 production. (C) Absorption spectra. (D) H_2 production rate by UCNPs-Pt@MOF and UCNPs-Pt@MOF/Au under excitation in the UV (200-400 nm), Vis (420-800 nm), NIR (980 nm) and solar light (Reprinted with the permission [549]. Copyright 2018, John Wiley & Sons).

6.2. Directed energy transfer reactions

Energy transfer (ET) is a key process for applications like photodynamic therapy, photocatalysis, or the implementation of solar cells. Due to the versatile structure of MOFs, donor and acceptor species can be precisely positioned, distributed, and oriented within the

framework facilitating directed ET. Different models have been introduced to describe ET processes. In solid-state materials, ET processes are normally described as the diffusion of localized (Frenkel) and delocalized (Wannier) excitons, as in semiconductors. MOFs are a special case of solid-state materials since their chromophores show only weak coupling. ET processes in MOFs are usually described by Förster and Dexter ET processes [588,589] (Fig. 41).

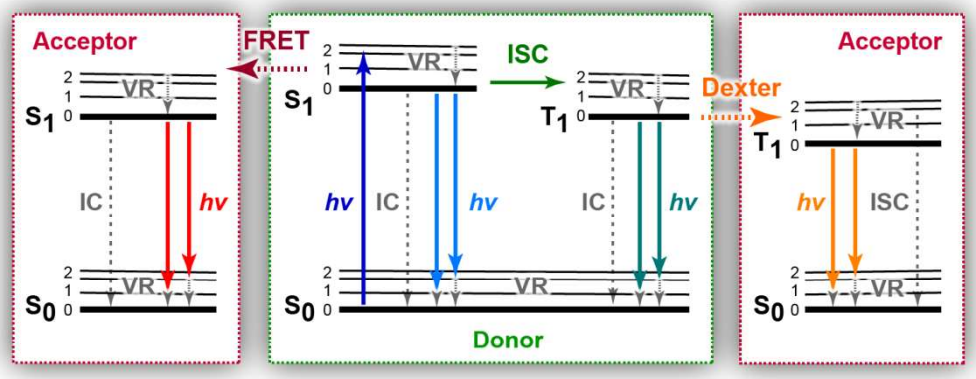

Figure 41. Simplified Jablonski diagrams of Förster and Dexter energy transfer processes. After direct excitation of the donor system from the singlet ground state S_0 to the corresponding excited state S_1, the excited donor D* in absence of an acceptor A can only relax *via* internal conversion, fluorescence, or intersystem crossing to the long-lived triplet state T_1 and consecutive phosphorescence. In the presence of an acceptor, energy can also be transferred *via* Förster resonance energy transfer after dipole-dipole interaction between both excited singlet states or *via* Dexter energy transfer after exchange interaction between the excited triplet states of the D*A system.

Three different protagonists in MOFs can act as donors responsible for energy uptake after light exposure: the organic linker, the metal node, or guest molecules, that might be present. The photoexcitation of usually the organic compound or the metal (complex) leads to a molecular excitation from the electronic ground state S_0 to an excited single state S_1 (Fig. 41). The excited donor relaxes rapidly back to the ground state either non-radiatively *via* internal conversion or radiatively *via* fluorescence or phosphorescence after intersystem crossing (ISC) to its triple-state T_1. Another possibility is the de-excitation *via* electron and energy transport processes to neighboring molecular units within the framework. Electron transport relies on the high redox activity of the excited state molecule [590,591]. Here, the excited donor transfers a single electron to a nearby acceptor resulting in a positively charged donor and negatively

charged acceptor unit (Fig. 42 A). Energy transfer, on the other hand, describes the photophysical process in which the electronically excited donor undergoes a transition to an energetically lower-lying state by transferring its energy to a second molecular species, *i.e.* the acceptor that is consecutively excited to an energetically higher state.

$$D^* + A \rightarrow D + A^* \qquad \text{(Eq. 13)}$$

As stated above, two different mechanisms for non-radiative ET processes are frequently proposed: Förster and Dexter ET transfer (Fig. 42 B, C). These processes reflect two fundamental electron-electron interactions: coulombic and exchange interactions.

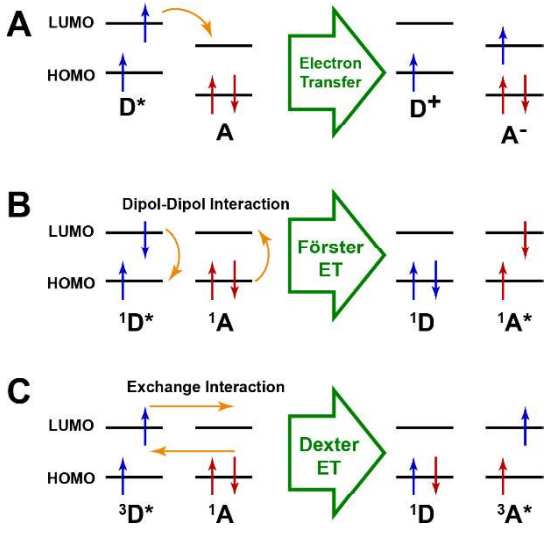

Figure 42. Energy and charge transport processes. Schematics of (A) electron transfer processes and (B) Förster and (C) Dexter energy transfer mechanism.

6.2.1. Förster resonance energy transfer

Förster resonance energy transfer (FRET) describes the distance-dependent transfer of energy between two molecular entities *via* a dipole–dipole (coulombic) interaction [588]. This antenna-receiver like mechanism is distance-dependent and sensitive between 3–10 nm [592]. After photoexcitation of the donor (Fig. 42 B, D*), the chromophore behaves like a dipole emitter showing electronic oscillation in the excited state. These oscillations can couple to the electronic ground state of the nearby receiver, *i.e.* the acceptor. For the ET to be efficient, the energies of donor and acceptor transitions $^1D^* \rightarrow {}^1D$ and $^1A \rightarrow {}^1A^*$ must be nearly identical (hence the term ‘resonance’). The donor de-excites to its electronic ground state non-radiatively

by transferring its full energy to the acceptor, which leads to a subsequent excitation of the acceptor (Fig. 42 B, A*). FRET depends inversely on the 6th power of the D-A distance r [593].

$$k_{FRET} \propto \left(\frac{R_0}{r}\right)^6 \qquad \text{(Eq. 14)}$$

The introduced Förster radius R_0 is dye-pair specific and refers to the distance, at which the energy transfer efficiency is 50%. It reflects the materials properties, relative spatial orientation of both molecules as well as their spectral properties. It depends on the spectral overlap integral $J(\lambda)$ between the normalized emission of the donor and the acceptor (Fig. 43).

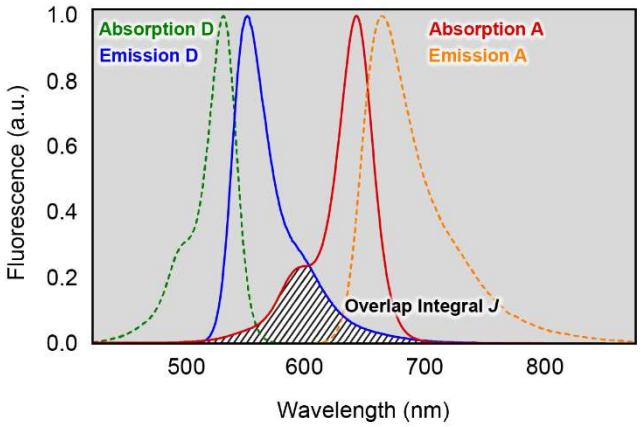

Figure 43. Spectral overlap between donor and acceptor. FRET results from dipole–dipole transitions between singlet-states of the excited D* and the ground-state A; J(λ) is defined based on the normalized donor fluorescence and acceptor absorption from $S_0 \rightarrow S_1$. Dexter ET is usually based on electron exchange between triplet states of the excited D* and the ground-state A; J(λ) is defined *via* the normalized spectrum of donor phosphorescence and acceptor absorption from $S_0 \rightarrow T_{1'}$.

6.2.2. Dexter energy transfer

As discussed above, the excited donor D* can de-excite also *via* internal conversion and intersystem crossing. The non-radiative decay by internal conversion is slow. Emission from the triplet state is spin-forbidden and leads to lifetimes beyond 100 ns. Both processes are sufficiently long enough to render an ET process possible to a close-by acceptor. FRET theory, however, is not suited to describe the energy transport starting from an excited molecule in the triplet state. Dexter ET describes the non-radiative transfer of energy between two molecular units, a donor and acceptor, by a simultaneous intermolecular exchange of ground-state and excited-state electrons (Fig. 42 C, D*). It is also referred to as ’sensitization‘ of the acceptor

with the triplet-excited donor being the 'sensitizer'. For this to happen, the wave function of both units must overlap. The exchange mechanism, therefore, requires quasi-direct contact between the donor and acceptor and is sensitive to distances below 1 nm [594]. The rate of energy transfer and hence the transfer efficiency drops exponentially with the D–A distance r [589].

$$k_{Dexter} \propto J(\lambda) \cdot exp\left(-\frac{2r}{L}\right) \qquad \text{(Eq. 15)}$$

It scales linearly with the spectral overlap integral $J(\lambda)$, which connects the phosphorescence of the donor and singlet-triplet absorption of the acceptor (Fig. 43) [595]. In the equation, L is the sum of the van der Waals radii of both molecules.

6.2.3. ET processes in MOFs

MOFs can be considered as multi chromophore ensembles in which various kinds of ET reactions are possible. These include dye-to-dye, dye-to-metal, metal-to-metal, and guest-to-host ET reactions (Fig. 44). Although different ET reactions can occur simultaneously, MOFs represent an excellent model system to investigate and design directed long-range energy transfer reactions.

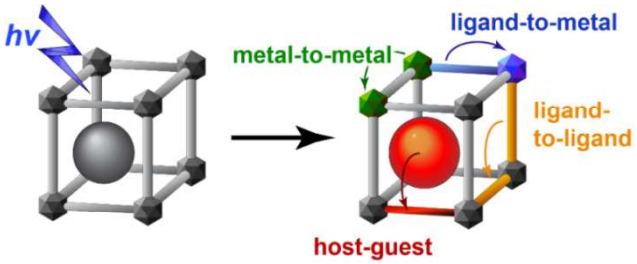

Figure 44. Electronic energy transport processes. Main energy transfer reactions in MOFs between the ligands, the metal clusters, ligand, and metal as well as between guest molecules and the framework. For clarity, only the interaction between guest and linker molecular is depicted.

Over the last years various strategies have been introduced to enhance the reach, directionality, and efficiency of ET processes. *(1)* The efficiency in energy transfer grows with a prolonged lifetime of the electronically excited states. Extended singlet state lifetimes can be obtained by linker rigidification in cyanine dyes. The restricted *cis-trans* isomerization eliminates additional pathways for non-radiative decay, which further enhances the quantum yield of the donor molecule [596]. *(2)* Another important parameter is the spectral overlap between the

excited state spectrum of the donor and the absorption spectrum of the acceptor. Inspired by light harvesting complexes in nature, porphyrin sensitizers are often used for Förster-type ET. Here, a promising approach for the design of enhanced porphyrin-derived linkers is the asymmetric modification of the porphyrin ring to *meso*-link porphyrin that possess enhanced Q band absorption (S_0 → S_1) and overlap integral [597]. *(3)* Directed energy transfer can be achieved by asymmetric arrangement of chromophores within the framework, *e.g.* within heterogeneous MOFs, like pillared Zn(II)-paddle-wheel-based Bodipy-porphyrin BOP-MOF [537].

6.2.3.1. ET reactions between organic molecules

In MOFs, two types of ET reactions between organic molecules can occur: either between ligands or between a guest molecule and a linker. In a pioneering work, Lee *et al.* [537] presented the Zn(II)-paddle-wheel-based Bodipy-porphyrin BOP-MOF (Fig. 45 A), in which FRET occurs between the two types of chromophores. In BOP-MOF, Zn-porphyrin coordinates pairs of Zn(II) ions forming two-dimensional sheets that are pillared by Bodipy struts (Fig. 45 B). With an inter-linker distance of ~15 Å and a good spectral overlap between the zinc porphyrin and the Bodipy, BOP-MOF shows emission only between 650–710 nm (Fig. 45 C) upon irradiation at 543 nm. No emission of the Bodipy linkers between 560–615 nm is observed in contrast to the isostructural BOB-MOF formed of Bodipy linkers (Fig. 45 C). The Bodipy-emission is fully quenched by the efficient linker-to-linker FRET process.

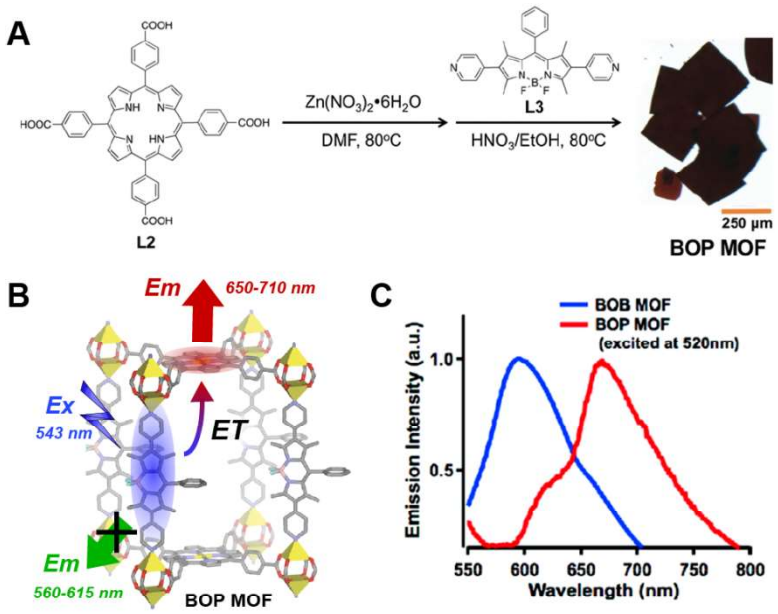

Figure 45. Strut-to-strut FRET between Bodipy and porphyrin linker. (A) Synthesis of BOP MOF. (B) Proposed ET mechanism. (C) Emission spectra after 520 nm excitation (Reprinted with the permission [537]. Copyright 2011, American Chemical Society).

In a follow-up publication, the directional exciton transport within pillared MOF layers was investigated using the controlled collapse of a 3D MOF structure to yield a 2D coordination polymer [598]. First, a heterogeneous, 3D pillared paddlewheel porphyrin containing MOF was formed on a glass substrate in a layer-by-layer fashion (Fig. 46). Layers of coordinated Zn clusters and tetratopic tetrakis(4-carboxyphenyl)porphyrin (tcpp) linkers were separated by bpy linker in a parallel fashion and showed interlayer distance of 14.7 Å. The final outward-facing layers consisted of non-luminescent Pd-porphyrin components (Pd-tcpp). In a subsequent step, SALE was employed to displace bipyridine by pyridine. Using FRET between the tcpp molecules as donors and Pd-tcpp as the acceptor at the final layer, the exciton migration length measured to be 9 Å in the 3D MOF and 11 Å in the collapsed 2D MOF. The over FRET efficiency between two tcpp in consecutive layers remained constant with an inter-tcpp distance of 14.3 Å.

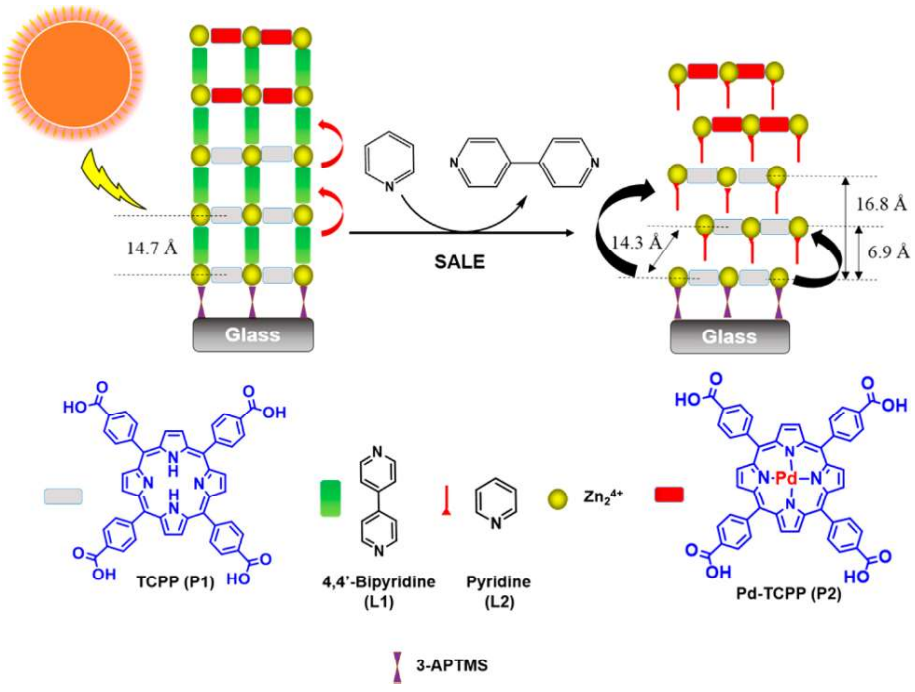

Figure 46. SALE-based collapse of pillared-3D MOFs for directional exciton transport. Free base porphyrin P1 and linker L1 were used for MOF thin films—followed by an even number of layers consisting of Pd-porphyrin P2 and Linker L1 (Reproduced with the permission [598]. Copyright 2016, American Chemical Society).

MOF as crystalline materials can show different properties as either 2D or 3D structures. Cao *et al.* [599] designed and synthesized 2D-MOF layers and 3D-MOFs from hafnium metal centers and mixed ligands to study the linker-linker energy transfer mechanism in 2D and 3D systems. Here, the donor ligand 4,4′,4″-(benzene-1,3,5-triyl-tris-(ethyne-2,1-diyl))-tribenzoate (bte) and acceptor ligand 3,3′,3″-nitro-4,4′,4″-(benzene-1,3,5-triyl-tris-(ethyne-2,1-diyl-))tribenzoate (bte-NO_2) were connected *via* Hf-oxo clusters (Fig. 47 a). The formed 2D MOF had the framework formula $Hf_{12}(\mu_3\text{-}O)_8(\mu_3\text{-}OH)_8(\mu_2\text{-}OH)_6(\mu_1\text{-}OH)_2(H_2O)_2(\eta_2\text{-}HCO_2)_4(bte)_4$ with a 3,6-connected *kgd* topology and consisted of 1-2 layers (Fig. 47 b). The 3D MOF showed no pillared layer structure, but an interconnected network with the framework formula $Hf_6(\mu_3\text{-}O)_4(\mu_3\text{-}OH)_4(H_2O)_4(bte)_4$ with 12-connected Hf_6 SBUs and 3-connected ligands to give 12,3-connected nets of *llj* topology (Fig. 47 c). The arrangement of the bte ligands can be described as two sets of honeycomb sheets perpendicular to each other and interconnected by sharing metal cluster nodes (Fig. 47 d).

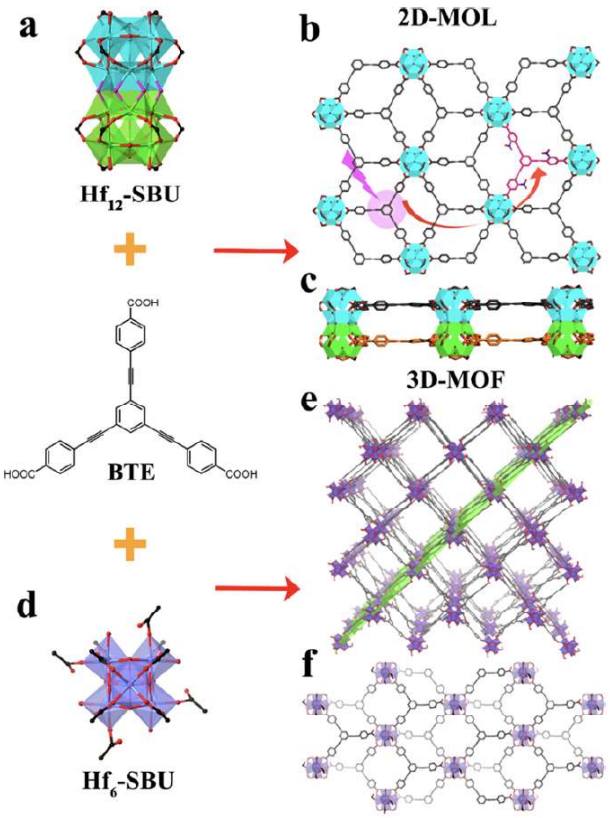

Figure 47. Exciton migration within MOFs in 2D and 3D. (A) Structure of the M12 SBU for the 2D system. (B) Crystal structure of the 2D layer in top and side view. (C) Structure of the Hf_6 SBU for the 3D MOF. (D) Crystal structure of the 3D MOF in top and side view (Reprinted with the permission [599]. Copyright 2017, American Chemical Society).

Owing to the inherent synthetic flexibility of MOFs, hybrid systems with core/shell-like hierarchical structure were recently introduced [600]. Two hierarchically hybridized zirconium MOFs were designed comprising two porphyrin ligands, tetrakis-(4-carboxyphenyl)-porphyrin (t) and its isomeric, "N-confused" porphyrin (NCP; Fig. 48). NCP had the same tetrapyrrolic backbone, but a modified pyrrole ring unit connected to the *meso*-carbon at the *α* and *β'* position. Following a seed-guided solvothermal ligand exchange reaction, NCP_{MOF}@$tcpp_{MOF}$ and $tcpp_{MOF}$@NCP_{MOF} hybrids were synthesized. They possess a class II core/shell structure and photo-physical properties that allow for broadband photon collection from the visible to the NIR region, owing to the NCP chromophore.

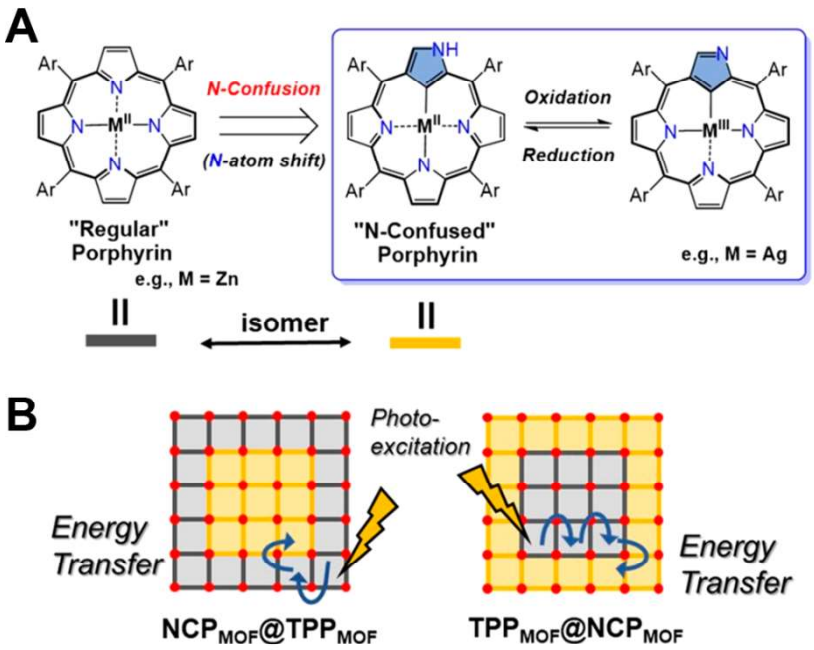

Figure 48. Energy migration in luminescent mixed-lanthanoid MOF thermometers. (A) Chemical structures of regular porphyrin and N-confused porphyrin. (B) Scheme of the photoinduced energy migration from tpp to NCP moieties in the hybrid MOF (Reprinted with the permission [600]. Copyright 2019, American Chemical Society).

6.2.3.2. ET reactions between metal ions and linker moieties

Ligand-sensitized luminescence has been extensively studied in MOFs that contain lanthanoids [559,601–607]. As discussed in section 6.1., emission from lanthanoids results from *f-f* transitions. Upon combination with organic ligands that act as a sensitizer to lanthanoid metal nodes in MOFs, a combined energy transfer and emission in the UV/Vis is observed.

Yang *et al.* [604] developed a single-component, white light-emitting MOF $([Eu_4(obb)_6(H_2O)_9]\cdot(H_2O))_\infty$ *via* self-assembly of the flexible ligand 4,4′-oxybisbenzoate (obb)

and trivalent europium. They observed photoluminescence from Eu^{3+}, after energy transfer from the linker, which could be spectrally tuned depending on the excitation wavelength. An identical behavior was found in two other isomorphic MOFs containing trivalent terbium or dysprosium. In a different approach, Wu *et al.* [602] designed thermosensitive MOFs containing both, Eu^{3+} and Tb^{3+} linked by a dicarboxylate linker (5-(4-(tetrazol-5-yl)phenyl isophthalic acid); H_2L). The isomorphic Ln-MOFs $[LnL(DMF)_2(NO_3)]_n$ (Ln: Eu, Tb) showed white-light emission. After UV excitation, blue emission originating from electron transitions of the H_2L ligand overlapped with green and red emissions by Tb^{3+} and Eu^{3+} after energy transfer from the ligand to the metal ions and between metal ions. Sensitized emission of lanthanoids was not only studied for incorporated metal ions, but also observed from guest cations within MOFs. Li *et al.* [603] employed the anionic MOF HPU-14 ($([Zn_3(L)_2{\cdot}2(Me_2NH)]{\cdot}3(CH_3OH){\cdot}5(H_2O))_n$) with an $(CH_3)_2NH^+$ filling as a platform for loading green-emitting Tb^{3+} and red-emitting Eu^{3+} into nanotube channels of the blue-emitting framework *via* ion-exchange. This was achieved by replacing the $(CH_3)_2NH^+$ filling by the cationic nitrate salts $Ln(NO_3)_3$ of Tb^{3+} and Eu^{3+}. The obtained framework HPU-14@Tb^{3+}@Eu^{3+} showed luminescence originating from all three compounds. A broad blue emission was observed by the host framework with a maximum at 431 nm, due to the energy transfer from the organic linker to the Zn^{2+} clusters. Additional energy transfer from the linker to the guest lanthanoid ions led to simultaneous emission around 520 nm due to Tb^{3+} and around 600 nm due to Eu^{3+}. The resulting material could act as a white LED with calorimetric sensitivity for gaseous HCl.

6.2.3.3. ET during host-guest interaction

MOFs that contain photosynthetic chromophore arrays, *e.g.* porphyrins, are an excellent platform to study the exciton transport within this well-defined structure. Synthetically, we are given the possibility to precisely position and orient, but also select the chromophores involved in the energy transfer process. Zhang *et al.* [593] studied the Förster energy transport of singlet excitons in two different light harvesting MOFs with truxene-based ligands. Surprisingly, a step-by-step exciton random hopping model between only nearest neighbors (as is used to explain Dexter ET) was not sufficient to describe the observed ET. It was found inadequate to evaluate Förster-type singlet exciton migration that involves direct jumping over longer distances (Fig. 49 A). The two MOFs (truMOF-1/2) were constructed from truxene-tribenzoate ligands (5,5',10,10',15,15'-hexaethyl-truxene-2,7,12-tribenzoic acid) and either of the two IBUs $Zn_{10}(\mu_4\text{-}O)_4$ (carboxylate)$_{12}$ and $Zn_4(\mu_4\text{-}O)(OH)_3(OH_2)_3$ (Fig. 49 B). Exciton migration

was observed between the truxene linker acting as the donor and adsorbed coumarin dye molecules as the acceptor (Fig. 49 C), which adhered to one of the benzene rings of the linker as determined by MD simulations. However, the intensity ratio of the coumarin emission, compared to those of the linker for samples with varying amounts of acceptor molecules, did not fit with the predictions of the nearest-neighbor step-by-step hopping (NNH) model. Measurements of the migration rate of singlet excitons within truMOF-1 and -2 revealed diffusivities of 1.8 and 2.3 x 10^{-2} cm^2/s. In both cases, the migration rate was faster than expected from a step-by step hopping mechanism, in which energy is passed on between neighboring truxene molecules. Additional exciton jumping beyond nearest neighbors (JBNN) was found to account for up to 67% of the ET rates in MOF systems with singlet excited states.

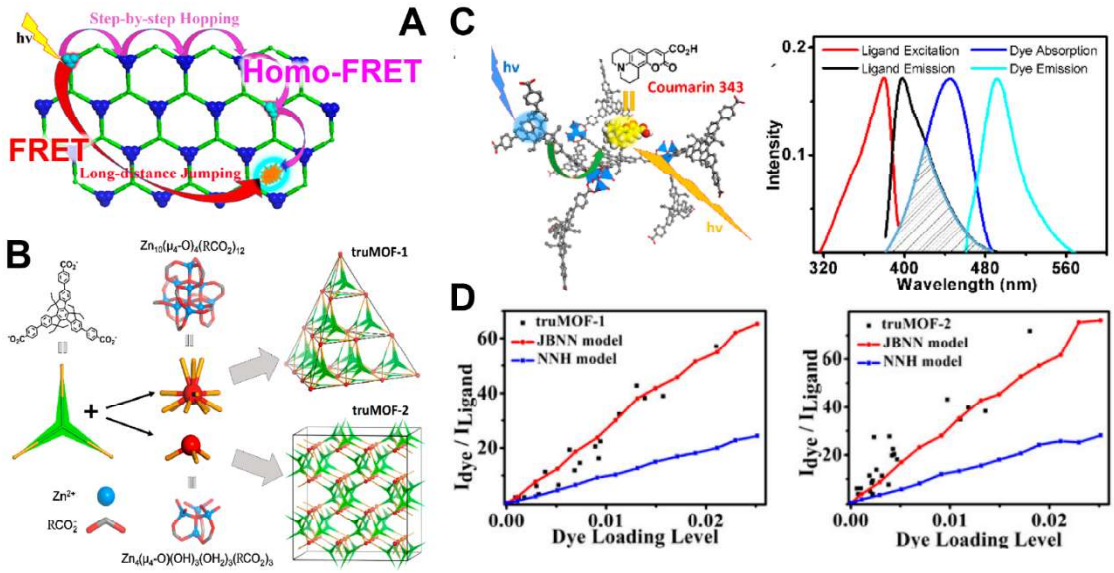

Figure 49. FRET beyond step-by-step-hopping. (A) Cartoon depicting two distinct pathways of exciton migration in a chromophoric network: (1) step-by-step nearest-neighbor hopping (NHH). (2) long-distance jumping beyond nearest neighbors (JBNN). (B) Investigated structures of truMOF-1 and truMOF-2. (C) Energy transfer between truxene ligand to coumarin guest molecules within the MOF. Excitation and emission spectra are recorded in DMF. (D) I_{dye}/I_{ligand} of dye@truMOFs as a function of the loading level, together with simulated values from the NNH model and the model including JBNN (Reprinted with the permission [593]. Copyright 2016, American Chemical Society).

Fullerenes (C_{60}) [608] are only one example aside from a plethora of organic chromophores that can enter semiconducting MOFs for light harvesting applications. In MOF-177, both kind of pores are sufficiently large to accommodate molecules like C_{60}. While the hosting material was found to be absorptive in the UV and emissive in the blue, it can act as both: donor and acceptor. In combination with the acceptor molecule, phenyl-C61-butyric acid methyl ester,

FRET occurred between the linker and guest-acceptor. An additional example presents the Zn-terephthalate MOFs, with TPA ligands exhibiting a luminescence over nearly 0.5 seconds [609]. The phosphorescence color could be tuned by the addition of guest solvents and molecules, like pyridine, that adjusts the electronic structures of the pristine MOF host structure. Stimuli-responsive, photo-luminescent lanthanoid MOFs (ZJU-88) were recently presented based on a MOF loading with diarylethene (DAE) derivatives [610]. Light triggered the switching of DAE between an open and closed isoform, which regulated the inactivation and activation of a photochromic FRET process between the DAE acceptor and lanthanoid donor. This allowed for reversible luminescence on-off switching of the lanthanoid emitting centers of MOF host was observed.

In a recent publication, a new strategy was presented to generate luminescent MOFs as white-light emitting-diodes. Liu *et al.* [611] employed the ZIF-8 MOF to encapsulate blue-, green-, and red-emitting dyes in the framework (Fig. 50). They investigated three different dyes@ZIF-8 approaches: *1)* multi-phase single-shell, *2)* single-phase single-shell, and *3)* single-phase multi-shell. This allowed for the systematic investigation, control, and modulation of the concentration and arrangement of encapsulated dyes within dyes@ZIF-8 structures. While model *1* led to a spectral separation of fluorescent emission, model *2* suffered from energy transfer occurring between the emissive dye molecules. Based on coumarin, fluorescein, and rhodamine B, that show efficient FRET in solution, an optimized "white-light-emitting" framework could be designed following the *3rd* approach.

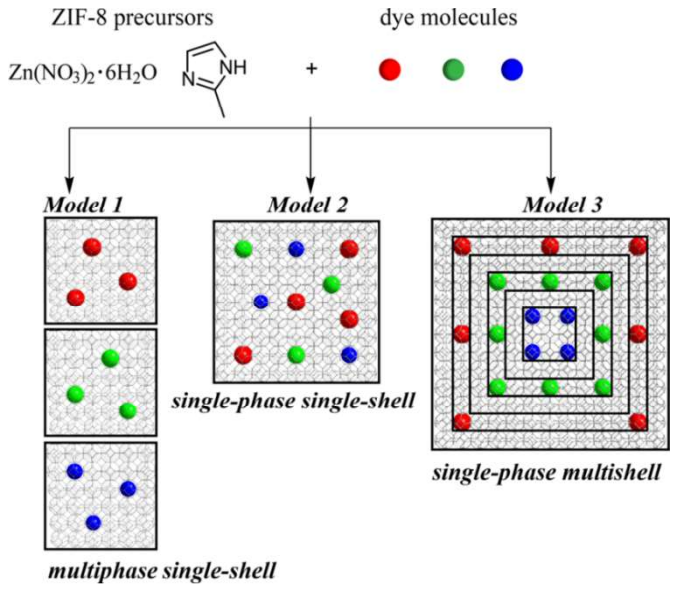

Figure 50. Synthesis strategies for the preparation of white-light-emitting MOFs. The simultaneous emission of blue, green, and red fluorescent dyes appears white. While randomly

mix addition of dyes leads to additional effects light quenching and FRET, separated phases allow for controlled the emission properties. Single-phase multi-shell MOFs facilitate the controlled emission of "white light" (Reprinted with the permission [611]. Copyright 2019, American Chemical Society).

6.3. Charge transfer reactions

MOFs as photo-catalysts have received great attention in the last years. They represent controllable, periodic scaffolds of organic molecules for tunable and inexpensive light absorption, and subsequent conversion to electrical and/or chemical energy. Solar energy conversion approaches can benefit from MOF in various ways: besides their periodic nature, MOFs can be grown as thin-films on transparent electrodes with nearly single-layer precision. Heterogeneous MOFs provide additional flexibility for using mixed species of chromophores. As already discussed in chapter 5 on conductivity, MOFs are usually semi-conducting. In this section, we will look at different approaches to enable and tune redox activity in MOF. As there are many excellent reviews [338,348,612–619] on conductivity, photochemistry, redox-activity, catalysis, and energy storage, we will focus on the underlying principle behind charge transfer reactions and discuss based on recent literature examples how these can be manipulated experimentally [620,621].

Three different strategies are pursued to enable directed charge transfer (CT) caused by sunlight. The first, considers photo- and redox-active guest molecules, which can be incorporated in the framework. The second, involves photo-induced charge separation within a redox-active linker, leading to the formation of localized holes and electrons, with subsequent charge transfer to catalytic units. The coordinating metal and exciton transport to the MOF's boundary is a good demonstration here. The third, photoexcitation of the metal-centers can free electrons that are transferred to neighboring clusters in the next step. Hence, photo-induced charge-transfer or electron-transfer (PET) processes play a fundamental role within the MOF as the node SBUs, linkers, and guest molecules all represent accessible sites for PET. They all can serve as a donor or an acceptor, depending on their relative ground- and excited-stated redox potentials [622]. The first step in a PET process is the photo-excitation of MOFs (section 6.1.), *i.e.* the uptake of light energy to power the CT, followed by a potential energy transfer within the MOF itself. The consecutive intramolecular CT is described by four separate steps [623].

Step 1: Delocalization of excitation on D-A complex

$$^{1,3}D^* + A \rightarrow {}^{1,3}(D\text{-}A)^* \qquad \text{(Eq. 16)}$$

Step 2: Partial charge transfer

$$^{1,3}(D\text{-}A)^* \rightarrow {}^{1,3}(D^{\delta+}\text{-}A^{\delta-})^* \quad \text{(Eq. 17)}$$

Step 3: Radical formation

$$^{1,3}(D^{\delta+}\text{-}A^{\delta-})^* \rightarrow {}^{1,3}(D^{+\cdot}\text{-}A^{-\cdot})^* \quad \text{(Eq. 18)}$$

Step 4: Charge separation

$$^{1,3}(D^{+\cdot}\text{-}A^{-\cdot})^* \rightarrow D^{+\cdot} + A^{-\cdot} \quad \text{(Eq. 19)}$$

These steps arise from the excited donor in either the singlet- or triplet state. MOFs with weakly coupled redox entities can be treated within the Marcus theory framework [623–628], that describes the transfer of charges from one single molecular entity to another—a theory for which R. A. Marcus received the Nobel prize in Chemistry in 1992. In MOFs, however, molecular bridging between donor and acceptor also occurs. Furthermore, the photo-induced charges are often delocalized across multiple donor or acceptor molecules. Here, theoretical approaches must treat donor and acceptor aggregates as a single super-molecule comprising the aggregated molecular units. Both cases can be managed within the generalized Marcus theory framework for multi-molecule delocalized CT in MOFs, which is beyond this review [629].

6.3.1. Host–guest interaction and long-range transport

A hindrance, to employ light-driven charge separation and CT reactions for photovoltaic applications, is the low exciton propagation in MOFs that leads to CT within redox-active molecules. The challenge lies in the finite thickness of the MOF layered system required for effective light harvesting, which is usually larger than the propagation distance before reabsorption. The main pathway responsible for charge transport in MOFs is a hopping mechanism. In this case, charges are spatially localized at moieties with discrete energy levels and charge hopping occurs to neighboring units exclusively. This mechanism (mediated along with the framework's linkages) is usually reported for CT in MOFs between metal and clusters or ligands.

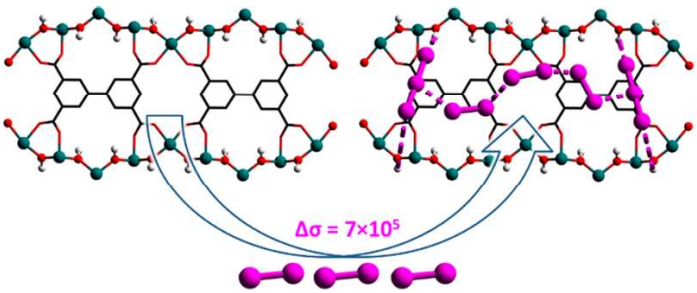

Figure 51. Electrical conductivity induced by host–guest charge transfer. Adsorption of iodine to the redox-active MOF leads to enhanced conductivity. View along b axis (Reprinted with the permission [630]. Copyright 2019, American Chemical Society).

An attractive strategy to facilitate long-range transport and electrical conductivity in porous MOFs is the inclusion of guest molecules within MOF cavities. A recent publication, Schröder and co-workers [630] compared the binding of iodine I_2 in a pair of redox-active MOFs, MFM-300(V(III)) and its oxidized, deprotonated analog MFM-300(V(IV)). MFM-300(V(III)) has the structure $[V_2(OH)_2(L)]$(H_4L = biphenyl-3,3′,5,5′-tetracarboxylic acid). Host–guest CT between I_2 and MFM-300(V(III)) led to a 70.000-fold enhancement in the electrical conductivity between the I_2-loaded and void MOF material. Upon addition of I_2 to MFM-300(V(III)), two species were formed with the MOF: triiodide I_3^- anions, which adhere to the hydroxyl group of the $[V(III)O_4(OH)_2]$ chains *via* hydrogen-bonded interactions and iodine that attached interstitially between two phenyl rings of neighboring ligand molecules (Fig. 51).

In a different approach by the Hupp lab, the redox-active molecule ferrocene (Fc) was incorporated into MOF NU-1000 (Fe-NU-1000). This framework possesses large pores (30 Å) and facilitates diffusion of solvent and electrolytes through films of variable thickness [631,632]. Using solvent-assisted ligand incorporation, a singly-carboxylated ferrocene was attached to the $Zr_6(\mu_3\text{-}O)_4(\mu_3\text{-}OH)_4(OH)_4(OH_2)_4$ nodes before layer formation on fluorine-doped tin oxide *via* electrophoretic deposition (Fig. 52 A) [631]. The pyrene-based MOF was formed from the connection of 1,3,6,8-tetrakis(*p*-benzoic acid)pyrene (H_4tbapy) to Zr nodes. The overall redox conductivity was explained by a site-to-site charge hopping from one Fc to the next. At low supporting electrolytic concentrations (50 mM), oxidation of the anchored Fc molecules dominated and made the porous MOF films repellent against cations in solution. The reduction of ferrocenium sites removed the cation-blocking behavior and turned the MOF layer into a membrane featuring bias-switchable permselectivity for anions. Li *et al.* [633] anchored redox-active pigment derived from tetraphenylporphyrinato Zn(II) (tppZn) post-synthetically within the 1D pores of the NU1000-MOF instead of ferrocene. The derived system exhibited a directed energy transfer from the excited MOF (NU-1000*) to tppZn and a CT from the excited tppZn* to the pyrene-linker in a wavelength-dependent manner.

Following this research, Hupp and co-workers [632] demonstrated that the kinetics of charge-hopping in Fe-NU-1000 could be substantially modulated by host–guest interaction that increases the rates of CT more than 30-fold. They employed β-cyclodextrin (β-CD), which has a several 1000-fold higher affinity for ferrocene then ferrocenium. To evaluate the kinetics of diffusive charge-transport within the MOF layers in the presence and absence of β-CD,

chronoamperometry was employed to measure the current over time. The current in Fc-NU-1000 films decreased in the presence of different amounts of β-CD (Fig. 52 B). The diffusion coefficient $D_{hopping}$—given by the slope of the linear plots—depends strongly on the concentration of β-CD and decreased by a factor of 30 in the presence of the saturating β-CD concentration of 20 mM. Binding of β-CD to ferrocenium allowed to adopt the speed in charge transfer, externally (Fig. 52 C).

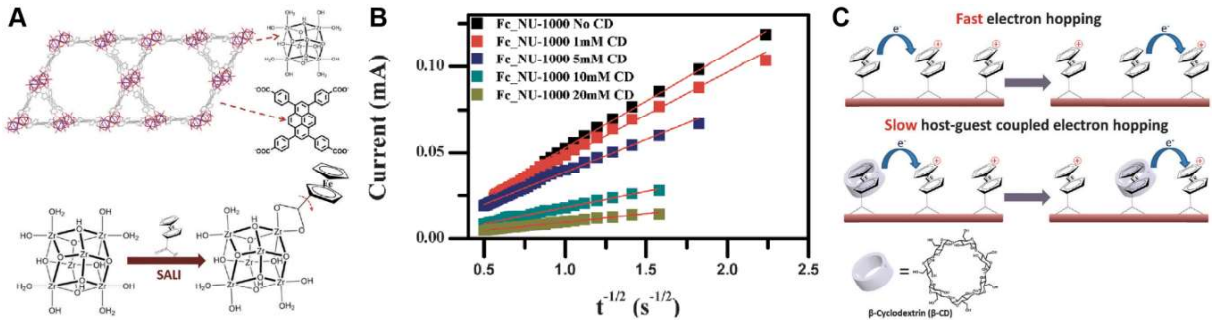

Figure 52. Modulation of charge transport rate by host–guest interaction. (A) Synthesized NU-1000 MOF with anchored ferrocene molecules. (B) Cottrell plots of current transients for Fc-NU-100 films in presence of different amounts of β-CD. (C) Host–guest modulated charge transfer mechanism in the presence of β-CD (Reprinted with the permission [632]. Copyright 2016, Royal Society of Chemistry).

In redox-active MOFs, the CT follows a redox hopping mechanism. While electrons hop between the redox-active moieties, ion diffusion occurs in parallel to balance the electroneutrality of the MOF. In a recent work, Meng *et al.* [634] studied the correlation between structure and charge diffusion within ferrocene-doped MOF films (Fc-MOF) on a conductive substrate. They found a direct correlation to pore size: an increase in pore size led to a negative effect on the electron transfer rate k_{e-hop} and a positive effect on the ion transfer k_{i-hop}. By quantitatively evaluating the diffusion and transport rate of electrons and ions *via* chronoamperometry in the ferrocene-doped MOF, an increase was found in diffusivity in the order Fc-MOF-808 < Fc-NU-1000 < Fc-NU-1003 (Fig. 53), relating to an increase in pore size. To extend to other Zr MOF systems, Palmer *et al.* [635] implanted the electroactive Fc in the framework of UiO-66 by solvent assisted ligand incorporation. Redox activity, however, was only observed in Fc closed to the external surface of UiO-66. In contrast to NU-100, UiO-66 has a 5-fold smaller pore size of ~6 Å. Consecutively, only Fc at the surface was electrochemically active, which is only the case for about 20% of the installed molecules. Surprisingly, CT diffusion coefficients in an oxidative and reductive stepping mode amounted

to 6.1 ± 0.8 × 10^{-11} and 2.6 ± 0.2 × 10^{-9} cm^2 in the presence of counter-ions from the KCl electrolyte.

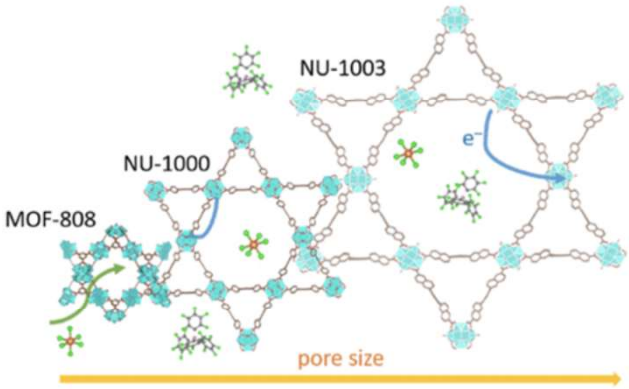

Figure 53. Electron transfer in MOFs is pore-size dependent. An increase in pore size leads to an increase in ion transport and a decrease in electron transport (Reprinted with the permission [634]. Copyright 2020, American Chemical Society).

Aside from Fc, further redox-active guest molecules are employed to enhance CT reactions between linkers. This brings us back to the case of Fc. Being incorporated in mesoporous tetrathiafulvalene (ttf)-based MOFs [636] they lead to an increase in electrical conductivity by two orders of magnitude due to CT interaction between the C_{60} and the hosting MOF. While the C_{60} in MOFs can serve as a potent electron acceptor, ttf exhibits interesting redox properties and a strong electron-donor character. The hosting material MUV-2 ($[H_4ttftb]_3[Fe_3(\mu_3\text{-}O)(COO)_6]_2$ with H_4ttftb = tetrathiafulvalene-3,4,5,6-tetrakis(4-benzoic acid)) was formed from a preformed cluster $[Fe_3O(CH_3COO)_6]ClO_4$ and H_4ttftb as the starting material (Fig. 54) [637]. The donor–acceptor interaction in C_{60}@MUV-2 led to a partial CT from the ttf to the Fc in the ground state. Time-dependent DFT calculations indicated a highly efficient CT from the ttf to the Fc in the S_1 of C_{60}@ttftb of nearly 1electron worth. These findings align with conductivity measurements, which showed an increase of two orders of magnitude in the presence of C_{60} within the MUV-2 material. Similar results were observed by Goswami *et al.* [638] when incorporating fullerenes in the zirconium-based MOF NU-901, with 1,3,6,8-tetrakis(*p*-benzoate) pyrene ($tbapy^{4-}$) linkers. CT between the donor linkers and fullerenes as an electron-acceptor led to an increase in conductivity from 10^{-14} to 10^{-3} S/cm.

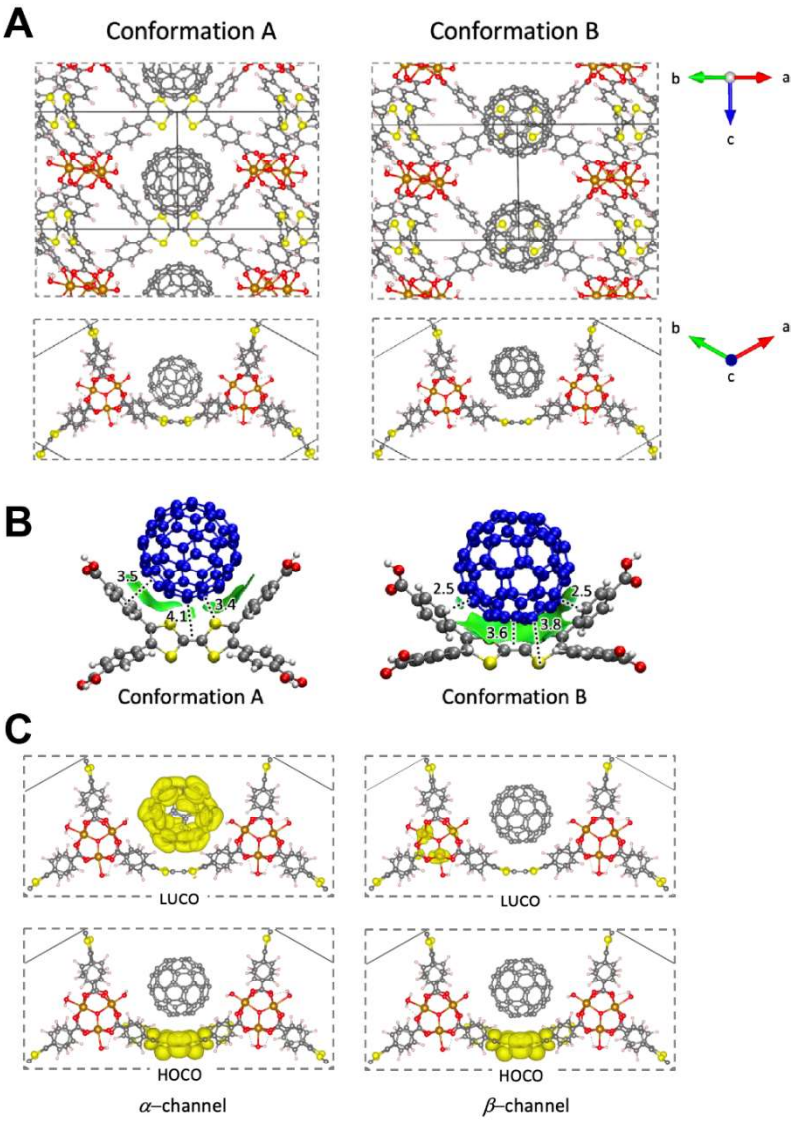

Figure 54. Host–guest mediated charge transfer in C_{60}@MUV-2. (A) Minimum-energy crystal structure and (B) supramolecular assembled of C_{60}@ttftb in the PBC-optimized C_{60}-MUV-2 system. (C) Highest occupied (HOCO) and lowest unoccupied (LUCO) crystal orbitals in the two spin channels for C_{60}@MUV-2 (licensed under CC-BY [636]).

To effectively transport charges, long-range ordering of donor and acceptor components are necessary. Crystalline MOFs offer the unique possibility to position and encapsulate guest molecules—simultaneously together with either donor or acceptor molecules as part of the framework. The incorporation of a strong reducer, such as ferrocene, or oxidizer, like fullerenes, holds great promises for catalytically active MOFs as future material for energy conversion and storage. Further successful reducer/oxidizer pairs, *i.e. D*/A pairs, for charge transfer applications in MOFs include TCNQ/btc in HKUST [401]; ttf/naphthalene-

tetracarboxydiimide (NTDI) [639,640], oligothiophene/[6,6]-phenyl-C_{61}-butyric acid methyl ester (PCBM) in MOF-177 [608] and *N,N'*-bis(4-pyridyl)-2,6-dipyrrolidyl napthalenediimide with methylviologen. In a recent publication, a synthetic MOF-based artificial light harvesting system was realized based on a tppZn-derived pigment as a guest molecule in NU-1000 [633]. The tppZn and linker formed a "special-pair"-like system, driving the charge-separation process in a wavelength-dependent manner [641]. Considering the wealth of electron redox agents available in photoredox catalysis [591] many more CT pairs with new properties will be certainly explored for artificial light harvesting.

6.3.2. Internal charge transfer reactions

Conductive MOFs grown on electrode surfaces are promising materials for future electricity-producing light harvesting devices. As seen in the last section, an important role is given to the pores accommodating small guest molecules and ions. Charge transfer, however, can also occur internally in homo- and heterogeneous MOFs between metal nodes, ligands, or simply between metal nodes and ligands by introducing: *(1)* mixed redox-active partners or *(2)* exploiting mixed valency approaches.

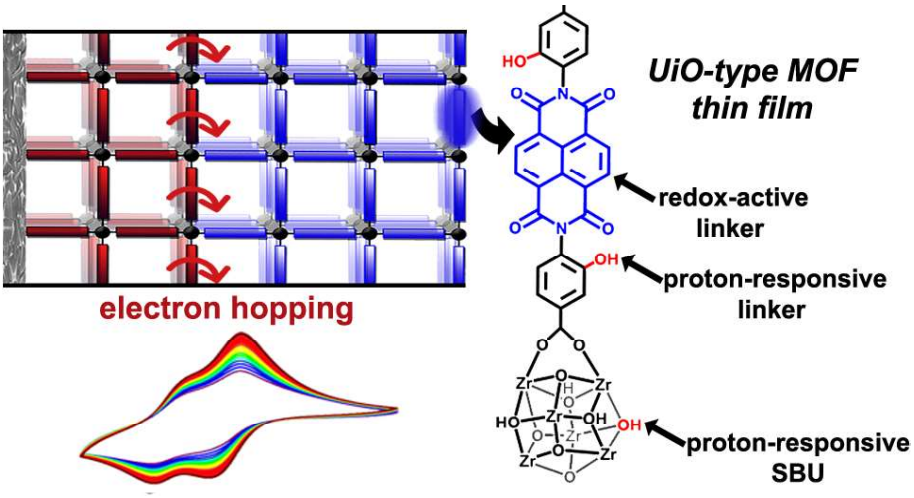

Figure 55. Electron hopping between linkers. The presence of counter-ions in the electrolyte can enhance or decrease the CT kinetics (Reprinted with the permission [642]. Copyright 2018, American Chemical Society).

In a recent example [642], redox-active naphthalene diimide linkers were implanted into a UiO/PIZOF-type MOF thin film. This highly stable framework offers large pores and surface area, in addition to excellent thermal, chemical, and catalytic stability. The electroactive Zr-MOF possesses $Zr_6O_4(OH)_4$ clusters connected by 12 linkers, which are based on

naphthalene diimide appended with carboxylic acid groups (dcphOH-ndi; Fig. 55). The synthesized Zr(dcphOH-ndi) MOF resembles the structure of UiO-66, although it exhibits a 2-fold interpenetrated structure, and possesses a pore size of 13 Å. Moreover, it exhibits proton-responsive behavior at both the Zr-SBUs and the hydroxyl-functionalized linker. Photo-induced CT occurred *via* linker-to-linker hopping, further balanced by the ion transport from the electrolyte.

MOFs with intra-framework CT have been reported using electroactive ligands with ligand-to-metal (LMCT) or metal-to-ligand charge (MLCT) transfer [418,424,620,643–645]. Gutierrez *et al.* [644] studied, for example, the LMCT in Zr-naphthalene MOFs *via* femtosecond spectroscopy and flash photolysis to follow photoinduced processes from the femto- to microsecond time scale: starting with an LMCT around 100-150 fs between the linker and Zr node, excimer formation and electron transfer between the linkers were observed on the ps time scale. Radiative electron-hole recombination was monitored consecutively in the later nano- to microsecond regime. An equally long lifetime of 3.5 µs for the charge-separated state in the case of MIL-100(Fe) was identified *via* combined steady-state and Fe K-edge X-ray transient absorption (XTA) spectroscopy [645]. While metal-to-metal charge transfer (MMCT) was reported in various mixed-metal MOF materials [621], ligand-to-ligand charge transfer (LLCT) in MOFs are still less frequent. A systematic study on LLCT reactions by Huo *et al.* [622] investigated the properties of three closely related manganese coordination 2D MOFs. The LLCT process within the MOFs occurred between TTF-bicarbonate (dimethylthio-tetrathiafulvalene-bicarboxylate), as an electron donor linker and different conjugated bipyridines (bpy, 1,2-bis(4-pyridyl)ethylene (bpe) and 4,4′-ethylenedipyridine (bpa)) as an electron acceptor linker achieved by metal coordination (Fig. 56 A). The compounds are referred to as MOF1: $[MnL(bpy)(H_2O)]_n{\cdot}nCH_3CN$, MOF2: $[MnL(bpe)_{0.5}(DMF)]_n{\cdot}2nH_2O$, and MOF3 $MnL(bpa)(H_2O)]_n{\cdot}2nH_2O$. with the linkers L = dimethylthio-tetrathiafulvalene-bicarboxylate (TTF), bpy, bpe, bpa. The LLCT was observed *via* optical diffuse reflection (Fig. 56 B) at 532 nm (MOF1), 582 nm (MOF2), and 498 nm (MOF3). Their calculated energy gap correlates with the experimental CT absorption band. Upon photoexcitation, LLCT between TTF and the linker occurs. The generated electron/hole charge separation (Fig. 56 C) leads to charge carriers that begin to move in opposite directions within the applied potential. The generated photocurrent is linearly proportional to the LLCT energy.

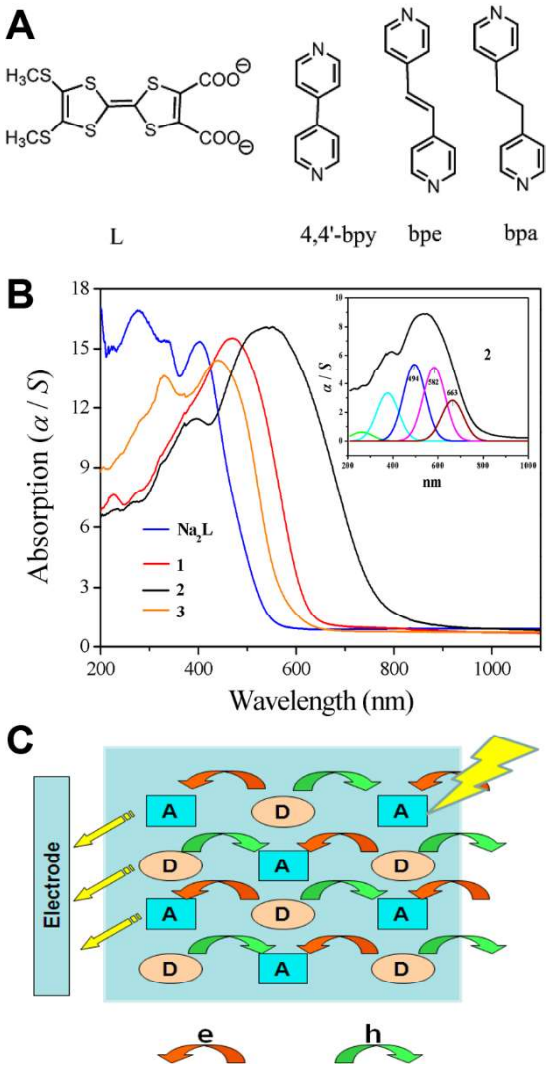

Figure 56. Ligand-to-ligand charge transfer in manganese-based MOFs with TTF- and bipyridine ligands. (A) Linker structures. (B) Optical diffuse-reflection spectra of acceptor ligands 1-3 and donor compound Na_2L for comparison in the solid-state. Inset: Optical diffuse-reflection spectra of 2 with peak separation. (C) Proposed LLCT mechanism in the synthesized MOF (Reprinted with the permission [622]. Copyright 2016, American Chemical Society).

A further strategy to enhance redox activity and conductivity in MOFs is the introduction of mixed valency either within metal nodes or linkers [612], *i.e.* the donor and acceptor moieties are identical but differ in their oxidation state. Regarding the metals [612], iron and copper are the most widely used redox couples to incorporate mixed valency in MOFs (although others are also employed). Mixed valency [646] was first shown in MIL-53(Fe)·H_2O. When used as an electrode in a lithium half-cell, entry and exit of Li^+ ions were accompanied by the reduction of Fe^{3+} into Fe^{2+}. Later, Sun *et al.* [647] prepared a series of MIL-53(Fe) type materials, Fe(bdc)(DMF,F), using different ratios of n($FeCl_3$)/n($FeCl_2$) leading to variable amounts of

Fe^{2+} in the framework (Fig. 57 (top)). The presence of Fe^{2+} within the framework and the associated increased catalytic activity of MIL-53(Fe)-derivatives, were investigated by monitoring the degradation of phenol with hydrogen peroxide as an oxidant at near-neutral pH and 35 °C. More significant results were observed for Fe(bdc)(DMF, F). Coexistent Fe^{2+} and Fe^{3+} nodes in the framework were additionally proven *via* Mössbauer spectroscopy (Fig. 57, (bottom)).

Sample	$n(FeCl_3)/n(FeCl_2)$	Fe^{2+}/%	Fe^{3+}/%
MIL-53(Fe)	---	0	100
FeMOF-71	7 : 1	0	100
FeMOF-31	3 : 1	0	100
FeMOF-11	1 : 1	9.0	91.0
FeMOF-13	1 : 3	18.7	81.3
FeMOF-17	1 : 7	20.5	79.5
Fe(BDC)(DMF,F)	0	26.0	74.0

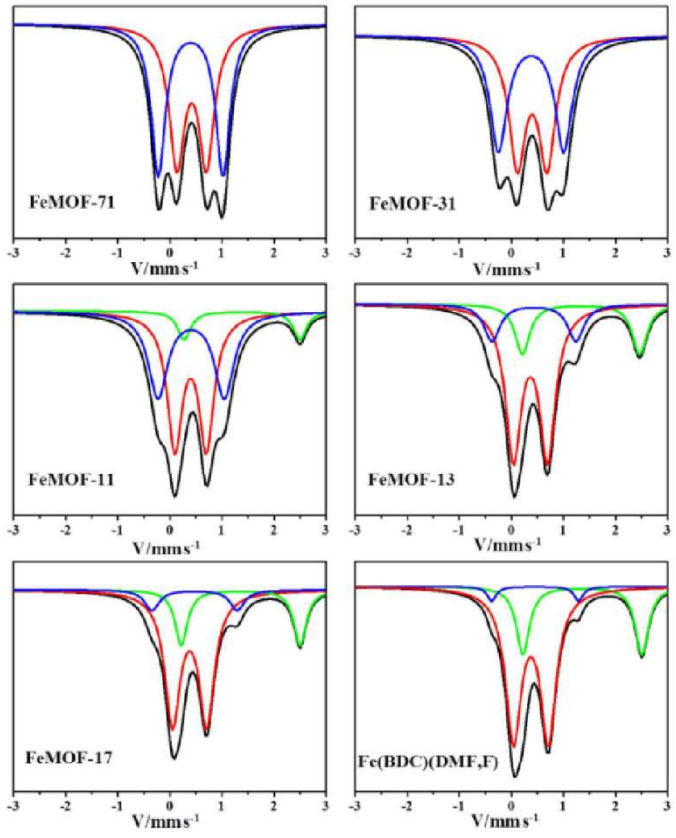

Figure 57. Mixed-valency Fe-containing MOF. (top) MOF synthesized with different molar ratios of $FeCl_3$ to $FeCl_2$ including the amount of Fe^{2+} determined by Mössbauer spectroscopy. (bottom) Corresponding ^{57}Fe Mössbauer spectra depicting the contributions of Fe^{3+}-OH, F (blue); Fe^{3+}-OH (red) and Fe^{2+} (green) (Reprinted with the permission [647]. Copyright 2016, Royal Society of Chemistry).

In a seminal work, Hua *et al.* [648] presented Zn(II) frameworks containing co-facial thiazolo[5,4-*d*]thiazoles (tztz) that led to a mixed-valence state upon (electro-)chemical reduction. The major framework formed was $[Zn_2(bpptztz)_2(tdc)_2]_n$, with bpptztz = 2,5-bis(4-(pyridine-4-yl)phenyl)thiazolo[5,4-d]thiazole) (Fig. 58 A). In this framework, tdc (= 2,5-thiophene dicarboxylate) co-ligands leads to aromatic π-stacking with the bpptztz ligands. The resulting inter-ligand distance, smaller than 3.8 Å, allows space-inter-valence charge transfer (IVCT) directly between the ligands, without the involvement of the surrounding framework (Fig. 58 C). This observation broadens the scope of possible CT pathways, aside from frequently reported internal through-bond transfer mechanism and site-by-site charge hopping mechanisms.

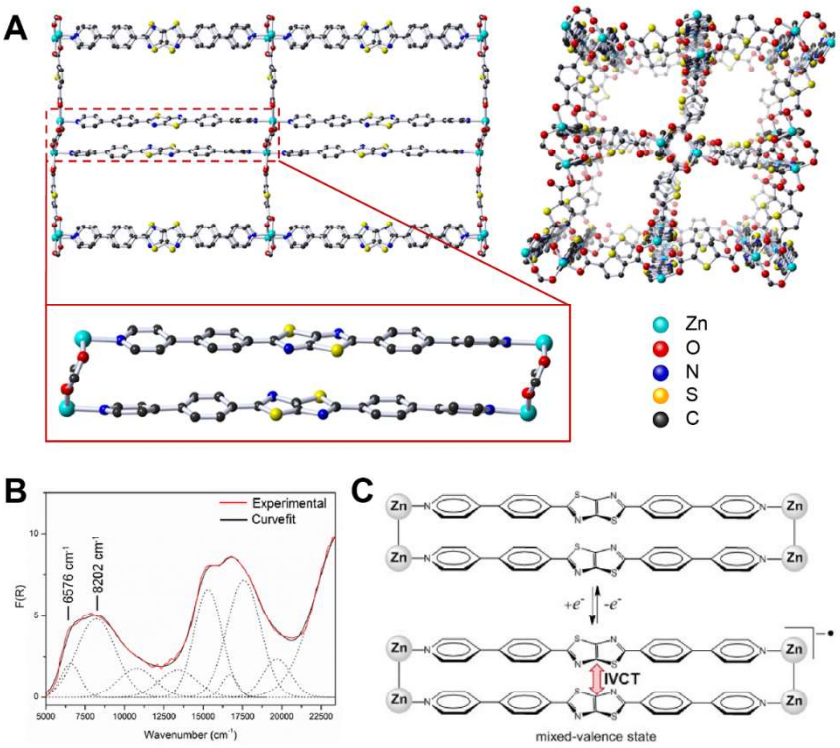

Figure 58. Inter-valence charge transfer. (A) Crystal structure along the c-axis (left) and a-axis (right). (bottom) Zoom into the "co-facial" pair of bpptztz ligands. (B) Comparison of computational predicted and experimental IVCT bands. The two lowest energy components of the NIR band are assigned to the mixed-valence form of $[Zn_2(bpptztz^{0/*-})_2(tdc)_2]_n$. (C) Schematics of the co-facial pair of bpptztz ligands showing reduction to the mixed-valence state that facilitates an IVCT interaction (Reprinted with the permission [648]. Copyright 2018, Royal Society of Chemistry).

Ding *et al.* [649] investigated two topologically Zn(II) and Cd(II) frameworks that feature co-facially stacked pairs of redox-active 2,5-bis-(4-(4-pyridinyl)-phenyl)-thiazolo-[5,4-*d*]-

thiazole (DPPzTz) ligands. Aromatic stacking interactions between the ligands led to a mixed-valence state upon electrochemical reduction. Differences in CT behavior of both MOFs systems are directly associated with the subtle changes in framework structure. The combination of theoretical modeling by Marcus theory, EPR (electron paramagnetic resonance), SEC (size-exclusion chromatography) and spectroelectrochemistry identified mixed-valence states and allowed deduction that electron transfer is less favorable in Cd-based MOF compared to the Zn-based MOF.

6.4. Summary

Global energy consumption has been rising over the past decades with approximately 80% usage relying on fossil fuels [650]. Renewable and sustainable approaches to generate "clean and affordable" light and energy [478], and to enable energy conversion and storage are key topics that need to be addressed by current research. In this chapter, we elucidated the physical principles underlying (artificial) photosynthesis in MOFs and discussed the three fundamental processes responsible for light harvesting, energy transport, and charge transport which are key to the underlying energy conversion and photo-catalysis phenomena. Based on these physical principles we discussed how chemical synthesis can control and improve each of the individual steps.

7. MOFs in heterogeneous catalysis

The modern chemical industry, in particular, the refining, petrochemical, and plastics industries, is largely based on catalytic processes involving heterogeneous solid-state catalysts [651]. Catalysts facilitate the course of the chemical reactions by lowering the energy barrier of the cycle of changes taking place and thus increase the rate of the chemical reactions. The research on the synthesis of new catalysts with well-developed porosity and high surface area is carried out in a broad scope in all modern and industrialized countries. Due to economic and ecological reasons, strong efforts are taken to replace homogeneous catalysts with heterogeneous ones characterized by high selectivity and activity. The catalyst development in the next decades will increasingly rely on the theoretical predictions and calculations based on catalysis principles, replacing empirical work. This approach will potentially allow to reducing the number of tested catalysts, necessary to choose the optimal one for a given process [652–661]. MOF materials attracted the attention of the scientific community because of their tremendous potential in the catalysis, which arises from their exceptional properties, first and foremost high porosity enabling the creation of a large number of active sites and an easy

functionalization of the surface. This provides numerous opportunities for the design of catalysts with high selectivity and activity. To demonstrate how MOF materials can contribute to the improvement of the course of individual catalytic processes, it is obligatory to understand their chemical and physical aspects. It was previously mentioned in the catalysis handbook by Domesic and co-workers [662] that the interdisciplinary nature of catalysis requires specialists from various fields such as surface, theory, engineering, kinetic, material, spectroscopy, and experimental chemistry as well as physics, and it can impede the developing process. Hence, it is important to identify the crucial aspects for designing of a catalyst. Especially to newcomers who start working with materials such as MOFs and COFs, understanding the origins of their exceptional catalytic performance can be non-trivial. The following short overview aims to provide researchers with the necessary information to approach the design and engineering of MOFs for catalytic applications.

7.1. Underlying principles in catalysis

Starting from the most fundamental aspects, the material that exhibits catalytic activity has to be able to create and cleave bonds with the surrounding molecules taking part in the ongoing reaction [663]. This means, the catalyst is not the substrate (A) nor the product (B) in the A → B conversion, but it provides convenient conditions for molecules to only change the reaction kinetics. In addition, it must be underlined that a catalyst cannot influence the thermodynamic equilibrium. The plain path from A to B would be an ideal case but between these points, many intermediate species are formed which differ in reaction enthalpies [664,665]. The nature of porous catalyst inherently creates confined local microenvironments where the concentration of these intermediates is not constant but varies throughout the catalytic process. When applying solid-state catalysts the Langmuir-Hinshelwood model assumes the three-steps mechanism of the catalytic reaction [666]: *i*) substrates adsorption and breakage of required bonds; *ii*) reaction on the surface between adsorbed molecules; *iii*) desorption of the products [667,668]. During the catalytic reactions, the diffusion of the reactants through a boundary layer surrounding the catalyst particles and intraparticle diffusion of the reactants/products through the catalysts pores or network channels occur. The diffusion rate of the adsorbed molecules depends on pore size of the catalyst, substrate molecular size, adsorption enthalpy, catalyst flexibility, and the presence of defects. Taking into consideration the degree of confinement of a sorbate within a porous material, four diffusional regimes that are known as molecular-, Knudsen-, intracrystalline diffusion, and molecular sieving have been described (Fig. 59) [669]. Modulating catalyst parameters directly affect diffusion behaviors which,

inherently, are connected to the kinetics and thus to the material catalytic performance. Designing pore sizes and pore networks that enable the free flow of adsorbed molecules (molecular diffusion) increases the catalytic reaction rate. However, it can reduce the selectivity of the catalyst by making its interior available to undesirable products. In Knudsen diffusion, the mean free path of diffusing reactant molecules is dominated by collisions between the reactant and the pore wall of the catalysts. When the pore diameter approaches the reactant molecular size, intracrystalline diffusion occurs, in which the most important is the strong interaction of the adsorbed molecules with the pore wall. The diffusion of the sorbate into the pores of the catalyst does not proceed if its size is larger than the available pores (molecular sieving).

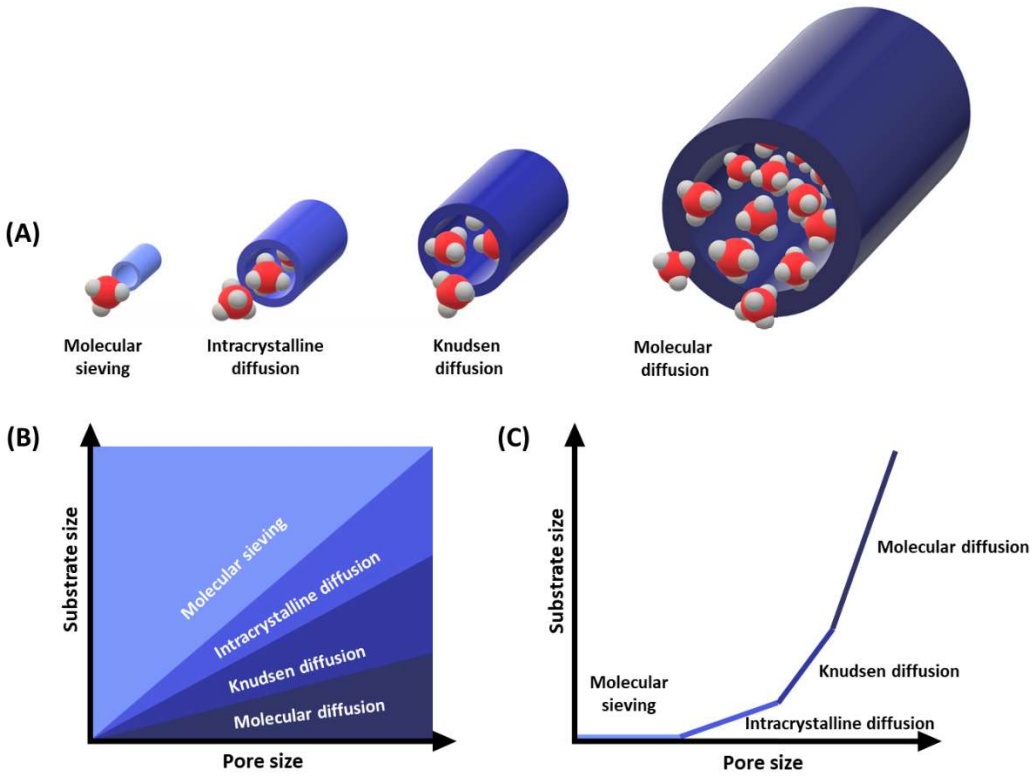

Figure 59. (A) The diffusion mechanism of adsorbate molecules in porous materials. (B) Relationship between substrate and pore size in diffusion processes. (C) Influence of pore size on diffusivity for a given sorbate.

In heterogeneous catalysis, the catalyst is a solid material usually in the form of a pellet, which is easily separable from the reactant mixture. For a specific catalytic reaction, the catalyst can run a certain number of conversion cycles before it deactivates, determined as turnover number (TON). More specifically, TON is the number of substrate molecules converted to a product by one catalyst molecule, also given over time as turnover frequency (TOF), which for

heterogeneous catalysis is used more often. The fundamental element in a catalyst are active sites—mostly at its surface—which are responsible for carrying out catalytic reactions by lowering the required activation energy (E_a) (the energy barrier). E_a varies for each process and is affected by different factors. For instance, the hydrogen activation applied in many important industrial processes (*e.g.* ammonia [670] or Fischer-Tropsch [671] synthesis) depends on electrons abundance at active sites. Thus, metals [672] or acid-base pairs are able to break covalent bonds between hydrogen and another atom, only if they provide enough electrons [673]. As far as the physical conditions are concerned, the temperature has also a significant impact on the catalysis. It influences catalyst and reactants stability, but also has an important role in determining which kinetics reactions (external on the surface or internal in the material) dominate and affect catalytic reaction rate. Internal reactions play a rate-limiting role at low temperatures, due to the faster diffusion through pores of the catalyst in comparison to rates of surface reactions. With increasing the temperature surface reactions start to dominate over internal reactions and the rate of the catalytic process begins to be controlled by intraparticle diffusion. In consequence, the value of the apparent activation energy becomes twice that of the intrinsic E_a (Fig. 60) [662]. Reactions with E_a lower than ~5 kcal/mol are diffusion-controlled, whereas reactions with E_a above this value are chemically controlled [674].

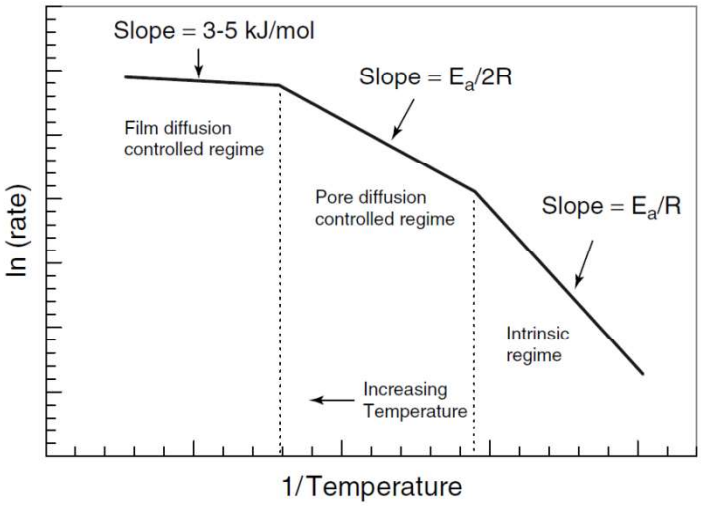

Figure 60. General effects of the temperature on the catalytic activity. The intrinsic activation energy is equal to E_a, and R is the gas constant (Reprinted with the permission [662]. Copyright 2008, John Wiley & Sons).

The temperature also plays an important role here by influencing the activation energy. It shows that the higher the E_a, the higher the sensitivity of the reaction to temperature. By using the Arrhenius equation (see chapter 3, Eq. 6) and knowing the temperature along with the reaction

rate, it is possible to determine the E_a. Despite the origin of this equation from the empirical observation, it is relevant for many rate constants over the wide temperatures range.

The importance of distinguishing whether the reaction is spontaneous diffusion or chemically controlled reaction can be a starting point in designing MOF catalysts. Fast diffusion promotes the reaction rate and the catalytic transformation is more effective if local intermediates do not disrupt [675]. Slow diffusion lowers the catalytic reaction rates, thereby the pore network must provide sufficient substrate and product transport. Applying pore tailoring it can be predesigned which reactants in terms of size can access a MOF. The difficulty arises in kinetics measurements due to the different reaction rates inside the material, compared to the external interaction rates at its surface. For this reason, it is elusive to precisely calculate catalytic parameters such as TOF for MOF materials [669]. Results of analytical techniques for the correct description of diffusion may vary dependently if the focus is either on the surface diffusion, internal interactions, or both. Examples of such techniques are: spectroscopic [676] or gravimetric [677] methods, zero-length column [678], quartz-crystal microbalance [679], quasi-elastic neutron scattering [680], pulsed-field gradient NMR [681], interference microscopy [682], or IR micro-imaging [683]. Nonetheless, decreasing MOF crystal size shortens the diffusion path, along keeping particle uniform both can prevent diffusion limitations and internal/external catalytic conversion differences [684].

The high porosity of many MOFs causes that most of the available catalyst sites are located at the internal surface of the material. In the case of idealized cubic Zn-based MOF-5 with dimension 0.25 mm, only 0.006% of metal clusters are accessible on the external crystal surfaces [669]. Therefore, it can be assumed that catalytic processes with porous MOF catalysts proceed at the far more abundant interstitial sites. However, when the substrate molecules diffusion is slower than the turnover of the MOF catalyst, and the activity of interfacial and interstitial catalyst sites are similar, the reaction will carry on at the external surface and only a few interstitial catalyst sites will contribute to catalytic performance (Fig. 61 A). Oppositely, if the substrate molecules diffusion is faster than the turnover of the catalyst, most of the catalytic active sites inside the framework will take part in the catalytic process (Fig. 61 B).

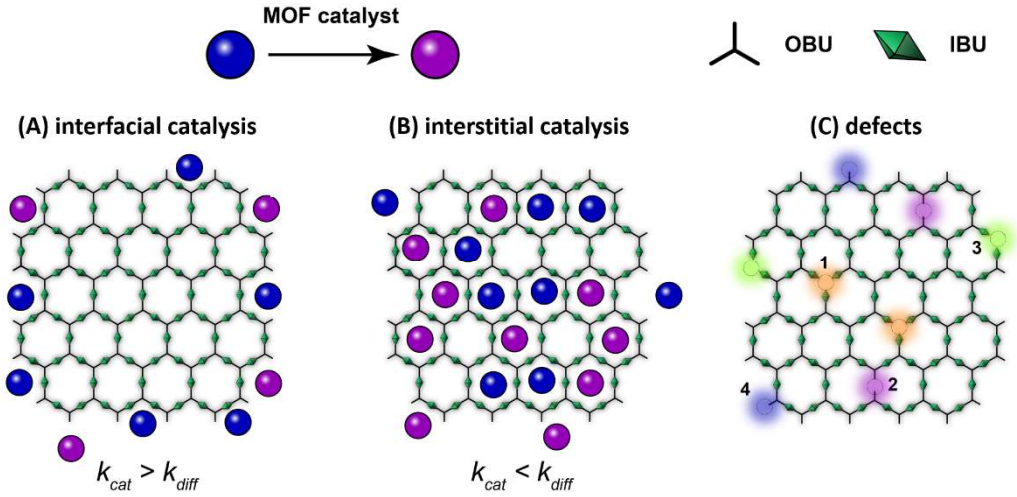

Figure 61. The relation between relative rates of catalyst turnover (k_{cat}) and substrate diffusion (k_{diff}) determines the potential reaction manner and its location in the MOF. (A) If $k_{cat} > k_{diff}$ the reaction proceeds at interfacial catalyst sites. (B) If $k_{cat} < k_{diff}$ interstitial catalyst sites will contribute to catalysis. (C) Various catalytically active defects can be located on the framework's surface: internally at CUS metal (1) and linker (2), and externally at CUS metal (3) and linker (4).

7.2. Fabrication strategies to employ MOFs as catalysts

Downsizing MOF particles or fabricating 2D thin layers are the main morphology-control approach in order to enhance catalytic performance by making easier access to the active sites [389]. These sites are divided with respect to their location in the framework: metallic nodes, functional groups of organic linkers, or encapsulated guest molecules [685]. MOFs can be described as single-site catalysts, meaning their catalytically active metal atom, ions, or clusters are coordinated on the framework surface by organic linkers. They usually have OMSs, also called CUSs as they are more exposed [686]. MOFs' predominance over homogeneous catalysts is that their active sites do not require stabilization or prevention from aggregation. The framework structure separates active sites and by consequence of their distribution, each of them has an own microenvironment. One could think that due to the repetitive composition and crystal nature it is easy to determine the amount of active sites and defects, adsorption enthalpies, TOF, or kinetics of MOFs. However, changes in the framework during catalytic conversion are currently challenging to investigate and internal kinetics impede a precise description of how exactly the catalytic reaction runs [687]. Up to now, only a few MOFs have been deeply investigated as catalysts [669]. The ideal approach in MOF catalyst design is to first define the catalytic application, reactants sizes, and required to overcome energy barriers. Subsequently, by taking into consideration available linkers and suitable metals, computational

calculations ought to give trial MOFs structure, as digital prototypes without empirical work [688,689]. If the synthesis and modifications are feasible and successful, the required material should be subjected to industrial application and be eventually implemented. In reality, it is difficult to combine all MOF design aspects, especially if experimental research is not aided by computation and with theoretical chemists and *vice versa*. Usually, researchers deal with creating novel structures or beneficial modifications of already known structures. Focusing on the MOFs' properties of the highest practical importance which are high internal surface and active site's density led to a whole new area of defect engineering. The rational design of more accessible active sites became an efficient way to increase catalyst performance. To quantify defects in the framework, elemental analysis, thermogravimetry (TGA) analysis, inductively coupled plasma atomic emission spectroscopy (ICP-OES), and ^{1}H NMR spectroscopy are suitable [33]. However, combining such data with kinetics and reaction yield has only a demonstrative character, while no precise information can be achieved, which types of defects are actively involved in the specific catalytic mechanism. Atomic-scale studies of dense bulk materials (such as ceramic oxides, metal oxides or metals [690–693]) show that their catalytically active surface is generally external, whereas in the case of MOFs the major fraction of their surface is internal. In MOFs with permanent porosity, long-range order indicate that all network atoms are at the surface. Both types of surfaces, inner and external reveal an order and roughness terraces separated by defects (Fig. 61 C). According to the surface defects and/or pore sizes of the catalyst, the reactant-catalyst energetic situation (enthalpy) is affected and therefore their reactivity.

Besides the confinement effects, the flexibility of MOF materials structure is an important aspect of their application in catalysis. Rigid surfaces undergo smaller relaxation and are most difficult for chemisorption-induced restructuring [694]. Flexible MOFs are thermodynamically more prone to adapt to the changing environment at the catalytic interface. Such dynamic materials, due to the conformation variety, breathing behavior and stimuli-responsive pores may be suitable for being a platform for an artificial switchable catalyst. For example, Zr-based MOF PCN-700 fabricated by Yuan and co-workers [695], was able to switch on or off its catalytic activity when it went upon reversible structural change. However, flexibility can lead to structural deformations which can weaken the size confinement effect. In consequence, more structural flexibility of the MOF can increase substrate conversion, but decrease selectivity towards the desired product [696].

Defects are associated with undermining the crystalline structure and indeed not all of them are beneficial. That is why their identification and quantification is essential [180,697–701]. In

order to increase the number of defects in MOFs the most common approach is the thermal pre-treatment to liberate labile ligands such as water or other electron-donor solvents to create missing linker defects [702]. Liberation generates CUSs and those metal sites without full coordination behave as Lewis acids. They indicate a strong affinity towards basic molecules or can become binding sites for small gas molecules such as CO_2. As those acid sites are situated in a confined pore environment, they can induce regioselectivity and shape- or size-selectivity towards guest molecules or reaction intermediates [703–705]. In the case of metal oxide cluster IBUs, after solvent removal, hydroxyl groups become more accessible and, accordingly, they can act as Lewis acid or Brønsted acid towards the substrate. The nature and strength of the MOF acid sites can be changed with the composition, by linker modification or by adopting a mixed linkers/metals approach [706,707]. The defect engineering in MOF crystal depends strongly on the reaction rate and temperature. If the reaction is slow and conditions provide thermodynamically stable growth, obtained MOF crystals usually are almost defect-free. On the contrary, if the reaction is fast and hence kinetically driven, IBUs and OBUs may encounter difficulties in achieving full coordination. Importantly, the number of missing building units should not prevent the formation of the intended original MOF structure formation. Lewis acid CUSs and basic active sites incorporated into MOF are suitable for catalytic transformations, such as cross-aldol and Knoevenagel condensation reactions [708–711]. For example, it was observed that an amino-functionalized UiO-66-NH_2 MOF exhibits a higher conversion (67%) than UiO-66 in the cross-aldol condensation of benzaldehyde with heptanal (30%) [711]. Related improvements were observed for a Knoevenagel condensation catalyzed by the amino-functionalized isoreticular MOF IRMOF-3 compared to its unfunctionalized version MOF-5. In this case, acid sites were present in the original MOF, Zn_4O clusters linked by 2-aminoterephthalic acid, thus no further enhancements were necessary [712,713]. MOFs acid-base activity can also promote cascade reactions, such as deacetalization-Knoevenagel reactions. Amino-functionalized MOF, MIL-101(Al)-NH_2, performs as a bifunctional acid-base catalyst [714]. These studies showed that MIL-101(Al)-NH_2 Brønsted acid and base sites promote both the deacetalization of benzaldehyde dimethylacetal and Knoevenagel condensation of benzaldehyde with malononitril. Additionally, this MOF catalyst can be applied for the one-pot reaction of benzaldehyde dimethylacetal and malononitrile to produce benzylidenemalononitrile. Among various MOF catalysts such as MIL-53(Al)-NH_2, MIL-53(Al), MIL-101(Cr)-NH_2, MIL-101(Cr), Zr-MOF-NH_2, Zr-MOF, Cu-MOF [$Cu_3(btc)_2$], and Ca-MOF (Ca-mtb), the MIL-101(Al)-NH_2 exhibited the highest catalytic activity in the benzylidenemalononitrile synthesis.

MOF catalysts can be prepared by introducing metalloligand active sites in a direct synthesis or with PSM. Pintado-Sierra and co-workers [715] introduced iridium complexes into UiO-66-NH_2 and IRMOF-3 through PSM resulting in the UiO-66-NH_2LIr and MOF-3-LIr structures. Those catalysts were used for the synthesis of mono N-alkylamines *via* reductive amination of aldehydes with nitroarenes, in a three-step cascade reaction. This type of reaction allowed making the process more sustainable because several steps occur in the same vessel without intermediate steps. Both materials exhibited higher selectivity towards secondary aromatic amines (the exact product depends on the applied aldehyde) than the corresponding homogeneous catalyst. In 2019 Liu *et al.* [716] synthesized bifunctional cationic Zr-based MTV-MOFs containing a salen-Co(III) motif and imidazolium. They used sequential mixed-ligands synthesis and post-synthetic ionization strategy to obtain MTV-MOFs with different amounts of Co and linker. The cationic MTV-MOF salen-Co(23%)⊂f(Br^-)etim-UiO-6 (etim = ethylimidazole) significantly enhanced the activity and selectivity of the CO_2 cycloaddition reaction with epoxides. More importantly, the catalyst revealed good thermal stability and it was reusable for at least five runs without a significant reduction of its catalytic activity and selectivity towards cyclic carbonates.

Another approach to control the number of defects in MOFs is using modulators during syntheses [717]. The modulator competes with the linker in coordination to the IBU, resulting in more available active sites. Using monocarboxylate modulators (*e.g.* acetic, benzoil, or trifluoroacetic acid (TFA)) during the synthesis of UiO-66 facilitates the control of the crystallite size as well as of the formation of defects [704]. In 2013, Vermootrele *et al.* [718] presented various examples of CUSs Zr_6 clusters through TFA incorporation. The addition of TFA increased the catalytic activity in several reactions such as cyclization of citronellal to isopulegol or Meerwein reduction of 4-tert-butylcyclohexanone. Moreover, the removal of this compound by thermal treatment enhanced the number of CUS. Jiang *et al.* [719] functionalized Al-based MOF USTC-253 synthesized by the reaction of $Al(NO_3)_3{\cdot}9H_2O$ and 4,4'-dibenzoic acid-2,2'-sulfone (sbpdc) in DMF with TFA. This procedure resulted in a defect-containing USTC-253-TFA, showing improved catalytic activity in the cycloaddition of CO_2 and epoxide (propylene oxide) in comparison to USTC-253 with increased yield from 74.4% to 81.3%. Yuan and co-workers [720] significantly enhanced the adsorbability of uranyl ions (from 24 to 357 mg/g) by tuning missing-linker defects of UiO-66. A tentative mechanism for the cycloaddition of CO_2 and epoxide into cyclic carbonate over USTC-253-TFA was proposed (Fig. 62) [719].

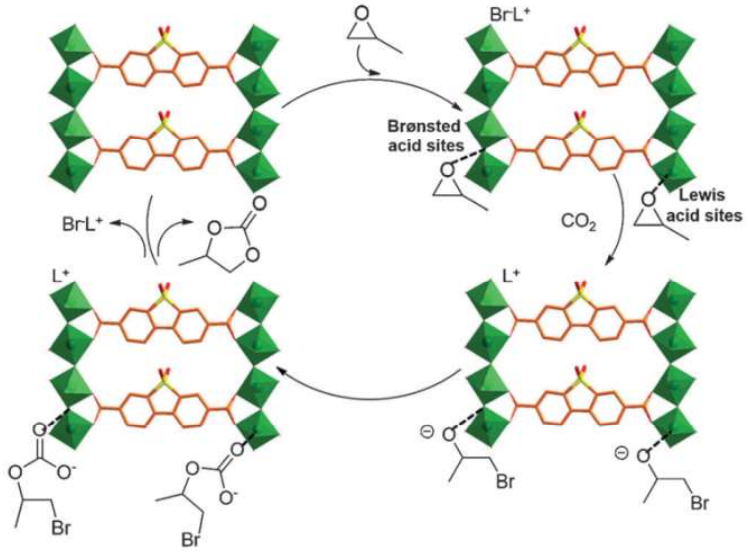

Figure 62. Proposed catalytic mechanism for the CO_2 cycloaddition of epoxide into cyclic carbonate over USTC-253-TFA (Reprinted with the permission [719]. Copyright 2015, John Wiley & Sons).

A different and very promising approach to enhancing catalytic performance is to construct bimetallic clusters in a porous framework. MOFs with free hydroxyl groups have attracted considerable attention due to their potential to anchor catalysts in an analogous way to traditional metal-oxosupports but having a much higher inner surface compared to those materials. Simple impregnation of MOFs with transition metal-containing species results already in active metal-based heterogeneous catalysts [721]. Both can be fabricated in the vapor phase *via* atomic layer deposition (ALD) in MOFs, and in condensed phase *via* solvothermal deposition in MOFs. Zr-based MOFs have a great application potential as solid supports in gas-phase catalysis and can be readily modified post-synthetically. For instance, in 2016 Li and co-workers [722] used ALD onto MOF to incorporate catalytically active metal centers. The method allowed the deposit of an atomic layer of metal on substrates. They introduced Ni on the node of a Zr-based MOF, NU-1000. The obtained material indicated high activity in terms of catalytic performance in gas-phase hydrogenation. Furthermore, its outstanding regenerability and long-term stability enhanced the longevity of these processes. The MOF's structure revealed the presence of isolated active sites. Between the deposited metal ions and the Zr_6 nodes, strong interaction occurred. Also, the organic linkers prevented the atom/ions from migration and agglomeration due to the isolation of support sites *via* lengthy organic spacers. It was confirmed that ALD is an effective strategy to produce stable single-site catalysts [722,723]. Noh *et al.* [724] explored the deposition of catalytically active molybdenum(VI) oxide on the node of NU-1000 by solvothermal deposition in MOFs. Its

catalytic activity was tested in the epoxidation of cyclohexene. MO-SIM achieved the high conversion of 93±2% (similar to a bulk Zr-supported analog), as well as excellent stability without leaching of the active species and loss in yield upon recycling.

The modifications of IBUs and OBUs enable the synthesis of specific MOF catalysts for asymmetric reactions, which are usually difficult to proceed by conventional inorganic catalysts such as zeolites. In addition, they are facing troublesome challenges in terms of low thermal-, water- and chemical stability, which reduces their applicability. Concerning this issue, in 2017 Chen *et al.* [725] combined bulky hydrophobic groups and chiral metal phosphonate linkers in obtaining a more stable MOF as the comprehensive asymmetric catalyst for several reactions: asymmetric allylboration, propargylation, Friedel-Crafts alkylation, and sulfoxidation. Phosphonates create strong bonds with metal ions and thanks to bulky *tert*-butyl groups asymmetric induction of mentioned reactions was controlled through the geometrical constraints. The stability of this framework was a result of the kinetic blocking through the protection of hydrolytically sensitive coordination backbones. The chiral dicarboxylate linker was derived from 1,1'-biphenol phosphoric acid and *tert*-butyl group, coordinated to the metal center *via* carboxylate and phosphonate groups. Consequently, 16 isostructural MOFs with chiral Lewis acidity could be synthesized. Furthermore, adjusting the catalytic feature *via* the insertion of different metals led to various catalytic activity in asymmetric reactions *i.e.* boration, propargylation, Friedel-Crafts alkylation, and sulfoxidation. It should be emphasized that those materials showed better efficiency than their homogeneous catalyst analogs that were not able to promote reaction with satisfactory enantioselectivity They also indicated good aqueous and thermal stability, along with acid/base tolerance. The combination of those properties together with recyclability makes them interesting candidates for pharmaceuticals and fine chemicals syntheses [725,726].

MOFs exhibit many attractive properties for electrocatalysis applications such as high surface area, permanent porosity, and site isolation. The high surface area gives the potential to load more catalytically active particles than in corresponding electrodes monolayers. Furthermore, permanent porosity facilitates fast substrate diffusion, whilst site isolation of catalyst molecules inside the framework inhibits bimolecular decomposition pathways. Nevertheless, MOFs are traditionally composed of the organic linker and redox-inert metal clusters (*e.g.* d^0 Zr^{4+}, d^{10} Zn^{2+}) which lead to poor charge transport to the MOF-embedded catalysts [727]. Hence, the realization of effective electrocatalytic MOFs has remained challenging. The UiO series of MOFs, usually exhibit outstanding thermal and chemical stability even under catalytic conditions (*i.e.* under irradiation, wide pH range, and at applied reductive and oxidative

potentials). Thus, these materials are excellent platforms for molecular catalysts immobilization. Nevertheless, the suitability of UiO-type MOFs as electrocatalysis platforms is presently limited because the Zr-based SBUs and their phenyl carboxylate linkers are redox-inactive within a reasonable potential window. In 2018 Johnson and co-workers [642] developed the first electroactive MOF with the UiO/PIZOF topology (Zr(dcphOH-ndi) by using redox-active naphthalene diimide linkers appended with carboxylic acid groups (dcphOH-ndi) (Fig. 63). The material revealed high stability, porosity, and charge transport properties required for electrocatalysis. Including hydroxyl groups on the dcphOH-ndi linker facilitated the proton transport through the material. The pK_a's of both the proton-responsive ndi linker and the Zr node demonstrated potential use in proton-coupled electron transfer (PCET) at pH range 3.4–6.1. The obtained Zr(dcphOH-NDI)@FTO thin film (1 μm) on the conducting fluorine-doped tin oxide displayed reversible electrochromic behavior due to the one-electron reductions of the redox-active NDI linker. 97 % of the NDI sites were electrochemically active at applied potentials. Additionally, the MOF thin film also confirmed to act efficiently in aqueous solutions, extending their further potential usefulness in electrocatalytic applications [642].

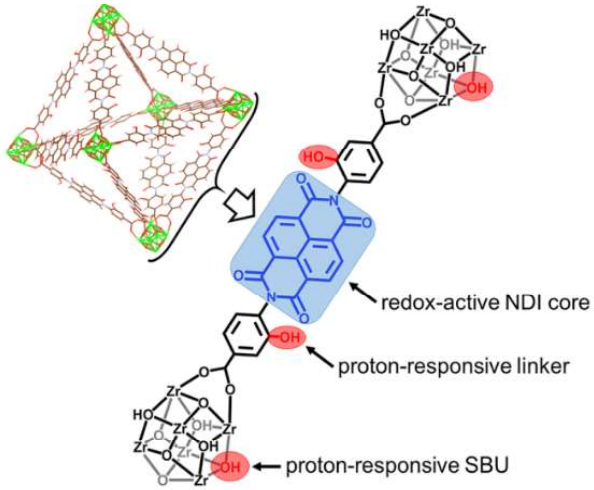

Figure 63. MOF design strategy for developing a redox-active framework featuring UiO topology with proton-responsive functionalities (Reprinted with the permission [642]. Copyright 2018, American Chemical Society).

Oxygen evolution reaction (OER) and hydrogen evolution reaction (HER) are the two core processes for electrochemical water splitting [728,729]. In the case of OER, MOFs operate in a *modus* that possess an energy cost significantly above thermodynamic requirements, showing a high overpotential and small TOF during oxygen evolution. Recently, a few 2D MOFs have been synthesized by Duan and co-workers [730]. They presented a strategy for the *in situ*

growth of ultrathin nanosheet arrays of 2D MOFs on different supports. They fabricated a Ni-Fe-based MOF which demonstrated several enhanced features for catalysis. Increased catalytic activity, more favorable kinetics, and strong endurance at electrocatalysis overall improved OER and HER. The material indicated superior electrocatalytic efficiency towards the oxygen evolution reaction. It revealed a small overpotential of 240 mV at 10 mA/cm^2, and robust operation for 20,000 seconds with no detectable decline in the catalytic activity. Moreover, the above mentioned MOF can be readily adaptable to prepare other 2D MOFs with different IBUs such as Co, Mn, Ti, and Mo [730].

In 2020, Fiaz and co-workers [731] reported a facile route for a low cost room temperature synthesis of TMS@MOF-5 (TMS, transition metal sulfide = MnS, FeS, CoS, NiS, CuS, and ZnS) composites by *in situ* incorporations of pre-synthesized TMS nanoparticles into MOF-5. All samples were coated on Ni-foam (NF). The comparison of OER catalytic activity between materials showed that NiS@MOF-5/NF is a highly efficient OER catalyst and it requires just 174 mV overpotential to deliver the 10 mA/cm^2 current density. It is still challenging to find intrinsically conductive, chemically, and electrochemically stable ORR (oxygen reduction reaction) electrocatalysts characterized by well-defined and tunable active sites. In another study, Miner *et al.* [428] presented a highly electron-conducting 2D MOF $Ni_3(HITP)_2$ (HITP=2, 3, 6, 7, 10, 11-hexaiminotriphenylene) with electrocatalytic ORR activity. It acted as a well-defined, tunable oxygen reduction electrocatalyst in alkaline solution. The MOF exhibited ORR activity and electrical conductivity (σ=40 S/cm) with no post-synthetic treatment or further modifications.

The pore size and shape tailorability of MOFs makes them promising materials for shape-selective catalysis, which aim to confine and thereby stabilize transition states on reaction intermediates. However, to the best of our knowledge, this kind of catalysis is still underexplored. MOFs assembled from transition metal diphosphine pincer complexes (pincer MOFs) are used extensively in heterogeneous catalysis due to their stability and they can take advantage of the effects of immobilization and site isolation. In 2018 Reiner *et al.* [732] synthesized and characterized 1-PdX = $\{Zr_6O_4(OH)_4(OAc)_{2.4}[L\text{-}PdX]_{2.4}\}Y_{2.4}$; (X=Cl (25%), I (75%); Y= Cl, I). After post-synthetic modification and ligand exchange at the pincer Pd sites, 1-PdTFA was synthesized. The oxidative I^-/TFA^- ligand exchange step achieved only ~50% yield, even after successful treatment with the hypervalent iodine reagent $PhI(TFA)_2$. Despite the good catalytic activity in intramolecular hydroamination of o-substituted alkynyl aniline, 1-PdTFA showed poor recyclability. It was proposed that the formation of a trifluoroacetamide side product caused catalyst deactivation. The comparison of catalytic activity of homogeneous

analogs indicated that substitution of TFA^- for a less reactive anion could inhibit catalyst deactivation and increase activity and recyclability. Hence, in 2018 Reiner and co-workers [65] reported the synthesis of 1-$PdBF_4$ through oxidative I^-/BF_4^- ligand exchange using the commercially available reagent $NOBF_4$. Generated material exhibited significantly better Lewis acid catalytic activity and recyclability than the previously reported TFA^- analog 1-PdTFA. Differences in reactivity can be caused by weaker coordinating nature of BF_4^- and its lower propensity to undergo unfavorable side reactions with substrates. $PdBF_4$ also showed a high selectivity degree to citronellal for the intramolecular hydroamination of 2-ethynylaniline over a self-dimerization process, while the homogeneous analog $^tBu_4$L-$PdBF_4$ generated a mixture of products.

The oxidation of alcohols into carbonyl compounds (ketone/aldehyde) is a very important topic due to their extensive application in the industry [734–736]. Traditionally oxidizing agents (*e.g.* MnO_2, CrO_3, or $KMnO_4$) are widely used in industry but only under severe conditions, such as high pressure or temperatures and highly acidic environment [737–739]. These chemical transformations often generate environmentally harmful toxic inorganic salts. Thus, the design of an effective, environmentally friendly, and sustainable oxidative catalyst is still an open challenge that needs to be addressed in the future. Polyoxometalates (POMs) may be an alternative because of their unique redox properties and tunable acidity [740–742]. However, only catalysts containing metals such as Co, Fe, Cu, or noble metals (Ru, Pd, Au) exhibit high efficiency in alcohol oxidation reactions [743]. Due to the high cost of noble metals, they are not suitable for the industrial synthesis of basic fine chemicals. Additionally, POMs' poor stability and low exposure of active sites impede their actual application in mass production. POM-based MOFs (POMOFs) utilize POMs and MOFs attributes and they can expand their applicability [744,745]. The spatial distances between POM anions can be significantly increased through the immobilization of functional POMs into MOFs, thereby enhancing anion clusters dispersity and exposing more active sites. In 2019 Li *et al.* [746] reported the synthesis of 3D Cu-based POMOF HENU-1. It was based on Dawson type phosphotungstates and *in situ* generated ligands $H[Cu_5^{I}Cu^{II}(pzc)_2(pz)_{4.5}\{P_2W_{18}\text{-}O_{62}\}]\cdot 6H_2O$ (Hpzc = pyrazine-2-carboxylic acid, pz = pyrazine). Through the pyrolysis of the pzc linker partially generated the secondary pz linker, and both the components participating in the MOF construction. The material was able to efficiently catalyze the oxidation of 1-phenylethanol, achieving a 97 % yield of the target product acetophenone after 3 h with a TOF of 9690 h^{-1}. HENU-1 exhibited good stability in the air as well as tolerance to basic and acidic media in the pH range of 1-12. It was also reused for at least five cycles without significant catalytic activity loss. Consequently,

incorporating the active transition metal ions and POMs to assemble POMOFs *via* the bridging of organic ligands may become an effective method to construct a POM-based heterogeneous catalytic platform for different organic reactions.

Although reticular chemistry holds the potential to design site-specific catalysts, a combination of theory and experimental efforts is required. In 2020, Yang and co-workers [747] reported an experimental and theoretical investigation of the catalytic dehydration of *t*-butyl alcohol (tba), which was used to examine the activity of OH groups of Zr_6O_8 nodes in the MOFs UiO-66 and MOF-808. The materials also differed in vacancy sites densities (Fig. 64) and pore sizes. The OH groups originated from the aqueous synthesis environment and behave like both Brønsted acid and base sites. It was shown that terminal OH groups on defect sites of Zr_6O_8 nodes of MOF-808 and UiO-66 catalyze the tba dehydration, with rates depending on ligands at defect sites and transport limitations. MOF-808 and UiO-66, which have approximately 6 and 1 vacancies per Zr_6O_8 node, respectively, were compared with alumina and zirconia. MOF-808 with higher vacancies nodes exhibited initially higher activity than UiO-66 material, but it must be noted that a higher amount of vacancies also reduces MOF catalyst stability. The OH groups in UiO-66 and MOF-808 act as Brønsted basic sites, and they are generated by the removal of formate/acetate ligands. The latter are initially present on the nodes *via* esterification reactions within the alcohol, which is shown by density functional theory calculations. It was proved that the binding of two tba molecules to node Zr atoms during the esterification reaction helped in lowering the total activation energy of this reaction.

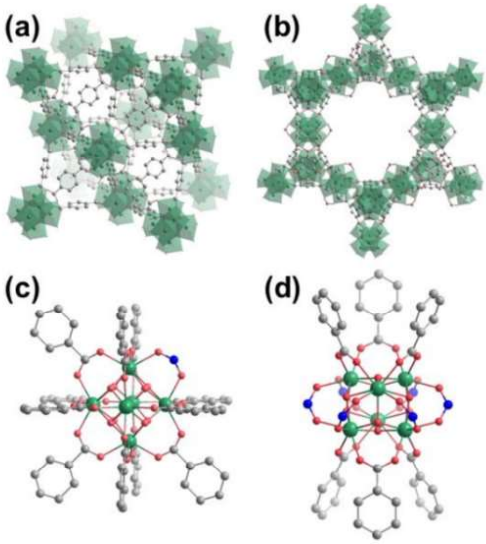

Figure 64. Crystal structures of (a) UiO-66 and (b) MOF-808, with details showing (c) missing-linker defects of UiO-66 and (d) structural vacancies of MOF-808. Ligands on defects/vacancies are shown in blue (Reprinted with the permission [747]. Copyright 2020, American Chemical Society).

P-xylene is an inexpensive industrial raw material, widely used in the synthesis of terephthalic acid, the precursor to polyester resins [748]. Interestingly, p-xylene is rarely oxidized to other oxygen-containing derivatives like hydroxymethylbenzoic acid (hmba) containing useful hydroxyl and carboxyl groups. The current synthesis method of hmba is not sensible due to the multistep process, long reaction times, low selectivity, and high reaction temperature and pressure. In 2019, Li and co-workers [748] presented efficient and simple hmba preparation by one-step p-xylene oxidation at 30 °C for 5 h. P-xylene's two methyl groups were oxidized to hydroxymethyl and carboxyl using Cu-MOF as the catalyst and acetonitrile as the solvent. Very high selectivity (99.2%) to 4-hydroxymethylbenzoic acid and good substrate conversion (85.5%) of p-xylene was achieved. These results indicate that Cu-MOF is a high-performance oxidation catalyst under mild conditions, which is also capable of proceeding the reaction three-times with the same activity.

An efficient approach to improve the stability of nanoparticles could be hierarchical nanoencapsulation [749–751]. For example, a mesoporous silica ($mSiO_2$) shell can significantly increase the mechanical properties of encapsulated MOFs. However, it is challenging due to the strong hydrophilic properties of $mSiO_2$. In 2018, Ying *et al*. [749] presented a simple method for the direct coating of MOF nanoparticles (MIL-101(Cr)) with a very thin hydrophobic $mSiO_2$ shell and the effect of the $mSiO_2$ shell on the MOFs in the oxidation of indene. The TOF value of the MIL-101(Cr)@$mSiO_2$ was 1.24 times greater than MIL-101(Cr). Thereby, MIL-101(Cr)@$mSiO_2$ performed improved catalytic activity, and also enhanced reusability as catalyst in the indene oxidation. In 2019, Gharib and co-workers [752] synthesized three new 3D Co(II)-based MOFs (TMU-49, TMU-50, and TMU-51) containing a highly π-conjugated amide-functionalized ligand. They were applied in the regioselective methanolysis of epoxides. Thereafter, to improve the MOF catalytic efficiency N1,N3-di(pyridine-4-yl) malonamide linker (S) was incorporated *via* SALE. New linker enhanced catalytic activity in the epoxide ring-opening reactions. The obtained isostructural materials (MOFs TMU-49S, TMU-50S and TMU-51S) could be reused without any significant loss in catalytic efficiency.

2-arylbenzoxazoles are a high potential class of pharmaceutically active compounds as they have anti-cancer, anti-inflammatory, antifungal, and antiviral properties. Currently, the synthesis method suffers from various drawbacks, such as the use of volatile organic solvents, the difficulty of catalyst recovery, and reuse with catalytic activity loss [753]. In 2017 Nguyen *et al.* [753] successfully synthesized a new superacidic MOF, based on the 6-connected Hf-oxo-cluster and the tritopic linker by sulfation method. The material exhibited unusual catalytic

performance for solvent-free heterocyclization of 2-arylbenzoxazoles synthesis. The reaction was performed with the high yield and ease of the catalyst recycling, with only a little reactivity loss, resulting in a 5% yield decrease after 5 catalytic cycles.

In 2015 Choi and co-workers [754] used strong sulfonic acid group ($-SO_3H$) and weak ammonium group ($-NH_3^+$) to incorporate them into a UiO-66 [$Zr_6O_4(OH)_4(bdc)_6$, separately and in a mixed way in the presence of 2.5 nm Pt NPs. The obtained materials were investigated in isomerization reactions of methyl-cyclopentane (MCP). The used functional groups play a key role in product activity and selectivity in the gas-phase conversion of MCP to acyclic isomer, olefins, cyclohexane, and benzene. Pt⊂nUiO-66-S catalytic activity was doubled comparing to the non-functionalized Pt⊂nUiO-66. Its selectivity to C_6-cyclic products (62.4 % and 28.6 % for cyclohexane and benzene, respectively) that contained no acyclic isomers products was the highest among the tested materials. All Pt⊂nUiO-66 catalysts with different functionalities maintained their morphology, crystal structure, and chemical composition without deactivation after 8 h of the process [754]. A similar case was explored in 2016 by Li *et al.* [755] in isoreticular UiO-66-X MOFs (X = H, NH_2, OMe) after Pd NPs encapsulation. These materials catalyzed the aerobic reaction between ethylene glycol and benzaldehyde. Pd@UiO-66-NH_2 exhibited high selectivity to benzaldehyde ethylene acetal of 94%, whereas both Pd@UiO-66-H and Pd@UiO-66-OMe revealed high selectivity (90% and 97%, respectively) to the ester 2-hydroxyethyl benzoate. These results demonstrate that the control of catalytic sites *via* their chemical surrounding at the molecular level creates interesting opportunities for the development of tunable metal-MOF catalysts for selective chemical transformations.

7.3. Summary

In this chapter, we showed how MOF materials can greatly improve heterogeneous catalysis despite their low-stability reputation. Their sophisticated structures offer interesting opportunities in *e.g.* gas-phase hydrogenation, redox-, or photoinduced catalysis. Moreover, they are also able to stabilize sensitive enzymes. MOFs outstanding performance (as seen by the increasing number of examples) stems from their inherent hierarchical arrangement of pores and building blocks network, which can accelerate reaction rates. By tuning their pore size, crystal defects, flexibility, and distribution of active sites the crucial confinement and diffusion mechanisms can be adapted. However, further investigations on correlating experimental conditions, surface barriers, adsorption enthalpies, kinetics, and catalytic performance must be considered. Many possible modifications (*e.g.* defect engineering or

functionalization), nodes, linkers combinations, and pore geometries could afford enzyme-like selectivity in terms of preferred substrate affinity/recognition and therefore allow the synthesis of the desired products with higher yields and greener pathways.

8. Concluding remarks

By venturing into the vast landscape of MOFs applications, we presented a comprehensive—albeit not necessarily complete—overview of how reticular diversity projected MOFs into so many technological areas, where they are currently a class of materials of primary importance. As diversity is an intrinsically flexible and inclusive concept that evolves along with the discovery of unknown properties or unseen aspects of already-known ones, we encourage established and emerging scientists to embrace its complex and ever-evolving meaning in reticular chemistry. We strongly believe that the combination of this mindset with the knowledge of the state of the art that herein we endeavored to provide will enable the next achievements in the field of MOFs, and new milestones in all the scientific fields they contribute to advance.

References

[1] H. Furukawa, U. Müller, O.M. Yaghi, "Heterogeneity within order" in metal-organic frameworks, Angew. Chemie - Int. Ed. 54 (2015) 3417–3430. https://doi.org/10.1002/anie.201410252.

[2] Z. Ji, H. Wang, S. Canossa, S. Wuttke, O.M. Yaghi, Pore Chemistry of Metal–Organic Frameworks, Adv. Funct. Mater. 2000238 (2020) 1–24. https://doi.org/10.1002/adfm.202000238.

[3] H. Furukawa, K.E. Cordova, M. O'Keeffe, O.M. Yaghi, The Chemistry and Applications of Metal-Organic Frameworks, Science (80-.). 341 (2013) 1230444–1230444. https://doi.org/10.1126/science.1230444.

[4] M. Lismont, L. Dreesen, S. Wuttke, Metal-organic framework nanoparticles in photodynamic therapy: current status and perspectives, Adv. Funct. Mater. 27 (2017) 1606314.

[5] P.Z. Moghadam, A. Li, S.B. Wiggin, A. Tao, A.G.P. Maloney, P.A. Wood, S.C. Ward, D. Fairen-Jimenez, Development of a Cambridge Structural Database subset: a collection of metal–organic frameworks for past, present, and future, Chem. Mater. 29 (2017) 2618–2625.

[6] N.W. Ockwig, O. Delgado-Friedrichs, M. O'Keeffe, O.M. Yaghi, Reticular chemistry: occurrence and taxonomy of nets and grammar for the design of frameworks, Acc. Chem. Res. 38 (2005) 176–182.

[7] M. O'Keeffe, M.A. Peskov, S.J. Ramsden, O.M. Yaghi, The reticular chemistry structure resource (RCSR) database of, and symbols for, crystal nets, Acc. Chem. Res. 41 (2008) 1782–1789.

[8] N. Stock, S. Biswas, Synthesis of Metal-Organic Frameworks (MOFs): Routes to Various MOF Topologies, Morphologies, and Composites, Chem. Rev. 112 (2012) 933–969. https://doi.org/10.1021/cr200304e.

[9] F. Haase, P. Hirschle, R. Freund, S. Furukawa, Z. Ji, S. Wuttke, Beyond Frameworks: Structuring Reticular Materials across Nano, Meso, and Bulk Regimes, Angew. Chemie Int. Ed. (2020).

[10] M. Eddaoudi, J. Kim, N. Rosi, D. Vodak, J. Wachter, M. O'Keeffe, O.M. Yaghi, Systematic design of pore size and functionality in isoreticular MOFs and their application in methane storage, Science (80-.). 295 (2002) 469–472.

[11] A. Gonzalez-Nelson, F.-X. Coudert, M.A. van der Veen, Rotational dynamics of linkers in metal–organic frameworks, Nanomaterials. 9 (2019) 330.

[12] A. Schneemann, V. Bon, I. Schwedler, I. Senkovska, S. Kaskel, R.A. Fischer, Flexible metal-organic frameworks, Chem. Soc. Rev. 43 (2014) 6062–6096. https://doi.org/10.1039/c4cs00101j.

[13] S. Dissegna, K. Epp, W.R. Heinz, G. Kieslich, R.A. Fischer, Metal–Organic Frameworks: Defective Metal-Organic Frameworks (Adv. Mater. 37/2018), Adv. Mater. 30 (2018) 1870280.

[14] S. Abednatanzi, P. Gohari Derakhshandeh, H. Depauw, F.X. Coudert, H. Vrielinck, P. Van Der Voort, K. Leus, Mixed-metal metal-organic frameworks, Chem. Soc. Rev. 48 (2019) 2535–2565. https://doi.org/10.1039/c8cs00337h.

[15] J.-S. Qin, S. Yuan, Q. Wang, A. Alsalme, H.-C. Zhou, Mixed-linker strategy for the construction of multifunctional metal–organic frameworks, J. Mater. Chem. A. 5 (2017) 4280–4291. https://doi.org/10.1039/C6TA10281F.

[16] A.G. Slater, A.I. Cooper, Function-led design of new porous materials, Science (80-.). 348 (2015) aaa8075–aaa8075. https://doi.org/10.1126/science.aaa8075.

[17] S. Canossa, S. Wuttke, Functionalisation chemistry of porous materials, Adv. Funct. Mater. (2020) 2003875. https://doi.org/10.1002/adfm.202003875.

[18] O.M. Yaghi, M.J. Kalmutzki, C.S. Diercks, N. Hanikel, O.M. Yaghi, Introduction to

Reticular Chemistry, Mol. Front. J. 4 (2019) eaat9180–eaat9180. https://doi.org/10.1142/s2529732519400054.

[19] A. Karmakar, A. V Desai, S.K. Ghosh, Ionic metal-organic frameworks (iMOFs): Design principles and applications, Coord. Chem. Rev. 307 (2016) 313–341. https://doi.org/10.1016/j.ccr.2015.08.007.

[20] G. Zhang, Z.A. Lan, X. Wang, Conjugated Polymers: Catalysts for Photocatalytic Hydrogen Evolution, Angew. Chemie - Int. Ed. 55 (2016) 15712–15727. https://doi.org/10.1002/anie.201607375.

[21] C.A. Fernandez, S.K. Nune, H. V Annapureddy, L.X. Dang, B.P. McGrail, F. Zheng, E. Polikarpov, D.L. King, C. Freeman, K.P. Brooks, Hydrophobic and moisture-stable metal–organic frameworks, Dalt. Trans. 44 (2015) 13490–13497. https://doi.org/10.1039/C5DT00606F.

[22] K. Jayaramulu, F. Geyer, A. Schneemann, Š. Kment, M. Otyepka, R. Zboril, D. Vollmer, R.A. Fischer, Hydrophobic Metal–Organic Frameworks, Adv. Mater. 31 (2019) 1900820. https://doi.org/10.1002/adma.201900820.

[23] L.H. Xie, M.M. Xu, X.M. Liu, M.J. Zhao, J.R. Li, Hydrophobic Metal–Organic Frameworks: Assessment, Construction, and Diverse Applications, Adv. Sci. 7 (2020). https://doi.org/10.1002/advs.201901758.

[24] L.K. Macreadie, E.J. Mensforth, R. Babarao, K. Konstas, S.G. Telfer, C.M. Doherty, J. Tsanaktsidis, S.R. Batten, M.R. Hill, CUB-5: A Contoured Aliphatic Pore Environment in a Cubic Framework with Potential for Benzene Separation Applications, J. Am. Chem. Soc. 141 (2019) 3828–3832. https://doi.org/10.1021/jacs.8b13639.

[25] Y. Peng, T. Gong, K. Zhang, X. Lin, Y. Liu, J. Jiang, Y. Cui, Engineering chiral porous metal-organic frameworks for enantioselective adsorption and separation, Nat. Commun. 5 (2014) 4406. https://doi.org/10.1038/ncomms5406.

[26] K. Gedrich, M. Heitbaum, A. Notzon, I. Senkovska, R. Fröhlich, J. Getzschmann, U. Mueller, F. Glorius, S. Kaskel, A family of chiral metal-organic frameworks, Chem. - A Eur. J. (2011). https://doi.org/10.1002/chem.201002568.

[27] L. Ma, J.M. Falkowski, C. Abney, W. Lin, A series of isoreticular chiral metal–organic frameworks as a tunable platform for asymmetric catalysis, Nat. Chem. 2 (2010) 838–846. https://doi.org/10.1038/nchem.738.

[28] Z.G. Gu, A. Pfriem, S. Hamsch, H. Breitwieser, J. Wohlgemuth, L. Heinke, H. Gliemann, C. Wöll, Transparent films of metal-organic frameworks for optical

applications, Microporous Mesoporous Mater. (2015). https://doi.org/10.1016/j.micromeso.2015.02.048.

[29] X. Jiang, L. Zhang, S. Liu, Y. Zhang, Z. He, W. Li, F. Zhang, Y. Shi, W. Lü, Y. Li, Q. Wen, J. Li, J. Feng, S. Ruan, Y.-J. Zeng, X. Zhu, Y. Lu, H. Zhang, Ultrathin Metal–Organic Framework: An Emerging Broadband Nonlinear Optical Material for Ultrafast Photonics, Adv. Opt. Mater. 6 (2018) 1800561. https://doi.org/10.1002/adom.201800561.

[30] R. Scatena, Y.T. Guntern, P. Macchi, Electron Density and Dielectric Properties of Highly Porous MOFs: Binding and Mobility of Guest Molecules in Cu3(BTC)2 and Zn3(BTC)2, J. Am. Chem. Soc. 141 (2019) 9382–9390. https://doi.org/10.1021/jacs.9b03643.

[31] L. Sun, M.G. Campbell, M. Dincə, Electrically Conductive Porous Metal-Organic Frameworks, Angew. Chemie - Int. Ed. 55 (2016) 3566–3579. https://doi.org/10.1002/anie.201506219.

[32] A.E. Baumann, D.A. Burns, B. Liu, V.S. Thoi, Metal-organic framework functionalization and design strategies for advanced electrochemical energy storage devices, Commun. Chem. 2 (2019) 1–14. https://doi.org/10.1038/s42004-019-0184-6.

[33] H. Babaei, A.J.H. McGaughey, C.E. Wilmer, Effect of pore size and shape on the thermal conductivity of metal-organic frameworks, Chem. Sci. 8 (2016) 583–589. https://doi.org/10.1039/C6SC03704F.

[34] J. Jiang, Y. Zhao, O.M. Yaghi, Covalent Chemistry beyond Molecules, J. Am. Chem. Soc. 138 (2016) 3255–3265. https://doi.org/10.1021/jacs.5b10666.

[35] S. Ali Akbar Razavi, A. Morsali, Linker functionalized metal-organic frameworks, Coord. Chem. Rev. 399 (2019) 213023. https://doi.org/10.1016/j.ccr.2019.213023.

[36] J.N. Hall, P. Bollini, Structure, characterization, and catalytic properties of open-metal sites in metal organic frameworks, React. Chem. Eng. 4 (2019) 207–222. https://doi.org/10.1039/c8re00228b.

[37] G. Férey, C. Serre, Large breathing effects in three-dimensional porous hybrid matter: Facts, analyses, rules and consequences, Chem. Soc. Rev. 38 (2009) 1380–1399. https://doi.org/10.1039/b804302g.

[38] Y. Hijikata, S. Horike, M. Sugimoto, H. Sato, R. Matsuda, S. Kitagawa, Relationship between channel and sorption properties in coordination polymers with interdigitated structures., Chemistry. 17 (2011) 5138–5144. https://doi.org/10.1002/chem.201003734.

[39] C.R. Murdock, B.C. Hughes, Z. Lu, D.M. Jenkins, Approaches for synthesizing breathing MOFs by exploiting dimensional rigidity, Coord. Chem. Rev. 258–259 (2014) 119–136. https://doi.org/10.1016/j.ccr.2013.09.006.

[40] D.-Y. Hong, Y.K. Hwang, C. Serre, G. Férey, J.-S. Chang, Porous Chromium Terephthalate MIL-101 with Coordinatively Unsaturated Sites: Surface Functionalization, Encapsulation, Sorption and Catalysis, Adv. Funct. Mater. 19 (2009) 1537–1552. https://doi.org/10.1002/adfm.200801130.

[41] D. Buso, J. Jasieniak, M.D.H. Lay, P. Schiavuta, P. Scopece, J. Laird, H. Amenitsch, A.J. Hill, P. Falcaro, Highly Luminescent Metal-Organic Frameworks Through Quantum Dot Doping, Small. 8 (2012) 80–88. https://doi.org/10.1002/smll.201100710.

[42] J.-W. Sun, P.-F. Yan, G.-H. An, J.-Q. Sha, G.-M. Li, G.-Y. Yang, Immobilization of Polyoxometalate in the Metal-Organic Framework rht-MOF-1: Towards a Highly Effective Heterogeneous Catalyst and Dye Scavenger, Sci. Rep. 6 (2016) 25595. https://doi.org/10.1038/srep25595.

[43] X. Lian, Y. Fang, E. Joseph, Q. Wang, J. Li, S. Banerjee, C. Lollar, X. Wang, H.-C. Zhou, Enzyme–MOF (metal–organic framework) composites, Chem. Soc. Rev. 46 (2017) 3386–3401. https://doi.org/10.1039/C7CS00058H.

[44] S.S. Park, C.H. Hendon, A.J. Fielding, A. Walsh, M. O'Keeffe, M. Dincă, The Organic Secondary Building Unit: Strong Intermolecular π Interactions Define Topology in MIT-25, a Mesoporous MOF with Proton-Replete Channels, J. Am. Chem. Soc. 139 (2017) 3619–3622. https://doi.org/10.1021/jacs.6b13176.

[45] J. Jin, X. Zhao, P. Feng, X. Bu, A Cooperative Pillar-Template Strategy as a Generalized Synthetic Method for Flexible Homochiral Porous Frameworks, Angew. Chemie Int. Ed. 57 (2018) 3737–3741. https://doi.org/10.1002/anie.201801116.

[46] L. Peng, S. Yang, S. Jawahery, S.M. Moosavi, A.J. Huckaba, M. Asgari, E. Oveisi, M.K. Nazeeruddin, B. Smit, W.L. Queen, Preserving Porosity of Mesoporous Metal-Organic Frameworks through the Introduction of Polymer Guests, J. Am. Chem. Soc. 141 (2019) 12397–12405. https://doi.org/10.1021/jacs.9b05967.

[47] Y. Fu, Z. Kang, J. Yin, W. Cao, Y. Tu, Q. Wang, X. Kong, Duet of Acetate and Water at the Defects of Metal-Organic Frameworks, Nano Lett. 19 (2019) 1618–1624. https://doi.org/10.1021/acs.nanolett.8b04518.

[48] S. Surblé, C. Serre, C. Mellot-Draznieks, F. Millange, G. Férey, A new isoreticular class of metal-organic-frameworks with the MIL-88 topology, Chem. Commun. (2006) 284–286. https://doi.org/10.1039/B512169H.

[49] G. Mehlana, G. Ramon, S. a Bourne, Methanol mediated crystal transformations in a solvatochromic metal organic framework constructed from Co(ii) and 4-(4-pyridyl) benzoate, CrystEngComm. 15 (2013) 9521. https://doi.org/10.1039/c3ce41064a.

[50] G. Mehlana, G. Ramon, S.A. Bourne, The role of C-H···π interactions in modulating the breathing amplitude of a 2D square lattice net: Alcohol sorption studies, CrystEngComm. 16 (2014) 8160–8168. https://doi.org/10.1039/c4ce00496e.

[51] D.N. Dybtsev, H. Chun, K. Kim, Rigid and Flexible: A Highly Porous Metal–Organic Framework with Unusual Guest-Dependent Dynamic Behavior, Angew. Chemie Int. Ed. 43 (2004) 5033–5036. https://doi.org/10.1002/anie.200460712.

[52] F. Millange, R.I. Walton, MIL-53 and its Isoreticular Analogues: a Review of the Chemistry and Structure of a Prototypical Flexible Metal-Organic Framework, Isr. J. Chem. 58 (2018) 1019–1035. https://doi.org/10.1002/ijch.201800084.

[53] Z. Fang, B. Bueken, D.E. De Vos, R.A. Fischer, Defect-Engineered Metal – Organic Frameworks, Angew. Chemie Int. Ed. 54 (2015) 7234–7254. https://doi.org/10.1002/anie.201411540.

[54] G. Barin, V. Krungleviciute, O. Gutov, J. T. Hupp, T. Yildirim, O. K. Farha, Defect Creation by Linker Fragmentation in Metal–Organic Frameworks and Its Effects on Gas Uptake Properties, Inorg. Chem. 53 (2014) 6914–6919. https://doi.org/10.1021/ic500722n.

[55] M.J. Cliffe, W. Wan, X. Zou, P.A. Chater, A.K. Kleppe, M.G. Tucker, H. Wilhelm, N.P. Funnell, F. Coudert, A.L. Goodwin, Correlated defect nanoregions in a metal–organic framework, Nat. Commun. 5 (2014) 4176. https://doi.org/10.1038/ncomms5176.

[56] Z. Fang, J.P. Dürholt, M. Kauer, W. Zhang, C. Lochenie, B. Jee, B. Albada, N. Metzler-Nolte, A. Pöppl, B. Weber, M. Muhler, Y. Wang, R. Schmid, R.A. Fischer, Structural Complexity in Metal–Organic Frameworks: Simultaneous Modification of Open Metal Sites and Hierarchical Porosity by Systematic Doping with Defective Linkers, J. Am. Chem. Soc. 136 (2014) 9627–9636. https://doi.org/10.1021/ja503218j.

[57] B. Li, X. Zhu, K. Hu, Y. Li, J. Feng, J. Shi, J. Gu, Defect creation in metal-organic frameworks for rapid and controllable decontamination of roxarsone from aqueous solution, J. Hazard. Mater. 302 (2016) 57–64. https://doi.org/10.1016/j.jhazmat.2015.09.040.

[58] S. Kim, A. Kim, J. Woon, H. Kim, Y. Bae, Creation of mesoporous defects in a microporous metal-organic framework by an acetic acid-fragmented linker co-

assembly and its remarkable effects on methane uptake, Chem. Eng. J. 335 (2018) 94–100. https://doi.org/10.1016/j.cej.2017.10.078.

[59] D.W. Lim, H. Kitagawa, Proton Transport in Metal-Organic Frameworks, Chem. Rev. (2020). https://doi.org/10.1021/acs.chemrev.9b00842.

[60] J. Canivet, M. Vandichel, D. Farrusseng, Origin of highly active metal–organic framework catalysts: defects? Defects!, Dalt. Trans. 45 (2016) 4090–4099. https://doi.org/10.1039/C5DT03522H.

[61] S. Dissegna, K. Epp, W.R. Heinz, G. Kieslich, R.A. Fischer, Defective Metal-Organic Frameworks, Adv. Mater. 30 (2018) 1–23. https://doi.org/10.1002/adma.201704501.

[62] U. Ravon, M. Savonnet, S. Aguado, M.E. Domine, E. Janneau, D. Farrusseng, Engineering of coordination polymers for shape selective alkylation of large aromatics and the role of defects, Microporous Mesoporous Mater. 129 (2010) 319–329. https://doi.org/10.1016/j.micromeso.2009.06.008.

[63] B. Tu, Q. Pang, D. Wu, Y. Song, L. Weng, Q. Li, Ordered Vacancies and Their Chemistry in Metal–Organic Frameworks, J. Am. Chem. Soc. 136 (2014) 14465–14471. https://doi.org/10.1021/ja5063423.

[64] P. Li, F.-F. Cheng, W.-W. Xiong, Q. Zhang, New synthetic strategies to prepare metal–organic frameworks, Inorg. Chem. Front. 5 (2018) 2693–2708. https://doi.org/10.1039/C8QI00543E.

[65] S. Yuan, L. Feng, K. Wang, J. Pang, M. Bosch, C. Lollar, Y. Sun, J. Qin, X. Yang, P. Zhang, Q. Wang, L. Zou, Y. Zhang, L. Zhang, Y. Fang, J. Li, H.-C. Zhou, Stable Metal-Organic Frameworks: Design, Synthesis, and Applications, Adv. Mater. 30 (2018) 1704303. https://doi.org/10.1002/adma.201704303.

[66] M.J. Cliffe, C. Mottillo, R.S. Stein, D.-K. Bučar, T. Friščić, Accelerated aging: a low energy, solvent-free alternative to solvothermal and mechanochemical synthesis of metal–organic materials, Chem. Sci. 3 (2012) 2495. https://doi.org/10.1039/c2sc20344h.

[67] L. Paseta, G. Potier, S. Sorribas, J. Coronas, Solventless synthesis of MOFs at high pressure, ACS Sustain. Chem. Eng. 4 (2016) 3780–3785. https://doi.org/10.1021/acssuschemeng.6b00473.

[68] B. Rühle, E. Virmani, H. Engelke, F.M. Hinterholzinger, T. von Zons, B. Brosent, T. Bein, A. Godt, S. Wuttke, A Chemiluminescent Metal–Organic Framework, Chem. - A Eur. J. (2019). https://doi.org/10.1002/chem.201806041.

[69] A.D. Burrows, C.G. Frost, M.F. Mahon, C. Richardson, Post-synthetic modification of

tagged metal-organic frameworks, Angew. Chemie - Int. Ed. 47 (2008) 8482–8486. https://doi.org/10.1002/anie.200802908.

[70] R.G. Pearson, Hard and Soft Acids and Bases, J. Am. Chem. Soc. 85 (1963) 3533–3539. https://doi.org/10.1021/ja00905a001.

[71] E.D. Bloch, D. Britt, C. Lee, C.J. Doonan, F.J. Uribe-romo, H. Furukawa, J.R. Long, O.M. Yaghi, Metal Insertion in a Microporous Metal - Organic Framework Lined with 2 , 2 ′ -Bipyridine, (2010) 14382–14384.

[72] L. Feng, S. Yuan, J.L. Li, K.Y. Wang, G.S. Day, P. Zhang, Y. Wang, H.C. Zhou, Uncovering Two Principles of Multivariate Hierarchical Metal-Organic Framework Synthesis via Retrosynthetic Design, ACS Cent. Sci. 4 (2018) 1719–1726. https://doi.org/10.1021/acscentsci.8b00722.

[73] J. Jiao, W. Gong, X. Wu, S. Yang, Y. Cui, Multivariate crystalline porous materials: Synthesis, property and potential application, Coord. Chem. Rev. 385 (2019) 174–190. https://doi.org/10.1016/j.ccr.2019.01.016.

[74] H. Deng, C.J. Doonan, H. Furukawa, R.B. Ferreira, J. Towne, C.B. Knobler, B. Wang, O.M. Yaghi, Multiple Functional Groups of Varying Ratios in Metal-Organic Frameworks, Science (80-.). 327 (2010) 846–850. https://doi.org/10.1126/science.1181761.

[75] L.J. Wang, H. Deng, H. Furukawa, F. Gándara, K.E. Cordova, D. Peri, O.M. Yaghi, Synthesis and characterization of metal-organic framework-74 containing 2, 4, 6, 8, and 10 different metals, Inorg. Chem. 53 (2014) 5881–5883. https://doi.org/10.1021/ic500434a.

[76] T. Tsuruoka, S. Furukawa, Y. Takashima, K. Yoshida, S. Isoda, S. Kitagawa, Nanoporous nanorods fabricated by coordination modulation and oriented attachment growth, Angew. Chemie. 121 (2009) 4833–4837.

[77] S. Canossa, A. Gonzalez-Nelson, L. Shupletsov, M. Carmen Martin, M.A. Van der Veen, Overcoming Crystallinity Limitations of Aluminium Metal-Organic Frameworks by Oxalic Acid Modulated Synthesis, Chem. – A Eur. J. 26 (2020) 3564–3570. https://doi.org/10.1002/chem.201904798.

[78] J. Ren, M. Ledwaba, N.M. Musyoka, H.W. Langmi, M. Mathe, S. Liao, W. Pang, Structural defects in metal–organic frameworks (MOFs): Formation, detection and control towards practices of interests, Coord. Chem. Rev. 349 (2017) 169–197. https://doi.org/https://doi.org/10.1016/j.ccr.2017.08.017.

[79] G.C. Shearer, S. Chavan, S. Bordiga, S. Svelle, U. Olsbye, K.P. Lillerud, Defect

Engineering: Tuning the Porosity and Composition of the Metal–Organic Framework UiO-66 via Modulated Synthesis, Chem. Mater. 28 (2016) 3749–3761. https://doi.org/10.1021/acs.chemmater.6b00602.

[80] A. Zimpel, N. Al Danaf, B. Steinborn, J. Kuhn, M. Höhn, T. Bauer, P. Hirschle, W. Schrimpf, H. Engelke, E. Wagner, Coordinative Binding of Polymers to Metal–Organic Framework Nanoparticles for Control of Interactions at the Biointerface, ACS Nano. 13 (2019) 3884–3895.

[81] R. Freund, U. Lächelt, T. Gruber, B. Rühle, S. Wuttke, Multifunctional Efficiency: Extending the Concept of Atom Economy to Functional Nanomaterials, ACS Nano. 12 (2018) 2094–2105. https://doi.org/10.1021/acsnano.8b00932.

[82] W.-Z. Wang, Environment-friendly synthesis of long chain semiaromatic polyamides, EXPRESS Polym. Lett. 3 (2009) 470–476. https://doi.org/10.3144/expresspolymlett.2009.58.

[83] S.M. Cohen, Postsynthetic Methods for the Functionalization of Metal–Organic Frameworks, Chem. Rev. 112 (2012) 970–1000. https://doi.org/10.1021/cr200179u.

[84] S.M. Cohen, The Postsynthetic Renaissance in Porous Solids, J. Am. Chem. Soc. 139 (2017) 2855–2863. https://doi.org/10.1021/jacs.6b11259.

[85] T. Islamoglu, S. Goswami, Z. Li, A. J. Howarth, O. K. Farha, J. T. Hupp, Postsynthetic Tuning of Metal–Organic Frameworks for Targeted Applications, Acc. Chem. Res. 50 (2017) 805–813. https://doi.org/10.1021/acs.accounts.6b00577.

[86] P. Cui, P. Wang, Y. Zhao, W.-Y. Sun, Fabrication of Desired Metal–Organic Frameworks via Postsynthetic Exchange and Sequential Linker Installation, Cryst. Growth Des. 19 (2019) 1454–1470. https://doi.org/10.1021/acs.cgd.8b01628.

[87] O.M. Yaghi, Reticular Chemistry: Molecular Precision in Infinite 2D and 3D, Mol. Front. J. 03 (2019) 66–83. https://doi.org/10.1142/s2529732519400054.

[88] C.S. Diercks, M.J. Kalmutzki, N.J. Diercks, O.M. Yaghi, Conceptual Advances from Werner Complexes to Metal-Organic Frameworks, ACS Cent. Sci. 4 (2018) 1457–1464. https://doi.org/10.1021/acscentsci.8b00677.

[89] O.M. Yaghi, Reticular Chemistry in All Dimensions, ACS Cent. Sci. 5 (2019) 1295–1300. https://doi.org/10.1021/acscentsci.9b00750.

[90] J.E. Mondloch, O. Karagiaridi, O.K. Farha, J.T. Hupp, Activation of metal-organic framework materials, CrystEngComm. 15 (2013) 9258–9264. https://doi.org/10.1039/c3ce41232f.

[91] C. Dietl, H. Hintz, B. Rühle, J. Schmedt auf der Günne, H. Langhals, S. Wuttke,

Switch-On Fluorescence of a Perylene-Dye-Functionalized Metal–Organic Framework through Postsynthetic Modification, Chem. Eur. J. 21 (2015) 10714–10720.

[92] A.P. Nelson, O.K. Farha, K.L. Mulfort, J.T. Hupp, Supercritical processing as a route to high internal surface areas and permanent microporosity in metal#organic framework materials, J. Am. Chem. Soc. 131 (2009) 458–460. https://doi.org/10.1021/ja808853q.

[93] J. An, C.M. Shade, D.A. Chengelis-Czegan, S. Petoud, N.L. Rosi, Zinc-adeninate metal-organic framework for aqueous encapsulation and sensitization of near-infrared and visible emitting lanthanide cations, J. Am. Chem. Soc. 133 (2011) 1220–1223. https://doi.org/10.1021/ja109103t.

[94] J. An, N.L. Rosi, Tuning MOF CO2 adsorption properties via cation exchange, J. Am. Chem. Soc. 132 (2010) 5578–5579. https://doi.org/10.1021/ja1012992.

[95] G. Calleja, J.A. Botas, M. Sánchez-Sánchez, M.G. Orcajo, Hydrogen adsorption over Zeolite-like MOF materials modified by ion exchange, Int. J. Hydrogen Energy. 35 (2010) 9916–9923. https://doi.org/10.1016/j.ijhydene.2010.02.114.

[96] R.E. Morris, L. Brammer, Coordination change, lability and hemilability in metal-organic frameworks, Chem. Soc. Rev. 46 (2017) 5444–5462. https://doi.org/10.1039/c7cs00187h.

[97] M. Kim, J.F. Cahill, Y. Su, K.A. Prather, S.M. Cohen, Postsynthetic ligand exchange as a route to functionalization of "inert" metal-organic frameworks, Chem. Sci. 3 (2012) 126–130. https://doi.org/10.1039/c1sc00394a.

[98] O. Karagiaridi, W. Bury, J.E. Mondloch, J.T. Hupp, O.K. Farha, Solvent-assisted linker exchange: An alternative to the de novo synthesis of unattainable metal-organic frameworks, Angew. Chemie - Int. Ed. 53 (2014) 4530–4540. https://doi.org/10.1002/anie.201306923.

[99] P. Deria, J.E. Mondloch, O. Karagiaridi, W. Bury, J.T. Hupp, O.K. Farha, Beyond post-synthesis modification: Evolution of metal-organic frameworks via building block replacement, Chem. Soc. Rev. 43 (2014) 5896–5912. https://doi.org/10.1039/c4cs00067f.

[100] W. Bury, D. Fairen-Jimenez, M.B. Lalonde, R.Q. Snurr, O.K. Farha, J.T. Hupp, Control over Catenation in Pillared Paddlewheel Metal–Organic Framework Materials via Solvent-Assisted Linker Exchange, Chem. Mater. 25 (2013) 739–744. https://doi.org/10.1021/cm303749m.

[101] B.J. Burnett, P.M. Barron, C. Hu, W. Choe, Stepwise Synthesis of Metal–Organic

Frameworks: Replacement of Structural Organic Linkers, J. Am. Chem. Soc. 133 (2011) 9984–9987. https://doi.org/10.1021/ja201911v.

[102] T. Li, M.T. Kozlowski, E.A. Doud, M.N. Blakely, N.L. Rosi, Stepwise Ligand Exchange for the Preparation of a Family of Mesoporous MOFs, J. Am. Chem. Soc. 135 (2013) 11688–11691. https://doi.org/10.1021/ja403810k.

[103] O. Karagiaridi, M.B. Lalonde, W. Bury, A.A. Sarjeant, O.K. Farha, J.T. Hupp, Opening ZIF-8: A catalytically active zeolitic imidazolate framework of sodalite topology with unsubstituted linkers, J. Am. Chem. Soc. 134 (2012) 18790–18796. https://doi.org/10.1021/ja308786r.

[104] O. Karagiaridi, W. Bury, A.A. Sarjeant, C.L. Stern, O.K. Farha, J.T. Hupp, Synthesis and characterization of isostructural cadmium zeolitic imidazolate frameworks via solvent-assisted linker exchange, Chem. Sci. 3 (2012) 3256–3260. https://doi.org/10.1039/c2sc20558k.

[105] M.B. Lalonde, J.E. Mondloch, P. Deria, A.A. Sarjeant, S.S. Al-Juaid, O.I. Osman, O.K. Farha, J.T. Hupp, Selective Solvent-Assisted Linker Exchange (SALE) in a Series of Zeolitic Imidazolate Frameworks, Inorg. Chem. 54 (2015) 7142–7144. https://doi.org/10.1021/acs.inorgchem.5b01231.

[106] H. Hintz, S. Wuttke, Postsynthetic modification of an amino-tagged MOF using peptide coupling reagents: A comparative study, Chem. Commun. 50 (2014) 11472–11475. https://doi.org/10.1039/c4cc02650k.

[107] H. Hintz, S. Wuttke, Solvent-Free and Time Efficient Postsynthetic Modification of Amino-Tagged Metal–Organic Frameworks with Carboxylic Acid Derivatives, Chem. Mater. 26 (2014) 6722–6728. https://doi.org/10.1021/cm502920f.

[108] S.M. Cohen, T. Islamoglu, S. Goswami, Z. Li, A.J. Howarth, O.K. Farha, J.T. Hupp, Postsynthetic Tuning of Metal-Organic Frameworks for Targeted Applications, Chem. Rev. 112 (2012) 970–1000. https://doi.org/10.1021/cr200179u.

[109] S.M. Cohen, Postsynthetic methods for the functionalization of metal-organic frameworks, Chem. Rev. 112 (2012) 970–1000. https://doi.org/10.1021/cr200179u.

[110] A.M. Fracaroli, P. Siman, D.A. Nagib, M. Suzuki, H. Furukawa, F.D. Toste, O.M. Yaghi, Seven Post-synthetic Covalent Reactions in Tandem Leading to Enzyme-like Complexity within Metal-Organic Framework Crystals, J. Am. Chem. Soc. 138 (2016) 8352–8355. https://doi.org/10.1021/jacs.6b04204.

[111] J.D. Evans, C.J. Sumby, C.J. Doonan, Post-synthetic metalation of metal–organic frameworks, Chem. Soc. Rev. 43 (2014) 5933–5951.

https://doi.org/10.1039/C4CS00076E.

[112] M. Bosch, S. Yuan, W. Rutledge, H.C. Zhou, Stepwise Synthesis of Metal-Organic Frameworks, Acc. Chem. Res. 50 (2017) 857–865. https://doi.org/10.1021/acs.accounts.6b00457.

[113] M.H. Mir, L.L. Koh, G.K. Tan, J.J. Vittal, Single-Crystal to Single-Crystal Photochemical Structural Transformations of Interpenetrated 3 D Coordination Polymers by [2+2] Cycloaddition Reactions, Angew. Chemie Int. Ed. 49 (2010) 390–393. https://doi.org/10.1002/anie.200905898.

[114] D. Liu, Z.-G. Ren, H.-X. Li, J.-P. Lang, N.-Y. Li, B.F. Abrahams, Single-Crystal-to-Single-Crystal Transformations of Two Three-Dimensional Coordination Polymers through Regioselective [2+2] Photodimerization Reactions, Angew. Chemie Int. Ed. 49 (2010) 4767–4770. https://doi.org/10.1002/anie.201001551.

[115] G. Férey, C. Mellot-Draznieks, C. Serre, F. Millange, J. Dutour, S. Surblé, I. Margiolaki, A Chromium Terephthalate-Based Solid with Unusually Large Pore Volumes and Surface Area, Science (80-.). 309 (2005) 2040–2042. https://doi.org/10.1126/science.1116275.

[116] P. Deria, W. Bury, I. Hod, C.W. Kung, O. Karagiaridi, J.T. Hupp, O.K. Farha, MOF functionalization via solvent-assisted ligand incorporation: Phosphonates vs carboxylates, Inorg. Chem. (2015). https://doi.org/10.1021/ic502639v.

[117] S. Yuan, W. Lu, Y.P. Chen, Q. Zhang, T.F. Liu, D. Feng, X. Wang, J. Qin, H.C. Zhou, Sequential linker installation: Precise placement of functional groups in multivariate metal-organic frameworks, J. Am. Chem. Soc. (2015). https://doi.org/10.1021/ja512762r.

[118] E.A. Kapustin, S. Lee, A.S. Alshammari, O.M. Yaghi, Molecular Retrofitting Adapts a Metal-Organic Framework to Extreme Pressure, ACS Cent. Sci. 3 (2017) 662–667. https://doi.org/10.1021/acscentsci.7b00169.

[119] Z. Tian, S. Dai, D. Jiang, Site Partition: Turning One Site into Two for Adsorbing CO 2, J. Phys. Chem. Lett. 7 (2016) 2568–2572. https://doi.org/10.1021/acs.jpclett.6b01141.

[120] X. Zhao, X. Bu, Q.-G. Zhai, H. Tran, P. Feng, Pore Space Partition by Symmetry-Matching Regulated Ligand Insertion and Dramatic Tuning on Carbon Dioxide Uptake, J. Am. Chem. Soc. 137 (2015) 1396–1399. https://doi.org/10.1021/ja512137t.

[121] H. Wang, J. Xu, D.S. Zhang, Q. Chen, R.M. Wen, Z. Chang, X.H. Bu, Crystalline capsules: Metal-organic frameworks locked by size-matching ligand bolts, Angew.

Chemie - Int. Ed. 54 (2015) 5966–5970. https://doi.org/10.1002/anie.201500468.

[122] S.-T. Zheng, X. Zhao, S. Lau, A. Fuhr, P. Feng, X. Bu, Entrapment of Metal Clusters in Metal–Organic Framework Channels by Extended Hooks Anchored at Open Metal Sites, J. Am. Chem. Soc. 135 (2013) 10270–10273. https://doi.org/10.1021/ja4044642.

[123] J. Hafizovic Cavka, S. Jakobsen, U. Olsbye, N. Guillou, C. Lamberti, S. Bordiga, K. Petter Lillerud, A New Zirconium Inorganic Building Brick Forming Metal Organic Frameworks with Exceptional Stability, J. Am. Chem. Soc. 130 (2008) 13850–13851. https://doi.org/10.1021/ja8057953.

[124] S. Yuan, J. Qin, H. Xu, J. Su, D. Rossi, Y. Chen, Z. Huang, X. Zou, H. Zhou, [Ti 8 Zr 2 O 12 (COO) 16] Cluster: An Ideal Inorganic Building Unit for Photoactive Metal − Organic Frameworks, ACS Cent. Sci. 4 (2018) 105–111. https://doi.org/10.1021/acscentsci.7b00497.

[125] J. Ha, J.H. Lee, H.R. Moon, Alterations to secondary building units of metal–organic frameworks for the development of new functions, Inorg. Chem. Front. 7 (2020) 12–27. https://doi.org/10.1039/c9qi01119f.

[126] M. Lalonde, W. Bury, O. Karagiaridi, Z. Brown, J.T. Hupp, O.K. Farha, Transmetalation: Routes to metal exchange within metal-organic frameworks, J. Mater. Chem. A. 1 (2013) 5453–5468. https://doi.org/10.1039/c3ta10784a.

[127] C.K. Brozek, M. Dincă, Cation exchange at the secondary building units of metal-organic frameworks, Chem. Soc. Rev. 43 (2014) 5456–5467. https://doi.org/10.1039/c4cs00002a.

[128] A.M. Hamisu, A. Ariffin, A.C. Wibowo, Cation Exchange in Metal-Organic Frameworks (MOFs): The Hard-Soft Acid-Base (HSAB) Principle Appraisal, Inorganica Chim. Acta. (2020) 119801. https://doi.org/10.1016/j.ica.2020.119801.

[129] C.K. Brozek, M. Dincə, Thermodynamic parameters of cation exchange in MOF-5 and MFU-4l, Chem. Commun. 51 (2015) 11780–11782. https://doi.org/10.1039/c5cc04249f.

[130] C.K. Brozek, L. Bellarosa, T. Soejima, T. V Clark, M. Dinca, N. Lõpez, M. Dincă, Solvent-dependent cation exchange in metal-organic frameworks, Chem. - A Eur. J. 20 (2014) 6871–6874. https://doi.org/10.1002/chem.201402682.

[131] S. Canossa, L. Fornasari, N. Demitri, M. Mattarozzi, D. Choquesillo-Lazarte, P. Pelagatti, A. Bacchi, MOF transmetalation beyond cation substitution: Defective distortion of IRMOF-9 in the spotlight, CrystEngComm. (2019). https://doi.org/10.1039/c8ce01808a.

[132] C. K. Brozek, M. Dincă, Ti3+-, V2+/3+-, Cr2+/3+-, Mn2+-, and Fe2+-Substituted MOF-5 and Redox Reactivity in Cr- and Fe-MOF-5, J. Am. Chem. Soc. 135 (2013) 12886–12891. https://doi.org/10.1021/ja4064475.

[133] M. Kim, J.F. Cahill, H. Fei, K.A. Prather, S.M. Cohen, Postsynthetic Ligand and Cation Exchange in Robust Metal–Organic Frameworks, J. Am. Chem. Soc. 134 (2012) 18082–18088. https://doi.org/10.1021/ja3079219.

[134] H. Fei, J.F. Cahill, K.A. Prather, S.M. Cohen, Tandem postsynthetic metal ion and ligand exchange in zeolitic imidazolate frameworks, Inorg. Chem. 52 (2013) 4011–4016. https://doi.org/10.1021/ic400048g.

[135] T.-F. Liu, L. Zou, D. Feng, Y.-P. Chen, S. Fordham, X. Wang, Y. Liu, H.-C. Zhou, Stepwise Synthesis of Robust Metal–Organic Frameworks via Postsynthetic Metathesis and Oxidation of Metal Nodes in a Single-Crystal to Single-Crystal Transformation, J. Am. Chem. Soc. 136 (2014) 7813–7816. https://doi.org/10.1021/ja5023283.

[136] Z. Wang, S.M. Cohen, Postsynthetic modification of metal-organic frameworks., Chem. Soc. Rev. 38 (2009) 1315–1329. https://doi.org/10.1039/b802258p.

[137] H. Cai, M. Li, X.-R. Lin, W. Chen, G.-H. Chen, X.-C. Huang, D. Li, Spatial, Hysteretic, and Adaptive Host-Guest Chemistry in a Metal-Organic Framework with Open Watson-Crick Sites, Angew. Chemie Int. Ed. 54 (2015) 10454–10459. https://doi.org/10.1002/anie.201502045.

[138] I. Akpinar, R.J. Drout, T. Islamoglu, S. Kato, J. Lyu, O.K. Farha, Exploiting π–π Interactions to Design an Efficient Sorbent for Atrazine Removal from Water, ACS Appl. Mater. Interfaces. 11 (2019) 6097–6103. https://doi.org/10.1021/acsami.8b20355.

[139] W. Xu, X. Pei, C.S. Diercks, H. Lyu, Z. Ji, O.M. Yaghi, A Metal–Organic Framework of Organic Vertices and Polyoxometalate Linkers as a Solid-State Electrolyte, J. Am. Chem. Soc. 141 (2019) 17522–17526. https://doi.org/10.1021/jacs.9b10418.

[140] A. Lanza, L.S. Germann, M. Fisch, N. Casati, P. Macchi, Solid-State Reversible Nucleophilic Addition in a Highly Flexible MOF, J. Am. Chem. Soc. (2015) 151002154626006–151002154626006. https://doi.org/10.1021/jacs.5b09231.

[141] A. Półrolniczak, S. Sobczak, A. Katrusiak, Solid-State Associative Reactions and the Coordination Compression Mechanism, Inorg. Chem. 57 (2018) 8942–8950. https://doi.org/10.1021/acs.inorgchem.8b00913.

[142] T. Kitao, Y. Zhang, S. Kitagawa, B. Wang, T. Uemura, Hybridization of MOFs and

polymers, Chem. Soc. Rev. 46 (2017) 3108–3133. https://doi.org/10.1039/C7CS00041C.

[143] M. Kalaj, K.C. Bentz, S. Ayala, J.M. Palomba, K.S. Barcus, Y. Katayama, S.M. Cohen, MOF-Polymer Hybrid Materials: From Simple Composites to Tailored Architectures, Chem. Rev. (2020) acs.chemrev.9b00575-acs.chemrev.9b00575. https://doi.org/10.1021/acs.chemrev.9b00575.

[144] C. Rösler, R.A. Fischer, Metal–organic frameworks as hosts for nanoparticles, CrystEngComm. 17 (2015) 199–217. https://doi.org/10.1039/C4CE01251H.

[145] T. Wang, L. Gao, J. Hou, S.J.A. Herou, J.T. Griffiths, W. Li, J. Dong, S. Gao, M.M. Titirici, R.V. Kumar, A.K. Cheetham, X. Bao, Q. Fu, S.K. Smoukov, Rational approach to guest confinement inside MOF cavities for low-temperature catalysis, Nat. Commun. 10 (2019) 1–9. https://doi.org/10.1038/s41467-019-08972-x.

[146] D. Fujita, M. Fujita, Fitting Proteins into Metal Organic Frameworks, ACS Cent. Sci. 1 (2015) 352–353. https://doi.org/10.1021/acscentsci.5b00315.

[147] Y. Chen, V. Lykourinou, C. Vetromile, T. Hoang, L.-J. Ming, R.W. Larsen, S. Ma, How Can Proteins Enter the Interior of a MOF? Investigation of Cytochrome c Translocation into a MOF Consisting of Mesoporous Cages with Microporous Windows, J. Am. Chem. Soc. 134 (2012) 13188–13191. https://doi.org/10.1021/ja305144x.

[148] K.W. Chapman, D.F. Sava, G. Halder, P.J. Chupas, T.M. Nenoff, Trapping guests within a nanoporous metal-organic framework through pressure-induced amorphization, J. Am. Chem. Soc. 133 (2011) 18583–18585. https://doi.org/10.1021/ja2085096.

[149] T.D. Bennett, P.J. Saines, D.A. Keen, J.-C. Tan, A.K. Cheetham, Ball-Milling-Induced Amorphization of Zeolitic Imidazolate Frameworks (ZIFs) for the Irreversible Trapping of Iodine, Chem. - A Eur. J. 19 (2013) 7049–7055. https://doi.org/10.1002/chem.201300216.

[150] C. Orellana-Tavra, E.F. Baxter, T. Tian, T.D. Bennett, N.K.H. Slater, A.K. Cheetham, D. Fairen-Jimenez, Amorphous metal-organic frameworks for drug delivery, Chem. Commun. 51 (2015) 13878–13881. https://doi.org/10.1039/c5cc05237h.

[151] D. Tanaka, K. Nakagawa, M. Higuchi, S. Horike, Y. Kubota, T.C. Kobayashi, M. Takata, S. Kitagawa, Kinetic gate-opening process in a flexible porous coordination polymer., Angew. Chem. Int. Ed. Engl. 47 (2008) 3914–3918. https://doi.org/10.1002/anie.200705822.

[152] H. Deng, M.A. Olson, J.F. Stoddart, O.M. Yaghi, Robust dynamics, Nat. Chem. 2 (2010) 439–443. https://doi.org/10.1038/nchem.654.

[153] K. Zhu, C.A. O'Keefe, V.N. Vukotic, R.W. Schurko, S.J. Loeb, A molecular shuttle that operates inside a metal–organic framework, Nat. Chem. 7 (2015) 514–519. https://doi.org/10.1038/nchem.2258.

[154] P.R. McGonigal, P. Deria, I. Hod, P.Z. Moghadam, A. Avestro, N.E. Horwitz, I.C. Gibbs-Hall, A.K. Blackburn, D. Chen, Y.Y. Botros, M.R. Wasielewski, R.Q. Snurr, J.T. Hupp, O.K. Farha, J.F. Stoddart, Electrochemically addressable trisradical rotaxanes organized within a metal–organic framework, Proc. Natl. Acad. Sci. 112 (2015) 11161–11168. https://doi.org/10.1073/pnas.1514485112.

[155] L.K. Knight, V.N. Vukotic, E. Viljoen, C.B. Caputo, S.J. Loeb, Eliminating the need for independent counterions in the construction of metal-organic rotaxane frameworks (MORFs), Chem. Commun. 4 (2009) 5585–5587. https://doi.org/10.1039/b911889f.

[156] K. Seki, Design of an adsorbent with an ideal pore structure for methane adsorption using metal complexes, Chem. Commun. (2001) 1496–1497. https://doi.org/10.1039/b104204c.

[157] H. Jasuja, Y. Jiao, N.C. Burtch, Y.G. Huang, K.S. Walton, Synthesis of cobalt-, nickel-, copper-, and zinc-based, water-stable, pillared metal-organic frameworks, Langmuir. (2014). https://doi.org/10.1021/la503269f.

[158] S. Henke, A. Schneemann, S. Kapoor, R. Winter, R.A. Fischer, Zinc-1,4-benzenedicarboxylate-bipyridine frameworks – linker functionalization impacts network topology during solvothermal synthesis, J. Mater. Chem. 22 (2012) 909–918. https://doi.org/10.1039/C1JM14791A.

[159] K. Koh, A.G. Wong-Foy, A.J. Matzger, A Porous Coordination Copolymer with over 5000 m 2 /g BET Surface Area, J. Am. Chem. Soc. 131 (2009) 4184–4185. https://doi.org/10.1021/ja809985t.

[160] K. Koh, A.G. Wong-Foy, A.J. Matzger, A Crystalline Mesoporous Coordination Copolymer with High Microporosity, Angew. Chemie Int. Ed. 47 (2008) 677–680. https://doi.org/10.1002/anie.200705020.

[161] L. Liu, K. Konstas, M. R. Hill, S. G. Telfer, Programmed Pore Architectures in Modular Quaternary Metal–Organic Frameworks, J. Am. Chem. Soc. 135 (2013) 17731–17734. https://doi.org/10.1021/ja4100244.

[162] A. Dutta, A.G. Wong-Foy, A.J. Matzger, Coordination copolymerization of three carboxylate linkers into a pillared layer framework, Chem. Sci. 5 (2014) 3729.

https://doi.org/10.1039/C3SC53549E.

[163] L.K. Macreadie, R. Babarao, C.J. Setter, S.J. Lee, O.T. Qazvini, A.J. Seeber, J. Tsanaktsidis, S.G. Telfer, S.R. Batten, M.R. Hill, Enhancing Multicomponent Metal–Organic Frameworks for Low Pressure Liquid Organic Hydrogen Carrier Separations, Angew. Chemie Int. Ed. 59 (2020) 6090–6098. https://doi.org/10.1002/anie.201916159.

[164] C.-X. Chen, Z. Wei, J.-J. Jiang, Y.-Z. Fan, S.-P. Zheng, C.-C. Cao, Y.-H. Li, D. Fenske, C.-Y. Su, Precise Modulation of the Breathing Behavior and Pore Surface in Zr-MOFs by Reversible Post-Synthetic Variable-Spacer Installation to Fine-Tune the Expansion Magnitude and Sorption Properties, Angew. Chemie Int. Ed. 55 (2016) 9932–9936. https://doi.org/10.1002/anie.201604023.

[165] S. Yuan, Y.P. Chen, J.S. Qin, W. Lu, L. Zou, Q. Zhang, X. Wang, X. Sun, H.C. Zhou, Linker Installation: Engineering Pore Environment with Precisely Placed Functionalities in Zirconium MOFs, J. Am. Chem. Soc. 138 (2016) 8912–8919. https://doi.org/10.1021/jacs.6b04501.

[166] X. Zhang, B.L. Frey, Y.-S. Chen, J. Zhang, Topology-Guided Stepwise Insertion of Three Secondary Linkers in Zirconium Metal–Organic Frameworks, J. Am. Chem. Soc. 140 (2018) 7710–7715. https://doi.org/10.1021/jacs.8b04277.

[167] J. Pang, S. Yuan, J. Qin, M. Wu, C. T. Lollar, J. Li, N. Huang, B. Li, P. Zhang, H.-C. Zhou, Enhancing Pore-Environment Complexity Using a Trapezoidal Linker: Toward Stepwise Assembly of Multivariate Quinary Metal–Organic Frameworks, J. Am. Chem. Soc. 140 (2018) 12328–12332. https://doi.org/10.1021/jacs.8b07411.

[168] M.J. Kalmutzki, N. Hanikel, O.M. Yaghi, Secondary building units as the turning point in the development of the reticular chemistry of MOFs, Sci. Adv. (2018). https://doi.org/10.1126/sciadv.aat9180.

[169] B. Tu, Q. Pang, E. Ning, W. Yan, Y. Qi, D. Wu, Q. Li, Heterogeneity within a Mesoporous Metal-Organic Framework with Three Distinct Metal-Containing Building Units, J. Am. Chem. Soc. 137 (2015) 13456–13459. https://doi.org/10.1021/jacs.5b07687.

[170] A. Schoedel, A.J. Cairns, Y. Belmabkhout, L. Wojtas, M. Mohamed, Z. Zhang, D.M. Proserpio, M. Eddaoudi, M.J. Zaworotko, The asc Trinodal Platform: Two-Step Assembly of Triangular, Tetrahedral, and Trigonal-Prismatic Molecular Building Blocks, Angew. Chemie Int. Ed. 52 (2013) 2902–2905. https://doi.org/10.1002/anie.201206042.

[171] M. Eddaoudi, J. Kim, J.B. Wachter, H.K. Chae, M. O'Keeffe, O.M. Yaghi, Porous metal-organic polyhedra: 25 Å cuboctahedron constructed from 12 Cu2(CO2)4 paddle-wheel building blocks [17], J. Am. Chem. Soc. 123 (2001) 4368–4369. https://doi.org/10.1021/ja0104352.

[172] J.J. Perry, J.A. Perman, M.J. Zaworotko, Design and synthesis of metal–organic frameworks using metal–organic polyhedra as supermolecular building blocks, Chem. Soc. Rev. 38 (2009) 1400–1417. https://doi.org/10.1039/b807086p.

[173] F. Nouar, J.F. Eubank, T. Bousquet, L. Wojtas, M.J. Zaworotko, M. Eddaoudi, Supermolecular building blocks (SBBs) for the design and synthesis of highly porous metal-organic frameworks, J. Am. Chem. Soc. 130 (2008) 1833–1835. https://doi.org/10.1021/ja710123s.

[174] V. Guillerm, D. Kim, J.F. Eubank, R. Luebke, X. Liu, K. Adil, M.S. Lah, M. Eddaoudi, A supermolecular building approach for the design and construction of metal-organic frameworks, Chem. Soc. Rev. 43 (2014) 6141–6172. https://doi.org/10.1039/c4cs00135d.

[175] Z. Wang, V.C. Kravtsov, M.J. Zaworotko, Ternary Nets formed by Self-Assembly of Triangles, Squares, and Tetrahedra, Angew. Chemie Int. Ed. 44 (2005) 2877–2880. https://doi.org/10.1002/anie.200500156.

[176] A.G. Wong-Foy, O. Lebel, A.J. Matzger, Porous Crystal Derived from a Tricarboxylate Linker with Two Distinct Binding Motifs, J. Am. Chem. Soc. 129 (2007) 15740–15741. https://doi.org/10.1021/ja0753952.

[177] X. Zhao, X. Wang, S. Wang, J. Dou, P. Cui, Z. Chen, D. Sun, X. Wang, D. Sun, Novel Metal–Organic Framework Based on Cubic and Trisoctahedral Supermolecular Building Blocks: Topological Analysis and Photoluminescent Property, Cryst. Growth Des. 12 (2012) 2736–2739. https://doi.org/10.1021/cg3002866.

[178] S.-T. Zheng, T. Wu, B. Irfanoglu, F. Zuo, P. Feng, X. Bu, Multicomponent Self-Assembly of a Nested Co24@Co48 Metal-Organic Polyhedral Framework, Angew. Chemie Int. Ed. 50 (2011) 8034–8037. https://doi.org/10.1002/anie.201103155.

[179] X. Kong, H. Deng, F. Yan, J. Kim, J.A. Swisher, B. Smit, O.M. Yaghi, J.A. Reimer, Mapping of Functional Groups in Metal-Organic Frameworks, Science (80-.). 341 (2013) 882–885. https://doi.org/10.1126/science.1238339.

[180] S. Canossa, Z. Ji, S. Wuttke, Circumventing Wear and Tear of Adaptive Porous Materials, Adv. Funct. Mater. (2020). https://doi.org/10.1002/adfm.201908547.

[181] H.D. Park, M. Dincă, Y. Román-Leshkov, Heterogeneous Epoxide Carbonylation by

Cooperative Ion-Pair Catalysis in Co(CO) 4 – -Incorporated Cr-MIL-101, ACS Cent. Sci. 3 (2017) 444–448. https://doi.org/10.1021/acscentsci.7b00075.

[182] Y.-B. Huang, J. Liang, X.-S. Wang, R. Cao, Multifunctional metal–organic framework catalysts: synergistic catalysis and tandem reactions, Chem. Soc. Rev. 46 (2017) 126–157. https://doi.org/10.1039/C6CS00250A.

[183] Z. Li, W. Sun, C. Chen, Q. Guo, X. Li, M. Gu, N. Feng, J. Ding, H. Wan, G. Guan, Deep eutectic solvents appended to UiO-66 type metal organic frameworks: Preserved open metal sites and extra adsorption sites for CO2 capture, Appl. Surf. Sci. 480 (2019) 770–778. https://doi.org/10.1016/j.apsusc.2019.03.030.

[184] S.M. Cohen, Z. Zhang, J.A. Boissonnault, Toward "metalloMOFzymes": Metal-Organic Frameworks with Single-Site Metal Catalysts for Small-Molecule Transformations, Inorg. Chem. 55 (2016) 7281–7290. https://doi.org/10.1021/acs.inorgchem.6b00828.

[185] Y. Ueda, H. Ito, D. Fujita, M. Fujita, Permeable Self-Assembled Molecular Containers for Catalyst Isolation Enabling Two-Step Cascade Reactions, J. Am. Chem. Soc. (2017). https://doi.org/10.1021/jacs.7b02745.

[186] C.S. Diercks, S. Lin, N. Kornienko, E.A. Kapustin, E.M. Nichols, C. Zhu, Y. Zhao, C.J. Chang, O.M. Yaghi, Reticular Electronic Tuning of Porphyrin Active Sites in Covalent Organic Frameworks for Electrocatalytic Carbon Dioxide Reduction, J. Am. Chem. Soc. 140 (2018) 1116–1122. https://doi.org/10.1021/jacs.7b11940.

[187] T.-Y. Zhou, B. Auer, S.J. Lee, S.G. Telfer, Catalysts Confined in Programmed Framework Pores Enable New Transformations and Tune Reaction Efficiency and Selectivity, J. Am. Chem. Soc. 141 (2019) 1577–1582. https://doi.org/10.1021/jacs.8b11221.

[188] P.D. Beer, P.A. Gale, D.K. Smith, Supramolecular chemistry, Oxford University Press, 1999.

[189] G. Yu, X. Chen, Host–guest chemistry in supramolecular theranostics, Theranostics. (2019). https://doi.org/10.7150/thno.31653.

[190] G. Wenz, An overview of host-guest chemistry and its application to nonsteroidal anti-inflammatory drugs, Clin. Drug Investig. (2000). https://doi.org/10.2165/00044011-200019002-00003.

[191] H. Cai, Y.L. Huang, D. Li, Biological metal–organic frameworks: Structures, host–guest chemistry and bio-applications, Coord. Chem. Rev. (2019). https://doi.org/10.1016/j.ccr.2017.12.003.

[192] K. Kim, Entering the recognition domain, Nat. Chem. (2009). https://doi.org/10.1038/nchem.419.

[193] B. Chen, S. Xiang, G. Qian, Metal-organic frameworks with functional pores for recognition of small molecules, Acc. Chem. Res. (2010). https://doi.org/10.1021/ar100023y.

[194] J. -M Lehn, Perspectives in Supramolecular Chemistry—From Molecular Recognition towards Molecular Information Processing and Self-Organization, Angew. Chemie Int. Ed. English. (1990). https://doi.org/10.1002/anie.199013041.

[195] N. Yanai, T. Uemura, M. Inoue, R. Matsuda, T. Fukushima, M. Tsujimoto, S. Isoda, S. Kitagawa, Guest-to-host transmission of structural changes for stimuli-responsive adsorption property, J. Am. Chem. Soc. (2012). https://doi.org/10.1021/ja2115713.

[196] J.S. Mugridge, Supramolecular Host-Guest Interactions, Dynamics and Structure, 2010.

[197] G. Cooke, V.M. Rotello, Methods of modulating hydrogen bonded interactions in synthetic host-guest systems, Chem. Soc. Rev. (2002). https://doi.org/10.1039/b103906g.

[198] L. Liu, J. Hao, Y. Shi, J. Qiu, C. Hao, Roles of hydrogen bonds and π-π stacking in the optical detection of nitro-explosives with a luminescent metal-organic framework as the sensor, RSC Adv. (2015). https://doi.org/10.1039/c4ra12835d.

[199] J.W. Steed, D.R. Turner, K.J. Wallace, Core Concepts in Supramolecular Chemistry and Nanochemistry, 2007. https://doi.org/10.1021/ja0769853.

[200] W.R. Zhuang, Y. Wang, P.F. Cui, L. Xing, J. Lee, D. Kim, H.L. Jiang, Y.K. Oh, Applications of π-π stacking interactions in the design of drug-delivery systems, J. Control. Release. (2019). https://doi.org/10.1016/j.jconrel.2018.12.014.

[201] X.H. Liu, C.X. Tan, J.Q. Weng, Synthesis, dimeric crystal structure, and fungicidal activity of 1-(4-methylphenyl)-2-(5-((3,5-dimethyl-1H-pyrazol-1-yl)methyl)-4-phenyl-4H-1,2, 4-triazol-3-ylthio)ethanone, Phosphorus, Sulfur Silicon Relat. Elem. 186 (2011) 558–564. https://doi.org/10.1080/10426507.2010.508060.

[202] G. Cavallo, P. Metrangolo, R. Milani, T. Pilati, A. Priimagi, G. Resnati, G. Terraneo, The Halogen Bond, Chem. Rev. 116 (2016) 2478–2601. https://doi.org/10.1021/acs.chemrev.5b00484.

[203] J. Li, Y. Qian, W. Duan, Q. Zeng, Advances in the study of the host-guest interaction by using coronene as the guest molecule, Chinese Chem. Lett. (2019). https://doi.org/10.1016/j.cclet.2018.05.037.

[204] O. Crespo-Biel, B.J. Ravoo, D.N. Reinhoudt, J. Huskens, Noncovalent nanoarchitectures on surfaces: From 2D to 3D nanostructures, J. Mater. Chem. (2006). https://doi.org/10.1039/b608858a.

[205] C. Bohne, Supramolecular dynamics, Chem. Soc. Rev. (2014). https://doi.org/10.1039/c3cs60352k.

[206] C.E. Chang, M.K. Gilson, Free energy, entropy, and induced fit in host-guest recognition: Calculations with the second-generation mining minima algorithm, J. Am. Chem. Soc. (2004). https://doi.org/10.1021/ja047115d.

[207] Y. Liu, Y. Chen, Cooperative binding and multiple recognition by bridged bis(β-cyclodextrin)s with functional linkers, Acc. Chem. Res. (2006). https://doi.org/10.1021/ar0502275.

[208] C.L.D. Gibb, B.C. Gibb, The Thermodynamics of Molecular Recognition, in: Supramol. Chem., 2012. https://doi.org/10.1002/9780470661345.smc005.

[209] K.N. Houk, A.G. Leach, S.P. Kim, X. Zhang, Binding Affinities of Host-Guest, Protein-Ligand, and Protein-Transition-State Complexes, Angew. Chemie - Int. Ed. (2003). https://doi.org/10.1002/anie.200200565.

[210] O. Danylyuk, V.P. Fedin, V. Sashuk, Kinetic trapping of the host–guest association intermediate and its transformation into a thermodynamic inclusion complex, Chem. Commun. (2013). https://doi.org/10.1039/c3cc37868c.

[211] Z. Dong, Y. Sun, J. Chu, X. Zhang, H. Deng, Multivariate Metal-Organic Frameworks for Dialing-in the Binding and Programming the Release of Drug Molecules, J. Am. Chem. Soc. (2017). https://doi.org/10.1021/jacs.7b07392.

[212] T. Ghanbari, F. Abnisa, W.M.A. Wan Daud, A review on production of metal organic frameworks (MOF) for CO2 adsorption, Sci. Total Environ. (2020). https://doi.org/10.1016/j.scitotenv.2019.135090.

[213] A.P. Cote, A.I. Benin, N.W. Ockwig, M. O'Keeffe, A.J. Matzger, O.M. Yaghi, Porous, crystalline, covalent organic frameworks, Science (80-.). 310 (2005) 1166–1170.

[214] H. Li, L. Li, R.-B. Lin, W. Zhou, Z. Zhang, S. Xiang, B. Chen, Porous metal-organic frameworks for gas storage and separation: Status and challenges, EnergyChem. 1 (2019) 100006. https://doi.org/10.1016/j.enchem.2019.100006.

[215] J. Liu, F. Zhang, X. Zou, G. Yu, N. Zhao, S. Fan, G. Zhu, Environmentally friendly synthesis of highly hydrophobic and stable MIL-53 MOF nanomaterials, Chem. Commun. (2013). https://doi.org/10.1039/c3cc42287a.

[216] O.K. Farha, I. Eryazici, N.C. Jeong, B.G. Hauser, C.E. Wilmer, A.A. Sarjeant, R.Q.

Snurr, S.T. Nguyen, A.Ö. Yazaydin, J.T. Hupp, Metal-organic framework materials with ultrahigh surface areas: Is the sky the limit?, J. Am. Chem. Soc. (2012). https://doi.org/10.1021/ja3055639.

[217] M. Kang, D.W. Kang, C.S. Hong, Post-synthetic diamine-functionalization of MOF-74 type frameworks for effective carbon dioxide separation, Dalt. Trans. (2019). https://doi.org/10.1039/c8dt04339f.

[218] B. Wang, L.H. Xie, X. Wang, X.M. Liu, J. Li, J.R. Li, Applications of metal–organic frameworks for green energy and environment: New advances in adsorptive gas separation, storage and removal, Green Energy Environ. (2018). https://doi.org/10.1016/j.gee.2018.03.001.

[219] B.M. Connolly, M. Aragones-Anglada, J. Gandara-Loe, N. Al Danaf, D.C. Lamb, J.P. Mehta, D. Vulpe, S. Wuttke, J. Silvestre-Albero, P.Z. Moghadam, Tuning porosity in macroscopic monolithic metal-organic frameworks for exceptional natural gas storage, Nat. Commun. 10 (2019) 1–11.

[220] L. Li, S. Tang, C. Wang, X. Lv, M. Jiang, H. Wu, X. Zhao, High gas storage capacities and stepwise adsorption in a UiO type metal–organic framework incorporating Lewis basic bipyridyl sites, Chem. Commun. (2014). https://doi.org/10.1039/c3cc48275h.

[221] S. Ullah, M.A. Bustam, M.A. Assiri, A.G. Al-Sehemi, F.A. Abdul Kareem, A. Mukhtar, M. Ayoub, G. Gonfa, Synthesis and characterization of iso-reticular metal-organic Framework-3 (IRMOF-3) for CO2/CH4 adsorption: Impact of post-synthetic aminomethyl propanol (AMP) functionalization, J. Nat. Gas Sci. Eng. (2019). https://doi.org/10.1016/j.jngse.2019.103014.

[222] T.M. McDonald, J.A. Mason, X. Kong, E.D. Bloch, D. Gygi, A. Dani, V. Crocellà, F. Giordanino, S.O. Odoh, W.S. Drisdell, B. Vlaisavljevich, A.L. Dzubak, R. Poloni, S.K. Schnell, N. Planas, K. Lee, T. Pascal, L.F. Wan, D. Prendergast, J.B. Neaton, B. Smit, J.B. Kortright, L. Gagliardi, S. Bordiga, J.A. Reimer, J.R. Long, Cooperative insertion of CO2 in diamine-appended metal-organic frameworks, Nature. (2015). https://doi.org/10.1038/nature14327.

[223] R.W. Flaig, T.M. Osborn Popp, A.M. Fracaroli, E.A. Kapustin, M.J. Kalmutzki, R.M. Altamimi, F. Fathieh, J.A. Reimer, O.M. Yaghi, The Chemistry of CO2 Capture in an Amine-Functionalized Metal-Organic Framework under Dry and Humid Conditions, J. Am. Chem. Soc. (2017). https://doi.org/10.1021/jacs.7b06382.

[224] X. Cui, Q. Yang, L. Yang, R. Krishna, Z. Zhang, Z. Bao, H. Wu, Q. Ren, W. Zhou, B. Chen, H. Xing, Ultrahigh and Selective SO2 Uptake in Inorganic Anion-Pillared

Hybrid Porous Materials, Adv. Mater. (2017). https://doi.org/10.1002/adma.201606929.

[225] G.W. Crabtree, M.S. Dresselhaus, The Hydrogen Fuel Alternative, MRS Bull. 33 (2008) 421–428. https://doi.org/10.1557/mrs2008.84.

[226] H. Furukawa, K.E. Cordova, M. O'Keeffe, O.M. Yaghi, The chemistry and applications of metal-organic frameworks, Science (80-.). (2013). https://doi.org/10.1126/science.1230444.

[227] Y. Li, R.T. Yang, Gas adsorption and storage in metal-organic framework MOF-177, Langmuir. (2007). https://doi.org/10.1021/la702466d.

[228] C. Petit, Present and future of MOF research in the field of adsorption and molecular separation, Curr. Opin. Chem. Eng. 20 (2018) 132–142. https://doi.org/10.1016/j.coche.2018.04.004.

[229] M.T. Kapelewski, T. Runčevski, J.D. Tarver, H.Z.H. Jiang, K.E. Hurst, P.A. Parilla, A. Ayala, T. Gennett, S.A. Fitzgerald, C.M. Brown, J.R. Long, Record High Hydrogen Storage Capacity in the Metal-Organic Framework Ni2(m-dobdc) at Near-Ambient Temperatures, Chem. Mater. (2018). https://doi.org/10.1021/acs.chemmater.8b03276.

[230] J.R. Li, R.J. Kuppler, H.C. Zhou, Selective gas adsorption and separation in metal-organic frameworks, Chem. Soc. Rev. (2009). https://doi.org/10.1039/b802426j.

[231] A. Schneemann, V. Bon, I. Schwedler, I. Senkovska, S. Kaskel, R.A. Fischer, Flexible metal-organic frameworks, Chem. Soc. Rev. (2014). https://doi.org/10.1039/c4cs00101j.

[232] S. Ullah, M.A. Bustam, A.G. Al-Sehemi, M.A. Assiri, F.A. Abdul Kareem, A. Mukhtar, M. Ayoub, G. Gonfa, Influence of post-synthetic graphene oxide (GO) functionalization on the selective CO2/CH4 adsorption behavior of MOF-200 at different temperatures; an experimental and adsorption isotherms study, Microporous Mesoporous Mater. (2020). https://doi.org/10.1016/j.micromeso.2020.110002.

[233] L. Maserati, S.M. Meckler, J.E. Bachman, J.R. Long, B.A. Helms, Diamine-Appended Mg2(dobpdc) Nanorods as Phase-Change Fillers in Mixed-Matrix Membranes for Efficient CO2/N2 Separations, Nano Lett. (2017). https://doi.org/10.1021/acs.nanolett.7b03106.

[234] S. Liu, L.T. Liu, L.X. Sun, Y.L. Zhou, F. Xu, Improved CO2 capture and separation performances of a Cr-based metal–organic framework induced by post-synthesis modification of amine groups, Polyhedron. (2018). https://doi.org/10.1016/j.poly.2018.09.033.

[235] Y. Zhang, B. Li, R. Krishna, Z. Wu, D. Ma, Z. Shi, T. Pham, K. Forrest, B. Space, S. Ma, Highly selective adsorption of ethylene over ethane in a MOF featuring the combination of open metal site and π-complexation, Chem. Commun. (2015). https://doi.org/10.1039/c4cc09774b.

[236] A. Ghosh, G. Das, Green synthesis of Sn(II)-BDC MOF: Preferential and efficient adsorption of anionic dyes, Microporous Mesoporous Mater. 297 (2020). https://doi.org/10.1016/j.micromeso.2020.110039.

[237] S.K. Sharma, Green chemistry for dyes removal from wastewater : research trends and applications, n.d.

[238] D. Jiang, M. Chen, H. Wang, G. Zeng, D. Huang, M. Cheng, Y. Liu, W. Xue, Z.W. Wang, The application of different typological and structural MOFs-based materials for the dyes adsorption, Coord. Chem. Rev. 380 (2019) 471–483. https://doi.org/10.1016/j.ccr.2018.11.002.

[239] G. Crini, E. Lichtfouse, Advantages and disadvantages of techniques used for wastewater treatment, Environ. Chem. Lett. (2019). https://doi.org/10.1007/s10311-018-0785-9.

[240] J. Goscianska, F. Ciesielczyk, Lanthanum enriched aminosilane-grafted mesoporous carbon material for efficient adsorption of tartrazine azo dye, Microporous Mesoporous Mater. 280 (2019) 7–19. https://doi.org/https://doi.org/10.1016/j.micromeso.2019.01.033.

[241] J. Goscianska, N.A. Fathy, R.M.M. Aboelenin, Adsorption of solophenyl red 3BL polyazo dye onto amine-functionalized mesoporous carbons, J. Colloid Interface Sci. 505 (2017) 593–604. https://doi.org/https://doi.org/10.1016/j.jcis.2017.06.052.

[242] J. Goscianska, M. Marciniak, R. Pietrzak, Mesoporous carbons modified with lanthanum(III) chloride for methyl orange adsorption, Chem. Eng. J. 247 (2014) 258–264. https://doi.org/https://doi.org/10.1016/j.cej.2014.03.012.

[243] J. Goscianska, M. Marciniak, R. Pietrzak, Ordered mesoporous carbons modified with cerium as effective adsorbents for azo dyes removal, Sep. Purif. Technol. 154 (2015) 236–245. https://doi.org/https://doi.org/10.1016/j.seppur.2015.09.042.

[244] E. Haque, J.W. Jun, S.H. Jhung, Adsorptive removal of methyl orange and methylene blue from aqueous solution with a metal-organic framework material, iron terephthalate (MOF-235), J. Hazard. Mater. 185 (2011) 507–511. https://doi.org/10.1016/j.jhazmat.2010.09.035.

[245] E. Haque, J.E. Lee, I.T. Jang, Y.K. Hwang, J.S. Chang, J. Jegal, S.H. Jhung,

Adsorptive removal of methyl orange from aqueous solution with metal-organic frameworks, porous chromium-benzenedicarboxylates, J. Hazard. Mater. 181 (2010) 535–542. https://doi.org/10.1016/j.jhazmat.2010.05.047.

[246] C. Chen, M. Zhang, Q. Guan, W. Li, Kinetic and thermodynamic studies on the adsorption of xylenol orange onto MIL-101(Cr), Chem. Eng. J. 183 (2012) 60–67. https://doi.org/10.1016/j.cej.2011.12.021.

[247] M.M. Modena, P. Hirschle, S. Wuttke, T.P. Burg, Mass measurements reveal preferential sorption of mixed solvent components in porous nanoparticles, Small. 14 (2018) 1800826.

[248] Q. Chen, Q. He, M. Lv, Y. Xu, H. Yang, X. Liu, F. Wei, Selective adsorption of cationic dyes by UiO-66-NH 2, Appl. Surf. Sci. (2015). https://doi.org/10.1016/j.apsusc.2014.11.103.

[249] R. Röder, T. Preiß, P. Hirschle, B. Steinborn, A. Zimpel, M. Höhn, J.O. Rädler, T. Bein, E. Wagner, S. Wuttke, Multifunctional nanoparticles by coordinative self-assembly of His-tagged units with metal–organic frameworks, J. Am. Chem. Soc. 139 (2017) 2359–2368.

[250] Q. Zha, X. Sang, D. Liu, D. Wang, G. Shi, C. Ni, Modification of hydrophilic amine-functionalized metal-organic frameworks to hydrophobic for dye adsorption, J. Solid State Chem. (2019). https://doi.org/10.1016/j.jssc.2019.04.001.

[251] Y. Lv, R. Zhang, S. Zeng, K. Liu, S. Huang, Y. Liu, P. Xu, C. Lin, Y. Cheng, M. Liu, Removal of p-arsanilic acid by an amino-functionalized indium-based metal–organic framework: Adsorption behavior and synergetic mechanism, Chem. Eng. J. (2018). https://doi.org/10.1016/j.cej.2018.01.139.

[252] J. Fei, T. Wang, Y. Zhou, Z. Wang, X. Min, Y. Ke, W. Hu, L. Chai, Aromatic organoarsenic compounds (AOCs) occurrence and remediation methods, Chemosphere. (2018). https://doi.org/10.1016/j.chemosphere.2018.05.145.

[253] H. Ali, E. Khan, I. Ilahi, Environmental chemistry and ecotoxicology of hazardous heavy metals: Environmental persistence, toxicity, and bioaccumulation, J. Chem. (2019). https://doi.org/10.1155/2019/6730305.

[254] H. Saleem, U. Rafique, R.P. Davies, Investigations on post-synthetically modified UiO-66-NH2 for the adsorptive removal of heavy metal ions from aqueous solution, Microporous Mesoporous Mater. (2016). https://doi.org/10.1016/j.micromeso.2015.09.043.

[255] K. Wang, J. Gu, N. Yin, Efficient Removal of Pb(II) and Cd(II) Using NH2-

Functionalized Zr-MOFs via Rapid Microwave-Promoted Synthesis, Ind. Eng. Chem. Res. (2017). https://doi.org/10.1021/acs.iecr.6b04997.

[256] H. Kim, S. Yang, S.R. Rao, S. Narayanan, E.A. Kapustin, H. Furukawa, A.S. Umans, O.M. Yaghi, E.N. Wang, Water harvesting from air with metal-organic frameworks powered by natural sunlight, Science (80-.). (2017). https://doi.org/10.1126/science.aam8743.

[257] P.H. Gleick, E. Pacific Institute for Studies in Development, Stockholm Environment Institute., Water in crisis : a guide to the world's fresh water resources, Oxford University Press, 1993.

[258] F. Fathieh, M.J. Kalmutzki, E.A. Kapustin, P.J. Waller, J. Yang, O.M. Yaghi, Practical water production from desert air, Sci. Adv. (2018). https://doi.org/10.1126/sciadv.aat3198.

[259] S. Bhattacharya, Traditional Water Harvesting Structures and Sustainable Water Management in India: A Socio-Hydrological Review, Int. Lett. Nat. Sci. (2015). https://doi.org/10.18052/www.scipress.com/ilns.37.30.

[260] M.J. Kalmutzki, C.S. Diercks, O.M. Yaghi, Metal–Organic Frameworks for Water Harvesting from Air, Adv. Mater. (2018). https://doi.org/10.1002/adma.201704304.

[261] L.G. Gordeeva, M. V. Solovyeva, A. Sapienza, Y.I. Aristov, Potable water extraction from the atmosphere: Potential of MOFs, Renew. Energy. (2020). https://doi.org/10.1016/j.renene.2019.12.003.

[262] C. Gropp, S. Canossa, S. Wuttke, F. Gándara, Q. Li, L. Gagliardi, O.M. Yaghi, Standard Practices of Reticular Chemistry, (2020).

[263] N. Hanikel, M.S. Prévot, O.M. Yaghi, MOF water harvesters, Nat. Nanotechnol. 15 (2020) 348–355. https://doi.org/10.1038/s41565-020-0673-x.

[264] H.L. Nguyen, N. Hanikel, S.J. Lyle, C. Zhu, D.M. Proserpio, O.M. Yaghi, A Porous Covalent Organic Framework with Voided Square Grid Topology for Atmospheric Water Harvesting, J. Am. Chem. Soc. (2020). https://doi.org/10.1021/jacs.9b13094.

[265] N. Ko, P.G. Choi, J. Hong, M. Yeo, S. Sung, K.E. Cordova, H.J. Park, J.K. Yang, J. Kim, Tailoring the water adsorption properties of MIL-101 metal-organic frameworks by partial functionalization, J. Mater. Chem. A. (2015). https://doi.org/10.1039/c4ta04907a.

[266] T. Pan, K. Yang, Y. Han, Recent Progress of Atmospheric Water Harvesting Using Metal-Organic Frameworks, Chem. Res. Chinese Univ. (2020). https://doi.org/10.1007/s40242-020-9093-6.

[267] M.W. Logan, S. Langevin, Z. Xia, Reversible Atmospheric Water Harvesting Using Metal-Organic Frameworks, Sci. Rep. (2020). https://doi.org/10.1038/s41598-020-58405-9.

[268] W. Shi, Y. Zhu, C. Shen, J. Shi, G. Xu, X. Xiao, R. Cao, Water sorption properties of functionalized MIL-101(Cr)-X (X=-NH2, –SO3H, H, –CH3, –F) based composites as thermochemical heat storage materials, Microporous Mesoporous Mater. 285 (2019) 129–136. https://doi.org/10.1016/j.micromeso.2019.05.003.

[269] A.J. Rieth, S. Yang, E.N. Wang, M. Dincă, Record Atmospheric Fresh Water Capture and Heat Transfer with a Material Operating at the Water Uptake Reversibility Limit, ACS Cent. Sci. (2017). https://doi.org/10.1021/acscentsci.7b00186.

[270] H. Furukawa, F. Gándara, Y.B. Zhang, J. Jiang, W.L. Queen, M.R. Hudson, O.M. Yaghi, Water adsorption in porous metal-organic frameworks and related materials, J. Am. Chem. Soc. (2014). https://doi.org/10.1021/ja500330a.

[271] T. Ma, E.A. Kapustin, S.X. Yin, L. Liang, Z. Zhou, J. Niu, L.H. Li, Y. Wang, J. Su, J. Li, X. Wang, W.D. Wang, W. Wang, J. Sun, O.M. Yaghi, Single-crystal x-ray diffraction structures of covalent organic frameworks, Science (80-.). (2018). https://doi.org/10.1126/science.aat7679.

[272] M. Peller, K. Böll, A. Zimpel, S. Wuttke, Metal–organic framework nanoparticles for magnetic resonance imaging, Inorg. Chem. Front. 5 (2018) 1760–1779. https://doi.org/10.1039/C8QI00149A.

[273] Z. Luo, S. Fan, C. Gu, W. Liu, J. Chen, B. Li, J. Liu, Metal–Organic Framework (MOF)-based Nanomaterials for Biomedical Applications, Curr. Med. Chem. 26 (2018) 3341–3369. https://doi.org/10.2174/0929867325666180214123500.

[274] S. Keskin, S. Kizilel, Biomedical Applications of Metal Organic Frameworks, Ind. Eng. Chem. Res. (2011). https://doi.org/10.1021/ie101312k.

[275] S. Wuttke, M. Lismont, A. Escudero, B. Rungtaweevoranit, W.J. Parak, Positioning metal-organic framework nanoparticles within the context of drug delivery – A comparison with mesoporous silica nanoparticles and dendrimers, Biomaterials. 123 (2017) 172–183. https://doi.org/https://doi.org/10.1016/j.biomaterials.2017.01.025.

[276] F. Peng, W. Zhang, F. Qiu, Self-assembling Peptides in Current Nanomedicine: Versatile Nanomaterials for Drug Delivery, Curr. Med. Chem. (2020).

[277] Y. Liu, Y. Zhao, X. Chen, Bioengineering of metal-organic frameworks for nanomedicine, Theranostics. (2019). https://doi.org/10.7150/thno.31918.

[278] F. Ke, Y.P. Yuan, L.G. Qiu, Y.H. Shen, A.J. Xie, J.F. Zhu, X.Y. Tian, L. De Zhang,

Facile fabrication of magnetic metal-organic framework nanocomposites for potential targeted drug delivery, J. Mater. Chem. (2011). https://doi.org/10.1039/c0jm01770a.

[279] S. Banerjee, C.T. Lollar, Z. Xiao, Y. Fang, H.C. Zhou, Biomedical Integration of Metal–Organic Frameworks, Trends Chem. (2020). https://doi.org/10.1016/j.trechm.2020.01.007.

[280] W. Zhu, J. Guo, S. Amini, Y. Ju, J.O. Agola, A. Zimpel, J. Shang, A. Noureddine, F. Caruso, S. Wuttke, SupraCells: Living Mammalian Cells Protected within Functional Modular Nanoparticle-Based Exoskeletons, Adv. Mater. 31 (2019) 1900545.

[281] W. Zhu, J. Guo, J.O. Agola, J.G. Croissant, Z. Wang, J. Shang, E. Coker, B. Motevalli, A. Zimpel, S. Wuttke, Metal–Organic Framework Nanoparticle-Assisted Cryopreservation of Red Blood Cells, J. Am. Chem. Soc. 141 (2019) 7789–7796.

[282] C. He, K. Lu, D. Liu, W. Lin, Nanoscale metal-organic frameworks for the co-delivery of cisplatin and pooled siRNAs to enhance therapeutic efficacy in drug-resistant ovarian cancer cells, J. Am. Chem. Soc. (2014). https://doi.org/10.1021/ja4098862.

[283] I. Imaz, M. Rubio-Martínez, L. García-Fernández, F. García, D. Ruiz-Molina, J. Hernando, V. Puntes, D. Maspoch, Coordination polymer particles as potential drug delivery systems, Chem. Commun. (2010). https://doi.org/10.1039/c003084h.

[284] L. Wang, M. Zheng, Z. Xie, Nanoscale metal-organic frameworks for drug delivery: A conventional platform with new promise, J. Mater. Chem. B. 6 (2018) 707–717. https://doi.org/10.1039/c7tb02970e.

[285] S. Wuttke, S. Braig, T. Preiß, A. Zimpel, J. Sicklinger, C. Bellomo, J.O. Rädler, A.M. Vollmar, T. Bein, MOF nanoparticles coated by lipid bilayers and their uptake by cancer cells, Chem. Commun. 51 (2015) 15752–15755.

[286] B. Illes, P. Hirschle, S. Barnert, V. Cauda, S. Wuttke, H. Engelke, Exosome-coated metal–organic framework nanoparticles: an efficient drug delivery platform, Chem. Mater. 29 (2017) 8042–8046.

[287] K. Böll, A. Zimpel, O. Dietrich, S. Wuttke, M. Peller, Clinically Approved MRI Contrast Agents as Imaging Labels for a Porous Iron-Based MOF Nanocarrier: A Systematic Investigation in a Clinical MRI Setting, Adv. Ther. 3 (2020) 1900126.

[288] B. Steinborn, P. Hirschle, M. Höhn, T. Bauer, M. Barz, S. Wuttke, E. Wagner, U. Lächelt, Core-Shell Functionalized Zirconium-Pemetrexed Coordination Nanoparticles as Carriers with a High Drug Content, Adv. Ther. 2 (2019) 1900120. https://doi.org/10.1002/adtp.201900120.

[289] E. Ploetz, A. Zimpel, V. Cauda, D. Bauer, D.C. Lamb, C. Haisch, S. Zahler, A.M.

Vollmar, S. Wuttke, H. Engelke, Metal–Organic Framework Nanoparticles Induce Pyroptosis in Cells Controlled by the Extracellular pH, Adv. Mater. 32 (2020) 1907267. https://doi.org/10.1002/adma.201907267.

[290] E. Ploetz, H. Engelke, U. Lächelt, S. Wuttke, The Chemistry of Reticular Framework Nanoparticles: MOF, ZIF, and COF Materials, Adv. Funct. Mater. (2020) 1909062.

[291] M.M. Modena, B. Rühle, T.P. Burg, S. Wuttke, Nanoparticle characterization: What to measure?, Adv. Mater. 31 (2019) 1901556.

[292] P. Hirschle, T. Preiß, F. Auras, A. Pick, J. Völkner, D. Valdepérez, G. Witte, W.J. Parak, J.O. Rädler, S. Wuttke, Exploration of MOF nanoparticle sizes using various physical characterization methods–is what you measure what you get?, CrystEngComm. 18 (2016) 4359–4368.

[293] A. Zimpel, T. Preiß, R. Röder, H. Engelke, M. Ingrisch, M. Peller, J.O. Rädler, E. Wagner, T. Bein, U. Lächelt, Imparting functionality to MOF nanoparticles by external surface selective covalent attachment of polymers, Chem. Mater. 28 (2016) 3318–3326.

[294] I. Abánades Lázaro, R.S. Forgan, Application of zirconium MOFs in drug delivery and biomedicine, Coord. Chem. Rev. (2019). https://doi.org/10.1016/j.ccr.2018.09.009.

[295] M.X. Wu, Y.W. Yang, Metal–Organic Framework (MOF)-Based Drug/Cargo Delivery and Cancer Therapy, Adv. Mater. 29 (2017) 1606134. https://doi.org/10.1002/adma.201606134.

[296] J.Y. Krzeszinski, Y. Wan, New therapeutic targets for cancer bone metastasis, Trends Pharmacol. Sci. (2015). https://doi.org/10.1016/j.tips.2015.04.006.

[297] S. Wuttke, A. Zimpel, T. Bein, S. Braig, K. Stoiber, A. Vollmar, D. Müller, K. Haastert-Talini, J. Schaeske, M. Stiesch, Validating Metal-Organic Framework Nanoparticles for Their Nanosafety in Diverse Biomedical Applications, Adv. Healthc. Mater. 6 (2017) 1600818.

[298] L.L. Tan, N. Song, S.X.A. Zhang, H. Li, B. Wang, Y.W. Yang, Ca2+, pH and thermo triple-responsive mechanized Zr-based MOFs for on-command drug release in bone diseases, J. Mater. Chem. B. (2016). https://doi.org/10.1039/c5tb01789k.

[299] T. Preiß, A. Zimpel, S. Wuttke, J.O. Rädler, Kinetic analysis of the uptake and release of fluorescein by metal-organic framework nanoparticles, Materials (Basel). (2017). https://doi.org/10.3390/ma10020216.

[300] S. Gadde, Multi-drug delivery nanocarriers for combination therapy, Medchemcomm. (2015). https://doi.org/10.1039/c5md00365b.

[301] C.M.J. Hu, L. Zhang, Nanoparticle-based combination therapy toward overcoming drug resistance in cancer, Biochem. Pharmacol. (2012). https://doi.org/10.1016/j.bcp.2012.01.008.

[302] B. Illes, S. Wuttke, H. Engelke, Liposome-coated iron fumarate metal-organic framework nanoparticles for combination therapy, Nanomaterials. (2017). https://doi.org/10.3390/nano7110351.

[303] N. Graber, H. Lüdi, H.M. Widmer, The use of chemical sensors in industry, Sensors Actuators B Chem. 1 (1990) 239–243. https://doi.org/https://doi.org/10.1016/0925-4005(90)80208-H.

[304] F.-G. Banica, Chemical sensors and biosensors: fundamentals and applications, John Wiley & Sons, 2012.

[305] X.-D. Wang, O.S. Wolfbeis, Fiber-Optic Chemical Sensors and Biosensors (2008–2012), Anal. Chem. 85 (2013) 487–508. https://doi.org/10.1021/ac303159b.

[306] S. Soloman, Sensors handbook, McGraw-Hill, Inc., 2009.

[307] J.R. Stetter, W.R. Penrose, S. Yao, Sensors, chemical sensors, electrochemical sensors, and ECS, J. Electrochem. Soc. 150 (2003) S11.

[308] J.D. Hol, T.B. Schön, F. Gustafsson, P.J. Slycke, Sensor fusion for augmented reality, in: 2006 9th Int. Conf. Inf. Fusion, FUSION, 2006. https://doi.org/10.1109/ICIF.2006.301604.

[309] R. Azuma, Y. Baillot, R. Behringer, S. Feiner, S. Julier, B. MacIntyre, Recent advances in augmented reality, IEEE Comput. Graph. Appl. 21 (2001) 34–47. https://doi.org/10.1109/38.963459.

[310] G. Schall, D. Wagner, G. Reitmayr, E. Taichmann, M. Wieser, D. Schmalstieg, B. Hofmann-Wellenhof, Global pose estimation using multi-sensor fusion for outdoor Augmented Reality, in: 2009 8th IEEE Int. Symp. Mix. Augment. Real., 2009: pp. 153–162. https://doi.org/10.1109/ISMAR.2009.5336489.

[311] M.I. Svechtarova, I. Buzzacchera, B.J. Toebes, J. Lauko, N. Anton, C.J. Wilson, Sensor Devices Inspired by the Five Senses: A Review, Electroanalysis. 28 (2016) 1201–1241. https://doi.org/10.1002/elan.201600047.

[312] A. Hulanicki, S. Głąb, F. Ingman, Chemical sensors definitions and classification, Pure Appl. Chem. 63 (1991) 1247–1250.

[313] Z. Brzózka, W. Wróblewski, Sensory Chemiczne, Oficyna Wydawnicza Politechniki Warszawskiej, Warszawa, 1999.

[314] J. Janata, Principles of Chemical Sensors, 2009. https://doi.org/10.1007/b136378.

[315] J. Janata, M. Josowicz, Chemical Modulation of Work Function as a Transduction Mechanism for Chemical Sensors, Acc. Chem. Res. 31 (1998) 241–248. https://doi.org/10.1021/ar9700668.

[316] F.A. Arris, A.M. Benoudjit, F. Sanober, W.W.A. Wan Salim, Characterization of electrochemical transducers for biosensor applications, in: Multifaceted Protoc. Biotechnol., 2019. https://doi.org/10.1007/978-981-13-2257-0_11.

[317] D.P. Jones, Biomedical sensors, Momentum press, 2010.

[318] S. Yin, P.B. Ruffin, F.T.S. Yu, Fiber optic sensors: Second edition, 2017. https://doi.org/10.1201/9781420053661.

[319] R. Lucklum, P. Hauptmann, Transduction mechanism of acoustic-wave based chemical and biochemical sensors, Meas. Sci. Technol. (2003). https://doi.org/10.1088/0957-0233/14/11/002.

[320] J.E. Lenz, A Review of Magnetic Sensors, Proc. IEEE. (1990). https://doi.org/10.1109/5.56910.

[321] P. Kinsler, Faraday's Law and Magnetic Induction: Cause and Effect, Experiment and Theory, Physics (College. Park. Md). (2020). https://doi.org/10.3390/physics2020009.

[322] J. Kennedy, Sensors in Biomedical Applications: Fundamentals, Technology and Applications Gábor Harsányi; CRC Press, Boca Raton, 2000, xviii +350 pages, ISBN 1-56676-885-3 ($189.95), Carbohydr. Polym. (2004). https://doi.org/10.1016/j.carbpol.2003.11.009.

[323] L. Esrafili, M. Gharib, A. Morsali, Selective detection and removal of mercury ions by dual-functionalized metal–organic frameworks: design-for-purpose, New J. Chem. 43 (2019) 18079–18091. https://doi.org/10.1039/C9NJ03951A.

[324] Y. Zhang, B. Li, H. Ma, L. Zhang, H. Jiang, H. Song, L. Zhang, Y. Luo, A nanoscaled lanthanide metal–organic framework as a colorimetric fluorescence sensor for dipicolinic acid based on modulating energy transfer, J. Mater. Chem. C. 4 (2016) 7294–7301. https://doi.org/10.1039/C6TC01022A.

[325] Q. Yang, L. Zhou, Y.X. Wu, K. Zhang, Y. Cao, Y. Zhou, D. Wu, F. Hu, N. Gan, A two dimensional metal–organic framework nanosheets-based fluorescence resonance energy transfer aptasensor with circular strand-replacement DNA polymerization target-triggered amplification strategy for homogenous detection of antibiotics, Anal. Chim. Acta. (2018). https://doi.org/10.1016/j.aca.2018.02.058.

[326] K. Kalantar-zadeh, B. Fry, Sensor Characteristics and Physical Effects. ln: Nanotechnology-Enabled Sensors, Springer, Boston, MA, 2008.

https://doi.org/https://doi.org/10.1007/978-0-387-68023-1_2.

[327] K.J. Bruemmer, S.W.M. Crossley, C.J. Chang, Activity-Based Sensing: A Synthetic Methods Approach for Selective Molecular Imaging and Beyond, Angew. Chemie Int. Ed. n/a (2019). https://doi.org/10.1002/anie.201909690.

[328] K. Müller-Buschbaum, F. Beuerle, C. Feldmann, MOF based luminescence tuning and chemical/physical sensing, Microporous Mesoporous Mater. 216 (2015) 171–199. https://doi.org/https://doi.org/10.1016/j.micromeso.2015.03.036.

[329] A.J. Bandodkar, I. Jeerapan, J. Wang, Wearable Chemical Sensors: Present Challenges and Future Prospects, ACS Sensors. 1 (2016) 464–482. https://doi.org/10.1021/acssensors.6b00250.

[330] S.K. Bhardwaj, N. Bhardwaj, R. Kaur, J. Mehta, A.L. Sharma, K.-H. Kim, A. Deep, An overview of different strategies to introduce conductivity in metal–organic frameworks and miscellaneous applications thereof, J. Mater. Chem. A. 6 (2018) 14992–15009. https://doi.org/10.1039/C8TA04220A.

[331] C.-S. Liu, J. Li, H. Pang, Metal-organic framework-based materials as an emerging platform for advanced electrochemical sensing, Coord. Chem. Rev. 410 (2020) 213222. https://doi.org/https://doi.org/10.1016/j.ccr.2020.213222.

[332] X. Liu, D. Huang, C. Lai, G. Zeng, L. Qin, H. Wang, H. Yi, B. Li, S. Liu, M. Zhang, R. Deng, Y. Fu, L. Li, W. Xue, S. Chen, Recent advances in covalent organic frameworks (COFs) as a smart sensing material, Chem. Soc. Rev. 48 (2019) 5266–5302. https://doi.org/10.1039/C9CS00299E.

[333] C.H. Pham, F. Paesani, Guest-Dependent Stabilization of the Low-Spin State in Spin-Crossover Metal-Organic Frameworks, Inorg. Chem. 57 (2018) 9839–9843. https://doi.org/10.1021/acs.inorgchem.8b00502.

[334] Q. Liu, J. Gao, Z. Zheng, D. Ning, Q. Wang, X.-M. Du, B. Zhao, W.-J. Ruan, Y. Li, Metal-organic frameworks based fluorescent sensor array for discrimination of flavonoids, Talanta. 203 (2019) 248–254. https://doi.org/https://doi.org/10.1016/j.talanta.2019.05.073.

[335] R.W. Day, D.K. Bediako, M. Rezaee, L.R. Parent, G. Skorupskii, M.Q. Arguilla, C.H. Hendon, I. Stassen, N.C. Gianneschi, P. Kim, M. Dincă, Single Crystals of Electrically Conductive Two-Dimensional Metal-Organic Frameworks: Structural and Electrical Transport Properties, ACS Cent. Sci. (2019). https://doi.org/10.1021/acscentsci.9b01006.

[336] B. Qian, Z. Chang, X.-H. Bu, Functionalized Dynamic Metal–Organic Frameworks as

Smart Switches for Sensing and Adsorption Applications, Top. Curr. Chem. 378 (2019) 5. https://doi.org/10.1007/s41061-019-0271-2.

[337] M. Drobek, J.-H. Kim, M. Bechelany, C. Vallicari, A. Julbe, S.S. Kim, MOF-Based Membrane Encapsulated ZnO Nanowires for Enhanced Gas Sensor Selectivity, ACS Appl. Mater. Interfaces. 8 (2016) 8323–8328. https://doi.org/10.1021/acsami.5b12062.

[338] G. Mínguez Espallargas, E. Coronado, Magnetic functionalities in MOFs: from the framework to the pore, Chem. Soc. Rev. 47 (2018) 533–557. https://doi.org/10.1039/C7CS00653E.

[339] T. Devic, P. Horcajada, C. Serre, F. Salles, G. Maurin, B. Moulin, D. Heurtaux, G. Clet, A. Vimont, J.M. Grenéche, B. Le Ouay, F. Moreau, E. Magnier, Y. Filinchuk, J. Marrot, J.C. Lavalley, M. Daturi, G. Férey, Functionalization in flexible porous solids: Effects on the pore opening and the host-guest interactions, J. Am. Chem. Soc. (2010). https://doi.org/10.1021/ja9092715.

[340] M.E. DMello, N.G. Sundaram, A. Singh, A.K. Singh, S.B. Kalidindi, An amine functionalized zirconium metal–organic framework as an effective chemiresistive sensor for acidic gases, Chem. Commun. 55 (2019) 349–352. https://doi.org/10.1039/C8CC06875E.

[341] M. Usman, S. Mendiratta, K.L. Lu, Semiconductor Metal–Organic Frameworks: Future Low-Bandgap Materials, Adv. Mater. (2017). https://doi.org/10.1002/adma.201605071.

[342] M.-H. Zeng, Q.-X. Wang, Y.-X. Tan, S. Hu, H.-X. Zhao, L.-S. Long, M. Kurmoo, Rigid Pillars and Double Walls in a Porous Metal-Organic Framework: Single-Crystal to Single-Crystal, Controlled Uptake and Release of Iodine and Electrical Conductivity, J. Am. Chem. Soc. 132 (2010) 2561–2563. https://doi.org/10.1021/ja908293n.

[343] A. Sengupta, S. Datta, C. Su, T.S. Herng, J. Ding, J.J. Vittal, K.P. Loh, Tunable Electrical Conductivity and Magnetic Property of the Two Dimensional Metal Organic Framework [Cu(TPyP)Cu2(O2CCH3)4], ACS Appl. Mater. Interfaces. 8 (2016) 16154–16159. https://doi.org/10.1021/acsami.6b03073.

[344] A. Dragässer, O. Shekhah, O. Zybaylo, C. Shen, M. Buck, C. Wöll, D. Schlettwein, Redox mediation enabled by immobilised centres in the pores of a metal–organic framework grown by liquid phase epitaxy, Chem. Commun. 48 (2012) 663–665. https://doi.org/10.1039/C1CC16580A.

[345] C.-W. Kung, K. Otake, C.T. Buru, S. Goswami, Y. Cui, J.T. Hupp, A.M. Spokoyny,

O.K. Farha, Increased Electrical Conductivity in a Mesoporous Metal–Organic Framework Featuring Metallacarboranes Guests, J. Am. Chem. Soc. 140 (2018) 3871–3875. https://doi.org/10.1021/jacs.8b00605.

[346] S. Han, S.C. Warren, S.M. Yoon, C.D. Malliakas, X. Hou, Y. Wei, M.G. Kanatzidis, B.A. Grzybowski, Tunneling Electrical Connection to the Interior of Metal–Organic Frameworks, J. Am. Chem. Soc. 137 (2015) 8169–8175. https://doi.org/10.1021/jacs.5b03263.

[347] B. Dhara, S.S. Nagarkar, J. Kumar, V. Kumar, P.K. Jha, S.K. Ghosh, S. Nair, N. Ballav, Increase in Electrical Conductivity of MOF to Billion-Fold upon Filling the Nanochannels with Conducting Polymer, J. Phys. Chem. Lett. 7 (2016) 2945–2950. https://doi.org/10.1021/acs.jpclett.6b01236.

[348] I. Stassen, N. Burtch, A. Talin, P. Falcaro, M. Allendorf, R. Ameloot, An updated roadmap for the integration of metal-organic frameworks with electronic devices and chemical sensors, Chem. Soc. Rev. (2017). https://doi.org/10.1039/c7cs00122c.

[349] M. Gilbert Gatty, A. Kahnt, L.J. Esdaile, M. Hutin, H.L. Anderson, B. Albinsson, Hopping versus Tunneling Mechanism for Long-Range Electron Transfer in Porphyrin Oligomer Bridged Donor–Acceptor Systems, J. Phys. Chem. B. 119 (2015) 7598–7611. https://doi.org/10.1021/jp5115064.

[350] V. Stavila, A.A. Talin, M.D. Allendorf, MOF-based electronic and opto-electronic devices, Chem. Soc. Rev. 43 (2014) 5994–6010. https://doi.org/10.1039/C4CS00096J.

[351] W. Volksen, R.D. Miller, G. Dubois, Low dielectric constant materials, Chem. Rev. 110 (2010) 56–110.

[352] K. Maex, M.R. Baklanov, D. Shamiryan, F. Lacopi, S.H. Brongersma, Z.S. Yanovitskaya, Low dielectric constant materials for microelectronics, J. Appl. Phys. 93 (2003) 8793–8841.

[353] C. Bartual-Murgui, A. Akou, C. Thibault, G. Molnár, C. Vieu, L. Salmon, A. Bousseksou, Spin-crossover metal–organic frameworks: promising materials for designing gas sensors, J. Mater. Chem. C. 3 (2015) 1277–1285. https://doi.org/10.1039/C4TC02441A.

[354] C. Bartual-Murgui, A. Akou, L. Salmon, G. Molnár, C. Thibault, J.A. Real, A. Bousseksou, Guest Effect on Nanopatterned Spin-Crossover Thin Films, Small. 7 (2011) 3385–3391. https://doi.org/10.1002/smll.201101089.

[355] C.-C. Chueh, C.-I. Chen, Y.-A. Su, H. Konnerth, Y.-J. Gu, C.-W. Kung, K.C.-W. Wu, Harnessing MOF materials in photovoltaic devices: recent advances, challenges, and

perspectives, J. Mater. Chem. A. 7 (2019) 17079–17095. https://doi.org/10.1039/C9TA03595H.

[356] X. Zhang, W. Wang, Z. Hu, G. Wang, K. Uvdal, Coordination polymers for energy transfer: Preparations, properties, sensing applications, and perspectives, Coord. Chem. Rev. 284 (2015) 206–235. https://doi.org/https://doi.org/10.1016/j.ccr.2014.10.006.

[357] P. Mahata, S.K. Mondal, D.K. Singha, P. Majee, Luminescent rare-earth-based MOFs as optical sensors, Dalt. Trans. 46 (2017) 301–328. https://doi.org/10.1039/C6DT03419E.

[358] E.J. D'Costa, Chemical sensor technology, volume 1. edited by T. Seiyama. Kodansha Ltd, Tokyo and Elsevier, Amsterdam, 1988, xvi + 250 pp. ISBN 0 444 98901 3. price:, Biosensors. (1989). https://doi.org/10.1016/0265-928x(89)80013-6.

[359] W.J. Peveler, M. Yazdani, V.M. Rotello, Selectivity and Specificity: Pros and Cons in Sensing, ACS Sensors. 1 (2016) 1282–1285. https://doi.org/10.1021/acssensors.6b00564.

[360] C.G. Siontorou, G.-P. Nikoleli, M.-T. Nikolelis, D.P. Nikolelis, Chapter 15 - Challenges and Future Prospects of Nanoadvanced Sensing Technology, in: Inamuddin, R. Khan, A. Mohammad, A.M.B.T.-A.B. for H.C.A. Asiri (Eds.), Elsevier, 2019: pp. 375–396. https://doi.org/https://doi.org/10.1016/B978-0-12-815743-5.00015-9.

[361] L.E. Kreno, K. Leong, O.K. Farha, M. Allendorf, R.P. Van Duyne, J.T. Hupp, Metal–Organic Framework Materials as Chemical Sensors, Chem. Rev. 112 (2012) 1105–1125. https://doi.org/10.1021/cr200324t.

[362] L.J. Small, R.C. Hill, J.L. Krumhansl, M.E. Schindelholz, Z. Chen, K.W. Chapman, X. Zhang, S. Yang, M. Schröder, T.M. Nenoff, Reversible MOF-Based Sensors for the Electrical Detection of Iodine Gas, ACS Appl. Mater. Interfaces. 11 (2019) 27982–27988. https://doi.org/10.1021/acsami.9b09938.

[363] G.-X. Wen, M.-L. Han, X.-Q. Wu, Y.-P. Wu, W.-W. Dong, J. Zhao, D.-S. Li, L.-F. Ma, A multi-responsive luminescent sensor based on a super-stable sandwich-type terbium(iii)–organic framework, Dalt. Trans. 45 (2016) 15492–15499. https://doi.org/10.1039/C6DT03057B.

[364] H. Li, M. Eddaoudi, M. O'Keeffe, O.M. Yaghi, Design and synthesis of an exceptionally stable and highly porous metal-organic framework, Nature. 402 (1999) 276–279.

[365] J.-H. Lee, T.-B. Nguyen, D.-K. Nguyen, J.-H. Kim, J.-Y. Kim, B.T. Phan, S.S. Kim,

Gas Sensing Properties of Mg-Incorporated Metal–Organic Frameworks, Sensors. 19 (2019) 3323. https://doi.org/10.3390/s19153323.

[366] M. Ding, X. Cai, H.-L. Jiang, Improving MOF stability: approaches and applications, Chem. Sci. 10 (2019) 10209–10230. https://doi.org/10.1039/C9SC03916C.

[367] D. Banerjee, S.J. Kim, J.B. Parise, Lithium Based Metal−Organic Framework with Exceptional Stability, Cryst. Growth Des. 9 (2009) 2500–2503. https://doi.org/10.1021/cg8014157.

[368] W.-M. Liao, M.-J. Wei, J.-T. Mo, P.-Y. Fu, Y.-N. Fan, M. Pan, C.-Y. Su, Acidity and Cd2+ fluorescent sensing and selective CO2 adsorption by a water-stable Eu-MOF, Dalt. Trans. 48 (2019) 4489–4494. https://doi.org/10.1039/C9DT00539K.

[369] P.Å. Öberg, F.A. Spelman, T. Togawa, P.Å. Öberg, J.D. Newman, A.P.F. Turner, S. Ueno, N. Iriguchi, K. Yamakoshi, A. Johansson, B. Hök, P. Rolfe, T. Tamura, B. Hensel, G. Czygan, I. Weiss, T. Nappholz, F.A. Spelman, P.J. French, D. Tanase, J.F.L. Goosen, T. Togawa, Front Matter, Sensors Med. Heal. Care. (2004) i–XXIV. https://doi.org/doi:10.1002/3527601414.fmatter.

[370] S.W. Lewis, Chemical Sensing and Detection in Forensic Science, Chemosensors. (2011) 475–496. https://doi.org/doi:10.1002/9781118019580.ch22.

[371] B. Gui, Y. Meng, Y. Xie, J. Tian, G. Yu, W. Zeng, G. Zhang, S. Gong, C. Yang, D. Zhang, C. Wang, Tuning the Photoinduced Electron Transfer in a Zr-MOF: Toward Solid-State Fluorescent Molecular Switch and Turn-On Sensor, Adv. Mater. 30 (2018) 1802329. https://doi.org/10.1002/adma.201802329.

[372] R. Goswami, S.C. Mandal, N. Seal, B. Pathak, S. Neogi, Antibiotic-triggered reversible luminescence switching in amine-grafted mixed-linker MOF: exceptional turn-on and ultrafast nanomolar detection of sulfadiazine and adenosine monophosphate with molecular keypad lock functionality, J. Mater. Chem. A. 7 (2019) 19471–19484. https://doi.org/10.1039/C9TA06632B.

[373] M. Jurcic, W.J. Peveler, C.N. Savory, D.-K. Bučar, A.J. Kenyon, D.O. Scanlon, I.P. Parkin, Sensing and Discrimination of Explosives at Variable Concentrations with a Large-Pore MOF as Part of a Luminescent Array, ACS Appl. Mater. Interfaces. 11 (2019) 11618–11626. https://doi.org/10.1021/acsami.8b22385.

[374] X.-D. Zhu, K. Zhang, Y. Wang, W.-W. Long, R.-J. Sa, T.-F. Liu, J. Lü, Fluorescent Metal–Organic Framework (MOF) as a Highly Sensitive and Quickly Responsive Chemical Sensor for the Detection of Antibiotics in Simulated Wastewater, Inorg. Chem. 57 (2018) 1060–1065. https://doi.org/10.1021/acs.inorgchem.7b02471.

[375] J.F. Eubank, H. Mouttaki, A.J. Cairns, Y. Belmabkhout, L. Wojtas, R. Luebke, M. Alkordi, M. Eddaoudi, The Quest for Modular Nanocages: tbo-MOF as an Archetype for Mutual Substitution, Functionalization, and Expansion of Quadrangular Pillar Building Blocks, J. Am. Chem. Soc. 133 (2011) 14204–14207. https://doi.org/10.1021/ja205658j.

[376] W. Hu, L. Wan, Y. Jian, C. Ren, K. Jin, X. Su, X. Bai, H. Haick, M. Yao, W. Wu, Electronic Noses: From Advanced Materials to Sensors Aided with Data Processing, Adv. Mater. Technol. 4 (2019) 1800488. https://doi.org/10.1002/admt.201800488.

[377] Q. Zhang, M. Lei, F. Kong, Y. Yang, A water-stable homochiral luminescent MOF constructed from an achiral acylamide-containing dicarboxylate ligand for enantioselective sensing of penicillamine, Chem. Commun. 54 (2018) 10901–10904. https://doi.org/10.1039/C8CC06274A.

[378] F.Y. Yi, D. Chen, M.K. Wu, L. Han, H.L. Jiang, Chemical Sensors Based on Metal–Organic Frameworks, Chempluschem. (2016). https://doi.org/10.1002/cplu.201600137.

[379] C. Qiao, X. Qu, Q. Yang, Q. Wei, G. Xie, S. Chen, D. Yang, Instant high-selectivity Cd-MOF chemosensor for naked-eye detection of Cu(ii) confirmed using in situ microcalorimetry, Green Chem. 18 (2016) 951–956. https://doi.org/10.1039/C5GC02393A.

[380] P.P. Leal, C.L. Hurd, S.G. Sander, E. Armstrong, P.A. Fernández, T.J. Suhrhoff, M.Y. Roleda, Copper pollution exacerbates the effects of ocean acidification and warming on kelp microscopic early life stages, Sci. Rep. 8 (2018) 14763. https://doi.org/10.1038/s41598-018-32899-w.

[381] J. Liu, J.-X. Hou, J.-P. Gao, J.-M. Liu, X. Jing, L.-J. Li, J.-L. Du, Stable Cd(II)-MOF as a fluorescent sensor for efficient detection of uranyl ions, Mater. Lett. 241 (2019) 184–186. https://doi.org/https://doi.org/10.1016/j.matlet.2019.01.090.

[382] J.-N. Hao, B. Yan, Simultaneous determination of indoor ammonia pollution and its biological metabolite in the human body with a recyclable nanocrystalline lanthanide-functionalized MOF, Nanoscale. 8 (2016) 2881–2886. https://doi.org/10.1039/C5NR06066D.

[383] W.W.E.-W. Wang, Introductory Chapter: What is Chemical Sensor?, in: IntechOpen, Rijeka, 2016: p. Ch. 1. https://doi.org/10.5772/64626.

[384] V. Chernikova, O. Yassine, O. Shekhah, M. Eddaoudi, K.N. Salama, Highly sensitive and selective SO2 MOF sensor: the integration of MFM-300 MOF as a sensitive layer

on a capacitive interdigitated electrode, J. Mater. Chem. A. 6 (2018) 5550–5554. https://doi.org/10.1039/C7TA10538J.

[385] R. Banerjee, H. Furukawa, D. Britt, C. Knobler, M. O'Keeffe, O.M. Yaghi, Control of Pore Size and Functionality in Isoreticular Zeolitic Imidazolate Frameworks and their Carbon Dioxide Selective Capture Properties, J. Am. Chem. Soc. 131 (2009) 3875–3877. https://doi.org/10.1021/ja809459e.

[386] J. Yang, Y.-B. Zhang, Q. Liu, C.A. Trickett, E. Gutiérrez-Puebla, M.Á. Monge, H. Cong, A. Aldossary, H. Deng, O.M. Yaghi, Principles of Designing Extra-Large Pore Openings and Cages in Zeolitic Imidazolate Frameworks, J. Am. Chem. Soc. 139 (2017) 6448–6455. https://doi.org/10.1021/jacs.7b02272.

[387] W. Li, Y. Zhang, C. Zhang, Q. Meng, Z. Xu, P. Su, Q. Li, C. Shen, Z. Fan, L. Qin, G. Zhang, Transformation of metal-organic frameworks for molecular sieving membranes, Nat. Commun. 7 (2016) 11315. https://doi.org/10.1038/ncomms11315.

[388] H. Tian, H. Fan, M. Li, L. Ma, Zeolitic Imidazolate Framework Coated ZnO Nanorods as Molecular Sieving to Improve Selectivity of Formaldehyde Gas Sensor, ACS Sensors. 1 (2016) 243–250. https://doi.org/10.1021/acssensors.5b00236.

[389] J. Hwang, A. Ejsmont, R. Freund, J. Goscianska, B.V.K.J. Schmidt, S. Wuttke, Controlling the morphology of metal–organic frameworks and porous carbon materials: metal oxides as primary architecture-directing agents, Chem. Soc. Rev. (2020). https://doi.org/10.1039/c9cs00871c.

[390] A. Das, N. Anbu, M. SK, A. Dhakshinamoorthy, S. Biswas, A functionalized UiO-66 MOF for turn-on fluorescence sensing of superoxide in water and efficient catalysis for Knoevenagel condensation, Dalt. Trans. 48 (2019) 17371–17380. https://doi.org/10.1039/C9DT03638E.

[391] W.P. Lustig, S. Mukherjee, N.D. Rudd, A. V Desai, J. Li, S.K. Ghosh, Metal–organic frameworks: functional luminescent and photonic materials for sensing applications, Chem. Soc. Rev. 46 (2017) 3242–3285. https://doi.org/10.1039/C6CS00930A.

[392] R. Zhang, D. Zhang, Y. Yao, Q. Zhang, Y. Xu, Y. Wu, H. Yu, G. Lu, Metal–Organic Framework Crystal-Assembled Optical Sensors for Chemical Vapors: Effects of Crystal Sizes and Missing-Linker Defects on Sensing Performances, ACS Appl. Mater. Interfaces. 11 (2019) 21010–21017. https://doi.org/10.1021/acsami.9b05933.

[393] A. Staerz, F. Roeck, U. Weimar, N. Barsan, Electronic Nose: Current Status and Future Trends1, Surf. Interface Sci. Vol. 9 Appl. I/Volume 10 Appl. II. (2020).

[394] T. Liu, Y. Chen, D. Li, T. Yang, J. Cao, Electronic Tongue Recognition with Feature

Specificity Enhancement, Sensors. 20 (2020) 772.

[395] C.W. Lee, J.M. Suh, H.W. Jang, Chemical Sensors Based on Two-Dimensional (2D) Materials for Selective Detection of Ions and Molecules in Liquid, Front. Chem. 7 (2019). https://doi.org/10.3389/fchem.2019.00708.

[396] M.C. Cha, M.P.A. Fisher, S.M. Girvin, M. Wallin, A.P. Young, Universal conductivity of two-dimensional films at the superconductor- insulator transition, Phys. Rev. B. (1991). https://doi.org/10.1103/PhysRevB.44.6883.

[397] M.G. Campbell, S.F. Liu, T.M. Swager, M. Dincă, Chemiresistive Sensor Arrays from Conductive 2D Metal–Organic Frameworks, J. Am. Chem. Soc. 137 (2015) 13780–13783. https://doi.org/10.1021/jacs.5b09600.

[398] M. Zhao, Y. Huang, Y. Peng, Z. Huang, Q. Ma, H. Zhang, Two-dimensional metal–organic framework nanosheets: synthesis and applications, Chem. Soc. Rev. 47 (2018) 6267–6295. https://doi.org/10.1039/C8CS00268A.

[399] M.-S. Yao, W.-X. Tang, G.-E. Wang, B. Nath, G. Xu, MOF Thin Film-Coated Metal Oxide Nanowire Array: Significantly Improved Chemiresistor Sensor Performance, Adv. Mater. 28 (2016) 5229–5234. https://doi.org/10.1002/adma.201506457.

[400] S. Wuttke, D.D. Medina, J.M. Rotter, S. Begum, T. Stassin, R. Ameloot, M. Oschatz, M. Tsotsalas, Bringing Porous Organic and Carbon-Based Materials toward Thin-Film Applications, Adv. Funct. Mater. 28 (2018) 1801545.

[401] A.A. Talin, A. Centrone, A.C. Ford, M.E. Foster, V. Stavila, P. Haney, R.A. Kinney, V. Szalai, F. El Gabaly, H.P. Yoon, F. Léonard, M.D. Allendorf, Tunable Electrical Conductivity in Metal-Organic Framework Thin-Film Devices, Science (80-.). 343 (2014) 66 LP – 69. https://doi.org/10.1126/science.1246738.

[402] D. Sheberla, J.C. Bachman, J.S. Elias, C.-J. Sun, Y. Shao-Horn, M. Dincă, Conductive MOF electrodes for stable supercapacitors with high areal capacitance, Nat. Mater. 16 (2017) 220–224. https://doi.org/10.1038/nmat4766.

[403] X. Song, X. Wang, Y. Li, C. Zheng, B. Zhang, C. Di, F. Li, C. Jin, W. Mi, L. Chen, W. Hu, 2D Semiconducting Metal–Organic Framework Thin Films for Organic Spin Valves, Angew. Chemie Int. Ed. 59 (2020) 1118–1123. https://doi.org/10.1002/anie.201911543.

[404] M.G. Campbell, D. Sheberla, S.F. Liu, T.M. Swager, M. Dincă, Cu 3 (hexaiminotriphenylene) 2 : An Electrically Conductive 2D Metal-Organic Framework for Chemiresistive Sensing, Angew. Chemie Int. Ed. 54 (2015) 4349–4352. https://doi.org/10.1002/anie.201411854.

[405] M. Huff, Process Variations in Microsystems Manufacturing, n.d.

[406] J. Cecil, M.B. Bharathi Raj Kumar, Y. Lu, V. Basallali, A review of micro-devices assembly techniques and technology, Int. J. Adv. Manuf. Technol. 83 (2016) 1569–1581. https://doi.org/10.1007/s00170-015-7698-6.

[407] M. Beidaghi, Y. Gogotsi, Capacitive energy storage in micro-scale devices: Recent advances in design and fabrication of micro-supercapacitors, Energy Environ. Sci. 7 (2014) 867–884. https://doi.org/10.1039/c3ee43526a.

[408] P. Falcaro, R. Ricco, C.M. Doherty, K. Liang, A.J. Hill, M.J. Styles, MOF positioning technology and device fabrication, Chem. Soc. Rev. 43 (2014) 5513–5560. https://doi.org/10.1039/c4cs00089g.

[409] L. Heinke, C. Wöll, Surface-Mounted Metal–Organic Frameworks: Crystalline and Porous Molecular Assemblies for Fundamental Insights and Advanced Applications, Adv. Mater. 31 (2019). https://doi.org/10.1002/adma.201806324.

[410] A. Walsh, K.T. Butler, C.H. Hendon, Chemical principles for electroactive metal-organic frameworks, MRS Bull. 41 (2016) 870–876. https://doi.org/10.1557/mrs.2016.243.

[411] B.G. Yacobi, Semiconductor Materials: An Introduction to Basic Principles, MICRODEVIC, Kluwer Academic Publisher, 2003. https://doi.org/10.1007/s00117-010-2057-y.

[412] L.S. Xie, G. Skorupskii, M. Dincă, Electrically Conductive Metal-Organic Frameworks, Chem. Rev. (2020). https://doi.org/10.1021/acs.chemrev.9b00766.

[413] S. Kasap, C. Koughia, H.E. Ruda, Springer Handbook of Electronic and Photonic Materials, Springer, 2017. https://doi.org/10.1007/978-3-319-48933-9.

[414] L. Wang, D. Beljonne, Flexible surface hopping approach to model the crossover from hopping to band-like transport in organic crystals, J. Phys. Chem. Lett. 4 (2013) 1888–1894. https://doi.org/10.1021/jz400871j.

[415] S.E. Gledhill, B. Scott, B.A. Gregg, Organic and nano-structured composite photovoltaics: An overview, J. Mater. Res. 20 (2005) 3167–3179. https://doi.org/10.1557/jmr.2005.0407.

[416] K.R. Dunbar, J.H. Ross, HYBRID MAGNETIC AND SEMICONDUCTING MATERIALS BASED ON, (2016).

[417] T. Mehtab, G. Yasin, M. Arif, M. Shakeel, R.M. Korai, M. Nadeem, N. Muhammad, X. Lu, Metal-organic frameworks for energy storage devices: Batteries and supercapacitors, J. Energy Storage. 21 (2019) 632–646.

https://doi.org/10.1016/j.est.2018.12.025.

[418] S.R. Ahrenholtz, C.C. Epley, A.J. Morris, Solvothermal Preparation of an Electrocatalytic Metalloporphyrin MOF Thin Film and its Redox Hopping Charge-Transfer Mechanism, J. Am. Chem. Soc. 136 (2014) 2464–2472. https://doi.org/10.1021/ja410684q.

[419] K.T. Butler, S.D. Worrall, C.D. Molloy, C.H. Hendon, M.P. Attfield, R.A.W. Dryfe, A. Walsh, Electronic structure design for nanoporous, electrically conductive zeolitic imidazolate frameworks, J. Mater. Chem. C. 5 (2017) 7726–7731. https://doi.org/10.1039/c7tc03150e.

[420] L. Sun, C.H. Hendon, S.S. Park, Y. Tulchinsky, R. Wan, F. Wang, A. Walsh, M. Dincă, Is iron unique in promoting electrical conductivity in MOFs?, Chem. Sci. 8 (2017) 4450–4457. https://doi.org/10.1039/c7sc00647k.

[421] L.S. Xie, L. Sun, R. Wan, S.S. Park, J.A. Degayner, C.H. Hendon, M. Dincă, Tunable Mixed-Valence Doping toward Record Electrical Conductivity in a Three-Dimensional Metal-Organic Framework, J. Am. Chem. Soc. 140 (2018) 7411–7414. https://doi.org/10.1021/jacs.8b03604.

[422] L.P. Tang, L.M. Tang, H. Geng, Y.P. Yi, Z. Wei, K.Q. Chen, H.X. Deng, Tuning transport performance in two-dimensional metal-organic framework semiconductors: Role of the metal d band, Appl. Phys. Lett. 112 (2018) 1–6. https://doi.org/10.1063/1.5000448.

[423] X. Huang, P. Sheng, Z. Tu, F. Zhang, J. Wang, H. Geng, Y. Zou, C.A. Di, Y. Yi, Y. Sun, W. Xu, D. Zhu, A two-dimensional π-d conjugated coordination polymer with extremely high electrical conductivity and ambipolar transport behaviour, Nat. Commun. 6 (2015) 1–8. https://doi.org/10.1038/ncomms8408.

[424] L.E. Darago, M.L. Aubrey, C.J. Yu, M.I. Gonzalez, J.R. Long, Electronic Conductivity, Ferrimagnetic Ordering, and Reductive Insertion Mediated by Organic Mixed-Valence in a Ferric Semiquinoid Metal–Organic Framework, J. Am. Chem. Soc. 137 (2015) 15703–15711. https://doi.org/10.1021/jacs.5b10385.

[425] J.A. DeGayner, I.R. Jeon, L. Sun, M. Dincă, T.D. Harris, 2D Conductive Iron-Quinoid Magnets Ordering up to Tc = 105 K via Heterogenous Redox Chemistry, J. Am. Chem. Soc. 139 (2017) 4175–4184. https://doi.org/10.1021/jacs.7b00705.

[426] D. Sheberla, L. Sun, M.A. Blood-forsythe, S. Er, C.R. Wade, C.K. Brozek, A. Aspuru-Guzik, M. Dinca, High Electrical Conductivity in Ni3(2,3,6,7,10,11-hexaiminotriphenylene)2, a Semiconducting Metal−Organic Graphene Analogue, J.

Am. Chem. Soc. 3 (2014) 2–5.

[427] P. Chaudhuri, C. Nazari Verani, E. Bill, E. Bothe, T. Weyhermüller, K. Wieghardt, Electronic Structure of Bis(o-iminobenzosemiquinonato)metal Complexes (Cu, Ni, Pd). The Art of Establishing Physical Oxidation States in Transition-Metal Complexes Containing Radical Ligands, J. Am. Chem. Soc. 123 (2001) 2213–2223. https://doi.org/10.1021/ja003831d.

[428] E.M. Miner, T. Fukushima, D. Sheberla, L. Sun, Y. Surendranath, M. Dincə, Electrochemical oxygen reduction catalysed by Ni3 (hexaiminotriphenylene)2, Nat. Commun. 7 (2016) 1–7. https://doi.org/10.1038/ncomms10942.

[429] A. Nazir, H.T.T. Le, C.W. Min, A. Kasbe, J. Kim, C.S. Jin, C.J. Park, Coupling of a conductive Ni3(2,3,6,7,10,11-hexaiminotriphenylene)2 metal-organic framework with silicon nanoparticles for use in high-capacity lithium-ion batteries, Nanoscale. 12 (2020) 1629–1642. https://doi.org/10.1039/c9nr08038d.

[430] J. Yang, P. Xiong, C. Zheng, H. Qiu, M. Wei, Metal-organic frameworks: A new promising class of materials for a high performance supercapacitor electrode, J. Mater. Chem. A. 2 (2014) 16640–16644. https://doi.org/10.1039/c4ta04140b.

[431] Poonam, K. Sharma, A. Arora, S.K. Tripathi, Review of supercapacitors: Materials and devices, J. Energy Storage. 21 (2019) 801–825. https://doi.org/10.1016/j.est.2019.01.010.

[432] A. Muzaffar, M.B. Ahamed, K. Deshmukh, J. Thirumalai, A review on recent advances in hybrid supercapacitors: Design, fabrication and applications, Renew. Sustain. Energy Rev. 101 (2019) 123–145. https://doi.org/10.1016/j.rser.2018.10.026.

[433] J. Park, M. Lee, D. Feng, Z. Huang, A.C. Hinckley, A. Yakovenko, X. Zou, Y. Cui, Z. Bao, Stabilization of Hexaaminobenzene in a 2D Conductive Metal-Organic Framework for High Power Sodium Storage, J. Am. Chem. Soc. 140 (2018) 10315–10323. https://doi.org/10.1021/jacs.8b06020.

[434] D. Sheberla, J.C. Bachman, J.S. Elias, C.J. Sun, Y. Shao-Horn, M. Dincă, Conductive MOF electrodes for stable supercapacitors with high areal capacitance, Nat. Mater. 16 (2017) 220–224. https://doi.org/10.1038/nmat4766.

[435] W.H. Li, K. Ding, H.R. Tian, M.S. Yao, B. Nath, W.H. Deng, Y. Wang, G. Xu, Conductive Metal–Organic Framework Nanowire Array Electrodes for High-Performance Solid-State Supercapacitors, Adv. Funct. Mater. 27 (2017) 1–7. https://doi.org/10.1002/adfm.201702067.

[436] S. Gao, Y. Sui, F. Wei, J. Qi, Q. Meng, Y. He, Facile synthesis of cuboid Ni-MOF for

high-performance supercapacitors, J. Mater. Sci. 53 (2018) 6807–6818. https://doi.org/10.1007/s10853-018-2005-1.

[437] J. Yang, Z. Ma, W. Gao, M. Wei, Layered Structural Co-Based MOF with Conductive Network Frames as a New Supercapacitor Electrode, Chem. - A Eur. J. 23 (2017) 631–636. https://doi.org/10.1002/chem.201604071.

[438] A.J. Clough, J.W. Yoo, M.H. Mecklenburg, S.C. Marinescu, Two-dimensional metal-organic surfaces for efficient hydrogen evolution from water, J. Am. Chem. Soc. 137 (2015) 118–121. https://doi.org/10.1021/ja5116937.

[439] I. Liberman, R. Shimoni, R. Ifraemov, I. Rozenberg, C. Singh, I. Hod, Active-Site Modulation in an Fe-Porphyrin-Based Metal-Organic Framework through Ligand Axial Coordination: Accelerating Electrocatalysis and Charge-Transport Kinetics, J. Am. Chem. Soc. 142 (2020) 1933–1940. https://doi.org/10.1021/jacs.9b11355.

[440] X. Gao, Y. Dong, S. Li, J. Zhou, L. Wang, B. Wang, MOFs and COFs for Batteries and Supercapacitors, Springer Singapore, 2020. https://doi.org/10.1007/s41918-019-00055-1.

[441] Y. Zhong, X. Xu, Y. Liu, W. Wang, Z. Shao, Recent progress in metal–organic frameworks for lithium–sulfur batteries, Polyhedron. 155 (2018) 464–484. https://doi.org/10.1016/j.poly.2018.08.067.

[442] M.T. Li, Y. Sun, K. Sen Zhao, Z. Wang, X.L. Wang, Z.M. Su, H.M. Xie, Metal-Organic Framework with Aromatic Rings Tentacles: High Sulfur Storage in Li-S Batteries and Efficient Benzene Homologues Distinction, ACS Appl. Mater. Interfaces. 8 (2016) 33183–33188. https://doi.org/10.1021/acsami.6b10946.

[443] A.E. Baumann, G.E. Aversa, A. Roy, M.L. Falk, N.M. Bedford, V.S. Thoi, Promoting sulfur adsorption using surface Cu sites in metal-organic frameworks for lithium sulfur batteries, J. Mater. Chem. A. 6 (2018) 4811–4821. https://doi.org/10.1039/c8ta01057a.

[444] F. Li, X. Zhang, X. Liu, M. Zhao, Novel Conductive Metal-Organic Framework for a High-Performance Lithium-Sulfur Battery Host: 2D Cu-Benzenehexathial (BHT), ACS Appl. Mater. Interfaces. 10 (2018) 15012–15020. https://doi.org/10.1021/acsami.8b00942.

[445] M. Fox, Optical properties of a-MnSe, Oxford University Press, 2001. https://doi.org/10.1103/PhysRevB.4.3425.

[446] O.A. Smyrnov, F. Biancalana, S. Malzer, Modulational instability and solitons in excitonic semiconductor waveguides, Phys. Rev. B - Condens. Matter Mater. Phys. 83 (2011) 1–7. https://doi.org/10.1103/PhysRevB.83.205207.

[447] S. Nojima, Photonic-crystal laser mediated by polaritons, Phys. Rev. B - Condens. Matter Mater. Phys. 61 (2000) 9940–9943. https://doi.org/10.1103/PhysRevB.61.9940.

[448] J. Yuen-Zhou, S.K. Saikin, N.Y. Yao, A. Aspuru-Guzik, Topologically protected excitons in porphyrin thin films, Nat. Mater. 13 (2014) 1026–1032. https://doi.org/10.1038/NMAT4073.

[449] G.M. Akselrod, P.B. Deotare, N.J. Thompson, J. Lee, W.A. Tisdale, M.A. Baldo, V.M. Menon, V. Bulovic, Visualization of exciton transport in ordered and disordered molecular solids, Nat. Commun. 5 (2014) 1–8. https://doi.org/10.1038/ncomms4646.

[450] Z. Sun, T. Liao, Springer Series in Materials Science 297 Responsive Nanomaterials for Sustainable Applications, n.d.

[451] L. Cao, Z. Lin, W. Shi, Z. Wang, C. Zhang, X. Hu, C. Wang, W. Lin, Exciton Migration and Amplified Quenching on Two-Dimensional Metal-Organic Layers, J. Am. Chem. Soc. 139 (2017) 7020–7029. https://doi.org/10.1021/jacs.7b02470.

[452] M. Oldenburg, A. Turshatov, D. Busko, S. Wollgarten, M. Adams, N. Baroni, A. Welle, E. Redel, C. Wöll, B.S. Richards, I.A. Howard, Photon Upconversion at Crystalline Organic–Organic Heterojunctions, Adv. Mater. 28 (2016) 8477–8482. https://doi.org/10.1002/adma.201601718.

[453] Y.A. Mezenov, A.A. Krasilin, V.P. Dzyuba, A. Nominé, V.A. Milichko, Metal–Organic Frameworks in Modern Physics: Highlights and Perspectives, Adv. Sci. 6 (2019). https://doi.org/10.1002/advs.201900506.

[454] V.A. Milichko, S. V Makarov, A. V Yulin, A. V Vinogradov, A.A. Krasilin, E. Ushakova, V.P. Dzyuba, E. Hey-Hawkins, E.A. Pidko, P.A. Belov, van der Waals Metal-Organic Framework as an Excitonic Material for Advanced Photonics, Adv. Mater. 29 (2017). https://doi.org/10.1002/adma.201606034.

[455] E. Castaldelli, K.D.G. Imalka Jayawardena, D.C. Cox, G.J. Clarkson, R.I. Walton, L. Le-Quang, J. Chauvin, S.R.P. Silva, G.J.F. Demets, Electrical semiconduction modulated by light in a cobalt and naphthalene diimide metal-organic framework, Nat. Commun. 8 (2017). https://doi.org/10.1038/s41467-017-02215-7.

[456] R. Ifraemov, R. Shimoni, W. He, G. Peng, I. Hod, A metal-organic framework film with a switchable anodic and cathodic behaviour in a photo-electrochemical cell, J. Mater. Chem. A. 7 (2019) 3046–3053. https://doi.org/10.1039/C8TA10483B.

[457] S. Goswami, M. Chen, M.R. Wasielewski, O.K. Farha, J.T. Hupp, Boosting Transport Distances for Molecular Excitons within Photoexcited Metal-Organic Framework Films, ACS Appl. Mater. Interfaces. 10 (2018) 34409–34417.

https://doi.org/10.1021/acsami.8b14977.

[458] A.J. Clough, J.M. Skelton, C.A. Downes, A.A. De La Rosa, J.W. Yoo, A. Walsh, B.C. Melot, S.C. Marinescu, Metallic Conductivity in a Two-Dimensional Cobalt Dithiolene Metal-Organic Framework, J. Am. Chem. Soc. 139 (2017) 10863–10867. https://doi.org/10.1021/jacs.7b05742.

[459] Y. He, E.D. Cubuk, M.D. Allendorf, E.J. Reed, Metallic Metal-Organic Frameworks Predicted by the Combination of Machine Learning Methods and Ab Initio Calculations, J. Phys. Chem. Lett. 9 (2018) 4562–4569. https://doi.org/10.1021/acs.jpclett.8b01707.

[460] J.H. Dou, L. Sun, Y. Ge, W. Li, C.H. Hendon, J. Li, S. Gul, J. Yano, E.A. Stach, M. Dincă, Signature of metallic behavior in the metal-organic frameworks M3(hexaiminobenzene)2 (M = Ni, Cu), J. Am. Chem. Soc. 139 (2017) 13608–13611. https://doi.org/10.1021/jacs.7b07234.

[461] X. Zhang, Y. Zhou, B. Cui, M. Zhao, F. Liu, Theoretical Discovery of a Superconducting Two-Dimensional Metal-Organic Framework, Nano Lett. 17 (2017) 6166–6170. https://doi.org/10.1021/acs.nanolett.7b02795.

[462] Z. Jin, J. Yan, X. Huang, W. Xu, S. Yang, D. Zhu, J. Wang, Solution-processed transparent coordination polymer electrode for photovoltaic solar cells, Nano Energy. 40 (2017) 376–381. https://doi.org/10.1016/j.nanoen.2017.08.028.

[463] T. Kambe, R. Sakamoto, T. Kusamoto, T. Pal, N. Fukui, K. Hoshiko, T. Shimojima, Z. Wang, T. Hirahara, K. Ishizaka, S. Hasegawa, F. Liu, H. Nishihara, Redox control and high conductivity of nickel bis(dithiolene) complex π-nanosheet: A potential organic two-dimensional topological insulator, J. Am. Chem. Soc. 136 (2014) 14357–14360. https://doi.org/10.1021/ja507619d.

[464] Y. Nonoguchi, D. Sato, T. Kawai, Crystallinity-dependent thermoelectric properties of a two-dimensional coordination polymer: Ni3(2,3,6,7,10,11-hexaiminotriphenylene)2, Polymers (Basel). 10 (2018). https://doi.org/10.3390/polym10090962.

[465] S. Chen, J. Dai, X.C. Zeng, Metal–organic Kagome lattices M 3 (2,3,6,7,10,11-hexaiminotriphenylene) 2 (M = Ni and Cu): from semiconducting to metallic by metal substitution, Phys. Chem. Chem. Phys. 17 (2015) 5954–5958. https://doi.org/10.1039/C4CP05328A.

[466] M.E. Foster, K. Sohlberg, M.D. Allendorf, A.A. Talin, Unraveling the Semiconducting/Metallic Discrepancy in Ni3(HITP)2, J. Phys. Chem. Lett. 9 (2018) 481–486. https://doi.org/10.1021/acs.jpclett.7b03140.

[467] H. Ibach, H. Luth, Solid-State Physics, an introduction to principles of material science., Springer, 2015. https://doi.org/10.1017/CBO9781107415324.004.

[468] H. Zhang, J. Hou, Y. Hu, P. Wang, R. Ou, L. Jiang, J. Zhe Liu, B.D. Freeman, A.J. Hill, H. Wang, Ultrafast selective transport of alkali metal ions in metal organic frameworks with subnanometer pores, Sci. Adv. 4 (2018). https://doi.org/10.1126/sciadv.aaq0066.

[469] P. Ramaswamy, N.E. Wong, G.K.H. Shimizu, MOFs as proton conductors-challenges and opportunities, Chem. Soc. Rev. 43 (2014) 5913–5932. https://doi.org/10.1039/c4cs00093e.

[470] C. Wang, X. Liu, N. Keser Demir, J.P. Chen, K. Li, Applications of water stable metal-organic frameworks, Chem. Soc. Rev. 45 (2016) 5107–5134. https://doi.org/10.1039/c6cs00362a.

[471] Y. Ye, L. Gong, S. Xiang, Z. Zhang, B. Chen, Metal-Organic Frameworks as a Versatile Platform for Proton Conductors, Adv. Mater. 1907090 (2020) 1907090. https://doi.org/10.1002/adma.201907090.

[472] V.G. Ponomareva, K.A. Kovalenko, A.P. Chupakhin, D.N. Dybtsev, E.S. Shutova, V.P. Fedin, Imparting high proton conductivity to a metal-organic framework material by controlled acid impregnation, J. Am. Chem. Soc. 134 (2012) 15640–15643. https://doi.org/10.1021/ja305587n.

[473] Z. Wang, Z. Wang, L. Yang, H. Wang, Y. Song, L. Han, K. Yang, J. Hu, H. Chen, F. Pan, Boosting interfacial Li+ transport with a MOF-based ionic conductor for solid-state batteries, Nano Energy. 49 (2018) 580–587. https://doi.org/10.1016/j.nanoen.2018.04.076.

[474] Y. Yoshida, K. Fujie, D.W. Lim, R. Ikeda, H. Kitagawa, Superionic Conduction over a Wide Temperature Range in a Metal–Organic Framework Impregnated with Ionic Liquids, Angew. Chemie - Int. Ed. 58 (2019) 10909–10913. https://doi.org/10.1002/anie.201903980.

[475] S. Bai, X. Liu, K. Zhu, S. Wu, H. Zhou, Metal-organic framework-based separator for lithium-sulfur batteries, Nat. Energy. 1 (2016). https://doi.org/10.1038/nenergy.2016.94.

[476] M. Li, Y. Wan, J.K. Huang, A.H. Assen, C.E. Hsiung, H. Jiang, Y. Han, M. Eddaoudi, Z. Lai, J. Ming, L.J. Li, Metal-Organic Framework-Based Separators for Enhancing Li-S Battery Stability: Mechanism of Mitigating Polysulfide Diffusion, ACS Energy Lett. 2 (2017) 2362–2367. https://doi.org/10.1021/acsenergylett.7b00692.

[477] R. Li, K. Li, G. Wang, L. Li, Q. Zhang, J. Yan, Y. Chen, Q. Zhang, C. Hou, Y. Li, H. Wang, Ion-Transport Design for High-Performance Na+-Based Electrochromics, ACS Nano. 12 (2018) 3759–3768. https://doi.org/10.1021/acsnano.8b00974.

[478] S. Chu, A. Majumdar, Opportunities and challenges for a sustainable energy future, Nature. 488 (2012) 294–303. https://doi.org/10.1038/nature11475.

[479] H. Dau, E. Fujita, L. Sun, Artificial Photosynthesis: Beyond Mimicking Nature, ChemSusChem. 10 (2017) 4228–4235. https://doi.org/10.1002/cssc.201702106.

[480] E. Shimoni, O. Rav-Hon, I. Ohad, V. Brumfeld, Z. Reich, Three-dimensional organization of higher-plant chloroplast thylakoid membranes revealed by electron tomography, Plant Cell. 17 (2005) 2580–2586. https://doi.org/10.1105/tpc.105.035030.

[481] A. Capretti, A.K. Ringsmuth, J.F. van Velzen, A. Rosnik, R. Croce, T. Gregorkiewicz, Nanophotonics of higher-plant photosynthetic membranes, Light Sci. Appl. 8 (2019) 5. https://doi.org/10.1038/s41377-018-0116-8.

[482] L.A. Staehelin, Chloroplast structure: from chlorophyll granules to supra-molecular architecture of thylakoid membranes, Photosynth. Res. 76 (2003) 185–196. https://doi.org/10.1023/a:1024994525586.

[483] G. McDermott, S.M. Prince, A.A. Freer, A.M. Hawthornthwaite-Lawless, M.Z. Papiz, R.J. Cogdell, N.W. Isaacs, Crystal structure of an integral membrane light-harvesting complex from photosynthetic bacteria, Nature. 374 (1995) 517–521. https://doi.org/10.1038/374517a0.

[484] A. Harriman, Artificial light-harvesting arrays for solar energy conversion, Chem. Commun. 51 (2015) 11745–11756. https://doi.org/10.1039/C5CC03577E.

[485] C. Creatore, A.W. Chin, M.A. Parker, S. Emmott, Emergent Models for Artificial Light-Harvesting, Front. Mater. 2 (2015). https://doi.org/10.3389/fmats.2015.00006.

[486] Z. Ding, C. Wang, S. Wang, L. Wu, X. Zhang, Light-harvesting metal-organic framework nanoprobes for ratiometric fluorescence energy transfer-based determination of pH values and temperature, Microchim. Acta. 186 (2019) 476. https://doi.org/10.1007/s00604-019-3608-1.

[487] J. Otsuki, Supramolecular approach towards light-harvesting materials based on porphyrins and chlorophylls, J. Mater. Chem. A. 6 (2018) 6710–6753. https://doi.org/10.1039/C7TA11274B.

[488] J.-J. Li, Y. Chen, J. Yu, N. Cheng, Y. Liu, A Supramolecular Artificial Light-Harvesting System with an Ultrahigh Antenna Effect, Adv. Mater. 29 (2017) 1701905. https://doi.org/10.1002/adma.201701905.

[489] L. Xu, Z. Wang, R. Wang, L. Wang, X. He, H. Jiang, H. Tang, D. Cao, B.Z. Tang, A Conjugated Polymeric Supramolecular Network with Aggregation-Induced Emission Enhancement: An Efficient Light-Harvesting System with an Ultrahigh Antenna Effect, Angew. Chemie Int. Ed. n/a (2019). https://doi.org/10.1002/anie.201907678.

[490] M. Hao, G. Sun, M. Zuo, Z. Xu, Y. Chen, X.-Y. Hu, L. Wang, A Supramolecular Artificial Light-Harvesting System with Two-Step Sequential Energy Transfer for Photochemical Catalysis, Angew. Chemie Int. Ed. n/a (2019). https://doi.org/10.1002/anie.201912654.

[491] C.-L. Sun, H.-Q. Peng, L.-Y. Niu, Y.-Z. Chen, L.-Z. Wu, C.-H. Tung, Q.-Z. Yang, Artificial light-harvesting supramolecular polymeric nanoparticles formed by pillar[5]arene-based host–guest interaction, Chem. Commun. 54 (2018) 1117–1120. https://doi.org/10.1039/C7CC09315B.

[492] Y. Liu, J. Jin, H. Deng, K. Li, Y. Zheng, C. Yu, Y. Zhou, Protein-Framed Multi-Porphyrin Micelles for a Hybrid Natural–Artificial Light-Harvesting Nanosystem, Angew. Chemie Int. Ed. 55 (2016) 7952–7957. https://doi.org/10.1002/anie.201601516.

[493] P.K. Dutta, R. Varghese, J. Nangreave, S. Lin, H. Yan, Y. Liu, DNA-Directed Artificial Light-Harvesting Antenna, J. Am. Chem. Soc. 133 (2011) 11985–11993. https://doi.org/10.1021/ja1115138.

[494] Y. Zeng, Y.-Y. Li, J. Chen, G. Yang, Y. Li, Dendrimers: A Mimic Natural Light-Harvesting System, Chem. – An Asian J. 5 (2010) 992–1005. https://doi.org/10.1002/asia.200900653.

[495] S. Hirayama, K. Oohora, T. Uchihashi, T. Hayashi, Thermoresponsive Micellar Assembly Constructed from a Hexameric Hemoprotein Modified with Poly(N-isopropylacrylamide) toward an Artificial Light-Harvesting System, J. Am. Chem. Soc. 142 (2020) 1822–1831. https://doi.org/10.1021/jacs.9b10080.

[496] X. Li, S. Qiao, L. Zhao, S. Liu, F. Li, F. Yang, Q. Luo, C. Hou, J. Xu, J. Liu, Template-Free Construction of Highly Ordered Monolayered Fluorescent Protein Nanosheets: A Bioinspired Artificial Light-Harvesting System, ACS Nano. 13 (2019) 1861–1869. https://doi.org/10.1021/acsnano.8b08021.

[497] L. Zhao, H. Zou, H. Zhang, H. Sun, T. Wang, T. Pan, X. Li, Y. Bai, S. Qiao, Q. Luo, J. Xu, C. Hou, J. Liu, Enzyme-Triggered Defined Protein Nanoarrays: Efficient Light-Harvesting Systems to Mimic Chloroplasts, ACS Nano. 11 (2017) 938–945. https://doi.org/10.1021/acsnano.6b07527.

[498] H. Sun, Q. Luo, C. Hou, J. Liu, Nanostructures based on protein self-assembly: From hierarchical construction to bioinspired materials, Nano Today. 14 (2017) 16–41. https://doi.org/https://doi.org/10.1016/j.nantod.2017.04.006.

[499] Y. Sun, F. Guo, T. Zuo, J. Hua, G. Diao, Stimulus-responsive light-harvesting complexes based on the pillararene-induced co-assembly of β-carotene and chlorophyll, Nat. Commun. 7 (2016) 12042. https://doi.org/10.1038/ncomms12042.

[500] H.-T. Feng, J.W.Y. Lam, B.Z. Tang, Self-assembly of AIEgens, Coord. Chem. Rev. 406 (2020) 213142. https://doi.org/https://doi.org/10.1016/j.ccr.2019.213142.

[501] Y. Li, Y. Dong, L. Cheng, C. Qin, H. Nian, H. Zhang, Y. Yu, L. Cao, Aggregation-Induced Emission and Light-Harvesting Function of Tetraphenylethene-Based Tetracationic Dicyclophane, J. Am. Chem. Soc. 141 (2019) 8412–8415. https://doi.org/10.1021/jacs.9b02617.

[502] S. Liu, S. Jiang, J. Xu, Z. Huang, F. Li, X. Fan, Q. Luo, W. Tian, J. Liu, B. Xu, Constructing Artificial Light-Harvesting Systems by Covalent Alignment of Aggregation-Induced Emission Molecules, Macromol. Rapid Commun. 40 (2019) 1800892. https://doi.org/10.1002/marc.201800892.

[503] X.-Y. Lou, N. Song, Y.-W. Yang, Fluorescence Resonance Energy Transfer Systems in Supramolecular Macrocyclic Chemistry, Molecules. 22 (2017). https://doi.org/10.3390/molecules22101640.

[504] J.M. Alex, P. McArdle, P.B. Crowley, Supramolecular stacking in a high Z′ calix[8]arene–porphyrin assembly, CrystEngComm. 22 (2020) 14–17. https://doi.org/10.1039/C9CE01646E.

[505] T. Xiao, W. Zhong, L. Zhou, L. Xu, X.-Q. Sun, R.B.P. Elmes, X.-Y. Hu, L. Wang, Artificial light-harvesting systems fabricated by supramolecular host–guest interactions, Chinese Chem. Lett. 30 (2019) 31–36. https://doi.org/https://doi.org/10.1016/j.cclet.2018.05.034.

[506] J. Chai, Y. Wu, B. Yang, B. Liu, The photochromism, light harvesting and self-assembly activity of a multi-function Schiff-base compound based on the AIE effect, J. Mater. Chem. C. 6 (2018) 4057–4064. https://doi.org/10.1039/C8TC00509E.

[507] S. Wang, J.-H. Ye, Z. Han, Z. Fan, C. Wang, C. Mu, W. Zhang, W. He, Highly efficient FRET from aggregation-induced emission to BODIPY emission based on host–guest interaction for mimicking the light-harvesting system, RSC Adv. 7 (2017) 36021–36025. https://doi.org/10.1039/C7RA05925F.

[508] Y. Shibuya, T. Itoh, S. Matsuura, A. Yamaguchi, Structural Stability of Light-

harvesting Protein LH2 Adsorbed on Mesoporous Silica Supports, Anal. Sci. 31 (2015) 1069–1074. https://doi.org/10.2116/analsci.31.1069.

[509] Y. Wang, M. Chen, D. Li, Z. Huang, Y. Mao, W. Han, T. Wang, D. Liu, Mesoporous silica hybrids as an antireflective coating to enhance light harvesting and achieve over 16% efficiency of organic solar cells, J. Mater. Chem. C. 7 (2019) 14962–14969. https://doi.org/10.1039/C9TC05301H.

[510] F. Cucinotta, B.P. Jarman, C. Caplan, S.J. Cooper, H.J. Riggs, J. Martinelli, K. Djanashvili, E. La Mazza, F. Puntoriero, Light-Harvesting Antennae using the Host–Guest Chemistry of Mesoporous Organosilica, ChemPhotoChem. 2 (2018) 196–206. https://doi.org/10.1002/cptc.201700144.

[511] L. Gartzia-Rivero, J. Bañuelos, I. López-Arbeloa, Photoactive Nanomaterials Inspired by Nature: LTL Zeolite Doped with Laser Dyes as Artificial Light Harvesting Systems, Mater. (Basel, Switzerland). 10 (2017) 495. https://doi.org/10.3390/ma10050495.

[512] X. Feng, X. Ding, L. Chen, Y. Wu, L. Liu, M. Addicoat, S. Irle, Y. Dong, D. Jiang, Two-dimensional artificial light-harvesting antennae with predesigned high-order structure and robust photosensitising activity, Sci. Rep. 6 (2016) 32944. https://doi.org/10.1038/srep32944.

[513] K. Chen, L. Yang, Z. Wu, C. Chen, J. Jiang, G. Zhang, A computational study on the tunability of woven covalent organic frameworks for photocatalysis, Phys. Chem. Chem. Phys. 21 (2019) 546–553. https://doi.org/10.1039/C8CP04373F.

[514] K. Lei, D. Wang, L. Ye, M. Kou, Y. Deng, Z. Ma, L. Wang, Y. Kong, A Metal-Free Donor–Acceptor Covalent Organic Framework Photocatalyst for Visible-Light-Driven Reduction of CO2 with H2O, ChemSusChem. n/a (2020). https://doi.org/10.1002/cssc.201903545.

[515] M. Li, J.-S. Chen, M. Cotlet, Efficient Light Harvesting Biotic–Abiotic Nanohybrid System Incorporating Atomically Thin van der Waals Transition Metal Dichalcogenides, ACS Photonics. 6 (2019) 1451–1457. https://doi.org/10.1021/acsphotonics.9b00090.

[516] B.K. Singh, A. Bijalwan, V. Rastogi, Enhancement of light harvesting efficiency of perovskite solar cells by using one-dimensional photonic crystals, Appl. Opt. 58 (2019) 8046–8054. https://doi.org/10.1364/AO.58.008046.

[517] Y.-N. Zhang, B. Li, L. Fu, Q. Li, L.-W. Yin, MOF-derived ZnO as electron transport layer for improving light harvesting and electron extraction efficiency in perovskite

solar cells, Electrochim. Acta. 330 (2020) 135280. https://doi.org/https://doi.org/10.1016/j.electacta.2019.135280.

[518] S. Huh, S.-J. Kim, Y. Kim, Porphyrinic metal–organic frameworks from custom-designed porphyrins, CrystEngComm. 18 (2016) 345–368. https://doi.org/10.1039/C5CE02106E.

[519] J. Liu, W. Zhou, J. Liu, Y. Fujimori, T. Higashino, H. Imahori, X. Jiang, J. Zhao, T. Sakurai, Y. Hattori, W. Matsuda, S. Seki, S.K. Garlapati, S. Dasgupta, E. Redel, L. Sun, C. Wöll, A new class of epitaxial porphyrin metal–organic framework thin films with extremely high photocarrier generation efficiency: promising materials for all-solid-state solar cells, J. Mater. Chem. A. 4 (2016) 12739–12747. https://doi.org/10.1039/C6TA04898F.

[520] N. Sharma, S.S. Dhankhar, C.M. Nagaraja, A Mn(II)-porphyrin based metal-organic framework (MOF) for visible-light-assisted cycloaddition of carbon dioxide with epoxides, Microporous Mesoporous Mater. 280 (2019) 372–378. https://doi.org/https://doi.org/10.1016/j.micromeso.2019.02.026.

[521] M.C. So, G.P. Wiederrecht, J.E. Mondloch, J.T. Hupp, O.K. Farha, Metal–organic framework materials for light-harvesting and energy transfer, Chem. Commun. 51 (2015) 3501–3510. https://doi.org/10.1039/C4CC09596K.

[522] D.E. Williams, N.B. Shustova, Metal–Organic Frameworks as a Versatile Tool To Study and Model Energy Transfer Processes, Chem. – A Eur. J. 21 (2015) 15474–15479. https://doi.org/10.1002/chem.201502334.

[523] T. Zhang, W. Lin, Metal–organic frameworks for artificial photosynthesis and photocatalysis, Chem. Soc. Rev. 43 (2014) 5982–5993. https://doi.org/10.1039/C4CS00103F.

[524] R. Haldar, L. Heinke, C. Wöll, Advanced Photoresponsive Materials Using the Metal–Organic Framework Approach, Adv. Mater. n/a (2019) 1905227. https://doi.org/10.1002/adma.201905227.

[525] H.-Q. Liang, Y. Guo, Y. Shi, X. Peng, B. Liang, B. Chen, A Light-Responsive Metal–Organic Framework Hybrid Membrane with High On/Off Photoswitchable Proton Conductivity, Angew. Chemie Int. Ed. 59 (2020) 7732–7737. https://doi.org/10.1002/anie.202002389.

[526] S.N. Misra, S.O. Sommerer, Absorption Spectra of Lanthanide Complexes in Solution, Appl. Spectrosc. Rev. 26 (1991) 151–202. https://doi.org/10.1080/05704929108050880.

[527] J. Dong, D. Zhao, Y. Lu, W.-Y. Sun, Photoluminescent metal–organic frameworks and their application for sensing biomolecules, J. Mater. Chem. A. 7 (2019) 22744–22767. https://doi.org/10.1039/C9TA07022B.

[528] T.N. Nguyen, F.M. Ebrahim, K.C. Stylianou, Photoluminescent, upconversion luminescent and nonlinear optical metal-organic frameworks: From fundamental photophysics to potential applications, Coord. Chem. Rev. 377 (2018) 259–306. https://doi.org/https://doi.org/10.1016/j.ccr.2018.08.024.

[529] Y. Cui, J. Zhang, H. He, G. Qian, Photonic functional metal–organic frameworks, Chem. Soc. Rev. 47 (2018) 5740–5785. https://doi.org/10.1039/C7CS00879A.

[530] W.P. Lustig, J. Li, Luminescent metal–organic frameworks and coordination polymers as alternative phosphors for energy efficient lighting devices, Coord. Chem. Rev. 373 (2018) 116–147. https://doi.org/https://doi.org/10.1016/j.ccr.2017.09.017.

[531] Y. Hao, S. Chen, Y. Zhou, Y. Zhang, M. Xu, Recent Progress in Metal-Organic Framework (MOF) Based Luminescent Chemodosimeters, Nanomater. (Basel, Switzerland). 9 (2019) 974. https://doi.org/10.3390/nano9070974.

[532] R. Medishetty, L. Nemec, V. Nalla, S. Henke, M. Samoć, K. Reuter, R.A. Fischer, Multi-Photon Absorption in Metal–Organic Frameworks, Angew. Chemie Int. Ed. 56 (2017) 14743–14748. https://doi.org/10.1002/anie.201706492.

[533] R. Medishetty, J.K. Zaręba, D. Mayer, M. Samoć, R.A. Fischer, Nonlinear optical properties, upconversion and lasing in metal–organic frameworks, Chem. Soc. Rev. 46 (2017) 4976–5004. https://doi.org/10.1039/C7CS00162B.

[534] H.-Q. Yin, X.-B. Yin, Metal–Organic Frameworks with Multiple Luminescence Emissions: Designs and Applications, Acc. Chem. Res. 53 (2020) 485–495. https://doi.org/10.1021/acs.accounts.9b00575.

[535] H. He, H. Li, Y. Cui, G. Qian, MOF-Based Organic Microlasers, Adv. Opt. Mater. 7 (2019) 1900077. https://doi.org/10.1002/adom.201900077.

[536] M.S.T. Gonçalves, Fluorescent Labeling of Biomolecules with Organic Probes, Chem. Rev. 109 (2009) 190–212. https://doi.org/10.1021/cr0783840.

[537] C.Y. Lee, O.K. Farha, B.J. Hong, A.A. Sarjeant, S.T. Nguyen, J.T. Hupp, Light-Harvesting Metal–Organic Frameworks (MOFs): Efficient Strut-to-Strut Energy Transfer in Bodipy and Porphyrin-Based MOFs, J. Am. Chem. Soc. 133 (2011) 15858–15861. https://doi.org/10.1021/ja206029a.

[538] L. Zhang, J. Lei, F. Ma, P. Ling, J. Liu, H. Ju, A porphyrin photosensitized metal–organic framework for cancer cell apoptosis and caspase responsive theranostics,

Chem. Commun. 51 (2015) 10831–10834. https://doi.org/10.1039/C5CC03028E.

[539] C. Liu, B. Liu, J. Zhao, Z. Di, D. Chen, Z. Gu, L. Li, Y. Zhao, Nd3+-Sensitized Upconversion Metal–Organic Frameworks for Mitochondria-Targeted Amplified Photodynamic Therapy, Angew. Chemie Int. Ed. 59 (2020) 2634–2638. https://doi.org/10.1002/anie.201911508.

[540] L. Zhang, L.L. Wang, L. Le Gong, X.F. Feng, M.B. Luo, F. Luo, Coumarin-modified microporous-mesoporous Zn-MOF-74 showing ultra-high uptake capacity and photo-switched storage/release of UVI ions, J. Hazard. Mater. 311 (2016) 30–36. https://doi.org/https://doi.org/10.1016/j.jhazmat.2016.01.082.

[541] M. Gutierrez, C. Martin, K. Kennes, J. Hofkens, M. Vander Auweraer, F. Sanchez, A. Douhal, New OLEDs Based on Zirconium Metal-Organic Framework, Adv. Opt. Mater. 6 (2018). https://doi.org/10.1002/adom.201701060.

[542] A. Gust, A. Zander, A. Gietl, P. Holzmeister, S. Schulz, B. Lalkens, P. Tinnefeld, D. Grohmann, A Starting Point for Fluorescence-Based Single-Molecule Measurements in Biomolecular Research, Molecules. 19 (2014). https://doi.org/10.3390/molecules191015824.

[543] X. Wang, W. Lu, Z.-Y. Gu, Z. Wei, H.-C. Zhou, Topology-guided design of an anionic bor-network for photocatalytic [Ru(bpy)3]2+ encapsulation, Chem. Commun. 52 (2016) 1926–1929. https://doi.org/10.1039/C5CC08614K.

[544] R. Sen, S. Koner, A. Bhattacharjee, J. Kusz, Y. Miyashita, K.-I. Okamoto, Entrapment of [Ru(bpy)3]2+ in the anionic metal–organic framework: Novel photoluminescence behavior exhibiting dual emission at room temperature, Dalt. Trans. 40 (2011) 6952–6960. https://doi.org/10.1039/C0DT01647K.

[545] L. Martins, L.K. Macreadie, D. Sensharma, S. Vaesen, X. Zhang, J.J. Gough, M. O'Doherty, N.-Y. Zhu, M. Rüther, J.E. O'Brien, A.L. Bradley, W. Schmitt, Light-harvesting, 3rd generation RuII/CoII MOF with a large, tubular channel aperture, Chem. Commun. 55 (2019) 5013–5016. https://doi.org/10.1039/C9CC00206E.

[546] C.R. McKeithan, L. Wojtas, R.W. Larsen, Guest to framework photoinduced electron transfer in a cobalt substituted RWLC-2 metal organic framework, Dalt. Trans. 47 (2018) 9250–9256. https://doi.org/10.1039/C8DT01287C.

[547] M. Shengqian, Elaboration And Applications Of Metal-organic Frameworks, World Scientific, 2018.

[548] C. Chen, W. Ma, J. Zhao, Semiconductor-mediated photodegradation of pollutants under visible-light irradiation, Chem. Soc. Rev. 39 (2010) 4206–4219.

https://doi.org/10.1039/B921692H.

[549] D. Li, S.-H. Yu, H.-L. Jiang, From UV to Near-Infrared Light-Responsive Metal–Organic Framework Composites: Plasmon and Upconversion Enhanced Photocatalysis, Adv. Mater. 30 (2018) 1707377. https://doi.org/10.1002/adma.201707377.

[550] Q. Tian, W. Yao, W. Wu, C. Jiang, NIR light-activated upconversion semiconductor photocatalysts, Nanoscale Horizons. 4 (2019) 10–25. https://doi.org/10.1039/C8NH00154E.

[551] Y. Tang, W. Di, X. Zhai, R. Yang, W. Qin, NIR-Responsive Photocatalytic Activity and Mechanism of NaYF4:Yb,Tm@TiO2 Core–Shell Nanoparticles, ACS Catal. 3 (2013) 405–412. https://doi.org/10.1021/cs300808r.

[552] H. Li, R. Liu, S. Lian, Y. Liu, H. Huang, Z. Kang, Near-infrared light controlled photocatalytic activity of carbon quantum dots for highly selective oxidation reaction, Nanoscale. 5 (2013) 3289–3297. https://doi.org/10.1039/C3NR00092C.

[553] J. Gao, Y. Chen, W. Ji, Z. Gao, J. Zhang, Synthesis of a CdS-decorated Eu-MOF nanocomposite for the construction of a self-powered photoelectrochemical aptasensor, Analyst. 144 (2019) 6617–6624. https://doi.org/10.1039/C9AN01606F.

[554] R. Kaur, A.L. Sharma, K.-H. Kim, A. Deep, A novel CdTe/Eu-MOF photoanode for application in quantum dot-sensitized solar cell to improve power conversion efficiency, J. Ind. Eng. Chem. 53 (2017) 77–81. https://doi.org/https://doi.org/10.1016/j.jiec.2017.04.002.

[555] J.-C.G. Bünzli, S. V Eliseeva, Intriguing aspects of lanthanide luminescence, Chem. Sci. 4 (2013) 1939–1949. https://doi.org/10.1039/C3SC22126A.

[556] C. Pagis, M. Ferbinteanu, G. Rothenberg, S. Tanase, Lanthanide-Based Metal Organic Frameworks: Synthetic Strategies and Catalytic Applications, ACS Catal. 6 (2016) 6063–6072. https://doi.org/10.1021/acscatal.6b01935.

[557] H. Xu, C.-S. Cao, X.-M. Kang, B. Zhao, Lanthanide-based metal–organic frameworks as luminescent probes, Dalt. Trans. 45 (2016) 18003–18017. https://doi.org/10.1039/C6DT02213H.

[558] A.D.G. Firmino, F. Figueira, J.P.C. Tomé, F.A.A. Paz, J. Rocha, Metal–Organic Frameworks assembled from tetraphosphonic ligands and lanthanides, Coord. Chem. Rev. 355 (2018) 133–149. https://doi.org/https://doi.org/10.1016/j.ccr.2017.08.001.

[559] Y. Su, J. Yu, Y. Li, S.F.Z. Phua, G. Liu, W.Q. Lim, X. Yang, R. Ganguly, C. Dang, C. Yang, Y. Zhao, Versatile bimetallic lanthanide metal-organic frameworks for tunable

emission and efficient fluorescence sensing, Commun. Chem. 1 (2018) 12. https://doi.org/10.1038/s42004-018-0016-0.

[560] S.-N. Zhao, G. Wang, D. Poelman, V.P. Voort, Luminescent Lanthanide MOFs: A Unique Platform for Chemical Sensing, Materials (Basel). 11 (2018). https://doi.org/10.3390/ma11040572.

[561] V. Poláchová, M. Pastucha, Z. Mikušová, M.J. Mickert, A. Hlaváček, H.H. Gorris, P. Skládal, Z. Farka, Click-conjugated photon-upconversion nanoparticles in an immunoassay for honeybee pathogen Melissococcus plutonius, Nanoscale. 11 (2019) 8343–8351. https://doi.org/10.1039/C9NR01246J.

[562] R. Singh, G. Dumlupinar, S. Andersson-Engels, S. Melgar, Emerging applications of upconverting nanoparticles in intestinal infection and colorectal cancer, Int. J. Nanomedicine. 14 (2019) 1027–1038. https://doi.org/10.2147/IJN.S188887.

[563] H. Li, X. Wang, D. Huang, G. Chen, Recent advances of lanthanide-doped upconversion nanoparticles for biological applications, Nanotechnology. 31 (2019) 72001. https://doi.org/10.1088/1361-6528/ab4f36.

[564] K. Green, K. Huang, H. Pan, G. Han, S.F. Lim, Optical Temperature Sensing With Infrared Excited Upconversion Nanoparticles, Front. Chem. 6 (2018). https://doi.org/10.3389/fchem.2018.00416.

[565] X. Zhu, J. Zhang, J. Liu, Y. Zhang, Recent Progress of Rare-Earth Doped Upconversion Nanoparticles: Synthesis, Optimization, and Applications, Adv. Sci. 6 (2019) 1901358. https://doi.org/10.1002/advs.201901358.

[566] Y. Liu, Y. Lu, X. Yang, X. Zheng, S. Wen, F. Wang, X. Vidal, J. Zhao, D. Liu, Z. Zhou, C. Ma, J. Zhou, J.A. Piper, P. Xi, D. Jin, Amplified stimulated emission in upconversion nanoparticles for super-resolution nanoscopy, Nature. 543 (2017) 229–233. https://doi.org/10.1038/nature21366.

[567] M.-F. Joubert, Photon avalanche upconversion in rare earth laser materials, Opt. Mater. (Amst). 11 (1999) 181–203. https://doi.org/https://doi.org/10.1016/S0925-3467(98)00043-3.

[568] W.D. Horrocks, J.P. Bolender, W.D. Smith, R.M. Supkowski, Photosensitized Near Infrared Luminescence of Ytterbium(III) in Proteins and Complexes Occurs via an Internal Redox Process, J. Am. Chem. Soc. 119 (1997) 5972–5973. https://doi.org/10.1021/ja9644211.

[569] L. Li, X. Zhang, J. Cui, L. Chen, A theoretical study of intrinsic optical bistability dynamics in Tm3+/Yb3+codoped systems with an upconversion avalanche

mechanism, J. Opt. A Pure Appl. Opt. 11 (2009) 105203. https://doi.org/10.1088/1464-4258/11/10/105203.

[570] N. Bloembergen, Solid State Infrared Quantum Counters, Phys. Rev. Lett. 2 (1959) 84–85. https://doi.org/10.1103/PhysRevLett.2.84.

[571] S. Wilhelm, Perspectives for Upconverting Nanoparticles, ACS Nano. 11 (2017) 10644–10653. https://doi.org/10.1021/acsnano.7b07120.

[572] G. Tessitore, G.A. Mandl, M.G. Brik, W. Park, J.A. Capobianco, Recent insights into upconverting nanoparticles: spectroscopy, modeling, and routes to improved luminescence, Nanoscale. 11 (2019) 12015–12029. https://doi.org/10.1039/C9NR02291K.

[573] S. Jafari, H. Derakhshankhah, L. Alaei, A. Fattahi, B.S. Varnamkhasti, A.A. Saboury, Mesoporous silica nanoparticles for therapeutic/diagnostic applications, Biomed. Pharmacother. 109 (2019) 1100–1111. https://doi.org/https://doi.org/10.1016/j.biopha.2018.10.167.

[574] P. Wang, F. Zhou, K. Guan, Y. Wang, X. Fu, Y. Yang, X. Yin, G. Song, X.-B. Zhang, W. Tan, In vivo therapeutic response monitoring by a self-reporting upconverting covalent organic framework nanoplatform, Chem. Sci. 11 (2020) 1299–1306. https://doi.org/10.1039/C9SC04875H.

[575] J. Li, C. Zhang, M. Yin, Z. Zhang, Y. Chen, Q. Deng, S. Wang, Surfactant-Sensitized Covalent Organic Frameworks-Functionalized Lanthanide-Doped Nanocrystals: An Ultrasensitive Sensing Platform for Perfluorooctane Sulfonate, ACS Omega. 4 (2019) 15947–15955. https://doi.org/10.1021/acsomega.9b01996.

[576] M. Li, S. Gul, D. Tian, E. Zhou, Y. Wang, Y. Han, L. Yin, L. Huang, Erbium(iii)-based metal–organic frameworks with tunable upconversion emissions, Dalt. Trans. 47 (2018) 12868–12872. https://doi.org/10.1039/C8DT02329H.

[577] H.S. Quah, W. Chen, M.K. Schreyer, H. Yang, M.W. Wong, W. Ji, J.J. Vittal, Multiphoton harvesting metal–organic frameworks, Nat. Commun. 6 (2015) 7954. https://doi.org/10.1038/ncomms8954.

[578] Z. Yuan, L. Zhang, S. Li, W. Zhang, M. Lu, Y. Pan, X. Xie, L. Huang, W. Huang, Paving Metal–Organic Frameworks with Upconversion Nanoparticles via Self-Assembly, J. Am. Chem. Soc. 140 (2018) 15507–15515. https://doi.org/10.1021/jacs.8b10122.

[579] C. Hao, X. Wu, M. Sun, H. Zhang, A. Yuan, L. Xu, C. Xu, H. Kuang, Chiral Core–Shell Upconversion Nanoparticle@MOF Nanoassemblies for Quantification and

Bioimaging of Reactive Oxygen Species in Vivo, J. Am. Chem. Soc. 141 (2019) 19373–19378. https://doi.org/10.1021/jacs.9b09360.

[580] J. Yu, Y. Cui, C.-D. Wu, Y. Yang, B. Chen, G. Qian, Two-Photon Responsive Metal–Organic Framework, J. Am. Chem. Soc. 137 (2015) 4026–4029. https://doi.org/10.1021/ja512552g.

[581] M. O'Keeffe, O.M. Yaghi, Deconstructing the Crystal Structures of Metal–Organic Frameworks and Related Materials into Their Underlying Nets, Chem. Rev. 112 (2012) 675–702. https://doi.org/10.1021/cr200205j.

[582] H. Deng, C.J. Doonan, H. Furukawa, R.B. Ferreira, J. Towne, C.B. Knobler, B. Wang, O.M. Yaghi, Multiple Functional Groups of Varying Ratios in Metal-Organic Frameworks, Science (80-.). 327 (2010) 846. https://doi.org/10.1126/science.1181761.

[583] S. Gharaati, C. Wang, C. Förster, F. Weigert, U. Resch-Genger, K. Heinze, Triplet–Triplet Annihilation Upconversion in a MOF with Acceptor-Filled Channels, Chem. – A Eur. J. 26 (2020) 1003–1007. https://doi.org/10.1002/chem.201904945.

[584] M. Li, Z. Zheng, Y. Zheng, C. Cui, C. Li, Z. Li, Controlled Growth of Metal–Organic Framework on Upconversion Nanocrystals for NIR-Enhanced Photocatalysis, ACS Appl. Mater. Interfaces. 9 (2017) 2899–2905. https://doi.org/10.1021/acsami.6b15792.

[585] Y. Li, Z. Di, J. Gao, P. Cheng, C. Di, G. Zhang, B. Liu, X. Shi, L.-D. Sun, L. Li, C.-H. Yan, Heterodimers Made of Upconversion Nanoparticles and Metal–Organic Frameworks, J. Am. Chem. Soc. 139 (2017) 13804–13810. https://doi.org/10.1021/jacs.7b07302.

[586] L. He, M. Brasino, C. Mao, S. Cho, W. Park, A.P. Goodwin, J.N. Cha, DNA-Assembled Core-Satellite Upconverting-Metal–Organic Framework Nanoparticle Superstructures for Efficient Photodynamic Therapy, Small. 13 (2017) 1700504. https://doi.org/10.1002/smll.201700504.

[587] S. Li, J. Liu, N.S. Ramesar, H. Heinz, L. Xu, C. Xu, N.A. Kotov, Single- and multi-component chiral supraparticles as modular enantioselective catalysts, Nat. Commun. 10 (2019) 4826. https://doi.org/10.1038/s41467-019-12134-4.

[588] T. Förster, Intramolecular energy migration and fluorescence, Ann. Phys. 2 (1948) 55–75.

[589] D.L. Dexter, A Theory of Sensitized Luminescence in Solids, J. Chem. Phys. 21 (1953) 836–850. https://doi.org/10.1063/1.1699044.

[590] C.K. Prier, D.A. Rankic, D.W.C. MacMillan, Visible Light Photoredox Catalysis with Transition Metal Complexes: Applications in Organic Synthesis, Chem. Rev. 113

(2013) 5322–5363. https://doi.org/10.1021/cr300503r.

[591] N.A. Romero, D.A. Nicewicz, Organic Photoredox Catalysis, Chem. Rev. 116 (2016) 10075–10166. https://doi.org/10.1021/acs.chemrev.6b00057.

[592] C.-B. Salem, E. Ploetz, D.C. Lamb, Chapter 2 - Probing dynamics in single molecules, in: C.K. Johnson (Ed.), Spectrosc. Dyn. Single Mol., Elsevier, 2019: pp. 71–115. https://doi.org/https://doi.org/10.1016/B978-0-12-816463-1.00002-X.

[593] Q. Zhang, C. Zhang, L. Cao, Z. Wang, B. An, Z. Lin, R. Huang, Z. Zhang, C. Wang, W. Lin, Förster Energy Transport in Metal–Organic Frameworks Is Beyond Step-by-Step Hopping, J. Am. Chem. Soc. 138 (2016) 5308–5315. https://doi.org/10.1021/jacs.6b01345.

[594] J.R. Lakowicz, Principles of Fluorescence Spectroscopy, 3rd ed., Springer, 2006.

[595] F. Strieth-Kalthoff, M.J. James, M. Teders, L. Pitzer, F. Glorius, Energy transfer catalysis mediated by visible light: principles, applications, directions, Chem. Soc. Rev. 47 (2018) 7190–7202. https://doi.org/10.1039/C8CS00054A.

[596] Z. Wei, Z.-Y. Gu, R.K. Arvapally, Y.-P. Chen, R.N. McDougald, J.F. Ivy, A.A. Yakovenko, D. Feng, M.A. Omary, H.-C. Zhou, Rigidifying Fluorescent Linkers by Metal–Organic Framework Formation for Fluorescence Blue Shift and Quantum Yield Enhancement, J. Am. Chem. Soc. 136 (2014) 8269–8276. https://doi.org/10.1021/ja5006866.

[597] M. Xie, F.-Q. Bai, J. Wang, Y.-Q. Zheng, Z. Lin, Theoretical investigations on the unsymmetrical effect of β-link Zn–porphyrin sensitizers on the performance for dye-sensitized solar cells, Phys. Chem. Chem. Phys. 20 (2018) 3741–3751. https://doi.org/10.1039/C7CP07115A.

[598] S. Goswami, L. Ma, A.B.F. Martinson, M.R. Wasielewski, O.K. Farha, J.T. Hupp, Toward Metal–Organic Framework-Based Solar Cells: Enhancing Directional Exciton Transport by Collapsing Three-Dimensional Film Structures, ACS Appl. Mater. Interfaces. 8 (2016) 30863–30870. https://doi.org/10.1021/acsami.6b08552.

[599] L. Cao, Z. Lin, W. Shi, Z. Wang, C. Zhang, X. Hu, C. Wang, W. Lin, Exciton Migration and Amplified Quenching on Two-Dimensional Metal–Organic Layers, J. Am. Chem. Soc. 139 (2017) 7020–7029. https://doi.org/10.1021/jacs.7b02470.

[600] Y. Yang, M. Ishida, Y. Yasutake, S. Fukatsu, C. Fukakusa, M. Morikawa, T. Yamada, N. Kimizuka, H. Furuta, Hierarchical Hybrid Metal–Organic Frameworks: Tuning the Visible/Near-Infrared Optical Properties by a Combination of Porphyrin and Its Isomer Units, Inorg. Chem. 58 (2019) 4647–4656.

https://doi.org/10.1021/acs.inorgchem.9b00251.

[601] X. Zhang, M.A. Ballem, Z.-J. Hu, P. Bergman, K. Uvdal, Nanoscale Light-Harvesting Metal–Organic Frameworks, Angew. Chemie Int. Ed. 50 (2011) 5729–5733. https://doi.org/10.1002/anie.201007277.

[602] L.-L. Wu, J. Zhao, H. Wang, J. Wang, A lanthanide(iii) metal–organic framework exhibiting ratiometric luminescent temperature sensing and tunable white light emission, CrystEngComm. 18 (2016) 4268–4271. https://doi.org/10.1039/C5CE02444G.

[603] H. Li, Q. Li, Z. Xu, Lanthanide cation encapsulated in a metal–organic framework as a white LED and selective naked-eye reversible HCl sensor, J. Mater. Chem. C. 7 (2019) 2880–2885. https://doi.org/10.1039/C8TC05956J.

[604] D. Yang, Y. Tian, W. Xu, X. Cao, S. Zheng, Q. Ju, W. Huang, Z. Fang, A Series of Lanthanide-Based Metal–Organic Frameworks: Synthesis, Structures, and Multicolor Tuning of Single Component, Inorg. Chem. 56 (2017) 2345–2353. https://doi.org/10.1021/acs.inorgchem.7b00074.

[605] L. Xu, Y. Li, Q. Pan, D. Wang, S. Li, G. Wang, Y. Chen, P. Zhu, W. Qin, Dual-Mode Light-Emitting Lanthanide Metal–Organic Frameworks with High Water and Thermal Stability and Their Application in White LEDs, ACS Appl. Mater. Interfaces. 12 (2020) 18934–18943. https://doi.org/10.1021/acsami.0c02999.

[606] X. Rao, T. Song, J. Gao, Y. Cui, Y. Yang, C. Wu, B. Chen, G. Qian, A Highly Sensitive Mixed Lanthanide Metal–Organic Framework Self-Calibrated Luminescent Thermometer, J. Am. Chem. Soc. 135 (2013) 15559–15564. https://doi.org/10.1021/ja407219k.

[607] W. Wang, J. Yang, R. Wang, L. Zhang, J. Yu, D. Sun, Luminescent Terbium-Organic Framework Exhibiting Selective Sensing of Nitroaromatic Compounds (NACs), Cryst. Growth Des. 15 (2015) 2589–2592. https://doi.org/10.1021/acs.cgd.5b00381.

[608] K. Leong, M.E. Foster, B.M. Wong, E.D. Spoerke, D. Van Gough, J.C. Deaton, M.D. Allendorf, Energy and charge transfer by donor–acceptor pairs confined in a metal–organic framework: a spectroscopic and computational investigation, J. Mater. Chem. A. 2 (2014) 3389–3398. https://doi.org/10.1039/C3TA14328G.

[609] X. Yang, D. Yan, Long-afterglow metal–organic frameworks: reversible guest-induced phosphorescence tunability, Chem. Sci. 7 (2016) 4519–4526. https://doi.org/10.1039/C6SC00563B.

[610] Z. Li, G. Wang, Y. Ye, B. Li, H. Li, B. Chen, Loading Photochromic Molecules into a

Luminescent Metal–Organic Framework for Information Anticounterfeiting, Angew. Chemie Int. Ed. 58 (2019) 18025–18031. https://doi.org/10.1002/anie.201910467.

[611] X.-Y. Liu, K. Xing, Y. Li, C.-K. Tsung, J. Li, Three Models To Encapsulate Multicomponent Dyes into Nanocrystal Pores: A New Strategy for Generating High-Quality White Light, J. Am. Chem. Soc. 141 (2019) 14807–14813. https://doi.org/10.1021/jacs.9b07236.

[612] J. Calbo, M.J. Golomb, A. Walsh, Redox-active metal–organic frameworks for energy conversion and storage, J. Mater. Chem. A. 7 (2019) 16571–16597. https://doi.org/10.1039/C9TA04680A.

[613] G. Xu, P. Nie, H. Dou, B. Ding, L. Li, X. Zhang, Exploring metal organic frameworks for energy storage in batteries and supercapacitors, Mater. Today. 20 (2017) 191–209. https://doi.org/https://doi.org/10.1016/j.mattod.2016.10.003.

[614] H. Wang, Q.-L. Zhu, R. Zou, Q. Xu, Metal-Organic Frameworks for Energy Applications, Chem. 2 (2017) 52–80. https://doi.org/https://doi.org/10.1016/j.chempr.2016.12.002.

[615] M.B. Solomon, T.L. Church, D.M. D'Alessandro, Perspectives on metal–organic frameworks with intrinsic electrocatalytic activity, CrystEngComm. 19 (2017) 4049–4065. https://doi.org/10.1039/C7CE00215G.

[616] L. Sun, M.G. Campbell, M. Dincă, Electrically Conductive Porous Metal–Organic Frameworks, Angew. Chemie Int. Ed. 55 (2016) 3566–3579. https://doi.org/10.1002/anie.201506219.

[617] Y.-Z. Chen, R. Zhang, L. Jiao, H.-L. Jiang, Metal–organic framework-derived porous materials for catalysis, Coord. Chem. Rev. 362 (2018) 1–23. https://doi.org/https://doi.org/10.1016/j.ccr.2018.02.008.

[618] Y. Zhang, S.N. Riduan, J. Wang, Redox Active Metal– and Covalent Organic Frameworks for Energy Storage: Balancing Porosity and Electrical Conductivity, Chem. – A Eur. J. 23 (2017) 16419–16431. https://doi.org/10.1002/chem.201702919.

[619] H. Bin Wu, X.W. Lou, Metal-organic frameworks and their derived materials for electrochemical energy storage and conversion: Promises and challenges, Sci. Adv. 3 (2017) eaap9252. https://doi.org/10.1126/sciadv.aap9252.

[620] J.G. Santaclara, F. Kapteijn, J. Gascon, M.A. van der Veen, Understanding metal–organic frameworks for photocatalytic solar fuel production, CrystEngComm. 19 (2017) 4118–4125. https://doi.org/10.1039/C7CE00006E.

[621] S. Abednatanzi, P. Gohari Derakhshandeh, H. Depauw, F.-X. Coudert, H. Vrielinck, P.

Van Der Voort, K. Leus, Mixed-metal metal–organic frameworks, Chem. Soc. Rev. 48 (2019) 2535–2565. https://doi.org/10.1039/C8CS00337H.

[622] P. Huo, T. Chen, J.-L. Hou, L. Yu, Q.-Y. Zhu, J. Dai, Ligand-to-Ligand Charge Transfer within Metal–Organic Frameworks Based on Manganese Coordination Polymers with Tetrathiafulvalene-Bicarboxylate and Bipyridine Ligands, Inorg. Chem. 55 (2016) 6496–6503. https://doi.org/10.1021/acs.inorgchem.6b00571.

[623] X. Li, K. Maindan, P. Deria, Metal-Organic Frameworks-Based Electrocatalysis: Insight and Future Perspectives, Comments Inorg. Chem. 38 (2018) 166–209. https://doi.org/10.1080/02603594.2018.1545225.

[624] R.A. Marcus, On the Theory of Oxidation-Reduction Reactions Involving Electron Transfer. I, J. Chem. Phys. 24 (1956) 966–978. https://doi.org/10.1063/1.1742723.

[625] R.A. Marcus, Chemical and Electrochemical Electron-Transfer Theory, Annu. Rev. Phys. Chem. 15 (1964) 155–196. https://doi.org/10.1146/annurev.pc.15.100164.001103.

[626] R.A. Marcus, N. Sutin, Electron transfers in chemistry and biology, Biochim. Biophys. Acta - Rev. Bioenerg. 811 (1985) 265–322. https://doi.org/https://doi.org/10.1016/0304-4173(85)90014-X.

[627] R.A. Marcus, Electron transfer reactions in chemistry. Theory and experiment, Rev. Mod. Phys. 65 (1993) 599–610. https://doi.org/10.1103/RevModPhys.65.599.

[628] S. Patwardhan, G.C. Schatz, Theoretical Investigation of Charge Transfer in Metal Organic Frameworks for Electrochemical Device Applications, J. Phys. Chem. C. 119 (2015) 24238–24247. https://doi.org/10.1021/acs.jpcc.5b06065.

[629] N.B. Taylor, I. Kassal, Generalised Marcus theory for multi-molecular delocalised charge transfer, Chem. Sci. 9 (2018) 2942–2951. https://doi.org/10.1039/C8SC00053K.

[630] X. Zhang, I. da Silva, R. Fazzi, A.M. Sheveleva, X. Han, B.F. Spencer, S.A. Sapchenko, F. Tuna, E.J.L. McInnes, M. Li, S. Yang, M. Schröder, Iodine Adsorption in a Redox-Active Metal–Organic Framework: Electrical Conductivity Induced by Host−Guest Charge-Transfer, Inorg. Chem. 58 (2019) 14145–14150. https://doi.org/10.1021/acs.inorgchem.9b02176.

[631] I. Hod, W. Bury, D.M. Gardner, P. Deria, V. Roznyatovskiy, M.R. Wasielewski, O.K. Farha, J.T. Hupp, Bias-Switchable Permselectivity and Redox Catalytic Activity of a Ferrocene-Functionalized, Thin-Film Metal–Organic Framework Compound, J. Phys. Chem. Lett. 6 (2015) 586–591. https://doi.org/10.1021/acs.jpclett.5b00019.

[632] I. Hod, O.K. Farha, J.T. Hupp, Modulating the rate of charge transport in a metal–organic framework thin film using host:guest chemistry, Chem. Commun. 52 (2016) 1705–1708. https://doi.org/10.1039/C5CC09695B.

[633] X. Li, J. Yu, D.J. Gosztola, H.C. Fry, P. Deria, Wavelength-Dependent Energy and Charge Transfer in MOF: A Step toward Artificial Porous Light-Harvesting System, J. Am. Chem. Soc. 141 (2019) 16849–16857. https://doi.org/10.1021/jacs.9b08078.

[634] M. Cai, Q. Loague, A.J. Morris, Design Rules for Efficient Charge Transfer in Metal–Organic Framework Films: The Pore Size Effect, J. Phys. Chem. Lett. 11 (2020) 702–709. https://doi.org/10.1021/acs.jpclett.9b03285.

[635] R.H. Palmer, J. Liu, C.-W. Kung, I. Hod, O.K. Farha, J.T. Hupp, Electroactive Ferrocene at or near the Surface of Metal–Organic Framework UiO-66, Langmuir. 34 (2018) 4707–4714. https://doi.org/10.1021/acs.langmuir.7b03846.

[636] M. Souto, J. Calbo, S. Mañas-Valero, A. Walsh, G. Mínguez Espallargas, Charge-transfer interactions between fullerenes and a mesoporous tetrathiafulvalene-based metal-organic framework, Beilstein J. Nanotechnol. 10 (2019) 1883–1893. https://doi.org/10.3762/bjnano.10.183.

[637] M. Souto, A. Santiago-Portillo, M. Palomino, I.J. Vitórica-Yrezábal, B.J.C. Vieira, J.C. Waerenborgh, S. Valencia, S. Navalón, F. Rey, H. García, G. Mínguez Espallargas, A highly stable and hierarchical tetrathiafulvalene-based metal-organic framework with improved performance as a solid catalyst, Chem. Sci. 9 (2018) 2413–2418. https://doi.org/10.1039/c7sc04829g.

[638] S. Goswami, D. Ray, K. Otake, C.-W. Kung, S.J. Garibay, T. Islamoglu, A. Atilgan, Y. Cui, C.J. Cramer, O.K. Farha, J.T. Hupp, A porous, electrically conductive hexazirconium(iv) metal–organic framework, Chem. Sci. 9 (2018) 4477–4482. https://doi.org/10.1039/C8SC00961A.

[639] C.F. Leong, B. Chan, T.B. Faust, D.M. D'Alessandro, Controlling charge separation in a novel donor–acceptor metal–organic framework via redox modulation, Chem. Sci. 5 (2014) 4724–4728. https://doi.org/10.1039/C4SC01551G.

[640] Z. Guo, D.K. Panda, M.A. Gordillo, A. Khatun, H. Wu, W. Zhou, S. Saha, Lowering Band Gap of an Electroactive Metal–Organic Framework via Complementary Guest Intercalation, ACS Appl. Mater. Interfaces. 9 (2017) 32413–32417. https://doi.org/10.1021/acsami.7b07292.

[641] Z. Guo, D.K. Panda, K. Maity, D. Lindsey, T.G. Parker, T.E. Albrecht-Schmitt, J.L. Barreda-Esparza, P. Xiong, W. Zhou, S. Saha, Modulating the electrical conductivity

of metal–organic framework films with intercalated guest π-systems, J. Mater. Chem. C. 4 (2016) 894–899. https://doi.org/10.1039/C5TC02232K.

[642] B.A. Johnson, A. Bhunia, H. Fei, S.M. Cohen, S. Ott, Development of a UiO-Type Thin Film Electrocatalysis Platform with Redox-Active Linkers, J. Am. Chem. Soc. (2018). https://doi.org/10.1021/jacs.7b13077.

[643] T. Song, P. Zhang, J. Zeng, T. Wang, A. Ali, H. Zeng, Tunable conduction band energy and metal-to-ligand charge transfer for wide-spectrum photocatalytic H2 evolution and stability from isostructural metal-organic frameworks, Int. J. Hydrogen Energy. 42 (2017) 26605–26616. https://doi.org/https://doi.org/10.1016/j.ijhydene.2017.09.081.

[644] M. Gutierrez, B. Cohen, F. Sánchez, A. Douhal, Photochemistry of Zr-based MOFs: ligand-to-cluster charge transfer, energy transfer and excimer formation, what else is there?, Phys. Chem. Chem. Phys. 18 (2016) 27761–27774. https://doi.org/10.1039/C6CP03791G.

[645] L. Hanna, P. Kucheryavy, C. Liu, X. Zhang, J. V Lockard, Long-Lived Photoinduced Charge Separation in a Trinuclear Iron-μ3-oxo-based Metal–Organic Framework, J. Phys. Chem. C. 121 (2017) 13570–13576. https://doi.org/10.1021/acs.jpcc.7b03936.

[646] G. Férey, F. Millange, M. Morcrette, C. Serre, M.-L. Doublet, J.-M. Grenèche, J.-M. Tarascon, Mixed-Valence Li/Fe-Based Metal–Organic Frameworks with Both Reversible Redox and Sorption Properties, Angew. Chemie Int. Ed. 46 (2007) 3259–3263. https://doi.org/10.1002/anie.200605163.

[647] Q. Sun, M. Liu, K. Li, Y. Han, Y. Zuo, J. Wang, C. Song, G. Zhang, X. Guo, Controlled synthesis of mixed-valent Fe-containing metal organic frameworks for the degradation of phenol under mild conditions, Dalt. Trans. 45 (2016) 7952–7959. https://doi.org/10.1039/C5DT05002B.

[648] C. Hua, P.W. Doheny, B. Ding, B. Chan, M. Yu, C.J. Kepert, D.M. D'Alessandro, Through-Space Intervalence Charge Transfer as a Mechanism for Charge Delocalization in Metal–Organic Frameworks, J. Am. Chem. Soc. 140 (2018) 6622–6630. https://doi.org/10.1021/jacs.8b02638.

[649] B. Ding, C. Hua, C.J. Kepert, D.M. D'Alessandro, Influence of structure-activity relationships on through-space intervalence charge transfer in metal-organic frameworks with cofacial redox-active units, Chem. Sci. 10 (2019) 1392–1400. https://doi.org/10.1039/c8sc01128a.

[650] B. Huskinson, M.P. Marshak, C. Suh, S. Er, M.R. Gerhardt, C.J. Galvin, X. Chen, A.

Aspuru-Guzik, R.G. Gordon, M.J. Aziz, A metal-free organic–inorganic aqueous flow battery, Nature. 505 (2014) 195–198. https://doi.org/10.1038/nature12909.

[651] A. Corma, J.M. Serra, Heterogeneous combinatorial catalysis applied to oil refining, petrochemistry and fine chemistry, in: Catal. Today, 2005: pp. 3–11. https://doi.org/10.1016/j.cattod.2005.07.117.

[652] Z. Karpinski, Elements of heterogeneous catalysis|(In Polish: Elementy Katalizy Heterogenicznej) by Barbara Grzybowska-Swierkosz, Wydawnictwo Naukowe PWN, Warszawa, 1993, 247 pp., ISBN 83-01-10511-9, (1994).

[653] P. Schlexer Lamoureux, K.T. Winther, J.A. Garrido Torres, V. Streibel, M. Zhao, M. Bajdich, F. Abild-Pedersen, T. Bligaard, Machine Learning for Computational Heterogeneous Catalysis, ChemCatChem. 11 (2019) 3581–3601. https://doi.org/10.1002/cctc.201900595.

[654] L. Grajciar, C.J. Heard, A.A. Bondarenko, M. V Polynski, J. Meeprasert, E.A. Pidko, P. Nachtigall, Towards operando computational modeling in heterogeneous catalysis, Chem. Soc. Rev. 47 (2018) 8307–8348. https://doi.org/10.1039/C8CS00398J.

[655] J.P. Reid, M.S. Sigman, Holistic prediction of enantioselectivity in asymmetric catalysis, Nature. 571 (2019) 343–348. https://doi.org/10.1038/s41586-019-1384-z.

[656] O. Engkvist, P.-O. Norrby, N. Selmi, Y. Lam, Z. Peng, E.C. Sherer, W. Amberg, T. Erhard, L.A. Smyth, Computational prediction of chemical reactions: current status and outlook, Drug Discov. Today. 23 (2018) 1203–1218.

[657] A.J. Medford, M.R. Kunz, S.M. Ewing, T. Borders, R. Fushimi, Extracting knowledge from data through catalysis informatics, ACS Catal. 8 (2018) 7403–7429.

[658] J.P. Reid, M.S. Sigman, Comparing quantitative prediction methods for the discovery of small-molecule chiral catalysts, Nat. Rev. Chem. 2 (2018) 290–305.

[659] E. Mansoor, J. Van der Mynsbrugge, M. Head-Gordon, A.T. Bell, Impact of long-range electrostatic and dispersive interactions on theoretical predictions of adsorption and catalysis in zeolites, Catal. Today. 312 (2018) 51–65.

[660] K.N. Houk, P.H.-Y. Cheong, Computational prediction of small-molecule catalysts, Nature. 455 (2008) 309–313. https://doi.org/10.1038/nature07368.

[661] K. Saravanan, J.R. Kitchin, O.A. von Lilienfeld, J.A. Keith, Alchemical Predictions for Computational Catalysis: Potential and Limitations, J. Phys. Chem. Lett. 8 (2017) 5002–5007. https://doi.org/10.1021/acs.jpclett.7b01974.

[662] J.A. Dumesic, G.W. Huber, M. Boudart, Principles of Heterogeneous Catalysis, in: Handb. Heterog. Catal., 2008. https://doi.org/10.1002/9783527610044.hetcat0001.

[663] M. Misono, Basis of heterogeneous catalysis, in: Stud. Surf. Sci. Catal., 2013. https://doi.org/10.1016/B978-0-444-53833-8.00001-6.

[664] R. Schlögl, Heterogeneous catalysis, Angew. Chemie - Int. Ed. (2015). https://doi.org/10.1002/anie.201410738.

[665] G. Ertl, H. Knözinger, J. Weitkamp, Handbook of Heterogeneous Catalysis, 2008. https://doi.org/10.1524/zpch.1999.208.part_1_2.274.

[666] D. Wolf, Kinetics of heterogeneous catalytic reactions, Springer Ser. Chem. Phys. (2004). https://doi.org/10.1016/s0166-9834(00)84492-9.

[667] G.W. Roberts, C.N. Satterfield, Effectiveness Factor for Porous Catalysts. Langmuir-Hinshelwood Kinetic Expressions, Ind. Eng. Chem. Fundam. 4 (1965) 288–293. https://doi.org/10.1021/i160015a009.

[668] K.V. Kumar, K. Porkodi, F. Rocha, Langmuir–Hinshelwood kinetics – A theoretical study, Catal. Commun. 9 (2008) 82–84. https://doi.org/https://doi.org/10.1016/j.catcom.2007.05.019.

[669] W.-Y. Gao, A.D. Cardenal, C.-H. Wang, D.C. Powers, In Operando Analysis of Diffusion in Porous Metal-Organic Framework Catalysts, Chem. – A Eur. J. 25 (2019) 3465–3476. https://doi.org/10.1002/chem.201804490.

[670] M. Hattori, S. Iijima, T. Nakao, H. Hosono, M. Hara, Solid solution for catalytic ammonia synthesis from nitrogen and hydrogen gases at 50 °C, Nat. Commun. 11 (2020) 2001. https://doi.org/10.1038/s41467-020-15868-8.

[671] A.G. Sault, An Auger Electron Spectroscopy Study of the Activation of Iron Fischer-Tropsch Catalysts: I. Hydrogen Activation, J. Catal. 140 (1993) 121–135. https://doi.org/https://doi.org/10.1006/jcat.1993.1072.

[672] Z. Deng, H. Yu, L. Wang, J. Liu, K.J. Shea, Ferrocene-based metal–organic framework nanosheets loaded with palladium as a super-high active hydrogenation catalyst, J. Mater. Chem. A. 7 (2019) 15975–15980. https://doi.org/10.1039/C9TA03403J.

[673] J. Jia, C. Qian, Y. Dong, Y.F. Li, H. Wang, M. Ghoussoub, K.T. Butler, A. Walsh, G.A. Ozin, Heterogeneous catalytic hydrogenation of CO2 by metal oxides: defect engineering – perfecting imperfection, Chem. Soc. Rev. 46 (2017) 4631–4644. https://doi.org/10.1039/C7CS00026J.

[674] G. Rothenberg, Catalysis: Concepts and Green Applications, 2008. https://doi.org/10.1002/9783527621866.

[675] E. Solel, N. Tarannam, S. Kozuch, Catalysis: Energy is the measure of all things,

Chem. Commun. (2019). https://doi.org/10.1039/c9cc00754g.

[676] V. Peksa, P. Lebrušková, H. Šípová, J. Štěpánek, J. Bok, J. Homola, M. Procházka, Testing gold nanostructures fabricated by hole-mask colloidal lithography as potential substrates for SERS sensors: sensitivity, signal variability, and the aspect of adsorbate deposition, Phys. Chem. Chem. Phys. 18 (2016) 19613–19620. https://doi.org/10.1039/C6CP02752K.

[677] S. Tanaka, K. Fujita, Y. Miyake, M. Miyamoto, Y. Hasegawa, T. Makino, S. Van der Perre, J. Cousin Saint Remi, T. Van Assche, G. V Baron, J.F.M. Denayer, Adsorption and Diffusion Phenomena in Crystal Size Engineered ZIF-8 MOF, J. Phys. Chem. C. 119 (2015) 28430–28439. https://doi.org/10.1021/acs.jpcc.5b09520.

[678] X. Hu, S. Brandani, A.I. Benin, R.R. Willis, Development of a Semiautomated Zero Length Column Technique for Carbon Capture Applications: Study of Diffusion Behavior of CO2 in MOFs, Ind. Eng. Chem. Res. 54 (2015) 5777–5783. https://doi.org/10.1021/acs.iecr.5b00515.

[679] O. Zybaylo, O. Shekhah, H. Wang, M. Tafipolsky, R. Schmid, D. Johannsmann, C. Wöll, A novel method to measure diffusion coefficients in porous metal–organic frameworks, Phys. Chem. Chem. Phys. 12 (2010) 8093–8098. https://doi.org/10.1039/B927601G.

[680] H. Jobic, D.I. Kolokolov, A.G. Stepanov, M.M. Koza, J. Ollivier, Diffusion of CH4 in ZIF-8 Studied by Quasi-Elastic Neutron Scattering, J. Phys. Chem. C. 119 (2015) 16115–16120. https://doi.org/10.1021/acs.jpcc.5b04259.

[681] F. Stallmach, S. Gröger, V. Künzel, J. Kärger, O.M. Yaghi, M. Hesse, U. Müller, NMR Studies on the Diffusion of Hydrocarbons on the Metal-Organic Framework Material MOF-5, Angew. Chemie Int. Ed. 45 (2006) 2123–2126. https://doi.org/10.1002/anie.200502553.

[682] L. Heinke, P. Kortunov, D. Tzoulaki, J. Kärger, The options of interference microscopy to explore the significance of intracrystalline diffusion and surface permeation for overall mass transfer on nanoporous materials, Adsorption. 13 (2007) 215–223. https://doi.org/10.1007/s10450-007-9048-y.

[683] H. Bux, C. Chmelik, J.M. van Baten, R. Krishna, J. Caro, Novel MOF-Membrane for Molecular Sieving Predicted by IR-Diffusion Studies and Molecular Modeling, Adv. Mater. 22 (2010) 4741–4743. https://doi.org/10.1002/adma.201002066.

[684] C. V McGuire, R.S. Forgan, The surface chemistry of metal–organic frameworks, Chem. Commun. 51 (2015) 5199–5217. https://doi.org/10.1039/C4CC04458D.

[685] J. Lee, O.K. Farha, J. Roberts, K.A. Scheidt, S.T. Nguyen, J.T. Hupp, Metal–organic framework materials as catalysts, Chem. Soc. Rev. 38 (2009) 1450–1459. https://doi.org/10.1039/B807080F.

[686] A. Zecchina, S. Bordiga, E. Groppo, The Structure and Reactivity of Single and Multiple Sites on Heterogeneous and Homogeneous Catalysts: Analogies, Differences, and Challenges for Characterization Methods, Sel. Nanocatalysts Nanosci. (2011) 1–27. https://doi.org/doi:10.1002/9783527635689.ch1.

[687] D. Yang, B.C. Gates, Catalysis by Metal Organic Frameworks: Perspective and Suggestions for Future Research, ACS Catal. (2019). https://doi.org/10.1021/acscatal.8b04515.

[688] V. Bernales, M.A. Ortuño, D.G. Truhlar, C.J. Cramer, L. Gagliardi, Computational Design of Functionalized Metal–Organic Framework Nodes for Catalysis, ACS Cent. Sci. 4 (2018) 5–19. https://doi.org/10.1021/acscentsci.7b00500.

[689] H. Lyu, Z. Ji, S. Wuttke, O.M. Yaghi, Digital Reticular Chemistry, Chem. (2020). https://doi.org/https://doi.org/10.1016/j.chempr.2020.08.008.

[690] M. Kumar Trivedi, Studies of the Atomic and Crystalline Characteristics of Ceramic Oxide Nano Powders after Bio field Treatment, Ind. Eng. Manag. (2015). https://doi.org/10.4172/2169-0316.1000161.

[691] I. MacLaren, Q.M. Ramasse, Aberration-corrected scanning transmission electron microscopy for atomic-resolution studies of functional oxides, Int. Mater. Rev. (2014). https://doi.org/10.1179/1743280413Y.0000000026.

[692] J.R. NOONAN, H.L. DAVIS, Atomic Arrangements at Metal Surfaces, Science (80-.). 234 (1986) 310 LP – 316. https://doi.org/10.1126/science.234.4774.310.

[693] W.L. Johnson, Bulk amorphous metal—An emerging engineering material, JOM. 54 (2002) 40–43. https://doi.org/10.1007/BF02822619.

[694] J.E. Warren, C.G. Perkins, K.E. Jelfs, P. Boldrin, P.A. Chater, G.J. Miller, T.D. Manning, M.E. Briggs, K.C. Stylianou, J.B. Claridge, M.J. Rosseinsky, Shape Selectivity by Guest-Driven Restructuring of a Porous Material, Angew. Chemie Int. Ed. 53 (2014) 4592–4596. https://doi.org/10.1002/anie.201307656.

[695] S. Yuan, L. Zou, H. Li, Y.-P. Chen, J. Qin, Q. Zhang, W. Lu, M.B. Hall, H.-C. Zhou, Flexible Zirconium Metal-Organic Frameworks as Bioinspired Switchable Catalysts, Angew. Chemie Int. Ed. 55 (2016) 10776–10780. https://doi.org/10.1002/anie.201604313.

[696] L. Chen, W. Zhan, H. Fang, Z. Cao, C. Yuan, Z. Xie, Q. Kuang, L. Zheng, Selective

Catalytic Performances of Noble Metal Nanoparticle@MOF Composites: The Concomitant Effect of Aperture Size and Structural Flexibility of MOF Matrices, Chem. – A Eur. J. 23 (2017) 11397–11403. https://doi.org/10.1002/chem.201702103.

[697] M. Taddei, When defects turn into virtues: The curious case of zirconium-based metal-organic frameworks, Coord. Chem. Rev. 343 (2017) 1–24.

[698] W. Schrimpf, J. Jiang, Z. Ji, P. Hirschle, D.C. Lamb, O.M. Yaghi, S. Wuttke, Chemical diversity in a metal-organic framework revealed by fluorescence lifetime imaging, Nat. Commun. (2018). https://doi.org/10.1038/s41467-018-04050-w.

[699] L. Liu, Z. Chen, J. Wang, D. Zhang, Y. Zhu, S. Ling, K.W. Huang, Y. Belmabkhout, K. Adil, Y. Zhang, B. Slater, M. Eddaoudi, Y. Han, Imaging defects and their evolution in a metal–organic framework at sub-unit-cell resolution, Nat. Chem. (2019). https://doi.org/10.1038/s41557-019-0263-4.

[700] D.S. Sholl, R.P. Lively, Defects in Metal–Organic Frameworks: Challenge or Opportunity?, J. Phys. Chem. Lett. 6 (2015) 3437–3444. https://doi.org/10.1021/acs.jpclett.5b01135.

[701] W. Schrimpf, G. Ossato, P. Hirschle, S. Wuttke, D.C. Lamb, Investigation of the Co-Dependence of Morphology and Fluorescence Lifetime in a Metal-Organic Framework, Small. (2016). https://doi.org/10.1002/smll.201600619.

[702] J. Canivet, M. Vandichel, D. Farrusseng, Origin of highly active metal–organic framework catalysts: defects? Defects!, Dalt. Trans. 45 (2016) 4090–4099. https://doi.org/10.1039/C5DT03522H.

[703] Y.K. Hwang, D.Y. Hong, J.S. Chang, S.H. Jhung, Y.K. Seo, J. Kim, A. Vimont, M. Daturi, C. Serre, G. Férey, Amine grafting on coordinatively unsaturated metal centers of MOFs: Consequences for catalysis and metal encapsulation, Angew. Chemie - Int. Ed. (2008). https://doi.org/10.1002/anie.200705998.

[704] D. Li, H.-Q. Xu, L. Jiao, H.-L. Jiang, Metal-organic frameworks for catalysis: State of the art, challenges, and opportunities, EnergyChem. 1 (2019) 100005. https://doi.org/10.1016/j.enchem.2019.100005.

[705] D. Jiang, S.M. Mahurin, S. Dai, eds., Materials for Carbon Capture, Wiley, 2020. https://doi.org/10.1002/9781119091219.

[706] C.A. Trickett, T.M. Osborn Popp, J. Su, C. Yan, J. Weisberg, A. Huq, P. Urban, J. Jiang, M.J. Kalmutzki, Q. Liu, J. Baek, M.P. Head-Gordon, G.A. Somorjai, J.A. Reimer, O.M. Yaghi, Identification of the strong Brønsted acid site in a metal–organic framework solid acid catalyst, Nat. Chem. 11 (2019) 170–176.

https://doi.org/10.1038/s41557-018-0171-z.

[707] Z. Hu, D. Zhao, Metal–organic frameworks with Lewis acidity: synthesis, characterization, and catalytic applications, CrystEngComm. 19 (2017) 4066–4081. https://doi.org/10.1039/C6CE02660E.

[708] M. Položij, M. Rubeš, J. Čejka, P. Nachtigall, Catalysis by Dynamically Formed Defects in a Metal-Organic Framework Structure: Knoevenagel Reaction Catalyzed by Copper Benzene-1,3,5-tricarboxylate, ChemCatChem. (2014). https://doi.org/10.1002/cctc.201402411.

[709] Y. Yang, H.F. Yao, F.G. Xi, E.Q. Gao, Amino-functionalized Zr(IV) metal-organic framework as bifunctional acid-base catalyst for Knoevenagel condensation, J. Mol. Catal. A Chem. (2014). https://doi.org/10.1016/j.molcata.2014.04.002.

[710] B. Li, Y. Zhang, D. Ma, L. Li, G. Li, G. Li, Z. Shi, S. Feng, A strategy toward constructing a bifunctionalized MOF catalyst: Post-synthetic modification of MOFs on organic ligands and coordinatively unsaturated metal sites, Chem. Commun. (2012). https://doi.org/10.1039/c2cc32384b.

[711] F. Vermoortele, A. Vimont, C. Serre, D. De Vos, An amino-modified Zr-terephthalate metal–organic framework as an acid–base catalyst for cross-aldol condensation, Chem. Commun. (2011). https://doi.org/10.1039/c0cc03038d.

[712] F.X.L.I. Xamena, F.G. Cirujano, A. Corma, An unexpected bifunctional acid base catalysis in IRMOF-3 for Knoevenagel condensation reactions, Microporous Mesoporous Mater. (2012). https://doi.org/10.1016/j.micromeso.2011.12.058.

[713] J. Gascon, U. Aktay, M.D. Hernandez-Alonso, G.P.M. van Klink, F. Kapteijn, Amino-based metal-organic frameworks as stable, highly active basic catalysts, J. Catal. (2009). https://doi.org/10.1016/j.jcat.2008.11.010.

[714] T. Toyao, M. Fujiwaki, Y. Horiuchi, M. Matsuoka, Application of an amino-functionalised metal-organic framework: An approach to a one-pot acid-base reaction, RSC Adv. (2013). https://doi.org/10.1039/c3ra44701d.

[715] M. Pintado-Sierra, A.M. Rasero-Almansa, A. Corma, M. Iglesias, F. Sánchez, Bifunctional iridium-(2-aminoterephthalate)-Zr-MOF chemoselective catalyst for the synthesis of secondary amines by one-pot three-step cascade reaction, J. Catal. (2013). https://doi.org/10.1016/j.jcat.2012.12.004.

[716] T.T. Liu, J. Liang, R. Xu, Y.B. Huang, R. Cao, Salen-Co(III) insertion in multivariate cationic metal-organic frameworks for the enhanced cycloaddition reaction of carbon dioxide, Chem. Commun. (2019). https://doi.org/10.1039/c8cc10268f.

[717] G. Cai, H.-L. Jiang, A Modulator-Induced Defect-Formation Strategy to Hierarchically Porous Metal–Organic Frameworks with High Stability, Angew. Chemie Int. Ed. 56 (2017) 563–567. https://doi.org/10.1002/anie.201610914.

[718] F. Vermoortele, B. Bueken, G. Le Bars, B. Van De Voorde, M. Vandichel, K. Houthoofd, A. Vimont, M. Daturi, M. Waroquier, V. Van Speybroeck, C. Kirschhock, D.E. De Vos, Synthesis modulation as a tool to increase the catalytic activity of metal-organic frameworks: The unique case of UiO-66(Zr), J. Am. Chem. Soc. (2013). https://doi.org/10.1021/ja405078u.

[719] Z.R. Jiang, H. Wang, Y. Hu, J. Lu, H.L. Jiang, Polar Group and Defect Engineering in a Metal-Organic Framework: Synergistic Promotion of Carbon Dioxide Sorption and Conversion, ChemSusChem. (2015). https://doi.org/10.1002/cssc.201403230.

[720] L. Yuan, M. Tian, J. Lan, X. Cao, X. Wang, Z. Chai, J.K. Gibson, W. Shi, Defect engineering in metal-organic frameworks: A new strategy to develop applicable actinide sorbents, Chem. Commun. (2018). https://doi.org/10.1039/c7cc07527h.

[721] V.R. Remya, M. Kurian, Synthesis and catalytic applications of metal–organic frameworks: a review on recent literature, Int. Nano Lett. (2019). https://doi.org/10.1007/s40089-018-0255-1.

[722] Z. Li, N.M. Schweitzer, A.B. League, V. Bernales, A.W. Peters, A.B. Getsoian, T.C. Wang, J.T. Miller, A. Vjunov, J.L. Fulton, J.A. Lercher, C.J. Cramer, L. Gagliardi, J.T. Hupp, O.K. Farha, Sintering-Resistant Single-Site Nickel Catalyst Supported by Metal-Organic Framework, J. Am. Chem. Soc. (2016). https://doi.org/10.1021/jacs.5b12515.

[723] S.M. George, Atomic layer deposition: An overview, Chem. Rev. (2010). https://doi.org/10.1021/cr900056b.

[724] H. Noh, Y. Cui, A.W. Peters, D.R. Pahls, M.A. Ortuno, N.A. Vermeulen, C.J. Cramer, L. Gagliardi, J.T. Hupp, O.K. Farha, An Exceptionally Stable Metal-Organic Framework Supported Molybdenum(VI) Oxide Catalyst for Cyclohexene Epoxidation, J. Am. Chem. Soc. (2016). https://doi.org/10.1021/jacs.6b08898.

[725] X. Chen, Y. Peng, X. Han, Y. Liu, X. Lin, Y. Cui, Sixteen isostructural phosphonate metal-organic frameworks with controlled Lewis acidity and chemical stability for asymmetric catalysis, Nat. Commun. (2017). https://doi.org/10.1038/s41467-017-02335-0.

[726] W. Lin, Asymmetric catalysis with chiral porous metal-organic frameworks, in: Top. Catal., 2010. https://doi.org/10.1007/s11244-010-9519-3.

[727] B. Pattengale, D.J. SantaLucia, S. Yang, W. Hu, C. Liu, X. Zhang, J.F. Berry, J. Huang, Direct Observation of Node-to-Node Communication in Zeolitic Imidazolate Frameworks, J. Am. Chem. Soc. 140 (2018) 11573–11576. https://doi.org/10.1021/jacs.8b06727.

[728] J. Wang, W. Cui, Q. Liu, Z. Xing, A.M. Asiri, X. Sun, Recent Progress in Cobalt-Based Heterogeneous Catalysts for Electrochemical Water Splitting, Adv. Mater. (2016). https://doi.org/10.1002/adma.201502696.

[729] K. Zeng, D. Zhang, Recent progress in alkaline water electrolysis for hydrogen production and applications, Prog. Energy Combust. Sci. (2010). https://doi.org/10.1016/j.pecs.2009.11.002.

[730] J. Duan, S. Chen, C. Zhao, Ultrathin metal-organic framework array for efficient electrocatalytic water splitting, Nat. Commun. (2017). https://doi.org/10.1038/ncomms15341.

[731] M. Fiaz, M. Kashif, M. Fatima, S.R. Batool, M.A. Asghar, M. Shakeel, M. Athar, Synthesis of Efficient TMS@MOF-5 Catalysts for Oxygen Evolution Reaction, Catal. Letters. (2020) 1–12. https://doi.org/10.1007/s10562-020-03155-6.

[732] B.R. Reiner, N.T. Mucha, A. Rothstein, J.S. Temme, P. Duan, K. Schmidt-Rohr, B.M. Foxman, C.R. Wade, Zirconium Metal-Organic Frameworks Assembled from Pd and Pt PNNNP Pincer Complexes: Synthesis, Postsynthetic Modification, and Lewis Acid Catalysis, Inorg. Chem. (2018). https://doi.org/10.1021/acs.inorgchem.7b03063.

[733] B.R. Reiner, A.A. Kassie, C.R. Wade, Unveiling reactive metal sites in a Pd pincer MOF: Insights into Lewis acid and pore selective catalysis, Dalt. Trans. (2019). https://doi.org/10.1039/c8dt03801e.

[734] T. Mallat, A. Baiker, Oxidation of alcohols with molecular oxygen on solid catalysts, Chem. Rev. (2004). https://doi.org/10.1021/cr0200116.

[735] Oxidation of Alcohols to Aldehydes and Ketones: A Guide to Current Common ... - Gabriel Tojo, Marcos I. Fernandez - Google Książki, (n.d.).

[736] H. Wang, W. Fan, Y. He, J. Wang, J.N. Kondo, T. Tatsumi, Selective oxidation of alcohols to aldehydes/ketones over copper oxide-supported gold catalysts, J. Catal. 299 (2013) 10–19. https://doi.org/10.1016/j.jcat.2012.11.018.

[737] A. Kamimura, H. Komatsu, T. Moriyama, Y. Nozaki, Sub-stoichiometric oxidation of benzylic alcohols with commercially available activated MnO2 under oxygen atmosphere: A green modification of the benzylic oxidation, Tetrahedron. (2013). https://doi.org/10.1016/j.tet.2013.04.109.

[738] J. Lou, Solvent free oxidation of alcohols catalyzed by KMnO4 adsorbed on Kieselguhr, Catal. Commun. 4 (2003) 647–649. https://doi.org/10.1016/j.catcom.2003.10.008.

[739] N.T. Thao, N.T. Nhu, K.-S. Lin, Liquid phase oxidation of benzyl alcohol to benzaldehyde over sepiolite loaded chromium oxide catalysts, J. Taiwan Inst. Chem. Eng. 83 (2018) 10–22. https://doi.org/10.1016/j.jtice.2017.11.034.

[740] J. Zhang, Y. Huang, G. Li, Y. Wei, Recent advances in alkoxylation chemistry of polyoxometalates: From synthetic strategies, structural overviews to functional applications, Coord. Chem. Rev. 378 (2019) 395–414. https://doi.org/https://doi.org/10.1016/j.ccr.2017.10.025.

[741] N.I. Gumerova, A. Rompel, Synthesis, structures and applications of electron-rich polyoxometalates, Nat. Rev. Chem. 2 (2018) 112. https://doi.org/10.1038/s41570-018-0112.

[742] S.-S. Wang, G.-Y. Yang, Recent Advances in Polyoxometalate-Catalyzed Reactions, Chem. Rev. 115 (2015) 4893–4962. https://doi.org/10.1021/cr500390v.

[743] L. Peng, S. Wu, X. Yang, J. Hu, X. Fu, M. Li, L. Bai, Q. Huo, J. Guan, Oxidation of benzyl alcohol over metal organic frameworks M-BTC (M = Co, Cu, Fe), New J. Chem. (2017). https://doi.org/10.1039/c7nj00588a.

[744] D.-Y. Du, J.-S. Qin, S.-L. Li, Z.-M. Su, Y.-Q. Lan, Recent advances in porous polyoxometalate-based metal–organic framework materials, Chem. Soc. Rev. 43 (2014) 4615–4632. https://doi.org/10.1039/C3CS60404G.

[745] C. Freire, D.M. Fernandes, M. Nunes, V.K. Abdelkader, POM & MOF-based Electrocatalysts for Energy-related Reactions, ChemCatChem. 10 (2018) 1703–1730. https://doi.org/10.1002/cctc.201701926.

[746] D. Li, Q. Xu, Y. Li, Y. Qiu, P. Ma, J. Niu, J. Wang, A Stable Polyoxometalate-Based Metal-Organic Framework as Highly Efficient Heterogeneous Catalyst for Oxidation of Alcohols, Inorg. Chem. (2019). https://doi.org/10.1021/acs.inorgchem.8b03589.

[747] D. Yang, C.A. Gaggioli, D. Ray, M. Babucci, L. Gagliardi, B.C. Gates, Tuning Catalytic Sites on Zr6O8 Metal Organic Framework Nodes via Ligand and Defect Chemistry probed with t-Butyl Alcohol Dehydration to Isobutylene, J. Am. Chem. Soc. (2020). https://doi.org/10.1021/jacs.0c03175.

[748] Y. Li, M. Wu, D. Chen, L. Jiang, J. He, Z. Luo, W. Wang, J. Wang, One-step highly selective oxidation of p-xylene to 4-hydroxymethylbenzoic acid over Cu-MOF catalysts under mild conditions, Mol. Catal. (2019).

https://doi.org/10.1016/j.mcat.2019.110542.

[749] J. Ying, A. Herbst, Y.X. Xiao, H. Wei, G. Tian, Z. Li, X.Y. Yang, B.L. Su, C. Janiak, Nanocoating of Hydrophobic Mesoporous Silica around MIL-101Cr for Enhanced Catalytic Activity and Stability, Inorg. Chem. (2018). https://doi.org/10.1021/acs.inorgchem.7b01992.

[750] A. Grigoropoulos, A.I. McKay, A.P. Katsoulidis, R.P. Davies, A. Haynes, L. Brammer, J. Xiao, A.S. Weller, M.J. Rosseinsky, Encapsulation of Crabtree's Catalyst in Sulfonated MIL-101(Cr): Enhancement of Stability and Selectivity between Competing Reaction Pathways by the MOF Chemical Microenvironment, Angew. Chemie Int. Ed. 57 (2018) 4532–4537. https://doi.org/10.1002/anie.201710091.

[751] J. Yu, C. Mu, B. Yan, X. Qin, C. Shen, H. Xue, H. Pang, Nanoparticle/MOF composites: preparations and applications, Mater. Horizons. 4 (2017) 557–569. https://doi.org/10.1039/C6MH00586A.

[752] M. Gharib, L. Esrafili, A. Morsali, P. Retailleau, Solvent-assisted ligand exchange (SALE) for the enhancement of epoxide ring-opening reaction catalysis based on three amide-functionalized metal-organic frameworks, Dalt. Trans. (2019). https://doi.org/10.1039/c9dt00941h.

[753] L.H.T. Nguyen, T.T. Nguyen, H.L. Nguyen, T.L.H. Doan, P.H. Tran, A new superacid hafnium-based metal-organic framework as a highly active heterogeneous catalyst for the synthesis of benzoxazoles under solvent-free conditions, Catal. Sci. Technol. (2017). https://doi.org/10.1039/c7cy01668a.

[754] K.M. Choi, K. Na, G.A. Somorjai, O.M. Yaghi, Chemical Environment Control and Enhanced Catalytic Performance of Platinum Nanoparticles Embedded in Nanocrystalline Metal-Organic Frameworks, J. Am. Chem. Soc. (2015). https://doi.org/10.1021/jacs.5b03540.

[755] X. Li, T.W. Goh, L. Li, C. Xiao, Z. Guo, X.C. Zeng, W. Huang, Controlling Catalytic Properties of Pd Nanoclusters through Their Chemical Environment at the Atomic Level Using Isoreticular Metal-Organic Frameworks, ACS Catal. (2016). https://doi.org/10.1021/acscatal.6b00397.